Functional Anatomy, Osteogenesis and Bone Microstructure of the Appendicular System of African Mole-Rats (Rodentia: Ctenohystrica: Bathyergidae)

Author: MSc. Germán Andrés Montoya-Sanhueza

Supervisor: Dr. Anusuya Chinsamy-Turan
Co-supervisor: Dr. Marcelo Sánchez-Villagra

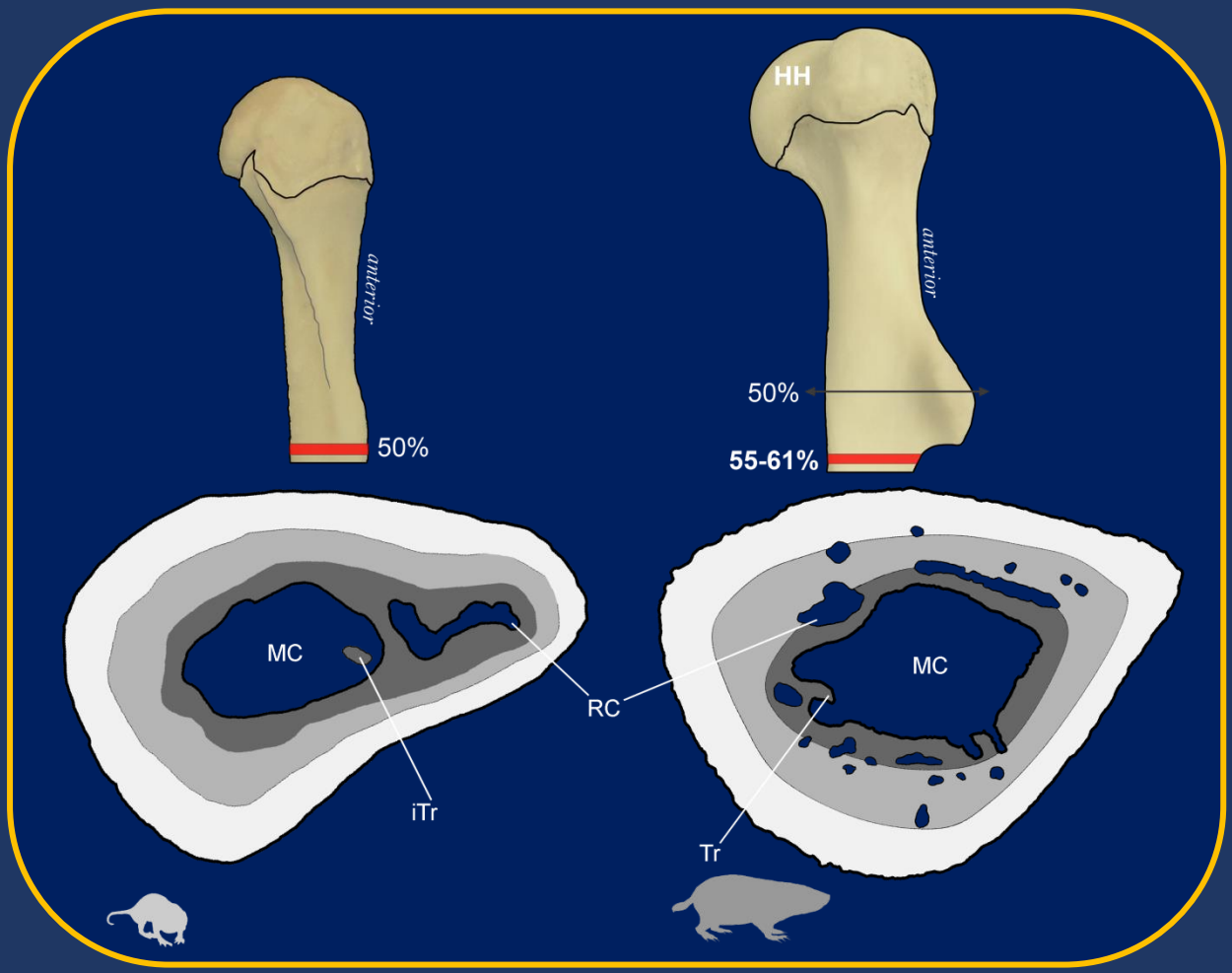

Thesis Presented for the Degree of
DOCTOR OF PHILOSOPHY

Functional Anatomy, Osteogenesis and Bone Microstructure of the Appendicular System of African Mole-Rats (Rodentia: Ctenohystrica: Bathyergidae)

Author: MSc. Germán Andrés Montoya-Sanhueza

Supervisor: Dr. Anusuya Chinsamy-Turan
Co-supervisor: Dr. Marcelo Sánchez-Villagra

Thesis Presented for the Degree of
DOCTOR OF PHILOSOPHY

Department of Biological Sciences
UNIVERSITY OF CAPE TOWN

February 2020

DECLARATIONS:

1. **I am presenting this dissertation in FULL/PARTIAL fulfilment of the requirements for my degree.**
2. **I know the meaning of plagiarism and declare that all of the work in the dissertation, save for that which is properly acknowledged, is my own.**
3. **I hereby grant the University of Cape Town free licence to reproduce for the purpose of research either the whole or any portion of the contents in any manner whatsoever of the above dissertation.**

Signed by candidate

Germán Montoya Sanhueza

10th of February 2020

I confirm that I have been granted permission by the University of Cape Town's Doctoral Degrees Board to include the following publication in my thesis, and where co-authorships are involved, my co-authors have agreed that I may include the publication:

- **Montoya-Sanhueza G**, Wilson LAB, Chinsamy A. 2019. Postnatal development of the largest subterranean mammal (*Bathyergus suillus*): Morphology, osteogenesis, and modularity of the appendicular skeleton. *Developmental Dynamics*.; 1–28. https://doi.org/10.1002/dvdy.81

Signature:	Signed by candidate
Date:	10/02/2020
Student name:	Germán Montoya-Sanhueza
Student number:	MNTGER002

SPECIAL ISSUE (II): ADVANCES IN EVOLUTIONARY AND DEVELOPMENTAL BIOLOGY

Cover photograph: (Bottom right) Double stained (alcian blue/alizarin red) of a newborn of the largest subterranean mammal (*Bathyergus suillus*). (Image © Germán Montoya-Sanhueza).

Somebody tell me frankly.
What times are these,
What century we live in,
What is the name of this country?

"Hope" (Esperanza)
Ariel Dorfman, 1978

In spite of this,
to oppression,
plundering and abandonment,
we respond with life.

"The Solitude of Latin America" (La soledad de América Latina)
Gabriel García Márquez, 1982

Acknowledgements

I would like to express my sincere thanks to my supervisors, Anusuya Chinsamy-Turan and Marcelo Sánchez-Villagra, without whom this work would have not been possible. They have been a fundamental support to develop and accomplish the present study, both by accepting me to be part of their research groups, as well as helping with the difficult task of providing funding for multiple activities including technical assistance, as well as to cover expenses for local and international conferences.

I am enormously grateful to the many academics that made this research possible by trusting, collaborating and dedicating their valuable time to this project, specifically by selecting and providing specimens. This was also possible thanks to their assistants who did the tedious work of preparing the samples. Among these researchers, I am most grateful to:

Prof. Nigel Bennett from *University of Pretoria* (UP - South Africa), who's support and kind contribution were fundamental to the accomplishment of this work, particularly with regard to the bone labelling experiments carried out in his laboratory.

Prof. Marietjie Oosthuizen also from UP was enormously helpful throughout this project by helping me with the experimental procedures, and other logistics of my research, especially during the many trips to Pretoria. Thank you very much Marietjie and Albert.

I wish to also acknowledge Prof. Jenny Jarvis and Justin O'Riain from *University of Cape Town* (UCT) for their help in this study, as well as for always giving me access to mole-rat specimens.

Prof. Radim Šumbera from *University of South Bohemia* (Czech Republic) for the constant support, enthusiasm and interest for this project, as well as to Honza (Jan) Okrouhlik and Matěj Lovy, who helped me in several aspects of this study. Thank you to the members of his team that prepared many specimens for this thesis.

Prof. Christine Dengler-Crish from *Northeast Ohio Medical University* (United States) for her enthusiastic collaboration in this study, and to her research assistant Katie Eckman.

Prof. Tim Clutton-Brock from the *University of Cambridge* (UK), which kindly gave me access to mole-rat specimens, as well as to the many members involved in the Kalahari Meerkat Project who helped me during my visit to the Kuruman station: Dave Gaynor, Tanja van de Ven, Jacob Brown, Carlijn Brands and Philippe Vullioud.

Prof. Sabine Begall from the *Universität Duisburg-Essen* (Germany), which kindly gave me access to specimens of mole-rats.

And finally to my co-supervisor Prof. Marcelo Sánchez-Villagra from the *Universität Zürich* (Switzerland) and the members of his team, Alexandra Wegmann and Heike Götzmann, that helped in diverse aspects of this thesis.

All the above researchers contributed to generate this comprehensive work, without the need of additional field collections or excessive deaths of wild specimens, thus proving that "recycling" in science can also be appropriately done through effective collaboration.

I am also grateful to the medical veterinarians Dr. Shabeer Bhoola for his help during injections of mole-rats at Terrace Road Veterinary Hospital (Johannesburg), and Dr. David Grant and Dr. Claire Havenga at the Rondebosch Veterinary Hospital (Cape Town), for their kindness and patience, and for enabling the X-rays of hundreds of mole-rat bones.

Several people from UCT also contributed in different ways to the accomplishment of this research. Tatiana Millard and Shakiera Sattar from the *Dept. of Molecular and Cell*

Biology (MCB – UCT), helped with staining procedures. Mrs Susan Cooper and Prof Dirk Lang from the *Confocal and light Microscope Imaging Facility* at the *Dept. of Human Biology,* were very kind and helpful during the process of imaging acquisition of bone fluorochromes. Prof. Nicola Illing and Keren Cooper assisted with the inspections of fluorescence microscopy at MCB.

I wish to also acknowledge that right at the beginning of this research, Dr. Charon de Villiers from the *South African Medical Research Council* (SAMRC - Cape Town) and Dr. Devin Finaughty from the *Dept. of Human Biology* (UCT), kindly gave me access to inspect of mole-rat habitats at SAMRC (Driftsands).

I am also grateful to Prof. Alejandra Echeverría from the *Universidad Nacional de Mar del Plata* (Argentina), who reviewed and discussed parts of this research (Chapter 3), and which considerably improved the quality of this study.

Dr. Rene Navarro is warmly thanked for guiding me through the "logics" of statistical and regression analysis. Also to Dr. Laura Wilson and Prof. Sue Hand for kindly receiving me at *University of New South Wales* (Australia) and for teaching me the use of software for allometric and ordination analyses. Dr. Sybrand van Sittert for helpful discussions on allometric analyses, and Prof. Kenneth D. Rose for his valuable comments on anatomical aspects of mammals.

The illustrators Joseph Trumpey, Jimmi Buscombe and Carmen Elisabeth are immensely thanked for giving me permission to use their beautiful artwork and material in this thesis (African mole-rats, wombat and pangolin, respectively, Fig. 1.1).

Thank you to my lab-mates in Prof. Anusuya's Paleolab: Emil, Matthew, Alberto, Carmen, Shafi, Iyra, Carla and Caitlin, as well as former colleagues Aurore, Debarati and Delphine, for their friendship and for our constant discussions on paleontology, evolution, morphology and science in general. It is in these instances when scientific consciousness and science grows. I am also grateful to the friends I have encountered along the path of this thesis, especially to Camilo López-Aguirre and Ottilie Katali, whom I wish all the best in this new year and future projects.

Thank you very much to my fellow Chileans Gonzalo Aguilar and Rene Navarro for their friendship, constant support and our eternal discussions trying to save this world during this "short" time (almost 7 years) of living in Cape Town.

Finally, I wish to express my heartfelt thanks to my family and friends, especially to my mom Isabel and brother Pablo for always supporting me during this, sometimes, unthinkable project. My grandma Fresia and my Aunties Paty and Licha, and Uncle Carlos for keeping the heart of the family alive. This work is for all of you. My partner Floriane for her tremendous support during this project and for her always stimulating and positive companionship during this journey. Brigitte Borgches, Matilda Smith and Paty Guevara thank you for always supporting and listening to me. Marietjie for your constant help and kindness. My friends that despite the distance, are always with me, Priscilla, Sergio and Miguel. Be strong my friends! Thanks to Halla, Eltahir and Anne for their beautiful friendship and help during my trip to Australia. You are a fantastic family! Thank you to all my friends have listened for more than four years to creepy stories of collecting, dissecting, burying, skeletonizing, measuring and analysing these fascinating underground creatures called mole-rats. I hope you also learned a bit about the unusual but extraordinary world and life of these "cuties".

I respectfully thank all the specimens used in this research, from which I am infinitely in debt.

This research would have not been possible without the initial support of my previous supervisors Prof. Karen Moreno (Universidad Austral de Chile), Prof. Guillermo D'Elia (Universidad Austral de Chile) and Prof. Sylvia Palma-Heldt (Universidad de Concepción).

This PhD Thesis was funded by the Government of Chile, CONICYT no. 72160463

Agradecimientos

Me gustaría expresar mi más sincero agradecimiento a mis supervisores, Anusuya Chinsamy-Turan y Marcelo Sánchez-Villagra, sin los cuales este trabajo no hubiera sido posible. Han sido un apoyo fundamental para realizar y finalizar con éxito el presente estudio, tanto al aceptarme como parte de sus grupos de investigación, como en ayudarme en la difícil tarea de brindar financiamiento para múltiples actividades incluyendo asistencia técnica, así como para cubrir gastos para conferencias locales e internacionales.

Estoy enormemente agradecido de todos los académicos que hicieron posible esta investigación, por confiar, colaborar y dedicar su valioso tiempo en este proyecto, específicamente seleccionando y brindando especímenes. Esto también fue posible gracias a sus asistentes que hicieron el tedioso trabajo de preparar las muestras. Entre estos investigadores, estoy muy agradecido de:

Prof. Nigel Bennett de la Universidad de Pretoria (UP - Sudáfrica), cuyo apoyo y amable contribución fueron fundamentales para realizar este trabajo, particularmente en lo que respecta a los experimentos de marcaje óseo llevados a cabo en su laboratorio.

Prof. Marietjie Oosthuizen y su esposo Albert Froneman, también de la UP, fue de valiosa ayuda durante este proyecto, específicamente con los procedimientos experimentales y otros aspectos logísticos de mi investigación durante todos los viajes a Pretoria. Muchas gracias Marietjie y Albert.

También deseo agradecer a los profesores Jenny Jarvis y Justin O'Riain de la Universidad de Ciudad del Cabo (UCT) por su ayuda en este estudio, así como también por darme siempre acceso a muestras de roedores.

Prof. Radim Šumbera de la Universidad de Bohemia del Sur (República Checa) por el constante apoyo, entusiasmo e interés por este proyecto, así como también a Honza (Jan) Okrouhlik y Matěj Lovy, quienes me ayudaron en varios aspectos de este estudio. Gracias a los miembros de su equipo que prepararon gran parte de los especímenes usados en esta tesis.

Prof. Christine Dengler-Crish de la Universidad Medica de Ohio del Noreste (Estados Unidos) por su entusiasmo para colaborar en este estudio, y a su asistente de investigación Katie Eckman.

Profesor Tim Clutton-Brock de la Universidad de Cambridge (Reino Unido), que amablemente dio acceso a muestras de ratas topo, así como a los miembros involucrados en el Proyecto Kalahari Meerkat que me ayudaron durante mi visita a la estación de Kuruman: Dave Gaynor, Tanja van de Ven, Jacob Brown, Carlijn Brands y Philippe Vullioud.

La profesora Sabine Begall de la Universität Duisburg-Essen (Alemania), que amablemente me dio acceso a muestras de ratas topo.

Y finalmente a mi co-supervisor Prof. Marcelo Sánchez-Villagra de la Universidad de Zurich (Suiza) y a los miembros de su equipo, Alexandra Wegmann y Heike Götzmann, que ayudaron en diversos aspectos de esta tesis.

Aquellos investigadores hicieron posible realizar este trabajo multidisciplinario, sin la necesidad de realizar nuevas recolecciones de campo y/o muertes excesivas de especímenes silvestres, así demostrando que el "reciclaje" en ciencia también es posible mediante la colaboración efectiva.

También estoy agradecido de los médicos veterinarios Dr. Shabeer Bhoola por su ayuda durante las inyecciones de ratas topo en el Terrace Road Veterinary Hospital (Johannesburgo), y al Dr. David Grant y a la Dra. Claire Havenga del Rondebosch Veterinary Hospital (Ciudad del Cabo), por su amabilidad y paciencia, y por permitir radiografiar cientos de huesos de rata topo.

Varios miembros de la UCT también contribuyeron de distintas maneras a la realización de esta investigación. Tatiana Millard y Shakiera Sattar del Departamento de Biología Celular y Molecular (MCB), ayudaron con la preparación de marcadores óseos. La Sra. Susan Cooper y el Prof. Dirk Lang del Centro de Imágenes de Microscopio Confocal y de Luz en el Departamento de Biología Humana, fueron muy amables durante el proceso de adquisición de imágenes de los fluorocromos. Prof. Nicola Illing y Keren Cooper también ayudaron con las observaciones de microscopía de fluorescencia iniciales en MCB.

También deseo reconocer la ayuda ofrecida al comienzo de esta investigación por la Dra. Charon de Villiers del Consejo de Investigación Médica de Sudáfrica (SAMRC - Ciudad del Cabo) y el Dr. Devin Finaughty del Departamento de Biología Humana (UCT), quienes amablemente dieron acceso a las instalaciones de SAMRC (Driftsands) para inspeccionar los hábitats de ratas topo.

También estoy agradecido a la Prof. Alejandra Echeverría de la Universidad Nacional de Mar del Plata (Argentina), quien revisó y discutió una parte importante de esta investigación (Capítulo 3), lo cual que mejoró considerablemente la calidad de este estudio.

Se agradece calurosamente al Dr. René Navarro por gentilmente guiarme a través de las "lógicas" del análisis estadístico y de regresión. También a la Dra. Laura Wilson y la Prof. Sue Hand por recibirme amablemente en la Universidad de Nueva Gales del Sur (Australia) y por guiarme en el uso de software para análisis alométricos y de ordenación. Al Dr. Sybrand van Sittert por las útiles discusiones sobre análisis alométrico, y al Prof. Kenneth D. Rose por sus valiosos comentarios sobre aspectos de anatomía de mamíferos.

Los ilustradores Joseph Trumpey, Jimmi Buscombe y Carmen Elisabeth son inmensamente agradecidos por darme permiso para utilizar sus hermosas obras de arte en esta tesis (ratas topo Africanas, wombat y pangolín, respectivamente, Fig. 1.1).

Gracias a mis compañeros de laboratorio en el Paleolab de la Prof. Anusuya Chinsamy: Emil, Matthew, Alberto, Carmen, Shafi, Iyra, Carla y Caitlin, así como también a los colegas anteriores Aurore, Debarati y Delphine, por su amistad y por nuestras constantes discusiones sobre paleontología, evolución, morfología y ciencia en general. Es en estas instancias cuando la conciencia científica y la ciencia crecen. También agradezco a todas las valiosas personas que me he encontrado en el camino de esta tesis, en especial a Camilo López-Aguirre y Ottilie Katali, a quienes les deseo todo lo mejor en este nuevo año y futuros proyectos.

Muchas gracias a mis compatriotas Gonzalo Aguilar y René Navarro por su amistad, apoyo constante y nuestras eternas discusiones tratando de salvar este mundo durante este "corto" tiempo (casi 7 años) viviendo en Ciudad del Cabo.

Finalmente, deseo expresar mi más sincero agradecimiento a mi familia y amigos, especialmente a mi mamá Isabel y mi hermano Pablo por apoyarme siempre en este proyecto, a veces impensable. A mi abuela Fresia y a mis tías Paty y Licha, y al tío Carlos por mantener vivo el corazón de la familia. Este trabajo es para todos ustedes. A mi compañera Floriane por su tremendo apoyo durante este proyecto y por su siempre estimulante y positivo compañerismo durante este viaje. Brigitte Borgches, Matilda Smith y Paty Guevara gracias por apoyarme y escucharme siempre. Marietjie por tu constante ayuda y amabilidad. Mis amigos que a pesar de la distancia, siempre están conmigo, Priscilla, Sergio y Miguel. ¡Sean fuertes amigos! Gracias a Halla, Eltahir y Anne por su hermosa amistad y ayuda durante mi viaje a Australia. ¡Son una familia fantástica! Gracias a todos mis amigos que han escuchado durante más de cuatro años las espeluznantes historias de recolectar, diseccionar, enterrar, esqueletonizar, medir y analizar estas fascinantes criaturas subterráneas llamadas ratas topo. Espero que también hayan aprendido un poco sobre el inusual pero extraordinario mundo y vida de estas "bellezas".

Agradezco respetuosamente a todos los ejemplares utilizados en esta investigación, de la que estoy infinitamente endeudado.

Esta investigación no hubiese sido posible sin el apoyo inicial de mis anteriores supervisores Prof. Karen Moreno (Universidad Austral de Chile), Prof. Guillermo D'Elía (Universidad Austral de Chile) y Prof. Sylvia Palma-Heldt (Universidad de Concepción).

Esta Tesis Doctoral fue financiada por el Gobierno de Chile, CONICYT no. 72160463

Functional Anatomy, Osteogenesis and Bone Microstructure of the Appendicular System of African Mole-Rats (Rodentia: Ctenohystrica: Bathyergidae)

Germán Andrés Montoya-Sanhueza
MSc Zoology

ABSTRACT

In comparison to their ecophysiological and behavioral aspects, the skeletal system of African mole-rats (Bathyergidae) has been relatively understudied. Only a few studies have assessed their skeletal system, but these have mostly focused on their cranial and dental systems, with little attention on their postcranial skeleton. This PhD thesis provides a considerable amount of information about the functional anatomy, morphological diversity and postnatal bone morphogenesis of the appendicular system of these subterranean mammals.

African mole-rats are small mammals highly adapted to the hypogeous niche that feed on underground roots and tubers. They forage, mate, breed and to some extent even disperse underground. For this, they build extensive burrow systems primarily with their chisel-like teeth, but also using their forelimbs for scratch-digging. One of the most exceptional features of bathyergids is their wide spectrum of social organization, which is unique among mammals and ranges from solitary, social and eusocial. Here, the eusocial naked mole-rat, *Heterocephalus glaber*, has been the most studied species. The physiology of African mole-rats is also exceptional among rodents and other mammals, showing low metabolic rates and body temperatures, as well as slow somatic growth rates. They also show enhanced fitness and prolonged longevity, features that have been associated to a life protected from both climatic extremes and predation, as well as to intergenerational transfer of information, communal care of young and shared foraging endeavors in social species. For these reasons, bathyergids represent a unique animal model to explore their skeletal adaptations to fossoriality and life underground. The aim of this research was to assess the patterns of bone growth and development to understand how adults attain their final phenotype.

A comprehensive sample (N = 506) of all six bathyergid genera including seven species and comprising individuals of both sexes and of different ontogenetic stages was studied. Stylopodial (humerus and femur) and zeugopodial (ulna and tibia-fibula) bones (n = 1133) were analyzed using multiple quantitative analyses of variance (ANOVA, MANOVA), ordination (PCA, DA) and regression (RMA, OLS, equality of slopes), as well as bone labeling techniques and detailed qualitative descriptions of their midshaft bone histology.

Chapter 3 shows that the specialized phenotype of the only scratch-digger bathyergid *Bathyergus suillus* underwent considerable morphological changes during ontogeny, e.g. juveniles showed externally more robust bones with thin cortical walls, whereas adults presented slender bones with significantly thicker cross-sections. Such changes are probably related to the increased digging demands and agonistic behaviors of the developing young. However, other aspects of their anatomy expressed perinatally, such as greater external epicondylar robustness, well-developed olecranon, teres major and deltoid processes, suggest a major role of genetic factors in their development. This chapter applied for first time the conceptualization of developmental modules to long bones, and showed that the periosteal module had higher variability and tended to grow faster than the endochondral module.

Chapter 4 analyzed the morphological diversity within Bathyergidae using comparative anatomy and morpho-functional indices and showed that most species shared a highly specialized fossorial morphology and that only the naked mole-rats were morphologically divergent (having a simplified phenotype), resembling the condition of non-fossorial closest relatives of the Bathyergidae. Nevertheless, the novel inclusion of three ecomorphological categories (solitary scratch-diggers, solitary chisel-tooth diggers and social chisel-tooth diggers) in this study, showed significant differences among the groups. In general, social species appeared to have a phenotype more specialized to

increase digging ability and locomotor performance, whereas solitary species showed a relatively less specialized fossorial phenotype, and a diminished locomotor ability. This may contribute to foraging strategies in social species which are known to have more complex and relatively longer burrow systems as compared to solitary species.

Chapter 5 assesses the ossification patterns of the endochondral and periosteal modules, and shows that in general most bathyergids have relatively similar endochondral growth rates, irrespective of social behavior or digging strategy, although the periosteal module showed relatively higher growth rates and a higher degree of variation as compared to the endochondral module, thus appearing to be considerably less dependent on body size and genetic factors. Naked mole-rats showed the lowest growth rates among bathyergids. Considering the basal phylogenetic position of *H. glaber* within the family, a neotenic condition is suggested for this species, and suggests accelerated bone growth rates for the evolution of the other bathyergids.

Chapter 6 provides a comprehensive description of the pattern of bone modelling in bathyergids and includes an assessment of their bone dynamics using fluorochrome labeling. All bathyergids analyzed showed increased cortical bone thickening during ontogeny, as well as low rates of endosteal bone resorption. Also, all species showed high histodiversity, limited remodeling (i.e. development of secondary osteons) and they do not ever develop Haversian bone tissues.

This thesis concludes that the combination of social strategy and type of excavation had an impact on the evolution of the bathyergid appendicular system. On one hand, it was evidenced that the development of fore- and hindlimbs are not constrained by intrinsic factors (as suggested for other mammals), and that the limbs develop at similar growth rates, resulting in relatively symmetrical limb proportions. This is suggested to improve locomotion within burrows and represents an adaptation to the subterranean lifestyle, which is also observed in other fossorial mammals. This thesis further discusses how environmental factors and specific behaviors and locomotor modes, may represent strong selective pressures on limb adaptation and evolution. Similarly, a proximo-distal pattern of variation was observed, where zeugopodial elements were more variable than stylopodial elements, probably because they are in direct interaction with the substrate, so they can evolve morphological adaptations for particular habitats and locomotor behaviors. Importantly, these adaptations are most likely mediated by heterochronic modifications of their ossification modules, especially intramembranous ossification, which is known to be more responsive to environmental factors, whilst the endochondral modules would be more conservative, perhaps because a stronger genetic regulation in postnatal life. Further research on long bone modules is necessary to understand the specificity of such changes.

Despite the comparatively simplified phenotype of *H. glaber,* they showed a larger morphospace as compared to other bathyergids, indicating a wider intraspecific variability. This agrees with previous observations suggesting skeletal plasticity for this species. It is suggested that living in large colonies results in diminished selective pressures for limb specialization but has an impact on increasing trait variability within members of the colony.

This study showed that the integration of multiscale techniques and multivariate analysis of combined skeletal phenotypes (i.e. forelimb + hindlimb) offer a better understanding of adaptations to the hypogeous environment. The findings of this study also highlight the importance of considering developmental modularity of long bones for assessment of bone adaptations, particularly for understanding the differential effects of intrinsic and extrinsic factors regulating endochondral and intramembranous ossification.

Contents

CHAPTER 1

Background

"Africa has produced many mammal curiosities, and the Bathyergidae take a high rank among these"

John Reeves Ellerman, 1956
(THE SUBTERRANEAN MAMMALS OF THE WORLD, p. 13)

1.1 INTRODUCTION

This thesis is composed of seven chapters. The first chapter (Ch. 1) provides a general background to the areas of study, including the rationale, aims, objectives and hypotheses. A second chapter (Ch. 2) is presented to include the materials and specimens used in this work, as well as to describe the general methods used to prepare the material. Four research chapters (Chapters 3-6), each of them representing a self-contained study, contain the analyses of this thesis. Three of them (Chapters 3-5) include quantitative analyses comprising a large amount of morphometric data, while the last one (Ch. 6) is principally qualitative. A final chapter (Ch. 7) includes a general discussion, concluding remarks and future directions.

1.1.1 The Hypogeous Environment, Subterranean Mammals and Fossoriality

The hypogeous (below-ground) niche comprises a unique set of physico-chemical conditions, such as i) low oxygen (hypoxia), ii) high carbon dioxide (CO_2) levels (hypercapnia), iii) high relative humidity, iv) little or no exposure to sunlight and v) a substrate that is energetically costly to burrow through (Nevo 1979, 1999; Bennett et al., 1988; Sherman et al, 1991; Bennett & Faulkes, 2000; Lacey *et al.*, 2000, McNab, 2002; Begall *et al.*, 2007; Burda *et al.*, 2007; Holtze *et al.,* 2018). These conditions make hypogeous environments considerably different to the epigeous (above-ground) niche, and impose a suite of challenges to the ecophysiology of organisms. For example, food and mate availability diminish significantly underground. However, the hypogeous niche also represents a relatively stable environment with a buffered thermic range in comparison to the surface, as well as provides shelter from predators and from extreme climatic fluctuations (Begall *et al.*, 2007; Burda *et al.*, 2007). These represent clear advantages for animals, and its preference over above-ground niches is reflected in the high biodiversity of extant mammals that successfully exploited this niche not only in the present but also during the Cenozoic (e.g. Hildebrand, 1985; Nevo, 1999; Busch *et al.*, 2000; Kley &

Kearney, 2007; Lessa *et al.*, 2008). Even the early evolution of non-mammalian therapsids during the Permo-Triassic transition (Botha & Chinsamy, 2004; Ray & Chinsamy, 2004), as well as the later rise of stem mammalian lineages during the Jurassic (Luo & Wible, 2005; Luo *et al.*, 2015), exhibit a rich fossil record associated with the hypogeous niche.

Mammals that use the hypogeous niche are usually defined as subterranean or fossorial (e.g. Nevo & Reig, 1990; Sherman *et al.*, 1991; Bennett & Faulkes, 2000; Lacey *et al.*, 2000; Begall *et al.*, 2007; Šumbera, 2019). However, these concepts are not equivalent and they involve different aspects of the biology of the species. Subterranean mammals live in burrows and conduct most of their life activities, including foraging and reproduction belowground, so they rarely explore the aboveground realm (Lacey *et al.*, 2000). This definition accounts for a more ecological aspect of the animal, and its study is oriented to understand how these organisms interact and adapt to the hypogeous environment. This definition also implies that these animals construct their own burrow systems, which vary in terms of dimensions and complexity, in the mechanisms used to build them, and in the level of cooperative or solitary work needed to build them, all of which will have a direct impact on the amount of energy spent building them (e.g. Nevo, 1999).

On the other hand, fossorial mammals are species that exhibit morphological specializations to build burrows, but spend considerable portions of their lives aboveground, either foraging and/or mating (e.g. Hildebrand, 1985; Lacey et al., 2000). This term represents a more functional explanation, since it focuses on the organism's ability to dig and hence it assesses the direct interaction between an organism's structural design and its digging behavior (e.g. Hildebrand, 1985). Nonetheless, this definition usually does not explain how the organism uses burrows or even for what purposes they dig. Because there are intermediate forms between digging and non-digging animals, some authors have also used the term semi-fossorial (e.g. Kinlaw, 1999; Pérez *et al.*, 2017), and also burrowing mammals (e.g. Goldstein, 1972; Reichman & Smith, 1990; Reichman & Seabloom, 2002; Hopkins & Davis, 2009). This latter term rather points to the capacity of animals to construct burrows, and actually not all fossorial mammals build their own burrows, e.g. ant eaters and pangolins generally do not build burrows but have very specialized forelimbs (Fig. 1.1) to dig out insects during foraging (Vizcaino *et al.*, 1999). Furthermore, the fossorial term has been widely used in ecomorphological studies to mainly assess the relationship between morphology (form and shape) and function, as well as to infer the paleobiology of extinct species through analyses of their skeletons (Reed, 1954; Hildebrand, 1985; Vizcaíno *et al.* 1999, 2016; Szalay & Sargis, 2001; White *et al.*, 2006; Pérez *et al.*, 2017).

Consequently, the subterranean definition represents a multidimensional aspect of life underground, since it involves the ecophysiological adaptations of the organism, as well as the different morphological and digging mechanisms utilized (level of fossoriality). In this study, both terms are used depending on the taxa and their particular lifestyle. The term semi-fossorial is avoided since it may include a wide spectrum of digging strategies within a continuum between fossorial and non-fossorial organisms. Examples of subterranean mammals are the marsupial mole (Notoryctidae), golden moles (Chrysochloridae), true moles (Talpidae), and

several rodent families like zokors (Myospalacinae), Middle East blind molerats (Spalacinae), Asian bamboo rats (Rhizomyinae) and African mole-rats (Bathyergidae) (Hildebrand, 1985, Nevo 1999; Lacey *et al.*, 2000). Figure 1.1 illustrates some of these taxa. Examples of fossorial mammals are the platypus (Ornithorhynchidae), wombats (Vombatidae), armadillos (Dasypodidae), badgers (Mustelidae), porcupines (Hystricidae), springhares (Pedetidae) and rabbits (Lagomorpha) (Hildebrand, 1985). One aspect present in several subterranean mammalian lineages is their highly reduced visual organs, although this feature should not be considered as a character to differentiate subterranean from fossorial mammals. In this work, different terrestrial species that live aboveground and have distinct locomotor mode such as ambulatory, cursorial or bipedal, are termed as surface-dwelling mammals (e.g. Šumbera, 2019).

1.1.2 African Mole-Rats (Phiomorpha, Bathyergidae)

African mole-rats (AMs) (Bathyergidae) are hystricognath rodents highly adapted to the hypogeous niche. They forage, mate, breed and to some extent even disperse underground (Bennett *et al.*, 1991; Seeman *et al.*, 1991; Bennett & Faulkes, 2000; Begall *et al.*, 2007). These features differentiate them from other rodents that despite having highly adapted fossorial features, they show a less specialized subterranean lifestyle (e.g. Lacey *et al.*, 2000). They are endemic to the sub-Saharan African region and represent one of the most speciose groups of subterranean rodents comprising six genera and ±20 species (IUCN, 2020), grouped within a monophyletic lineage, the Phiomorpha (plus Thryonomyidae and Petromuridae) (Lavocat, 1978; Jarvis & Bennett, 1990; Faulkes *et al.*, 2004; Van Daele *et al.*, 2007; Upham & Patterson, 2015). Figure 1.2 shows the six extant genera (*Heterocephalus, Heliophobius, Fukomys*, *Cryptomys, Georychus* and *Bathyergus*), as well as their phylogenetic relationships. As with many other mammals, the fossil record of Bathyergidae appears to be more widely distributed and diversified than they are today. They have the second oldest fossil history among subterranean rodents and one of the longest records of generic stability during their first 14 million years of history (Cook *et al.*, 2000). Molecular data suggest that extant genera such as *Heterocephalus* had the earliest divergence times dated to the early Oligocene (31.2 Ma), just when the main four caviomorph superfamilies (Erethizonoidea and Cavioidea at 32.4 Mya, Chinchilloidea and Octodontoidea at 32.8 Mya) appeared in South America (Patterson & Upham, 2014; Upham & Patterson, 2015). The oldest bathyergid skulls known in the fossil record (Lavocat, 1973; Mein & Pickford 2008) are more similar to those of *Heterocephalus* and *Heliophobius*, both of which belong to ancient lineages (Faulkes *et al.*, 2004; Van Daele *et al.*, 2007; Patterson & Upham 2014). The oldest fossil representatives of the Bathyergoidea lineage (all extinct genera), occur in the early Miocene deposits of Namibia (*Bathyergoides* and *Geofossor*) and eastern Africa (*Bathyergoides*, *Geofossor*, and *Proheliophobius*) (Jarvis & Bennett, 1990; Cook *et al.* 2000; Winkler *et al.* 2010; and references therein). All these fossils share several cranial features associated with fossorial specializations such as procumbent (pick-like) incisors used for excavation (Lavocat, 1978; Jarvis & Bennett, 1990).

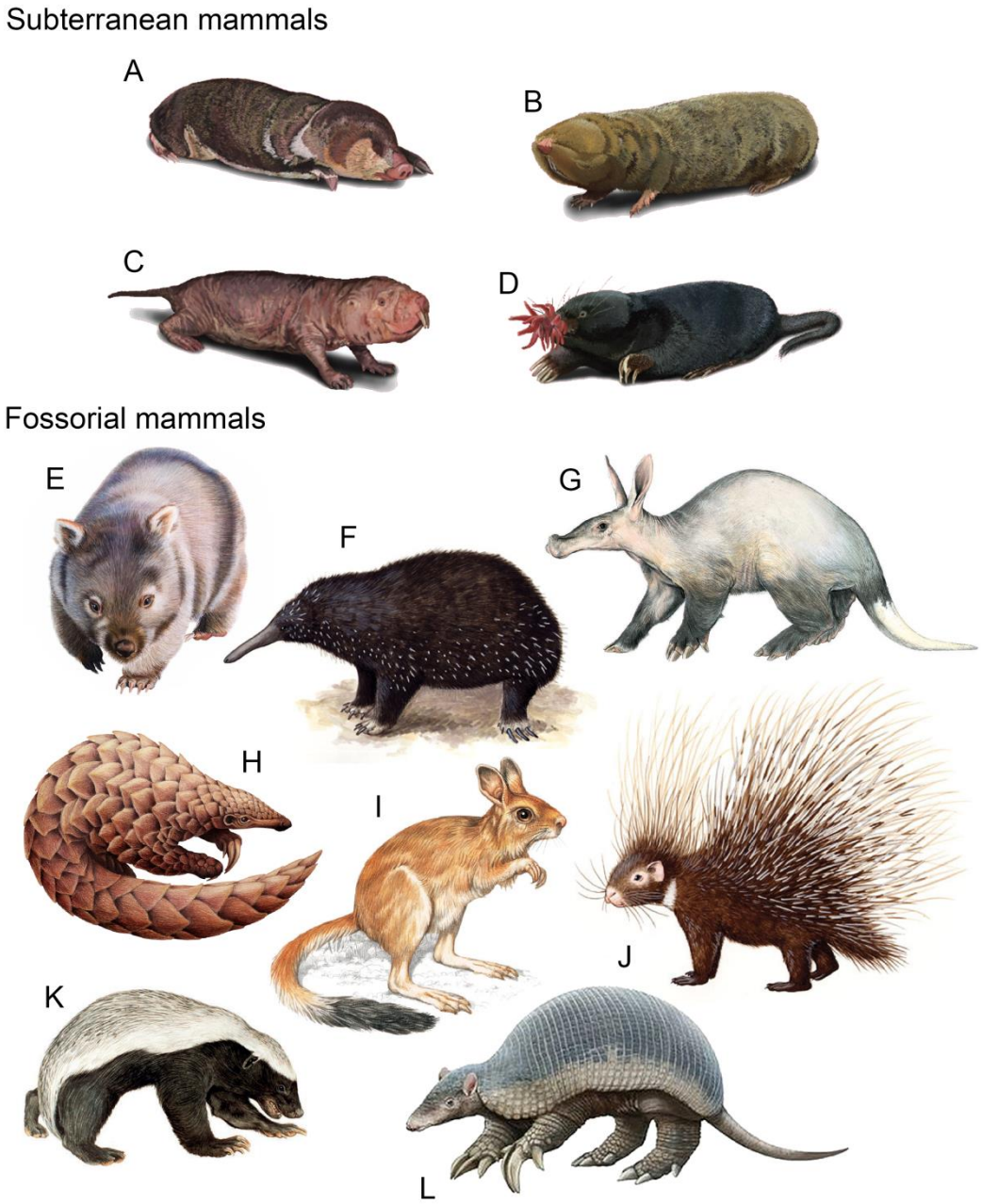

FIGURE 1.1. Subterranean (A-D) and fossorial (E-L) mammals. A) Cape golden mole (*Chrysochloris asiatica*). B) Blind molerat (*Nannospalax galili*). C) Naked mole-rat (*Heterocephalus glaber*). D) Star-nosed mole (*Condylura cristata*) [A-D, illustrations by Michelle Leveille, extracted from Partha *et al.* (2017)]. E) Common wombat (*Vombatus ursinus*) (Illustrated by Jimmi Buscombe). F) Long-beaked echidna (*Zaglossus*). G) Aardvark (*Orycteropus afer*) (Extracted and modified from Kingdom *et al.*, 2013). H) Giant pangolin (*Manis gigantea*) (Illustrated by Carmen Elisabeth). I) Springhare (*Pedetes capensis*) (Extracted and modified from Skinner & Chimimba, 2005). J) Cape porcupine (*Hystrix africaeaustralis*). K) Honey badger or ratel (*Mellivora capensis*) (Extracted and modified from Kingdon & Hoffmann, 2013). L) Giant armadillo (*Priodontes maximus*) (National Geographic). F and J extracted from www.animaldiversity.org. Illustrations not at scale.

The first fossils of extant bathyergids correspond to one species of *Heterocephalus* and have been found in Plio-Pleistocene fossil beds of the north of Tanzania in the Lower Laetolil Beds (3.85–4.4 Ma) (Denys, 2011). Recently,

Patterson & Upham (2014) proposed a distinct family for naked mole-rats (*H. glaber*) due to their earlier and "independent" evolution from the rest of AMs. This taxonomic re-arrangement poses questions for the evolution and interrelationships of fossil and extant AMs, but does not change their monophyletic condition (e.g. Faulkes *et al.* 2004) or their historical ecological relationship with the hypogeous niche. For this reason, throughout this manuscript, the traditional –and more parsimonious– taxonomic view of AMs as a single family including naked mole-rats (*H. glaber*) is maintained (Lavocat, 1978; De Graaff, 1981; Honeycutt *et al.*, 1991; Jarvis & Bennett, 1990). The fact that all extinct members of this group have apparently maintained fossorial adaptations indicates that they have a remarkable hypogeous evolutionary history, probably maintained due to the low metabolic rates and speciation rates suggested for subterranean rodents in comparison to surface-dwelling relatives (e.g. Martin & Palumbi, 1993; Churakov *et al.* 2010; Spradling *et al.* 2011). Since bathyergids show the widest variety of social systems among mammals, such evolutionary scenario also raises the question of the social status of the ancestor of all AMs (Bennett & Faulkes, 2000). The latter is beyond the scope of this study, but it is anticipated that the study of their postcranial anatomy can contribute to understanding the evolution of certain traits related to the origin of their sociality and fossoriality.

1.1.3 Skeletal Adaptations in African Mole-Rats: An Overview

Among mammals, one of the most exceptional features of AMs is their wide spectrum of social organizations, which ranges from solitary, social and eusocial (Jarvis, 1981, 2003, 2013; Jarvis & Bennett, 1991; Burda *et al.,* 2000). However, they also show different strategies for building burrows: all genera are primarily chisel-tooth diggers, so they use their continuously growing extra-buccal and highly procumbent incisors to excavate tunnels (Genelly, 1965; Jarvis & Sale, 1971; Berkovitz & Faulkes, 2001), while only *Bathyergus* is a scratch-digger, and uses primarily its forelimbs with long claws for tunnel excavation (Bennett *et al.*, 2009). In this sense, all genera except *Bathyergus* have exceptionally very short claws in their feet (Fig. 1.3), and only *H. glaber* shows extremely reduced claws (Fig. 1.3, 1.4). Figure 1.4 shows some extremes in morphology and life history traits among bathyergids: *B. suillus,* which is solitary and the largest species having the shortest lifespan (6-12? years, pers. comm., J. Jarvis, 2016), while *H. glaber* is eusocial and the smallest taxon (~35 g), but having the longest lifespan (~30 years) among the family (Dammann & Burda, 2007).

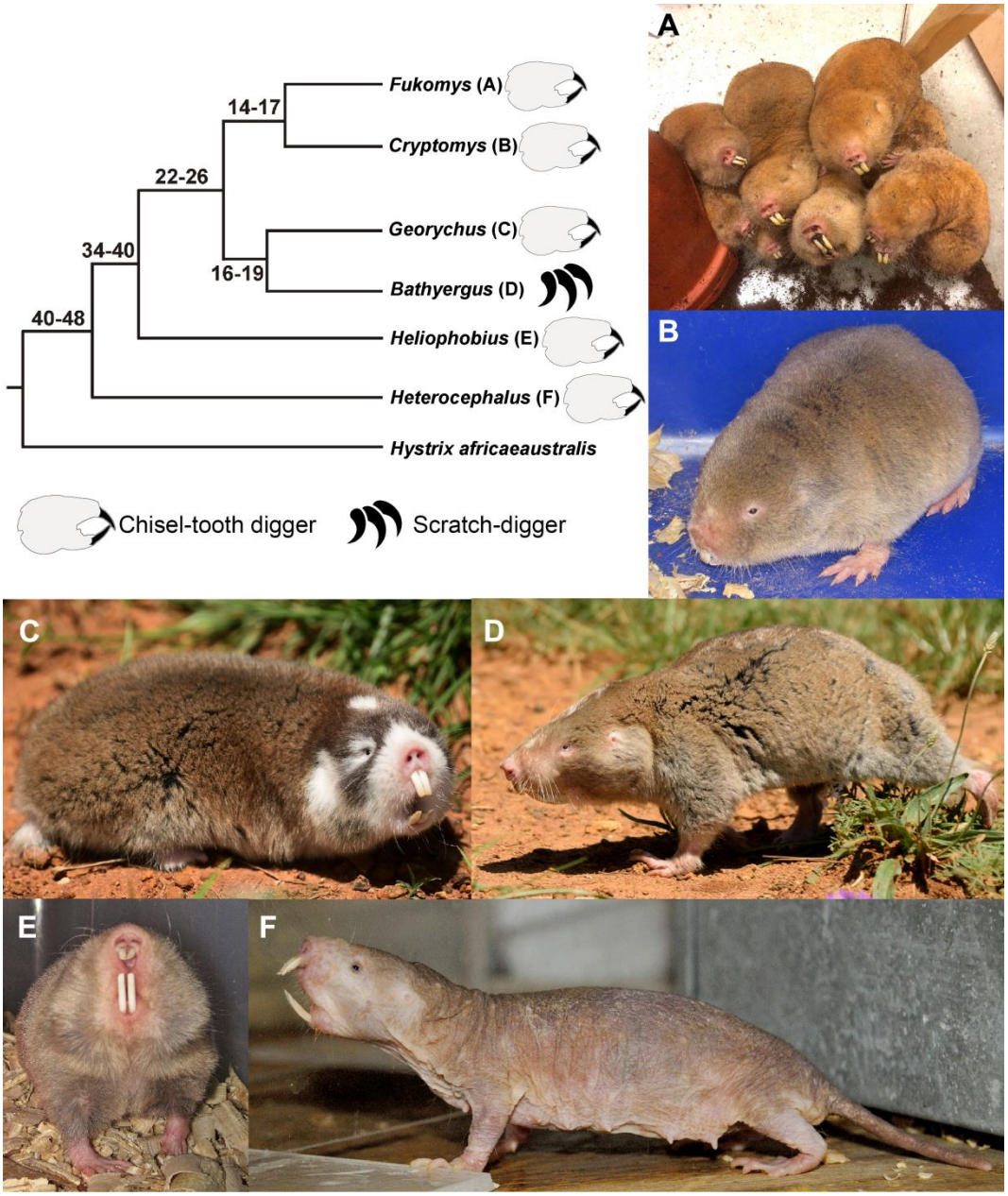

FIGURE 1.2. Phylogenetic relationships among African mole-rats and their six extant genera. The cladogram shows the phylogenetic relationships of African mole-rat species and one outgroup species, the Cape porcupine (*Hystrix africaeaustralis*). A) Mechow's mole-rat (*Fukomys mechowii*). B) Mahali's mole-rat (*Cryptomys hottentotus mahali*). C) Cape mole-rat (*Georychus capensis*). D) Cape dune mole-rat (*Bathyergus suillus*). E) Silvery mole-rat (*Heliophobius argenteocinereus*). F) Naked mole-rat (*Heterocephalus glaber*). Cladogram extracted and modified from Seney *et al.* (2009), but see more details in Faulkes *et al.* (2004). Images are not at scale. Photographs by Germán Montoya-Sanhueza.

FIGURE 1.3. Morphological adaptations of the forefeet of African mole-rats, including scratch-diggers and chisel-tooth diggers. A) Cape dune mole-rat (*Bathyergus suillus*). B) Cape mole-rat (*Georychus capensis*). C) Silvery mole-rat (*Heliophobius argenteocinereus*). D) Mechow's mole-rat (*Fukomys mechowii*). E). Mahali's mole-rat (*Cryptomys hottentotus mahali*). D) Naked mole-rat (*Heterocephalus glaber*). See Figure 1.2 for legend. Images are not at scale. Photographs by Germán Montoya-Sanhueza.

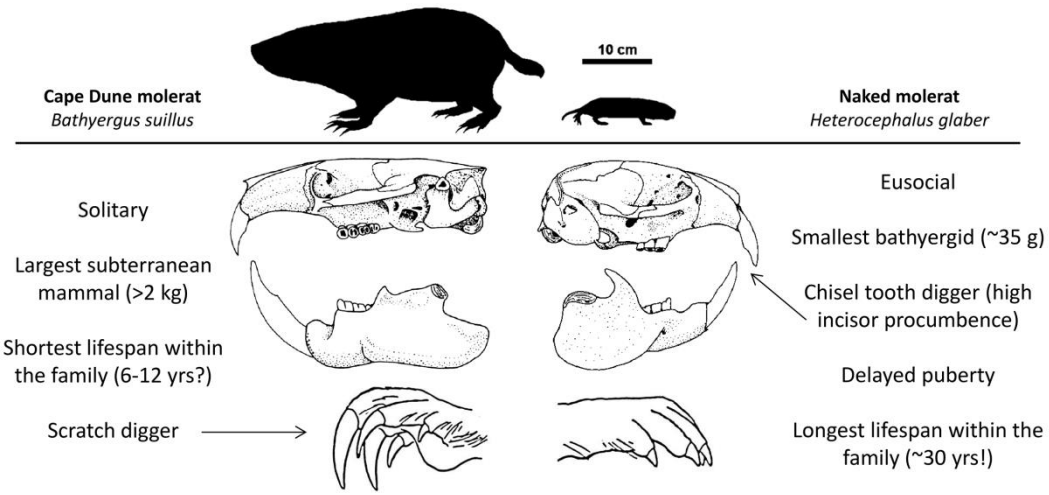

FIGURE 1.4. Most conspicuous morphological and ecological features of two contrasting fossorial types among African mole-rats: *Bathyergus suillus* (left) and *Heterocephalus glaber* (right). Skull and hand illustrations extracted and modified from Happold (2013) and Stein (2000).

As a result of these extraordinary behavioral and life history traits, bathyergids have been subject to a wide range of studies, especially in terms of their social behavior, activity patterns, energetics, ecology, mineral metabolism,

reproductive physiology, endocrinology, sensory function, genomics, and most recently, biomedical and aging studies (e.g., Buffenstein and Yahav, 1991; Buffenstein *et al.*, 1994; Bennett, 2009; Faulkes and Bennett, 2009; Buffenstein and Pinto, 2009; Pinto *et al.*, 2010; Boyles *et al.*, 2011; Edrey *et al.*, 2011; Tian *et al.*, 2013; Fang *et al.*, 2014; Stathopoulos *et al.*, 2014; Davies *et al.*, 2015; Omerbasic *et al.*, 2016; Park *et al.*, 2017; Retief *et al.*, 2017; Skulachev *et al.*, 2017; Ruby *et al.*, 2018; Šumbera, 2019). These studies highlight the distinctiveness of their physiology when compared to other mammals, such as low metabolism, extended longevity, non-dependent vitamin D mineral metabolism, resistance to anoxia and cancer, absence of pain sensitization and delayed puberty (see references above). Surprisingly, little is known about their skeletal system, particularly pertaining to its development and evolution. Only few studies have reported the general somatic growth trends of bathyergid populations (e.g. Bennett *et al.*, 1991; Bennett & Aguilar, 1995; Scharff *et al.* 1999). Because most AMs are chisel-tooth diggers, their craniodental adaptations have also received considerably more attention as compared to their postcranial anatomy (e.g., Barčiová *et al.*, 2009; Van Daele *et al.*, 2009; Cox & Faulkes, 2014; Gomes Rodrigues & Šumbera, 2015; Gomes Rodrigues *et al.*, 2015; Mason *et al.*, 2016; McIntosh & Cox, 2016a, b; Van Wassenbergh *et al.*, 2017). Furthermore, the postcranial system of scratch-digging species is also mentioned only in more general comparative studies of adults (e.g., Hildebrand, 1978, 1985; Stein, 2000; Samuels & Van Valkenburg, 2008; Prochel *et al.*, 2014), and the postcranial system of social species is practically not mentioned. Some key studies on their skeletal system are briefly summarized here.

Lumbar elongation. One of the most striking features of the skeletal system of bathyergids is based on observations made on naked mole-rat queens (i.e. reproductive females), which are physically distinct from non-reproductive members of the colony, i.e. queens have significantly longer lumbar vertebrae for their body size compared to all other colony members (Jarvis *et al.*, 1991; O'Riain *et al.*, 2000; Dengler-Crish & Catania, 2007, 2009; Henry *et al.*, 2007). This phenomenon resembles the puberty-like "growth spurt" typically observed in humans and other mammals once sexual maturity has occurred (usually coinciding with skeletal maturity), but it differs from them in that a net gain in lumbar bone length is achieved long after skeletal maturity and throughout each breeding cycle to accommodate large litters (Henry *et al.*, 2007). Similar trends of intra-colony morphological divergence have been found in the social Damaraland mole-rat (*Fukomys damarensis*) (Young & Bennett, 2010; Thorley *et al.*, 2018), as well as in a cooperative carnivore, the meerkat (*Suricata suricatta*) (Russell *et al.*, 2004), but apparently not in solitary AMs (see Montoya-Sanhueza *et al.*, 2019). This suggests that sex steroids related to pregnancy may have an important role in bone growth and body size in social AMs (Henry *et al.*, 2007), and also that this phenomenon may be more widespread among female vertebrates than previously thought (Russell *et al.*, 2004).

Dental replacement. The solitary silvery mole-rat *Heliophobius argenteocinereus* has recently been reported to show continuous dental replacement, i.e. its dentition is constantly replaced by supernumerary teeth moving secondarily towards the front of the jaw (Gomes Rodrigues *et al.*, 2011). This, in combination with the progressive eruption of high-crowned teeth of this

and other AMs, it constitutes an exceptional adaptation among rodents, most likely related to enhance hyper-chisel-tooth digging, which usually involves high dental wear (Gomes Rodrigues *et al.*, 2011).

Reduced osteopenia. Another recent discovery of the bathyergid musculoskeletal system is their reduced bone loss (osteopenia), as well as the maintenance of lean muscle mass throughout ontogeny (Pinto *et al.*, 2010; O'Connor *et al.*, 2002; Montoya-Sanhueza, 2014; Montoya-Sanhueza & Chinsamy, 2017, 2018). This results in individuals having long bones with thick cortical walls and differing from most surface-dwelling mammals, which naturally undergo osteopenia with aging (e.g. Duque & Watanabe, 2011). The initial study of Pinto *et al.* (2010) on naked mole-rats focused on the elucidation of the mechanisms facilitating sustained bone structure and strength in hypogonadic subordinates, and yielded important cues about the bone development of mammal species with delayed puberty (Buffenstein *et al.*, 2012). Naked mole-rat queens can suppress the reproductive expression of subordinates (for as long as 10 years in some cases) by her aggressive social behavior (Sherman *et al.*, 1991). Pinto *et al.* (2010) showed that male and female subordinates have similar femoral phenotype in comparison to queens, which show greater femoral diameter, femoral cortical area and thickness, as well as elongated vertebrae (see references above). These major morphological changes observed of queens are related with the attainment of sexual maturity and pregnancy, and also points to the relevance of hormones regulating late postnatal bone development to reach the "reproductive adult phenotype" (e.g. Dengler-Crish & Catania, 2007, 2009). In the solitary Cape dune mole-rat, *Bathyergus suillus*, a systemic thickening of their long bones occurs mainly due to periosteal and endosteal bone formation as well as reduced endosteal bone resorption (Montoya-Sanhueza & Chinsamy, 2017). This positively imbalanced bone modeling occurs in long bones with thick cortical walls and therefore high levels of bone quality are maintained throughout ontogeny, most probably to ensure the maintenance of skeletal function and performance during digging activities, as also suggested for *H. glaber* (Pinto *et al.*, 2010; Montoya-Sanhueza & Chinsamy, 2017, 2018).

Bone resorption and secondary reconstruction typically occurring in the bone structure of reproductive mammalian females (e.g. Purdie *et al.*, 1988), have also been observed in *B. suillus* (Montoya-Sanhueza & Chinsamy, 2018), and only briefly noted for queen naked mole-rats (Pinto *et al.*, 2010).

These characteristics evidence the peculiarities of the musculoskeletal system of AMs, which are probably adaptations to the challenges of their subterranean lifestyle, but also related their complex social systems. These raise several questions about how intrinsic (genetic), environmental (e.g., ecological, biomechanical, geographical) and/or its combination (epigenetic) regulate skeletal specializations in social and solitary species. These specializations also indicate that despite their long evolutionary history and apparently conserved and convergent phenotype, their skeletons have undergone unique physiological and molecular developmental pathways, which were not appropriately considered before, probably because of the obvious inability of visualizing their skeletons.

1.1.4 Rationale of this Work

Rodents represent a distinctive placental order encompassing more than 40% of mammalian biodiversity (Fabre *et al.*, 2015). The repeated colonization of different ecosystems, from aquatic to desert areas, and their presence on most continents are indicative of their extraordinary adaptive capabilities. Their small to medium size, short generation times (Martin & Palumbi, 1993), and effective population size (Spradling, 2001), have been suggested to be fundamental for such success. As a result of their adaptation to diverse ecological niches, rodents show a wide range of locomotor repertories and therefore a considerable phenotypic diversity (disparity) of their postcranial skeleton (e.g. Samuels & Van Valkenburgh, 2008; Cox & Hautier, 2015). These features make them a unique mammalian model to assess different evolutionary processes (Hautier & Cox, 2015). However, most morpho-functional studies of the musculoskeletal system of rodents have been focused to understand their cranial anatomy, whilst their postcranium has been less studied, probably because they are often depicted as "terrestrial generalists" (Vianey-Liaud *et al.*, 2015). Given these circumstances, it is evident that studies on postcranial elements are needed to improve our knowledge of them, as well as to generate a more complete understanding of skeletal development, adaptation and evolution of this diverse group of mammals (Wilson & Geiger, 2015; Morgan, 2015).

Skeletal adaptations in mammals are best known for surface-dwelling species such as laboratory rodents (e.g. Ruth, 1953; Tomlin *et al.* 1953; Bateman, 1954; Frandsen *et al.* 1954; Pratt, 1957, 1959; Enlow, 1962, 1963; Li & Klein, 1990; Biewener & Bertram, 1993; Erben, 1996; Hörner *et al.* 1997; Lelovas *et al.* 2008; Hall, 2015). Regarding the specific adaptations of subterranean and fossorial mammals, studies have mostly focused on adults and have analyzed few specimens (Vizcaíno *et al.*, 2002, 2006, 2016; Elissamburu & Vizcaíno, 2004; Lagaria & Youlatos, 2006; Candela & Picasso, 2008; Samuels & Van Valkenburgh, 2008; Hopkins & Davis, 2009; Elissamburu, 2010; Elissamburu & De Santis, 2011; Meier *et al.*, 2013; Rose *et al.*, 2014; Marcy *et al.*, 2016; Morgan *et al.*, 2017; Sansalone *et al.*, 2018). For these reasons, our knowledge concerning the ontogenetic and intraspecific variation of these highly specialized mammals is also lacking. Furthermore, most of the previous studies have focused on one anatomical dimension of their skeletal system, either their external morphology (using 2D or 3D morphometrics) or their comparatively much less investigated bone microstructure. The integration of different dimensions of bone structure such as histomorphometry and functional anatomy of cortical bone, trabecular bone and diaphyseal bone elongation under a multiscale approach would considerably contribute to understand bone growth and adaptation in mammals.

The present study aims to fill this gap by a series of studies: i) integrating different aspects of limb bones such as bone microstructure and external anatomy (Ch. 3), ii) by assessing their appendicular morphological disparity (Ch. 4), iii) by analyzing ontogenetic patterns of different species (Ch. 5) and iv) by comprehensively describing their patterns of osteogenesis during ontogeny (Ch. 6).

It is important to note that skeletal adaptations in subterranean mammals have been mostly associated with cranial and postcranial features specialized to maximize digging activity. However, skeletal adaptaions can also include locomotor (e.g. posture and limb proportions) and reproductive (e.g. vertebral

elongation, pelvic modifications) specializations (Eilam *et al.*, 1995; O'Riain *et al.*, 2000; Montoya-Sanhueza *et al.*, 2019). This study recognizes such differences and addresses primarily limb bone specializations linked to digging behavior, although the effects of within-burrow locomotion in the appendicular system are also considered in some sections (e.g. chapters 3 and 4). The multiple aspects analyzed in this study are for first time assessed in rodents simultaneously and therefore will considerably contribute to our knowledge of bone growth and adaptation in mammals.

1.2 AIMS OF THE STUDY

The aim of this research is to assess the patterns of bone growth and development of the appendicular phenotype of African mole-rats (Rodentia: Bathyergidae). The proposed research is novel since it will provide substantial quantitative and qualitative information on the processes of skeletal morphogenesis of a highly specialized group of subterranean mammals. This research will consolidate several aspects of their skeletal biology, such as comparative bone anatomy, osteogenesis, bone (re)modeling and function, thus providing a more integrated view of the process of morphogenesis in non-model group.

1.3 OBJECTIVES, RESEARCH QUESTIONS, HYPOTHESES AND PREDICTIONS

1.3.1 Objective Chapter 3

This chapter focuses on the determination of the postnatal development of limb bones of the only scratch-digging bathyergid genus (*Bathyergus*). It integrates multivariate analysis and a multiscale approach including different dimensions of bone structure (i.e. external morphology and bone microstructure).

Question 1: What morphological changes occur during the ontogeny of *Bathyergus suillus*, and when do these occur?

Question 2: Do certain parts of the skeleton develop at different rates (e.g., intralimb and interlimb variability)?

Question 3: Do endochondral and periosteal bone modules show different growth trends in relation to body size?

1.3.2 Objective and Hypothesis of Chapter 4

This chapter focuses on determining the morphological diversity (disparity) of the appendicular system of adult African mole-rats by analyzing morpho-functional indices based on their external anatomy.

***Hypothesis A**:* The type of social strategy observed in bathyergids influence the morphology of their appendicular skeleton, since a cooperative lifestyle would compensate for individual optimization of anatomical structures for burrow construction. It is expected that solitary species (*Heliophobius, Georychus* and *Bathyergus*) will show a more specialized ("morphologically divergent") appendicular anatomy as compared to social species (*Heterocephalus, Fukomys* spp. and *Cryptomys*), which will have a more generalized or simplified limb

morphology. It is also expected that scratch-digging species (*Bathyergus*) will show a higher degree of morphological specialization in their limbs as compared to chisel-tooth digging taxa (*Heterocephalus*, *Fukomys* spp., *Cryptomys*, *Heliophobius* and *Georychus*), due to increased anatomical specializations to maximize scratch-digging behavior (i.e. soil breakup).

1.3.3 Objective and Hypothesis of Chapter 5

This chapter focuses on determining and comparing the relative rates of bone growth and osteogenesis of different developmental modules (i.e. intramembranous and endochondral ossification) to elucidate general patterns of appendicular heterochrony in African mole-rats.

Hypothesis B: Because the pectoral girdle and forelimb bones are fundamental for burrow construction, these elements are functionally prioritized during development, so the humerus and ulna will show faster growth rates as compared to hindlimb bones. It is expected that the forelimb bones will mature earlier than hindlimb bones.

Hypothesis C: Endochondral and intramembranous ossifications have different rates of bone growth during ontogeny. It is expected that because of the differences in the timing of epithelial cell production and growth plate conservatism (predetermination), endochondral ossification will show a more stable pattern of bone growth, and therefore faster growth rates as compared to intramembranous ossification which will be more variable due to the constant *de novo* cell formation at periosteal and endosteal surfaces.

1.3.4 Objective and Hypothesis of Chapter 6

This chapter focuses on comparing the bone microstructure of African mole-rats during postnatal ontogeny to determine the patterns of bone modeling and remodeling among species.

Hypothesis D: All bathyergid species will show similar bone modeling patterns, which will be evidenced by similar composition of bone tissue matrices (histodiversity) in diaphyseal cortical bone microanatomy.

Hypothesis E: Differences in growth rates will be reflected by showing either increased amounts of rapidly deposited bone tissues (i.e. woven bone, compact coarse cancellous bone and perhaps more parallel-fibered than lamellar bone) bone tissues, or slowly deposited bone tissues (lamellar bone, lamellated bone, and perhaps less amount of parallel-fibered bone tissues).

Hypothesis F: Due to the relevance of the pectoral girdle and forelimb bones during excavation and burrow construction, the humerus and ulna will show faster growth rates as compared to hindlimb bones. This will be evidenced by forelimb bones maturing earlier than hindlimb bones, and this will be reflected by the humerus and ulna showing rapidly deposited bone tissues as compared to the femur and tibia of the same individual. A similar pattern is expected for zeugopodial and stylopodial elements, where the first will show tissues with higher bone growth rates.

CHAPTER 2

General Material and Methods

This chapter provides a general overview of the specimens used throughout this study, as well as it describes the general methods used to prepare such material. Information about the origin of the specimens, location, biological information and sampling methods are described here. Nevertheless, the detailed methods used for each of the research chapters (Chapters 3-6), are specifically outlined in each respective chapter. At the end of this chapter, a list of abbreviations and symbols used throughout the manuscript is also provided.

2.1 THE STUDY SAMPLE AND DATA COLLECTION

Comprehensive postnatal ontogenetic sequences of skeletons of all six genera of extant African mole-rats genera (*Bathyergus, Heliophobius, Georychus, Fukomys, Cryptomys* and *Heterocephalus*) were obtained for this study (Fig. 1.2; Table 2.1). The sample included male and female individuals, which were usually equally sampled (1:1). A total of 1133 bones pertaining to 506 individuals of eight bathyergid species were analyzed (Table 2.1). As Table 2.1 indicates, specimens were obtained from different researchers and institutions from around the world, and they were collected from the wild on field collections or from captive colonies, or in some cases collected in the field and then kept in captivity for some period. Majority of the individuals already had data pertaining to body mass (BM), body length (BL) and skull length (SKL), which were taken at the time of death (Table 2.1). However, for specimens that lacked such morphological data, these were taken during this study (see details in Table 2.1). A Mitutoyo digital caliper (0.01 mm) was used to measure BL and SKL, while a standard electronic balance (0.01 g) was used to quantify BM. BL (mm) was measured from the tip of the snout to the base of the tail and SKL (mm) from the tip of the incisor alveolus to the posterior part of the skull (Fig. 2.1). The weight of some frozen specimens was obtained only after they were completely defrosted (Table 2.1). Additional data such as locality, reproductive status, date of birth (DOB) and date of death (DOD) was available only for some specimens (Table 2.1). In the cases of unknown sex (e.g. naked molerats), this was determined by visual inspection under the guidance of Emeritus Associate Prof. Jennifer Jarvis, who is preeminent on the study of naked mole-rats around the world due to her pioneering work in Kenya and her comprehensive study of captive colonies at the University of Cape Town (UCT). Additional references were also utilized (e.g. Seney *et al.*, 2009).

As indicated above, the specimens analyzed in this study were either already skeletonized or were frozen carcasses. In the latter case, once defrosted, a surgical scalpel was used to remove the skull, forelimbs (scapula, humerus, ulna, radius) and hindlimbs (femur, tibia-fibula) of each specimen, although it was not always possible to get the four limb bones of each individual. Limb bones were taken preferentially from the left side, although in some cases they were recovered from the right side. After muscles and soft tissues were removed, the bones were skeletonized using worm colonies (Tenebrionidae) at UCT. This process required approximately 1-2 months and left the skeletons mostly free of soft tissues. Bones that still retained remnants of soft tissues (usually tendons) were kept in jars of water and left for around 6 weeks to promote bacterial growth with the consequent consummation of the remaining flesh (no chemicals or soap were used during this process). Since tenebrionid worms can also eat the small bones of young individuals, especially the poorly mineralized epiphyses, or even the bones of small species (e.g. naked molerats), such specimens were skeletonized exclusively using bacterial activity, and they were carefully monitored. All materials skeletonized during this study were fixed in ethanol (96%) for at least 48 hours, and thereafter in acetone for around two hours. In the cases were specimens obtained were already stored in ethanol or formaldehyde, such material was directly analyzed without additional treatment.

Once bones were skeletonized, high resolution photographs from anterior and posterior views were either taken with a DSLR camera (Nikon D200) or using a stereomicroscope (Nikon SMZ 745T and Leica EZ4 HD), depending on the size of the bone. Prior to sectioning procedures for histological analysis, X-rays of all bones were performed with the help of Dr. David Grant and Dr. Claire Havenga at the Rondebosch Veterinary Hospital (Cape Town, South Africa).

2.2 MORPHOLOGY, RELATIVE AGE AND SKELETAL MATURITY

Life in burrows imposes strong morphological constraints on subterranean mammals which usually results in phenotypes with elongated cylindrical body shapes and short limbs (Fig. 1.1A-D). The general morphology of a bathyergid is schematized in Figure 2.1, which also shows the principal bones analyzed here, as well as general anatomical nomenclature used in this study. Several morphological measurements of the appendicular system were obtained in this study. The main data set comprises a range of linear measurements such as lengths (from proximal to distal articular surfaces) and diameters (epiphyseal and diaphyseal) obtained from the stylopods (humerus, femur) and zeugopods (ulna and tibia-fibula) of each individual (Fig. 2.1). This was used in chapters 3-5 to test multiple hypothesis outlined in sections 1.3.1-1.3.3 (Ch. 1). The full description of such linear measurements was mostly detailed in Ch. 3, although some parameters are also described in Ch. 4, and subsequently used for Ch. 5 too.

In this chapter, the relative age classes and/or skeletal maturity of the specimens is outlined. The relative age classes of almost all individuals were determined from patterns of molar eruption and wear from previous studies on AMs (e.g. Taylor *et al.*, 1985; Janse van Rensburg *et al.,* 2004; Hart *et al.*, 2007; Chimimba *et al.,* 2010; Gomes Rodrigues *et al.,* 2011).

Skeletal maturity was assessed principally on the degree of epiphyseal fusion of long bones. Three main stages were defined: i) epiphyseal line is totally visible around the bone (unfused), ii) at least half of the epiphyseal line is observed (semifused), and iii) epiphyseal line is absent or considerably restricted to one sector of the bone (fused) (Fig. 2.2).

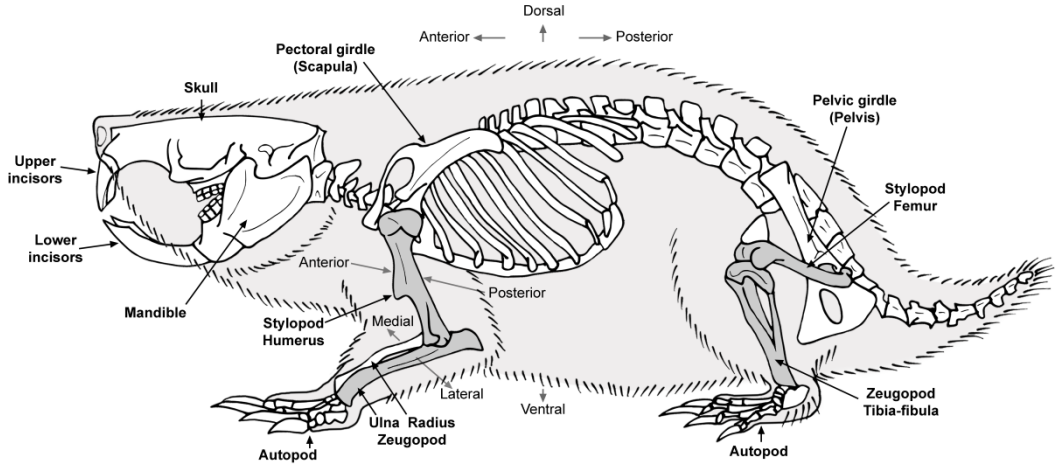

FIGURE 2.1. Schematic representation of the morphology of a bathyergid skeleton showing the main anatomical features of their cranial and appendicular skeleton. Bones used in this study are shown in grey. Based on *Bathyergus suillus*.

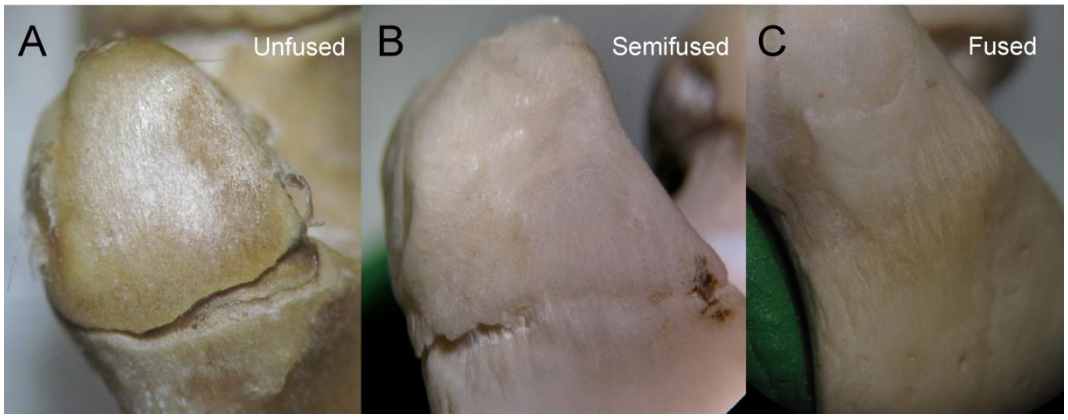

FIGURE 2.2. Three stages of epiphyseal fusion recorded in bathyergids. A) Unfused (#337). B) Semifused (#1338). C) Fused (#220). Examples correspond to the greater trochanter of males of *Bathyergus suillus*.

Table 2.1. General information of the species and bathyergid individuals analyzed in this study: collector (institution), location - original provenance (city), number of individuals (*N*), date of birth (DOB) and death (DOD), reproductive status (RS). The asterisk (*) in *G. capensis* indicates that some individuals have an unknown origin. *Abbreviations*: Body mass (BM); body length (BL); skull length (SKL); captivity (C); wild (W); Cape Town (CT); Van Zylsrus (VZ); Northeast Ohio Medical University (NOMU); University of Cambridge (UC); University of Cape Town (UCT); University of Pretoria (UP); University of South Bohemia (USB); measured (Y); measured and taken by G. Montoya-Sanhueza (Yg); not measured (N).

Species	Common name (Abbreviation)	Location (city)	*N*	BM	BL	SKL	RS	DOB	DOD	Condition	Collector (Institution)	Country
Bathyergus suillus	Cape dune mole-rat (CDM)	Airport (CP)	48	Y	Y	Y	Y	N	Y	Wild	Justin O'Riain (UCT)	South Africa
Bathyergus suillus	Cape dune mole-rat (CDM)	Darling (CP)	88				N	N	Y	Wild	Nigel Bennett (UP), Jan Okrouhlik (USB)	South Africa, Czech Republic
Bathyergus janetta	Namaqua dune mole-rat (NDM)	-	6				N			Wild	Jennifer Jarvis (UCT)	South Africa
Georychus capensis	Cape mole-rat (CPM)	Darling (CP)*	62	Y	Yg	Yg				Wild	Nigel Bennett (UP), Jan Okrouhlik (USB)	South Africa, Czech Republic
Heliophobius argenteocinereus	Silvery mole-rat (SYM)	-	30	Y	Y	N		Y	Y		Radim Šumbera (USB)	Czech Republic
Heliophobius argenteocinereus	Silvery mole-rat (SYM)	-	4		Yg	Yg	N				Nigel Bennett (UP)	South Africa
Fukomys mechowii	Mechow's mole-rat (MWM)	-	32	Y	Y	N	Y	Y	Y		Radim Šumbera (USB)	Czech Republic
Fukomys damarensis	Damaraland mole-rat (DLM)	-	7		Y	Yg	N	N			Nigel Bennett (UP), Jennifer Jarvis (UCT)	South Africa
Fukomys damarensis	Damaraland mole-rat (DLM)	Kuruman (VZ)	25	Y	N	N	Y	Y	Y	Captivity	Tim Clutton-Brock (UC)	UK
Cryptomys hottentotus	Common Hottentot mole-rat (CHM)	-	53	Y	Yg	Yg	N	N		Wild	Andrew Spinks (UCT)	South Africa
Cryptomys h. natalensis	Natal Mole-rat (NLM)	-	10	Y	Y	Y	N		Y	W+C	Nigel Bennett (UP)	South Africa
Heterocephalus glaber	Naked mole-rat (NKM)	UCT colony	73	Yg	Yg	Yg				Captivity	Jennifer Jarvis (UCT), Nigel Bennett (UP)	South Africa
Heterocephalus glaber	Naked mole-rat (NKM)	US colony	10	Y	N	N	Y	Y	Y	Captivity	Christine Dengler-Crish (NOMU)	USA
Total			**448**									

2.3 ABBREVIATIONS AND SYMBOLS

APDH: Anteroposterior diameter of the humerus (mm)
APDF: Anteroposterior diameter of the femur (mm)
APDT: Anteroposterior diameter of the tibia (mm)
APDU: Anteroposterior diameter of the ulna (mm)
BL: Body length (mm)
BM: Body mass (g)
D: Distal fusion of epiphysis
DLH: Origin of deltoid tubercle (mm)
DT: Deltoid tubercle
DTFJ: Length of the distal tibio-fibular junction (mm)
EF: Femoral condylar width (mm)
EH: Humeral epicondylar width (mm)
FH: Femoral head diameter (mm)
FL: Femoral length (mm)
FUL: Functional length of the ulna (mm)
HH: Humeral head diameter (mm)
HL: Humeral length (mm)
OL: Olecranon length (mm)
P: Proximal fusion of epiphysis
TL: Tibio-fibular or tibial length (mm)
TDH: Transversal diameter of the humerus (mm)
TDU: Transversal diameter of the ulna (mm)
TDF: Transversal diameter of the femur (mm)
TDT: Transversal diameter of the tibia (mm)
SKL: Skull length (mm)
UL: Ulnar length (mm)
UTL: Length of the tibial tuberosity (mm)
VL: Vertebral length (mm)

BI: Brachial index
CI: Crural index
CDIh: Cortico-diaphyseal index of the humerus
CDIf: Cortico-diaphyseal index of the femur
EIh: Humeral epicondylar index
EIf: Femoral condylar index
FHI: Femoral head index
FRI: Robustness of the femur
HRI: Humerus robustness index
HHI: Humeral head index
IFA: Index of fossorial ability
IMI: Intermembral index
RDP: Relative position of the deltoid tubercle
SGD: Suggested bone growth direction
TRI: Robustness of the tibia (transverse - mediolateral)
TRI*: Robustness of the tibia (anteroposterior - modified version)
TSI: Tibial spine index
TJI: Tibio-fibular junction index
URI: Transverse robustness of the ulna
URI*: Robustness of the forearm (anteroposterior - modified version)
VI: Vertebral index

CCCB: Compact coarse cancellous bone
ELB: Endosteal lamellar bone
FLB: Fibrolamellar bone
PLB: Periosteal lamellar bone
LB: Lamellar bone
LLB: Lamellated lamellar bone
WB: Woven bone
LAG: Lines of Arrested Growth
GM: Growth Mark
RC: Resorption Cavity
MC: Medullary Cavity

Ci: Confidence intervals
DA: Discriminant Analysis
DF1: Discriminant Function 1
DF2: Discriminant Function 2
F: Females
M: Males
MA: Major Axis Regression
PCA: Principal Component Analysis
OLS: Ordinary Least Square Regression
OS: Ontogenetic stage
RMA: Reduced Major Axis Regression
SMA: Standardized Major Axis (Type II) Regression
SD: Standard Deviation
R^2/r^2: Coefficient of Determination
(I): Isometry
(-): Negative allometry
(+): Positive allometry

Biological Sciences

Prof. Anusuya Chinsamy-Turan
Department of Biological Sciences
University of Cape Town
Private Bag X3, Rhodes Gift, 7701 South Africa
Tel: +27 (0) 21 650 4007 Fax: +27 (0) 21 650 3301
http://www.biologicalsciences.uct.ac.za/
anusuya.chinsamy-turan@uct.ac.za

7/01/2020

To whom it may concern

I confirm that the following article was published by Germán Montoya-Sanhueza and it forms an important part of his PhD research, which I supervised. As supervisor I basically read and commented on the drafts of the manuscript.

Montoya-Sanhueza G, Wilson LAB, Chinsamy A. *Postnatal development of the largest subterranean mammal (*Bathyergus suillus*): Morphology, osteogenesis, and modularity of the appendicular skeleton*. Developmental Dynamics. 2019;1–28. https://doi.org/10.1002/dvdy.81

I fully support that the content of this publication is acceptable as a chapter of Germán's dissertation.

Signature Removed

Prof. Anusuya Chinsamy-Turan

Supervisor

9 January 2020

To whom it may concern:

I hereby declare my agreement that the article “Postnatal development of the largest subterranean mammal (*Bathyergus suillus*): Morphology, osteogenesis, and modularity of the appendicular skeleton” may be included as a chapter in the Ph.D dissertation of Mr. Germán Montoya-Sanhueza. He has conducted the research presented in this paper as part of this doctoral dissertation and he successfully submitted the manuscript before the completion of his Ph.D. As a co-author of this paper, I assisted Mr. Montoya-Sanhueza by teaching him the methods to conduct the analyses he performed in this paper. I also read and commented on drafts of the manuscript that Mr. Montoya-Sanhueza prepared.

Ref: Montoya-Sanhueza G, Wilson LAB, Chinsamy A. Postnatal development of the largest subterranean mammal (Bathyergus suillus): Morphology, osteogenesis, and modularity of the appendicular skeleton. Developmental Dynamics. 2019;1–28. https://doi.org/10.1002/dvdy.81

I fully support the inclusion of this manuscript as a chapter in Mr. Montoya-Sanhueza’s dissertation.

Yours sincerely,

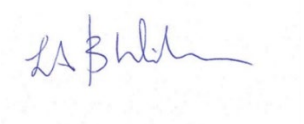

Dr. Laura A. B. Wilson
Australian Research Council (ARC), Discovery Early Career Research (DECRA) Fellow
University of New South Wales, Sydney, NSW 2052, Australia

CHAPTER 3

Postnatal Development of the Largest Subterranean Mammal *(Bathyergus suillus)*: Morphology, Osteogenesis and Modularity of the Appendicular Skeleton

Germán Montoya-Sanhueza[1]*, Laura A. B. Wilson[2], Anusuya Chinsamy[1]

Published in: *Developmental Dynamics*. 2019;1–28. https://doi.org/10.1002/dvdy.81

ABSTRACT

Background: Subterranean mammals show a suite of musculoskeletal adaptations that enables efficient digging. However, little is known about their development. We assessed ontogenetic changes in functionally relevant skeletal traits, and ossification patterns (periosteal and endochondral bone modules) in a truly subterranean scratch-digging rodent, *Bathyergus*. We studied 52 individuals (202 long bones) from a wild population by using a multiscale approach involving internal and external morphology. **Results**: Multivariate analysis showed significant morphological changes during ontogeny. A specialized phenotype is expressed perinatally (e.g., greater external robustness and developed olecranon, teres major, and deltoid tubercle), whereas adults presented slender bones with significantly thicker cross-sections. Ossification modules scaled mostly isometrically with body size parameters. Periosteal modules showed high variability and tended to grow faster than endochondral modules. **Conclusions**: Scratch-digging adaptations appear at perinatal age and then specialize in subadults. Early development of agonistic and digging behaviors and onset of sexual maturation seems to contribute to its development, although genetic factors also seem to play an important role. Ontogenetic differences are probably a trade-off to counteract weaker cortical bone properties and poor muscle development in juveniles, whereas slender but thicker cortical bones maximize bone resistance

[1] *Department of Biological Sciences, University of Cape Town, Private Bag X3, Rhodes Gift 7701, South Africa.*
[2] *School of Biological, Earth and Environmental Sciences, University of New South Wales, Sydney, NSW 2052, Australia.*
*Corresponding author: GM-S, getamoo@gmail.com

during burrow construction without compromising locomotor performance in adults.

3.1 INTRODUCTION

One of the most important aspects of the skeletal system in subterranean mammals is to increase bone strength to withstand the greater loads exerted during digging activity. Compared to their more cursorial relatives, subterranean and fossorial mammals show more robust skeletons due to both modifications of their external anatomy (e.g. wider (epi)condyles and wider diaphyses) and bone microstructure (e.g. thicker cortical walls) (Hildebrand, 1985; Biknevicius, 1993; Casinos *et al.*, 1993; Montoya-Sanhueza & Chinsamy, 2017). Such morphological changes in shape and form are the result of evolutionary modifications in the patterns of bone modeling, specifically involving the interplay between endochondral ossification (axial bone elongation) and intramembranous ossification (radial bone apposition) (e.g. Enlow, 1963). However, there is a considerable gap in our understanding of the mechanisms facilitating bone adaptation, as well as the processes involved in the acquisition of the subterranean skeletal phenotype in mammals. Specifically, the developmental relationship between external anatomy and cross-sectional properties of bones (e.g. bone geometry and bone microanatomy) has been largely neglected in subterranean mammals as well as in surface-dwelling mammals (Young *et al.*, 2010).

With the exception of few ontogenetic studies mostly focused on cranial anatomy (e.g. Cubo *et al.*, 2006; Goswami & Prochel, 2007; Hart *et al.*, 2007; Verzi *et al.*, 2010; Ventura & Casado-Cruz, 2011; Echeverría *et al.*, 2014; Vassallo *et al.*, 2016), most of the research assessing the musculoskeletal phenotype of extant and extinct subterranean and fossorial mammals has focused on morpho-functional comparisons of adults only (or at "endpoints" of ontogeny) where most of somatic (and/or skeletal) growth of the individual has been attained (e.g., Lessa & Stein, 1992; Vizcaíno *et al.*, 2002, 2006, 2016; Elissamburu & Vizcaíno, 2004; Lagaria & Youlatos, 2006; Candela & Picasso, 2008; Samuels & Van Valkenburgh, 2008; Hopkins & Davis, 2009; Elissamburu, 2010; Elissamburu & De Santis, 2011; Meier *et al.*, 2013; Rose *et al.*, 2014; Marcy *et al.*, 2016; Morgan *et al.*, 2017; Sansalone *et al.*, 2018; Calede *et al.*, 2019). Additionally, most of these studies have focused on few specimens and have used a particular anatomical dimension for analysis, either their external morphology (2D or 3D) or their bone microanatomy.

The analysis of ontogenetic series as well as the integration of different levels of structural organization has the potential to provide relevant insights regarding the adaptive strategies associated with the subterranean lifestyle. Its study becomes even more relevant considering the wide diversity of subterranean and fossorial organisms adapted to the hypogeous niche, which show highly specialized forms not only in the present (e.g. Nevo, 1999; Busch *et al.*, 2000), but also from the early evolution of nonmammalian therapsids (Botha & Chinsamy, 2004; Ray & Chinsamy, 2004) and stem mammalian lineages (Luo & Wible, 2005; Chen & Wilson, 2015; Luo *et al.*, 2015).

In this study, we integrate different quantitative and qualitative approaches to determine the postnatal ontogeny of the appendicular and axial skeleton of a fully subterranean scratch-digger, the Cape dune molerat *Bathyergus suillus* (Fig. 3.1). Scratch-digger species dig by extending their forefeet to the earth and then drawing their long claws more or less downward, toward, or under the body (Hildebrand, 1985). Since this solitary species builds extensive burrow systems that can extend over 250 m of total length and 220 mm in diameter (Chimimba & Bennett, 2005; Bennett *et al.*, 2009; Bray *et al.*, 2012; Jarvis, 2013), it represents a valuable model to understand the development of such skeletal adaptations in organisms that experience naturally strenuous biomechanical conditions over their lives. Cape dune molerats represent the largest species of all African molerats (Bathyergidae) and the largest truly subterranean mammal in the world, reaching a body mass over 2 kg (Davies & Jarvis, 1986; Nevo, 1999; Chimimba & Bennett, 2005; Bray *et al.*, 2012; Jarvis, 2013), whereby its study contributes to understanding skeletal adaptations under extreme conditions.

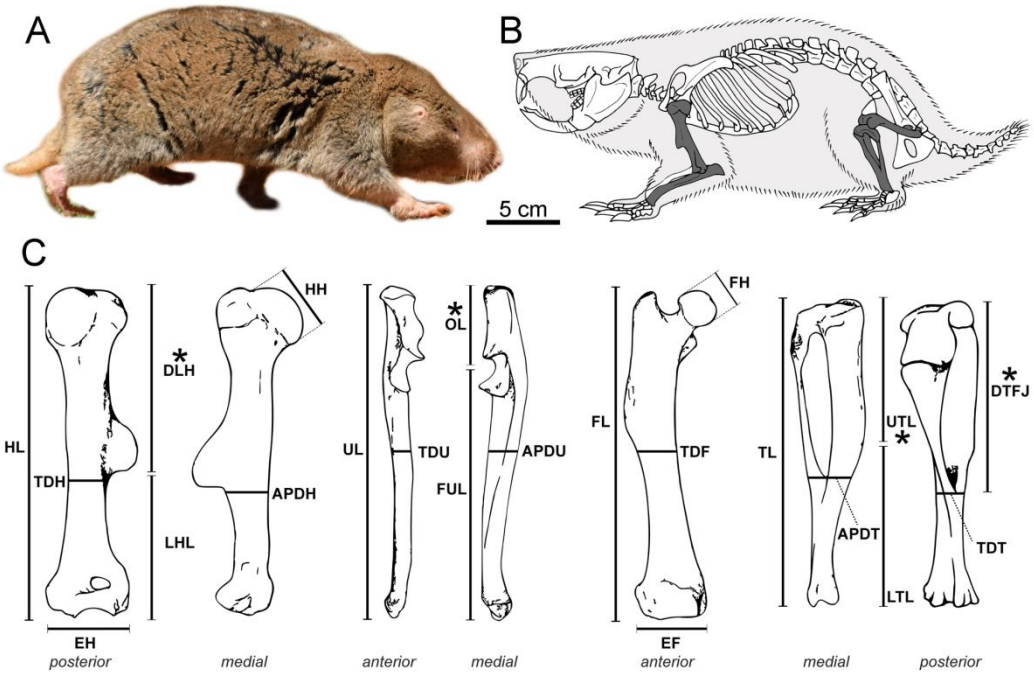

FIGURE 3.1. A) Adult specimen of *Bathyergus suillus* moving aboveground. B) Skeletal representation showing the bones studied here (dark grey). C) Linear measurements of the long bones analyzed. Asterisk (*) indicates bone superstructures calculated in this study. The individual in (A) was provided by Jan Okrouhlik and Nigel Bennett, University of Pretoria (South Africa). Abbreviations: Total lengths of humerus (HL), ulna (UL), femur (FL), and tibia-fibula (TL). Transversal diameters of humerus (TDH), ulna (TDU), femur (TDF) and tibia-fibula (TDT). Anteroposterior diameters of humerus (APDH), ulna (APDU), and tibia-fibula (APDT). Deltoid tubercle length (DLH). Humeral head diameter (HH). Humeral (EH) and femoral (EF) condylar widths. Olecranon length (OL). Functional length of the ulna (FUL). Length of the distal tibio-fibular junction (DTFJ). Tibial tuberosity (UTL). See descriptions of measurements in text.

3.1.1 Long Bone Growth in *Bathyergus suillus*

A recent quantitative and qualitative study has shown that adult limb bones of *B. suillus* undergo systemic thickening of their cortical bone walls (Montoya-Sanhueza & Chinsamy, 2017). Furthermore, the femora of this species do not experience bone loss (osteopenia) during adulthood (Montoya-Sanhueza & Chinsamy, 2018), which seems to be a systemic process also occurring in the humerus and zeugopodial bones of this species (Montoya-Sanhueza & Chinsamy, 2017). This suggests that microstructural bone adaptations such as cortical thickening in adults and scarce bone resorption throughout ontogeny, act in synergy to promote high levels of bone integrity during life, thus ensuring the maintenance of skeletal function and performance. However, juveniles of *B. suillus* have relatively thin cortical walls and high intracortical porosity as compared to adults (Montoya-Sanhueza & Chinsamy, 2018), so the mechanical properties of their long bones are expected to be reduced and therefore more prone to fracture risk due to weaker bone properties (e.g., Main & Biewener, 2006). The implications of these conditions become especially relevant considering that digging and tunneling begins at ~6 weeks old (Chimimba & Bennett, 2005), whilst dispersal at around two months of age (<200 - 300 g of body weight; Bennett *et al.*, 1991). Given the early occurrence of digging behavior in this species, it is expected that some morphological adaptations associated with digging capabilities and increased robusticity may be established early in ontogeny to reduce fracture risks, and probably synchronous with the beginning of such activities, as has been suggested for other subterranean species (e.g., Cubo *et al.*, 2006; Echeverría *et al.*, 2014).

Long bones of mammals increase their bone mass either by increasing bone density and/or bone size (Wall, 1983; Mora & Gilsanz, 2010). The first is positively correlated with cortical bone thickening (e.g. Webber *et al.*, 2015), which results from intramembranous ossification throughout bone modeling dynamics such as endosteal and periosteal bone apposition (Enlow, 1963; Wall, 1983; Montoya-Sanhueza & Chinsamy, 2017). This process is responsible for most of the bulk of long bones (Hall, 1978; Wall, 1983). The second aspect is, at least in terrestrial mammals, the result of bone elongation (Mora & Gilsanz, 2010), which results from chondrocyte proliferation and bone matrix production throughout endochondral ossification at growth plates (Kronenberg, 2003). Consequently, peak bone mass in long bones is attained by a dual process involving endochondral and intramembranous ossification, which are regulated by different genes (Beamer *et al.*, 1996; Klein *et al.*, 1998; Sarges *et al.*, 2011; Wongdee *et al.*, 2012). Because these osteogenic processes represent relatively independent developmental entities (Atchley & Hall, 1991; Hall, 2015), they can be considered as organizational modules (e.g. Esteve-Altava, 2017; see also Experimental Procedures), and therefore their growth dynamics are relevant to understanding patterns of skeletal modularity in long bones. Similarly, since both bone thickening and bone elongation are affected by different factors (Moss-Salentijn, 1991; Taylor, 1991), the study of modularity could provide important insights into the mechanisms driving bone adaptation in subterranean mammals. In this sense, although the pattern of bone modeling in *B. suillus* has been comprehensively described previously (Montoya-Sanhueza & Chinsamy, 2017), it remains unknown how both bone thickening and elongation relate to age and whole-body size parameters. Additionally, subterranean

mammals have typically been described as having elongated cylindrical body shapes with short limbs (Eilam *et al.*, 1995; Eilam, 1997; Nevo, 1999, Stein, 2000), but no morphological studies have yet demonstrated how this "subterranean phenotype" is reached.

In this study we use a multiscale approach including morpho-functional indices to quantify ontogenetic morphological changes associated with the functional ability of bone designs to either favor strength or speed. We also use linear measurements (length and diameter) and different proxies of body size to identify the modular patterns of endochondral and periosteal bone formation during ontogeny. Bone fusion sequences are also included in this analysis, especially for the estimation of bone growth direction and to assess how plate closure may affect the postnatal development of specific functional traits. Considering the above, the main questions addressed in this study are: i) what morphological changes occur during the ontogeny of *B. suillus*, and when do these occur? ii), do certain parts of the skeleton develop at different rates (e.g., intralimb and interlimb variability)? iii) do endochondral and periosteal bone modules show different growth trends in relation to body size? Considering that *B. suillus* mostly use their forelimbs to break-up the soil during burrow construction (Jarvis, 2013), we expect that the forelimbs would reach the adult phenotype (skeletal maturity) earlier than hindlimbs. This would be further supported by humeral and ulnar traits showing faster growth rates as compared to femoral and tibio-fibular traits. Secondarily, differences in trait variability are expected to occur between ossification modules due to differential effects of the environment and development (e.g. Atchley & Hall, 1991; Moss-Salentijn, 1991; Taylor, 1991). The results of this study are mostly discussed in terms of development and function, although aspects of behavior, locomotion, and sex differences are also included. This study provides the first integrative assessment of limb bone growth of a subterranean mammal involving different dimensions of anatomical analysis (i.e. external morphology and bone microstructure), thus providing a comprehensive understanding of the patterns of morphological adaptation in a highly specialized mammal.

3.2 EXPERIMENTAL PROCEDURES

3.2.1 Species and Specimens

Forty-six Cape dune molerats, *Bathyergus suillus,* were analyzed in this study (Fig. 3.3.1A, B), comprising 11 juveniles (six females, five males), 17 subadults (eight females, nine males) and 18 adults (11 females, seven males). Data collection methods and biological aspects of these specimens are presented in previous studies (Hart *et al.*, 2007; Montoya-Sanhueza & Chinsamy, 2017, 2018). Ontogenetic stages were based on the relative age classes (from 2 to 9) determined on patterns of molar eruption and wear (Hart *et al.*, 2007). Given that newborns were unavailable for *B. suillus*, we studied a newborn individual of its closest relative, the Namaqua dune molerat, *B. janetta* (Visser *et al.*, 2014), as well as a juvenile and four adults of this taxon. Namaqua dune molerats are a medium to large size species, reaching body masses of about 500 g and have a similar lifestyle to *B.*

suillus (Bennett *et al.*, 1991; Herbst *et al.*, 2004; Jarvis, 2013). These species occur mostly allopatrically, with *B. suillus* being endemic to the Cape Peninsula in the Western Cape Province (South Africa), and *B. janetta* endemic to the north-western parts of the Northern Cape (South Africa), but also extending to the south of Namibia. Hybridization of these species has been postulated at the border of their distributions (see Visser *et al.*, 2014, and references therein), although recent molecular studies have suggested a higher genetic variation within *Bathyergus*, leading to a paraphyletic placement of these taxa and indicating that a systematic revision is needed (Ingram *et al.* 2004; Visser *et al.*, 2014). Both species are scratch-diggers (Jarvis, 2013) closely associated with coastal sand dunes and alluvial sands along rivers. As compared to *B. suillus*, *B. janetta* produce smaller burrow systems, ranging between 57-175 m and 136 mm in diameter (Jarvis, 2013). The pattern of molar eruption and wear of *B. janetta,* along with its humeral and femoral bone histology (G. Montoya-Sanhueza, unpubl. data, 2018) confirms advanced stages of somatic maturity in adults. The neonate and juvenile of *B. janetta* were donated by J. Jarvis and were already cleared and stained with alcian blue for cartilage, and alizarin red for bone/osteoid. All specimens are housed in the Department of Biological Sciences at the University of Cape Town (UCT), South Africa.

3.2.2 Measurements

Twenty linear measurements were recorded from forelimbs (humerus and ulna) and hindlimbs (femur and tibia-fibula) of each specimen (Fig. 3.1C). Linear measurements were recorded using a digital caliper (0.01 mm). Some small bones (especially from neonates and juveniles) were photographed using a stereomicroscope (Nikon SMZ 745T), and then analyzed in Image Pro-Plus version 4.5 (Media Cybernetics, Silver Spring, USA). Measurements, presented in mm (mean ± *SD*), follow standard linear measurements from previous studies (Fig. 3.1). Total bone lengths are the maximum distance from the proximal articular surface to the distal articular surface (Fig. 3.1). In the humerus, transversal (TDH) and anteroposterior diameters (APDH) were measured below the deltoid tubercle (DT) (~60% from proximal epiphysis). The location of the DP within the diaphysis (DLH) was measured from the humeral head to the distal origin of this structure. The humeral head diameter (HH) is the maximum distance in its major breadth. Humeral (EH) and femoral (EF) condylar widths were measured as the maximum distance between the medial and lateral edges of the (epi)condyles. In the ulna, the olecranon length (OL) is the distance from the tip of the olecranon to the center of the trochlear notch. The functional length of the ulna (FUL) is the difference between UL and OL (Fig. 3.1). The transversal (TDU) and anteroposterior diameters of the ulna (APDU) were taken at 50% from the proximal epiphysis. In the femur, the transversal diameter (TDF) was measured at the 50% of the FL from its proximal epiphysis (usually below the third trochanter). Due to the circular shape of the femoral head, its diameter (FH) was measured as the maximum distance between the medial edge to the lateral edge. In the tibio-fibula, the length of the distal tibio-fibular junction (DTFJ) is the distance from the proximal articular surface to the tibio-fibular junction (which is usually located at ~58% from the proximal epiphysis in this species). The transversal (TDT) and

anteroposterior diameters (APDT) were measured at the distal tibio-fibular junction. The tibial tuberosity (UTL) was measured between the proximal articular surface to the distal point of this feature. Three additional composite measures were added to the analysis: forelimb length (HL+FUL), hindlimb length (FL+TL) and vertebral length (BL-SKL). We also explored morphological changes in the relative position of bone superstructures (i.e. projections that serve for tendon and ligament insertion or articulation) on the diaphysis of long bones since their position is crucial for musculoskeletal functionality (Stern *et al.*, 2015). We calculated the mean relative percentage to the total length of four bone superstructures; i) distal origin of deltoid tubercle (DLH%), ii) distal origin of olecranon (OL%), iii) extension of the tibial tuberosity (UTL%) and iv) distal tibio-fibular junction (DTFJ%) (Fig. 3.1C). In order to determine the direction of bone growth we recorded the general pattern of epiphyseal fusion of *B. suillus* (Table 3.6), considering two main stages: fused (epiphyseal line partially present or absent) and non-fused epiphyses (epiphyseal line totally visible).

3.2.3 Morpho-Functional Indices

To assess the degree of morphological change in the postcranial skeleton we used morpho-functional indices and limb proportions which are readily recorded on neonatal/juvenile specimens (Table 3.1). The use of these indices allowed us to identify which specific aspects of the bone shape undergoes change, i.e. either its length or its diameter. Nineteen indices were calculated from linear measurements (see details in Table 3.1): 14 were taken from previous studies; two represent a modification of some of them (see below); and three were developed in this study. Their calculation and biomechanical/ecomorphological function are presented in Table 3.1. The indices representing robustness of the ulna (URI) and tibia (TRI) have been typically measured as the quotient between the transversal (mediolateral) diameter of the bone and its functional length (e.g., Vizcaíno *et al.*, 2016). These indices are thought to demonstrate the robustness and strength of such bones, as well as the available surface for muscle attachment. Specifically, the use of transverse diameters reflects the resistance to bending in one direction, the mediolateral axis of the bone. However, the higher bending stresses in the forearm of mammals performing parasagittal movements during scratch-digging behavior, like *B. suillus* (Hildebrand, 1985), are expected to occur mainly in the anteroposterior axis of the bone (Biewener & Taylor, 1986; Carter & Beaupré, 2001; Leppänen *et al.*, 2006), which is usually longer and hence designed to resist higher bending stresses as compared to its orthogonal, shorter mediolateral axis. The wider anteroposterior ulnar section also provides a larger surface for attachment of flexor muscles such as the m. extensor carpi ulnaris, m. flexor carpi ulnaris and m. flexor digitorum profundus (e.g., Holliger, 1916). Therefore, to assess the bending resistance of such bones in a more precise manner we included two indices indicating the robustness of the ulna and tibia in the anteroposterior axis (URI* and TRI*, respectively). Other indices vary in the way that they have been previously measured. For instance, the humerus robustness index (HRI) is sometimes calculated with its anteroposterior axis (e.g., Echeverría *et al.*, 2014), and other times with its mediolateral axis (e.g., Elissamburu & Vizcaíno, 2004;

Vizcaíno *et al.*, 2016). We followed the former authors since their calculation is more in accordance with the biomechanical approach explained above.

The cortical area of tubular long bones is generally considered to reflect a section's rigidity to pure axial (compressive or tensile) loadings (e.g., Heinrich & Biknevicius, 1998). For this reason, we included a dimensionless parameter of bone thickness, the cortico-diaphyseal index (CDI) (Castanet *et al.*, 2000; Montoya-Sanhueza & Chinsamy, 2018), which is a basic estimator of cortical area and bone strength (Currey, 2002). This index also provides information on osteogenic dynamics when analyzed along with estimations of bone area (see Montoya-Sanhueza & Chinsamy, 2018). This parameter quantifies the ratio between the cortical thickness and the radius of the cross-section (see Girondot & Laurin, 2003), so that higher values indicate thicker cortical walls and hence a higher rigidity to resist bending and torsional strains (e.g. Heinrich *et al.*, 1999). Both humeral (CDIh) and femoral (CDIf) parameters were calculated using binary images of bone area and empty space; the medullary cavity and resorption cavities are considered as empty spaces (thus increasing bone porosity), while nutrient arteries and void space are not included, thus minimizing the intrinsic bone porosity levels of the bone, but still keeping the general microanatomical design of the whole cross-section (see Montoya-Sanhueza & Chinsamy, 2018). Since peak bending strains generally occur in the midshaft of quadrupedal mammals (Biewener & Taylor, 1986; Carter & Beaupré, 2001; Young *et al.*, 2014), bone cross-sections were done at ~50% of the femoral diaphysis, and below the deltoid tubercle in the humerus (at ~58-60% from the proximal articular surface). CDI values were obtained from the software Bone Profiler Version 4.5.7 (Girondot & Laurin, 2003).

We also assessed the intermembral index (IMI) (Howell, 1965) and the vertebral index (VI) (developed in this study). Apart from indicating leaping ability, the IMI has not shown clear functional correlates in mammals, especially those associated with either higher speed or lack of it (Howell, 1965). However, this index has never been applied to assess ontogenetic patterns. Subterranean mammals, which are usually ascribed to have cylindrical body shapes with short limbs (Eilam *et al.*, 1995; Eilam, 1997; Nevo, 1999, Stein, 2000), also appears to have a symmetric limb length ratio, i.e. high IMI ~1.0. We expect high IMI values in *B. suillus*, as a strategy facilitating bidirectional locomotion in narrow burrow systems (e.g., Eilam *et al.*, 1995; Eilam, 1997).

Henry *et al.* (2007) and Dengler-Crish and Catania (2007, 2009) have reported that the lumbar vertebrae elongate in queens of the eusocial naked molerat, *Heterocephalus glaber* (Bathyergidae), likely as an adaptation to provide more space within the body (longitudinally) and thereby increasing the abdominal capacity for pups. In this study, the vertebral index (VI) included lengths of the cervical, thoracic, lumbar and sacral vertebrae. Higher values of VI will represent a longer relative spine length, which it is expected to increase during ontogeny, especially in females.

3.2.4 Allometric Analysis

Long bone allometry of *B. suillus* was assessed in relation to body mass (BM) and body length (BL), although skull length (naso-occipital length) (SKL) was also included for comparative purposes due to their frequent use in studies on fossorial mammals (e.g., Schleich & Vassallo, 2003; Bidau *et al.*, 2011; Echeverría *et al.*, 2014) (Table 3.5). To assess the amount of variance of each of these proxies, we used the coefficient of determination (R^2) obtained from RMA regressions. Only for the assessment of linear relationships among proxies of body size, we used relative age (2-9) as an "independent" variable.

A large proportion of structural evolution can be fully described in terms of relative growth and heterochrony, today better known as allometric trends (Gould, 1966). One important aspect of using bone allometry and linear regressions in this study is to provide information on mechanisms explaining structural modifications, especially associated with patterns of ossification among different skeletal elements and within bone elements. Long bone osteogenesis in vertebrates undergoes two main processes during growth; endochondral and intramembranous (perichondral/periosteal) ossification, which represent independent developmental entities (Hall, 2015). The integration of allometric approaches permits the quantification of such tissue-mediated mechanisms responsible for the final phenotype observed among species (e.g., Sanger *et al.*, 2011; Koyabu *et al.*, 2011). For this reason, in this study, linear measurements associated with bone elongation (HL, DLH, UL, OL, FUL, FL, TL, UTL and DTFJ) were considered to reflect patterns of the endochondral bone module, while the measurements associated to radial bone thickening (TDH, APDH, TDU, APDU, TDF, TDT and APDT) were considered to reflect the periosteal bone module. The ossification of secondary centers (HH, FH) reflects another module, although since the (epi)condyles (EH and EF) are located in the interface (metaphysis) between endochondral and periosteal bone formations (Hall, 1978; Moss-Salentijn, 1991), these traits most likely involve the interaction of two different developmental modules.

Linear measurements were analyzed by standardized major axis (SMA) estimation (Model II regression) (Warton *et al.*, 2006). We chose SMA (=RMA), over ordinary least square regressions (OLS) and major axis (MA) estimation types because we intended to determine the relationship between two variables not necessarily independent in the strict sense, and with both variables containing error to some extent (Warton *et al.*, 2006). Departures from isometry were assessed by inspection of slopes (b) and fitting to the 95% confidence intervals (CI) by testing the null hypothesis $b = 1.0$ when comparisons of the scalars are equivalent (e.g. BL vs SKL), and $b = 0.33$ when comparisons involve different scalars (e.g. BM vs BL). If the CI excluded a value of 1.0 (or 0.33), then allometry was considered significant. If the slope is 1 (or 0.33), the change is isometric (I); if the slope is <1.0 (or <0.33) there will be an increase in size of the x variable and hence negative (-) allometry; if the slope is >1.0 (or >0.33), there will be an increase in size of the variable y and hence positive (+) allometry. Patterns of bone growth in *B. janetta* were assessed using SKL only. In this study, body size variables are always plotted in the x axis, to highlight the effect on the y variable (e.g., positive allometry denotes increase in y).

3.2.5 Statistical Analysis

To assess postnatal morphological changes, functional indices were analyzed by two-way multivariate analysis of variance (MANOVA). Factors used in the MANOVA were ontogenetic stage (OS) (juveniles, subadults and adults), sex (female, male) and its interaction (OS*sex). We performed Scheffe's *F* post hoc tests for the MANOVA. We also explored the data using non-parametric MANOVA (NPMANOVA) (Euclidean distance), which gave similar results (OS: $F = 16.279$, $P < 0.001$; Sex: $F = 2.144$, $P > 0.05$) as compared to the parametric procedure. We opted to show the parametric model due to the more complete output of the MANOVA, which allowed us to carry out a discriminant function analysis (DFA) with the standardized canonical coefficients. The DFA permits a visualization of the differences in the morpho-functional indices that most contribute to the differentiation between groups based on OS centroids. An alpha level of 0.05 for all statistical tests was used. For all the allometric analyses and morpho-functional indices, data were previously $\log_{10}$ transformed. Tests and plots were performed in Microsoft Excel (2010), PAST version 2.17c (Hammer *et al.*, 2001) and IBM SPSS version 25 (IBM, 2017) Statistical Package for Social Sciences.

3.3 RESULTS

3.3.1 Multivariate Analysis (MANOVA) of Morpho-Functional Indices

Nineteen morpho-functional indices were analyzed (Table 3.1 and 3.2). Significant differences were found among ontogenetic stages (OS) (Wilks' $\lambda = 0.045$; $F_{38, 40} = 3.936$; $P < 0.001$), but not between sexes (Wilks' $\lambda = 0.453$; $F_{19, 20} = 1.273$; $P > 0.05$) or the sex*OS interaction (Wilks' $\lambda = 0.185$; $F_{38, 40} = 1.397$; $P > 0.05$). Univariate ANOVAs showed that 13 out of 19 morpho-functional indices were significantly different ($P < 0.05$) among ontogenetic groups (Fig. 3.2): humerus robustness index (HRI: $F = 6.154$), humeral head index (HHI: $F = 23.154$), humeral epicondylar index (EIh: $F = 66.815$), index of fossorial ability (IFA: $F = 11.224$), anteroposterior robustness of the forearm (URI*: $F = 4.232$), brachial index (BI: $F = 3.769$): femoral condylar index (EIf: $F = 88.646$), femoral head index (FHI: $F = 51.237$), tibial spine index (TSI: $F = 3.924$), crural index (CI: $F = 9.172$), intermembral index (IMI: $F = 6.495$), and cortico-diaphyseal index of the humerus (CDIh: $F = 15.858$) and femur (CDIf: $F = 23.811$). The rest of the indices i.e., the relative position of the deltoid tubercle (RDP), transverse robustness of the ulna (URI), robustness of the femur (FRI), transverse (TRI) and anteroposterior (TRI*) robustness of the tibia, as well as the vertebral index (VI) showed non-significant differences among ontogenetic stages ($P > 0.05$). The ontogenetic invariability of these indices also indicates a relatively proportional growth of their bone modules from juvenile to adult stages (Table 3.2; Fig. 3.3).

Index		Calculation	Functional significance
RDP	Relative position of the deltoid process	Humeral head-distal origin of deltoid process length divided by humeral length (DLH/HL)	An estimator of in-lever arm of the deltoid and pectoral muscles. Higher in specialized forms.
HRI	Humerus robustness index	Anteroposterior diameter at diaphysis divided by humeral length (APDH/HL)	Indicates robustness of the humerus and its ability to resist bending stresses in the anteroposterior axis.
Elh	Humeral epicondylar index	Epicondylar width of the humerus divided by humeral length (EH/HL)	Indicates the relative area available for the origin of the forearm flexors, pronators, and supinators and hence their degree of development.
HHI•	Humeral head index	Maximum diameter (anteroposterior) of humeral head divided by humeral length (HH/HL)	Represents the relative amount of articular surface of the glenohumeral joint and gives an idea of the extensiveness for anteroposterior movements of the humerus.
IFA	Index of fossorial ability	Olecranon length divided by the functional ulnar length (OL/FUL)	This index reflects the mechanical advantage of the triceps and dorsoepitrochlearis muscles during elbow extension.
URI	Robustness of the forearm	Transverse diameter of the ulna at the diaphyseal midpoint divided by functional ulnar length (TDU/FUL)	Reflects the resistance of the ulna to bending in the mediolateral axis and also indicates the relative surface available for the insertion of muscles involved in pronation and supination of the forearm and flexion of the manus and digits.
URI*	Robustness of the forearm (modified version)	Anteroposterior diameter of the ulna at the diaphyseal midpoint divided by functional ulnar length (APDU/FUL)	Similar to URI, but it reflects the resistance of the ulna to bending in the anteroposterior axis.
BI	Brachial index	Functional ulnar length divided by humeral length (FUL/HL)	Indicates the relative proportions of proximal (humerus) and middle (ulna) elements of forelimbs (forearm) and gives an indication of the extent to which the forelimb is apt for fast movement.
FRI	Femur robustness index	Transverse diameter of the femur at the diaphyseal midpoint divided by the functional femoral length (TDF/FL)	Indicates robustness of the femur and its ability to resist bending in the mediolateral axis and shearing stresses.
Eif	Femoral epicondylar index	Epicondylar width of the femur divided by femoral length (EF/FL)	Indicates the relative area available for the origins of the gastrocnemius and soleus muscles used in extension of the knee and plantar-flexion of the pes.
FHI•	Femoral head index	Maximum diameter of femoral head divided by femoral length (FH/FL)	Indicates the dimension of the femoral head.
TSI	Tibial spine index	Proximal tibia length (distance from the proximal articular surface of the tibia to the distal point of the tibial tuberosity), divided by the tibial length (UTL/TL)	Reflects the strength of the leg and the relative width available for the insertion of the gracilis, semitendinosus, and semimembranosus muscles and the foot flexors. Also hamstrings and biceps femoris muscles acting across the knee and hip joints.
TRI	Robustness of the tibia	Transverse diameter of the tibia divided by the tibial length (TDT/TL)	Indicates robustness of the tibia and its ability to resist bending in the mediolateral axis and shearing stresses.
TRI*	Robustness of the tibia (modified version)	Anteroposterior diameter of the tibia divided by the tibial length (APDT/TL)	Indicates robustness of the tibia and its ability to resist bending in the anteroposterior axis and shearing stresses.
CI	Crural index	Tibial length divided by femoral length (TL/FL)	Indicates the relative proportions of proximal (femur) and middle (tibia) elements of the hindlimb (foreleg). Indicates of how well the hindlimbs are apt for speed.
IMI	Intermembral index	Forelimb length divided by the hindlimb length [in this case, (HL + FUL)/(FL + TL)]	Indicates the length symmetry between fore and hindlimbs.
VI•	Vertebral index	Vertebral length divided by the total length of the individual (without considering tail length)	Indicates the proportion of the vertebral length in relation to body size, and it may evidence specific locomotor and reproductive features of the organism.
CDIh†	Cortico-diaphyseal index of the humerus	Ratio between the cortical thickness and the radius of the cross section	An index of strength and stiffness of tubular bones. Higher values would increase buckling resistance.
CDIf†	Cortico-diaphyseal index of the femur	Ratio between the cortical thickness and the radius of the cross section	An index of strength and stiffness of tubular bones. Higher values would increase buckling resistance.

TABLE 3.1 (*previous page*). Morpho-functional indices analyzed in this study, their calculation and functional significance. Measurements indicated above are illustrated in Figure 1. (†) Indices calculated with Bone Profiler (Girondot & Laurin, 2003). (*) Indices modified in this study (see text). (•) Indices created in this study. Indices and measurements follow mainly Howell (1965), Hildebrand (1985), Rose (1989), Vizcaíno *et al.* (1999, 2016), Currey (2002), Salton & Sargis (2008), Echeverría *et al.* (2014), Wilson & Geiger (2015) and references therein.

TABLE 3.2. Descriptive statistics (mean ± *SD*) of morpho-functional indices of *Bathyergus suillus* (top) and *B. janetta* (bottom). Females (F), males (M). Statistically significant indices (P < 0.001) are shown in bold (see text). See abbreviations in Table 3.1.

B. suillus	**Juveniles**		**Subadults**		**Adults**	
Index	**F (n = 5)**	**M (n = 5)**	**F (n = 8)**	**M (n = 8)**	**F (n = 12)**	**M (n = 6)**
RDP	0.589 ± 0.020	0.583 ± 0.029	0.599 ± 0.023	0.586 ± 0.017	0.592 ± 0.018	0.595 ± 0.020
HRI	0.134 ± 0.014	0.124 ± 0.007	0.120 ± 0.008	0.113 ± 0.008	0.120 ± 0.008	0.116 ± 0.011
HHI	0.238 ± 0.010	0.248 ± 0.007	0.235 ± 0.006	0.230 ± 0.010	0.220 ± 0.009	0.218 ± 0.009
EIh	0.381 ± 0.014	0.376 ± 0.017	0.346 ± 0.006	0.330 ± 0.017	0.322 ± 0.016	0.297 ± 0.012
IFA	0.372 ± 0.032	0.341 ± 0.023	0.339 ± 0.028	0.349 ± 0.023	0.315 ± 0.022	0.311 ± 0.019
URI	0.058 ± 0.006	0.058 ± 0.010	0.058 ± 0.006	0.061 ± 0.007	0.053 ± 0.006	0.050 ± 0.003
URI*	0.081 ± 0.006	0.082 ± 0.007	0.088 ± 0.007	0.088 ± 0.005	0.089 ± 0.007	0.085 ± 0.004
BI	0.867 ± 0.055	0.902 ± 0.047	0.872 ± 0.045	0.846 ± 0.020	0.903 ± 0.047	0.893 ± 0.015
FRI	0.109 ± 0.008	0.115 ± 0.007	0.121 ± 0.007	0.119 ± 0.009	0.121 ± 0.009	0.113 ± 0.005
EIf	0.302 ± 0.019	0.290 ± 0.008	0.250 ± 0.011	0.250 ± 0.013	0.231 ± 0.011	0.227 ± 0.009
FHI	0.158 ± 0.005	0.154 ± 0.008	0.144 ± 0.004	0.140 ± 0.008	0.130 ± 0.007	0.127 ± 0.006
TSI	0.453 ± 0.037	0.478 ± 0.028	0.488 ± 0.018	0.490 ± 0.018	0.490 ± 0.023	0.487 ± 0.019
TRI	0.087 ± 0.004	0.093 ± 0.007	0.095 ± 0.006	0.092 ± 0.007	0.097 ± 0.006	0.095 ± 0.006
TRI*	0.108 ± 0.009	0.131 ± 0.012	0.123 ± 0.011	0.123 ± 0.006	0.129 ± 0.015	0.128 ± 0.008
CI	0.993 ± 0.043	0.939 ± 0.041	0.935 ± 0.013	0.929 ± 0.027	0.923 ± 0.030	0.906 ± 0.023
IMI	0.835 ± 0.040	0.844 ± 0.017	0.845 ± 0.027	0.847 ± 0.011	0.857 ± 0.032	0.891 ± 0.016
VI	0.789 ± 0.017	0.795 ± 0.015	0.798 ± 0.008	0.799 ± 0.013	0.792 ± 0.011	0.790 ± 0.005
CDIh	0.373 ± 0.071	0.423 ± 0.082	0.459 ± 0.047	0.500 ± 0.065	0.523 ± 0.036	0.517 ± 0.031
CDIf	0.385 ± 0.064	0.415 ± 0.100	0.493 ± 0.114	0.591 ± 0.082	0.587 ± 0.048	0.638 ± 0.033

B. janetta			
Index	**Newborns** ***n* = 1**	**Juveniles** ***n* = 1**	**Adults** ***n* = 3; †(*n* = 2)**
RDP	0.567	0.528	0.554 ± 0.030
HRI	0.143	0.117	0.115 ± 0.008
HHI	0.298	0.236	0.214 ± 0.007
EIh	0.370	0.407	0.310 ± 0.015
IFA	0.366	0.291	0.286 ± 0.005 †
URI	0.071	0.070	0.050 ± 0.002 †
URI*	0.106	0.086	0.083 ± 0.006 †
BI	0.841	0.971	0.950 ± 0.015 †
FRI	0.098	0.083	0.110 ± 0.003
EIf	0.286	0.342	0.223 ± 0.007
FHI	0.143	0.161	0.128 ± 0.007
TSI	0.383		0.438 ± 0.023 †
TRI	0.107	0.082	0.088 ± 0.009 †
TRI*	0.148	0.125	0.136 ± 0.010 †
CI	0.927	0.951	0.972 ± 0.028 †
IMI	0.945	0.910	0.904 ± 0.033 †
VI	0.619	0.678	0.804 ± 0.002 †

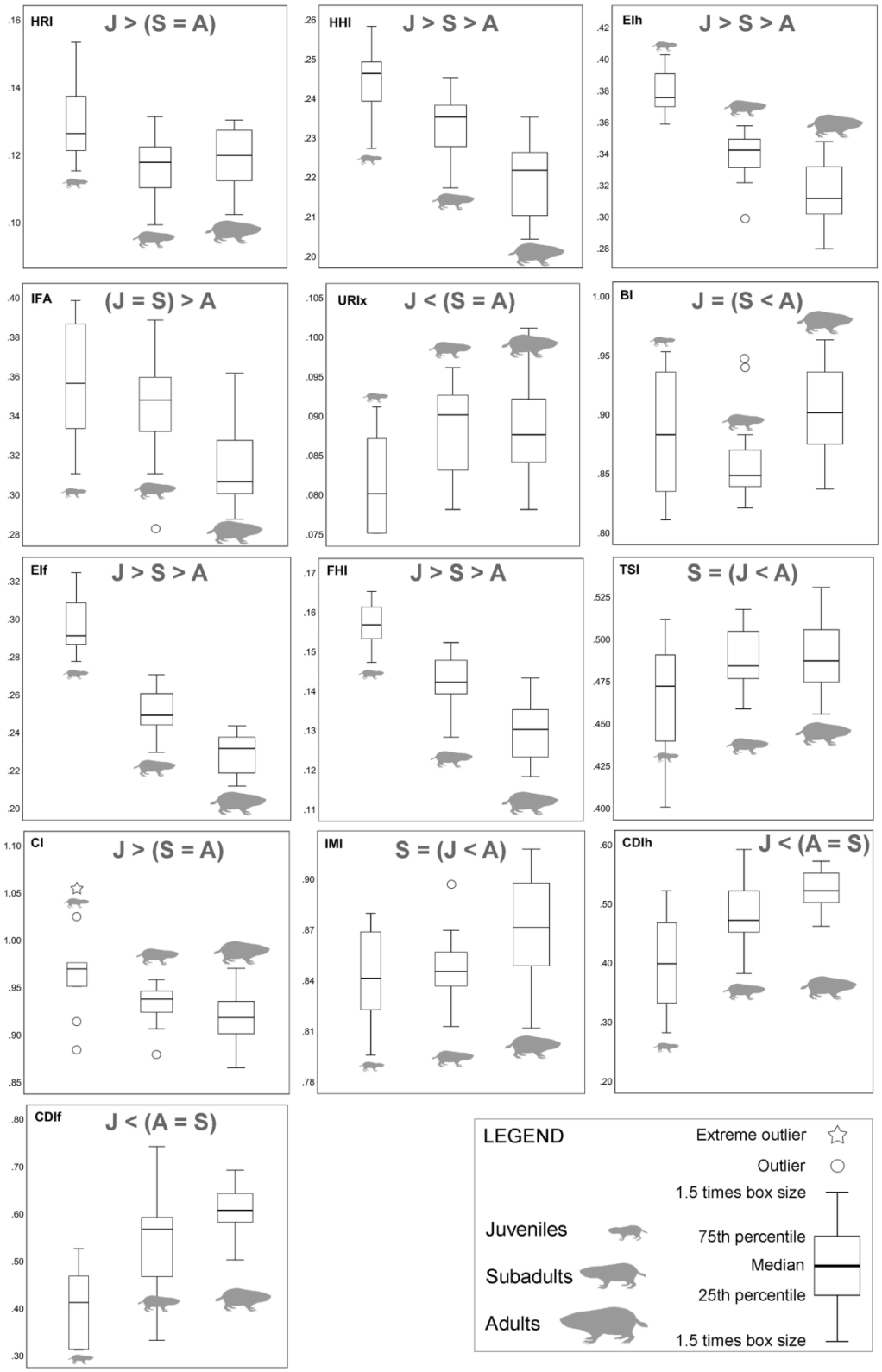

FIGURE 3.2. Box and whisker plots showing ontogenetic trends of statistically significant morpho-functional indices (13) of *Bathyergus suillus*. Significant differences, after post hoc correction (Scheffe's *F*) among juveniles (J), subadults (S) and adults (A) are shown for each index. Width of the boxes indicates sample size. Abbreviations: Humerus robustness index (HRI); Humeral head index (HHI); Humeral epicondylar index (EIh); Index of fossorial ability (IFA); Anteroposterior robustness of the forearm (modified version) (URI*); Brachial index (BI); Femoral condylar index (EIf); Femoral head index (FHI); Tibial spine index (TSI); Crural index (CI); Intermembral index (IMI); Cortico-diaphyseal index of the humerus (CDIh) and femur (CDIf).

Scheffe's *F* post hoc tests indicated that the humeral (HHI) and femoral head (FHI) indices, as well as the humeral (EIh) and femoral condylar (EIf) indices decreased from juvenile to adult stages (Fig. 3.2). Similarly, the index of fossoriality (IFA), humeral robustness (HRI) and crural index (CI) were higher in juveniles as compared to adults, although subadults showed variable values (Table 3.2; Fig. 3.2, 3.3). These trends contrast with the ontogenetic increase of the anteroposterior robustness of the forearm (URI*) and the cortico-diaphyseal index of the humerus (CDIh) and femur (CDIf), with subadults and adults showing similar means, but higher than juveniles (Table 3.2; Fig. 3.3, 3.2). Similarly, the tibial spine (TSI) and intermembral (IMI) indices also increased during ontogeny, with subadults displaying a more variable morphology. The brachial index (BI) of subadults tended to have lower values as compared to juveniles. In general, these data indicated that certain functional indices associated with better digging ability decreased with age (e.g., HRI, IFA), while others increased (e.g., URI*, CDIh). Similarly, indices associated to locomotor performance (i.e. CI, BI and IMI) showed different ontogenetic trends, although adults had a more symmetrical limb proportion than juveniles (IMI; Fig. 3.2).

The discriminant function analysis (DFA) showed a significant morphological differentiation between ontogenetic groups (Wilks' λ = 0.063; $F_{26, 60}$ = 6.825; P < 0.0001). The analysis yielded two discriminant functions (DF) accounting for 100% of the total variance of the data (Table 3.3; Fig. 3.4). The first axis (DF1) explained most of the morphological variability (91.8%), where the femoral condylar index (EIf) and crural index (CI) contributed the most to this function (Table 3.3; Fig. 3.4). This indicates that the most noticeable morphological changes in *B. suillus* occurred were observed in the hindlimb. The second discriminant function (DF2) accounted for 8.13% of variance, where the brachial index (BI) contributed the most (Table 3.3). Correlations obtained between ontogenetic groups and canonical variables for DF1 (Table 3.3) showed that juveniles and most subadults had negative DF1 scores for HRI, HHI, EIh, IFA, EIf, FHI and CI, which are correlated with more robust humeral diaphyses (HRI), greater humeral and femoral head articular surfaces (HHI and FHI), wider humeral and femoral condyles (EIh and EIf), longer olecranon processes (higher IFA) and more symmetric femoral and tibio-fibular proportions (CI) (Fig. 3.4). Adults (and some subadults) had positive DF1 scores for URI*, BI, TSI, IMI, CDIh and CDIf, indicating thicker anteroposterior ulnae, thicker cortical humeral (CDIh) and femoral (CDIf) cortical walls, larger tibial spine index (TSI) and more symmetrical forelimb (BI) and intermembral (IMI) proportions (Table 3.3; Fig. 3.4). Negative scores of (epi)condylar diameters (EIh and EIf) and size of the femoral head (FHI), as well as positive scores for cortico-diaphyseal indices (CDIh and CDIf) contributed the most to discriminate between ontogenetic groups (Table 3.3). Correlations of the DF2 were negative for HHI, EIh, IFA, URI*, FHi, TSI, CDIh and CDIf. Most subadults, some adults and two juveniles were represented by these negative scores, representing an intermediate group between the juvenile and adult centroids, although more closely related to adults, except for the index of fossorial ability, which is more similar to juveniles and one of the variables contributing most to this function (Table 3.3).

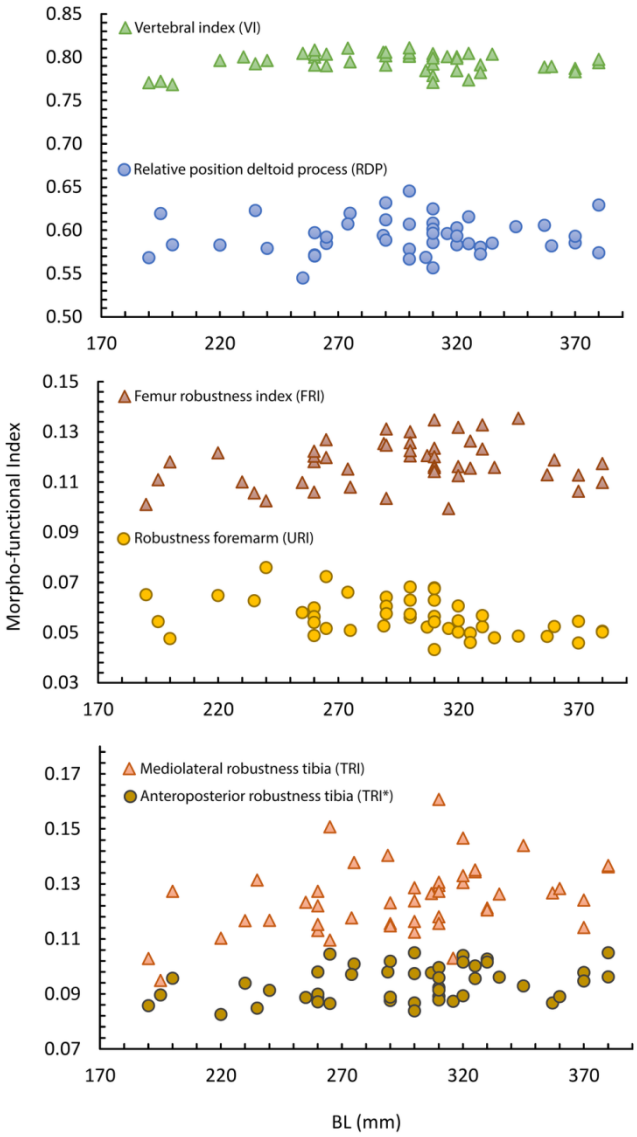

FIGURE 3.3. Growth trends of non-ontogenetically significant morpho-functional indices of *Bathyergus suillus*. Body length (BL) is used as the proxy of body size. Abbreviations: Relative position of the deltoid tubercle (RDP); transverse robustness of the ulna (URI); robustness of the femur (FRI); transverse (TRI) and anteroposterior (modified version, TRI*) robustness of the tibia; vertebral index (VI).

	Standardized canonical discriminant function coefficients		Correlations dependent vs canonical variables	
Functional index	DF1	DF2	DF1	DF2
HRI	0.22	0.415	−0.1489	0.35555
HHI	0.055	−0.539	−0.36366	−0.26923
EIh	−0.301	−0.071	−0.51435	−0.00298
IFA	0.347	−0.026	−0.25184	−0.34453
URI*	0.485	0.224	0.14403	−0.28333
BI	0.331	1.142	0.07235	0.51086
EIf	−1.09	0.734	−0.74997	0.16681
FHI	−0.319	−0.416	−0.55553	−0.24294
TSI	0.03	−0.304	0.14405	−0.22121
CI	0.793	−0.222	−0.20347	0.08391
IMI	0.274	−0.231	0.15256	0.24544
CDIh	0.16	−0.356	0.31706	−0.09125
CDIf	−0.108	0.487	0.35632	−0.14252
Eigenvalue	8.116	0.718		
% Variance	91.869	8.131		
Wilks' λ	0.064	0.582		

TABLE 3.3. Standardized canonical discriminant function coefficients, coefficient vs variable correlations, eigenvalues, Wilk's lambda and proportion of variance explained by each function.

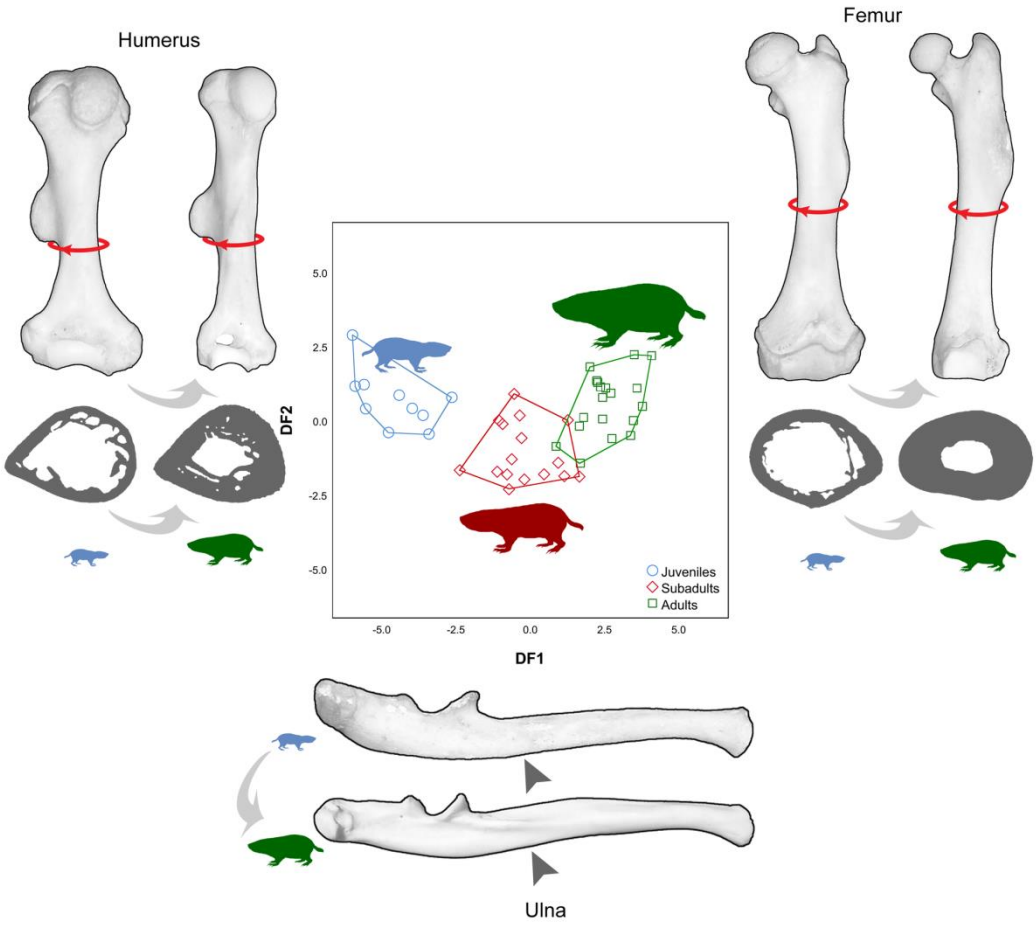

FIGURE 3.4. Scatterplot of DF1 and DF2 values showing ontogenetic morphological differentiation of the appendicular skeleton of *Bathyergus suillus*. Bones around the graph show the main differences of the external morphology and bone microanatomy between juveniles and adults (bones scaled to same size). Location of long bone cross-sections are indicated by a red ring. The arrow head in the ulna shows the area subjected to morphological change (URI*). Ulnae do not show the distal epiphysis.

3.3.2 Limb Bone Allometry

We reported a comprehensive data set of linear measurements and allometric growth trajectories for *B. suillus* (Table 3.4, 3.5; Fig. 3.5). Figure 5 shows the growth trends of the main endochondral and periosteal modules, where the longest and shortest bones are the ulna and humerus, respectively (Fig. 3.5A), the thickest and thinnest in anteroposterior direction are the tibia-fibula and ulna, respectively (Fig. 3.5B), and the thicker and narrower in mediolateral direction are the femur and ulna, respectively (Fig. 3.5C). RMA regressions of body size proxies against age classes (2-9) showed that the most variable proxy was body mass (BM, R^2 = 0.649), followed by body length (BL, R^2 = 0.711) and skull length (SKL, R^2 = 0.763). This is similar to previous reports of *B. suillus* showing considerable intrapopulation variability in BM later in ontogeny, which results in marked male-biased sexual dimorphism of adults (Hart *et al.*, 2007). These three proxies scaled isometrically with each other (Table 3.5). Regarding postcranial elements, most of them scaled isometrically with BM (65%) and BL (61%), although when scaled against SKL, a higher number of positive correlations were obtained (43%), with only 39%

showing isometry (Table 3.5). These data indicate that some postcranial elements have a distinct growth pattern in relation to SKL; particularly the forelimb length (H+U), humeral length (HL), ulnar length (UL) and femoral length (FL), among others, showed positive allometry with respect to the skull, although an isometric relationship with vertebral length (VL) persisted (Table 3.5). In general, 13 measures showed consistent scaling patterns for all proxies (Table 3.4). Seven showed isometry (TDH, APDH, TDU, UTL, DTFJ, FL+TL, VL), indicating that both endochondral and periosteal modules show proportional growth patterns with respect to body size. Two showed positive allometry (APDU, APDT) (Table 3.5), indicating that periosteal modules tended to grow proportionally larger than endochondral modules respect to proxies of body size. Four showed negative allometry (EH, OL, FH, EF), indicating that all epiphyseal and metaphyseal traits, associated to secondary centers of ossification, have a reduced contribution to the total growth of the bone (Table 3.5).

3.3.3 Endochondral Modules

The forelimb (H+U) showed higher slopes in comparison to the hindlimb (F+T) (Table 3.5). Particularly, the tibial length (TL) showed the slowest slopes for bone lengths, which explain the smaller size of this bone in comparison to the rest of the bones analyzed (Tables 4, 5; Fig. 3.5). The fact that the deltoid tubercle length (DLH) and functional ulnar length (FUL) showed higher slopes as compared to their respective total bone lengths (HL and UL, respectively), indicates a negative effect of their distal and proximal epiphysis, respectively, on the total elongation of these bones. This is because the growth plates of the distal humerus and proximal ulna fused before their contrary epiphyses.

3.3.4 Periosteal Module

Diaphyseal thickening (anteroposterior and mediolateral diameters) showed the highest slopes for each bone, except for the humerus, where an endochondral module showed the highest values (i.e. DLH; Table 3.5). Based on this, bone thickening was attained quickly in ontogeny in *B. suillus*. As mentioned before, in the humerus, bone elongation is prioritized over bone thickening, and transversal thickening (TDH) is prioritized over anteroposterior (APDH) thickening. The contrary occurs in the ulna, where anteroposterior thickening is prioritized. In general, all regressions showed high coefficients of determination ($R^2 > 0.80$; Table 3.5), although endochondral modules showed lower degrees of variation for those traits, and periosteal modules a higher degree of variation, especially the APDH and TDU.

TABLE 3.4 (*next page*). Descriptive statistics (mean ± *SD*) of linear measurements of *Bathyergus suillus*. See abbreviations in Table 3.1 and Figure 3.1.

B. suillus						
	Juveniles		**Subadults**		**Adults**	
Measurements	**F (n = 4)**	**M (n = 5)**	**F (n = 8)**	**M (n = 8)**	**F (n = 12)**	**M (n = 6)**
BM$^{(I)}$	370.500 ± 152.511	459.200 ± 124.560	623.250 ± 178.062	843.250 ± 225.816	991.670 ± 203.930	1497.670 ± 193.517
BL$^{(I)}$	228.750 ± 27.801	243.000 ± 26.599	275.380 ± 13.071	308.130 ± 13.076	317.750 ± 9.411	369.500 ± 9.670
VL$^{(I)}$	181.793 ± 25.245	193.396 ± 24.426	219.821 ± 11.188	246.216 ± 10.558	251.656 ± 7.494	291.960 ± 8.834
SKL$^{(I)}$	46.960 ± 2.765	49.606 ± 2.245	55.559 ± 2.895	61.914 ± 5.006	66.098 ± 4.272	77.543 ± 1.814
HL	27.823 ± 2.119	28.790 ± 2.026	34.414 ± 2.495	38.189 ± 3.379	40.279 ± 2.054	47.405 ± 1.989
HH	6.710 ± 0.734	7.138 ± 0.552	8.088 ± 0.478	8.761 ± 0.499	8.863 ± 0.286	10.300 ± 0.182
EH$^{(-)}$	10.655 ± 0.512	10.824 ± 0.983	11.900 ± 0.852	12.563 ± 0.824	12.937 ± 0.682	14.058 ± 0.353
DLH	16.535 ± 1.147	16.766 ± 1.226	20.645 ± 2.053	22.386 ± 2.138	23.860 ± 1.325	28.223 ± 1.841
TDH$^{(I)}$	3.388 ± 0.230	3.610 ± 0.274	4.296 ± 0.281	4.701 ± 0.311	4.885 ± 0.372	5.705 ± 0.405
APDH$^{(I)}$	3.765 ± 0.231	3.586 ± 0.318	4.141 ± 0.321	4.284 ± 0.286	4.832 ± 0.408	5.472 ± 0.400
UL	33.003 ± 3.612	34.792 ± 2.296	40.145 ± 3.324	43.578 ± 4.014	47.793 ± 3.313	55.495 ± 2.038
OL$^{(-)}$	8.795 ± 0.650	8.846 ± 0.619	10.126 ± 0.859	11.235 ± 0.945	11.403 ± 0.569	13.157 ± 0.454
FUL	24.208 ± 3.140	25.946 ± 1.880	30.019 ± 2.799	32.343 ± 3.245	36.391 ± 2.956	42.338 ± 2.009
TDU$^{(I)}$	1.873 ± 0.190	2.012 ± 0.350	2.314 ± 0.246	2.619 ± 0.256	2.528 ± 0.216	2.795 ± 0.186
APDU$^{(+)}$	2.678 ± 0.283	2.870 ± 0.222	3.529 ± 0.351	3.833 ± 0.284	4.257 ± 0.376	4.740 ± 0.229
FL	31.158 ± 3.103	33.448 ± 2.221	39.404 ± 2.478	43.201 ± 3.879	46.590 ± 3.002	52.837 ± 1.764
FH$^{(-)}$	4.880 ± 0.486	5.154 ± 0.296	5.675 ± 0.375	6.040 ± 0.271	6.045 ± 0.268	6.727 ± 0.355
EF$^{(-)}$	9.185 ± 0.412	9.692 ± 0.733	9.834 ± 0.271	10.779 ± 0.585	10.720 ± 0.376	11.992 ± 0.323
TDF	3.420 ± 0.172	3.854 ± 0.379	4.785 ± 0.519	5.116 ± 0.508	5.636 ± 0.527	5.968 ± 0.184
TL	30.403 ± 2.265	31.388 ± 2.286	36.831 ± 2.057	40.093 ± 3.485	42.953 ± 2.176	47.860 ± 1.353
UTL$^{(I)}$	14.145 ± 0.823	14.958 ± 0.570	17.980 ± 1.494	19.645 ± 2.028	21.043 ± 1.342	23.285 ± 1.186
DTFJ$^{(I)}$	17.948 ± 0.838	19.026 ± 0.964	21.976 ± 1.344	24.368 ± 1.985	25.590 ± 1.429	28.765 ± 1.288
TDT	2.668 ± 0.265	2.906 ± 0.261	3.496 ± 0.337	3.698 ± 0.397	4.150 ± 0.378	4.545 ± 0.367
APDT$^{(+)}$	3.335 ± 0.512	4.100 ± 0.332	4.539 ± 0.564	4.933 ± 0.443	5.554 ± 0.633	6.105 ± 0.341

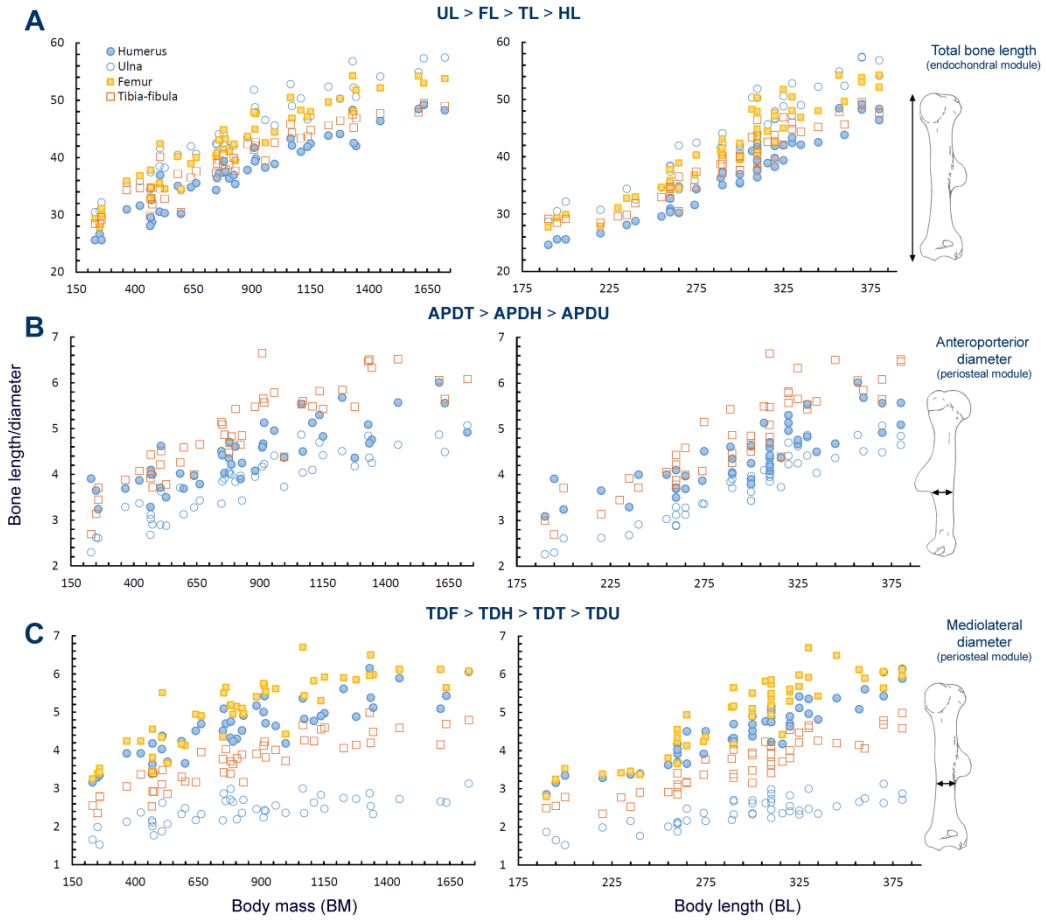

FIGURE 3.5. Ontogenetic growth trends of bone modules (elongation and thickening) in *Bathyergus suillus* plotted against body mass and body length. A) Endochondral bone modules showing the total bone lengths of the humerus (HL), ulna (UL), femur (FL) and tibia-fibula (TL). B) Periosteal bone module showing the anteroposterior diameters of the humerus (APDH), ulna (APDU) and tibia-fibula (APDT). C) Periosteal bone modules showing the mediolateral diameters of the humerus (TDH), ulna (TDU), femur (TDF) and tibia-fibula (TDT). Allometric equations are presented in Table 3.5.

TABLE 3.5 (*next page*). Regressions describing the ontogenetic postcranial growth patterns of *Bathyergus suillus*. Scaling relationship of 23 linear measurements of the appendicular system and vertebrae were assessed against body mass (BM), body length (BL) and skull length (SKL). Isometry (I), positive (+) and negative (-) allometry are showed next to the slope. See abbreviations in Table 3.1 and Figure 3.1.

BM vs							BL vs					SKL vs				
Bone	**Variable**	***Y*-intercept**	**Slope**		**CI limits (slope)**	R^2	***Y*-intercept**	**Slope**		**CI limits (slope)**	R^2	***Y*-intercept**	**Slope**		**CI limits (slope)**	R^2
Body size	BL	1.596	0.304	(I)	0.270; 0.339	0.885										
Skull size	SKL	0.869	0.317	(I)	0.277; 0.343	0.906	−0.698	1.004	(I)	0.850; 1.110	0.903					
Humerus	HL	0.560	0.349	(I)	0.311; 0.377	0.912	−1.138	1.095	(I)	0.966; 1.179	0.930	−0.396	1.100	(+)	1.041; 1.159	0.970
	HH	0.153	0.268	(−)	0.245; 0.293	0.885	−1.237	0.875	(−)	0.822; 0.935	0.941	−0.644	0.880	(I)	0.775; 1.001	0.896
	EH	0.495	0.207	(−)	0.179; 0.231	0.819	−0.565	0.670	(−)	0.585; 0.730	0.830	−0.105	0.670	(−)	0.586; 0.764	0.815
	DLH	0.296	0.362	(I)	0.315; 0.397	0.894	−1.482	1.142	(I)	0.979; 1.249	0.890	−0.704	1.146	(+)	1.062; 1.243	0.938
	TDH	−0.313	0.336	(I)	0.283; 0.377	0.791	−2.000	1.075	(I)	0.943; 1.174	0.885	−1.264	1.076	(I)	0.9749; 1.18	0.861
	APDH	−0.209	0.296	(I)	0.229; 0.352	0.666	−1.656	0.931	(I)	0.713; 1.077	0.720	−1.033	0.941	(I)	0.801; 1.076	0.786
Ulna	UL	0.633	0.348	(I)	0.303; 0.377	0.897	−1.067	1.094	(I)	0.913; 1.191	0.885	−0.315	1.094	(+)	1.031; 1.162	0.947
	OL	0.225	0.279	(−)	0.233; 0.315	0.791	−1.100	0.863	(−)	0.707; 0.975	0.840	−0.524	0.873	(−)	0.799; 0.940	0.893
	FUL	0.419	0.379	(I)	0.326; 0.412	0.885	−1.440	1.195	(+)	1.018; 1.312	0.864	−0.611	1.190	(+)	1.104; 1.279	0.926
	TDU	−0.519	0.312	(I)	0.250; 0.369	0.584	−1.966	0.950	(I)	0.764; 1.103	0.697	−1.331	0.960	(I)	0.770; 1.120	0.635
	APDU	−0.550	0.390	(+)	0.332; 0.432	0.836	−2.487	1.239	(+)	1.091; 1.338	0.906	−1.648	1.246	(+)	1.110; 1.369	0.896
Forelimb	H + U	0.804	0.360	(I)	0.316; 0.387	0.915	−0.957	1.133	(I)	0.973; 1.223	0.911	−0.180	1.133	(+)	1.073; 1.206	0.963
Femur	FL	0.645	0.339	(I)	0.305; 0.366	0.910	−1.080	1.094	(I)	0.954; 1.187	0.915	−0.327	1.094	(+)	1.020; 1.174	0.961
	FH	0.170	0.207	(−)	0.177; 0.234	0.822	−0.877	0.665	(−)	0.538; 0.754	0.832	−0.417	0.664	(−)	0.575; 0.753	0.843
	EF	0.525	0.172	(−)	0.151; 0.189	0.831	−0.311	0.539	(−)	0.455; 0.606	0.837	0.058	0.539	(−)	0.488; 0.588	0.863
	TDF	−0.418	0.386	(I)	0.323; 0.432	0.772	−2.452	1.273	(+)	1.079; 1.416	0.833	−1.547	1.256	(+)	1.097; 1.411	0.837
Tibio-fibula	TL	0.715	0.304	(−)	0.268; 0.327	0.896	−0.781	0.961	(I)	0.820; 1.056	0.897	−0.114	0.957	(I)	0.894; 1.017	0.947
	UTL	0.331	0.329	(I)	0.279; 0.364	0.858	−1.405	1.086	(I)	0.920; 1.198	0.877	−0.648	1.080	(I)	0.969; 1.190	0.917
	DTFJ	0.496	0.303	(I)	0.261; 0.331	0.863	−1.053	0.981	(I)	0.824; 1.076	0.887	−0.374	0.978	(I)	0.907; 1.056	0.941
	TDT	−0.478	0.362	(I)	0.303; 0.406	0.817	−2.276	1.150	(I)	0.960; 1.289	0.831	−1.486	1.150	(+)	1.029; 1.258	0.869
	APDT	−0.460	0.399	(+)	0.342; 0.448	0.840	−2.485	1.285	(+)	1.106; 1.441	0.833	−1.568	1.265	(+)	1.094; 1.443	0.833
Hindlimb	F + T	0.983	0.321	(I)	0.286; 0.345	0.910	−0.624	1.025	(I)	0.889; 1.118	0.913	0.327	0.889	(I)	0.709; 1.068	0.867
Vertebrae	BL-SKL	1.488	0.307	(I)	0.271; 0.349	0.846	−0.141	1.017	(I)	0.992; 1.058	0.993	0.565	1.013	(I)	0.868; 1.181	0.849

3.3.5 Development of Diaphyseal Bone Superstructures

The position of superstructures within the diaphysis does not undergo considerable changes (i.e., scarce longitudinal diaphyseal drift). The distal origin of the deltoid tubercle (DLH%) is similar between sexes and ages: juveniles (♀ = 58.28%; ♂ = 58.40%); subadults (♀ = 59.91%; ♂ = 59.91%); adults (♀ = 59.25%; ♂ = 59.64%). This is also reflected by the RDP index (Fig. 3.3). The olecranon (OL%) tended to decrease in relative size, becoming restricted to the distal portion of the ulna: juveniles (♀ = 26.35%; ♂ = 25.43%); subadults (♀ = 25.22%; ♂ = 25.54%); adults (♀ = 23.72%; ♂ = 23.40%). This is also reflected in the IFA index (Fig. 3.2). The distal point of the tibial tuberosity (UTL%) increases slightly during ontogeny: juveniles (♀ = 45.43%; ♂ = 47.80%); subadults (♀ = 48.77%; ♂ = 49.10%); adults (♀ = 49.01%; ♂ = 48.87%). This is also observed in the TSI index (Fig. 3.2). The position of the distal tibio-fibular junction (DTFJ%) does not change in males, although females have a more proximal tibio-fibular junction than males in early ontogeny: juveniles (♀ = 57.49%; ♂ = 60.62%); subadults (♀ = 59.67%; ♂ = 60.75%); adults (♀ = 59.58%; ♂ = 60.04%). Overall, this indicates an isometric position of superstructures during ontogeny, and that juvenile females have a shorter tibial tuberosity and tibio-fibular junction than males, although a larger olecranon process.

3.3.6 Epiphyseal Fusion

In general, except for the humerus, growth plates fused quite late in ontogeny (Table 3.6). From all growth plates analyzed, the distal humerus fused first; some juveniles showed totally fused epiphyses, while all subadults and adults have fused them. The proximal epiphysis of the humerus never fuses. In the ulna, only a few adults fused the olecranon (mainly females), whereas the styloid process never fuses in males and it was fused in only one female. In the femur, only a few adults showed the femoral head and greater trochanter fused, but the condyles were never fused. In the tibia-fibula, the proximal epiphysis never fused, whereas the cochlea is fused in all the adults.

3.3.7 Sex Differences of Morpho-Functional Indices

Although the MANOVA did not show sex differences, the univariate ANOVAs found significant differences ($P < 0.05$) for the humeral robustness index (HRI: $F = 5.844$), epicondylar index (EIh: $F = 11.592$), robustness of the tibia (TRI: $F = 4.757$), crural index (CI: $F = 7.566$) and cortico-diaphyseal index of the femur (CDIf: $F = 5.27$). Females have wider anteroposterior (higher HRI) and epicondylar humeral diameters (higher EIh) than males (Table 3.2). Females also have a more symmetric bone growth between the femur and the tibio-fibula (higher CI). However, males have wider mediolateral thicknesses of the tibia (TRI) and thicker cortical femoral walls (CDIf) as compared to females. In general, these differences indicated that periosteal and (epi)condylar modules grew relatively more in the humeri and tibiae of females and that the periosteal/endosteal apposition was higher in the hindlimbs of males.

TABLE 3.6. Number of specimens showing proximal (p) and distal (d) fusion of epiphysis in *Bathyergus suillus* and *B. janetta*. The suggested bone growth direction (SGD), based on fusion and allometric growth trajectories (see Table 3.5) is also indicated. Sample size is shown in parentheses.

B. suillus					
Bone	**Epiphyses**	**Juveniles**	**Subadults**	**Adults**	**SGD**
Humerus	Humeral head (p)	0 (10)	0 (17)	0 (19)	Proximal
	Trochlea + Capitellum (d)	8 (10)	17 (17)	19 (19)	
Ulna	Olecranon (p)	0 (10)	0 (17)	8 (19)	Distal
	Styloid process (d)	0 (10)	0 (17)	1 (19)	
Femur	Femoral head (p)	0 (11)	0 (17)	4 (19)	Distal?
	Greater trocanter (p)	0 (11)	0 (17)	13 (19)	
	Condyles (d)	0 (11)	0 (17)	3 (19)	
Tibia-fibula	Condyles (p)	0 (11)	0 (17)	0 (19)	Proximal
	Cochlea (d)	0 (11)	2 (17)	17 (17)	
B. janetta					
Bone	**Epiphyses**	**Newborns**	**Adults**		**SGD**
Humerus	Humeral head (P)	0 (1)	0 (4)		Proximal
	Trochlea + Capitellum (D)	0 (1)	4 (4)		
Ulna	Olecranon (P)	0 (1)	0 (2)[1]		Distal
	Styloid process (D)	0 (1)	0 (2)		
Femur	Femoral head (P)	0 (1)	0 (4)[1]		Distal
	Greater trocanter (P)	0 (1)	0 (4)[2]		
	Condyles (D)	0 (1)	0 (4)		
Tibia-fibula	Condyles (P)	0 (1)	0 (2)		Proximal
	Cochlea (D)	0 (1)	0 (2)[2]		

3.3.8 Developmental Functional Morphology of Namaqua Dune Molerats (*Bathyergus janetta*)

The inclusion of *B. janetta* in this study helped to understand the initial stages of perinatal limb bone development in the scratch-digger lineage, *Bathyergus*. Since only six specimens were studied for *B. janetta*, we only describe the main developmental and morphological changes of *B. janetta* and highlight its differences with *B. suillus*. Gross anatomical shape is attained early in postnatal ontogeny (Fig. 3.6). In the two days old newborn, the primary ossification fronts are widely spread towards the bone ends, and chondroepiphyses are already quite differentiated, but apparently still lacking secondary centers of ossification (Fig. 3.6). Secondary centers are usually developed a few days after birth in rodents (Johnson, 1933; Patton & Kaufman, 1995; Sánchez-Villagra, 2002; Farnum, 2007). In this specimen, the teres major process of the scapula, which is a ventral prolongation associated with the origin of the teres major muscle, and therefore, highly developed in adult subterranean rodents (Fernández *et al.*, 2000; Echeverría *et al.*, 2014), was already differentiated and well-developed but still cartilaginous (Fig. 3.6). Similarly, in the humerus, the deltoid tubercle was also well formed in anterolateral projection and mostly ossified, although cartilage still evident on the edges (Fig. 3.6). In the juvenile specimen, the cartilaginous portion of the teres major process has considerably been reduced, and the secondary centers of ossification are visible. In this specimen, the deltoid tubercle was totally ossified (i.e. no remnants of cartilage). The ulna of the newborn has a well differentiated

and robust olecranon process which extends considerably behind the elbow, but it is also still cartilaginous, while the trochlear notch is ossified. In the juvenile, these features appear considerably more ossified, and the cartilaginous portions reduced. In the femur of the newborn and juvenile, the greater trochanter is well differentiated but still cartilaginous, and the third trochanter is well ossified in the juvenile. The fibula is already fused to the tibia along the distal third of their diaphysis, but still shows a groove at their distal portions (Fig. 3.6). The anteromedial position of the tibia and the posterolateral position of the fibula do not change from newborn to adult stages, although the distal groove between the fused tibia and fibula disappears in the latter. In general, the ossification process seems to occur more rapidly in the forelimb.

Out of 17 morpho-functional indices calculated for *B. janetta*, most of them (11) tended to decrease during ontogeny (HRI, HHI, EIh, IFA, URI, URI*, EIf, FHI, TRI, TRI*, IMI), five tended to increase (FRI, TSI, CI, VI, BI), and one maintained their values (RDP; Table 3.2). Most indices showed a similar ontogenetic pattern to *B. suillus*, although some differences were noted when adults were compared; *B. janetta* showed a more proximally located deltoid tubercle (RDP), a higher brachial (BI) and crural indices (CI), as well as lower tibial spine index (TSI) and tibial robustness (TRI). Interestingly, the index of fossorial ability (IFA) in *B. janetta* showed slightly lower values as compared to *B. suillus*, although it also decreases during ontogeny.

Regarding the development of superstructures in *B. janetta*, the DLH% does not vary during ontogeny [newborn = 56.68%; juvenile = 52.78; adults (n = 4) = 55.42%], OL% decreased [newborn = 26.80%; juvenile = 22.53; adults (n = 2) = 22.25%], UTL% increased [newborn = 38.29%; adults (n = 2) = 43.81%], and DTFJ% also decreases [newborn = 61.00%; juvenile = 60.17%; adults (n = 2) = 55.95%]. In general, these features showed some similar growth trends during ontogeny as compared to *B. suillus* (except DTFJ%), although the deltoid tubercle (DLH%), tibial tuberosity (UTL%) and distal tibio-fibular junction (DTFJ%) are more proximally located in *B. janetta*.

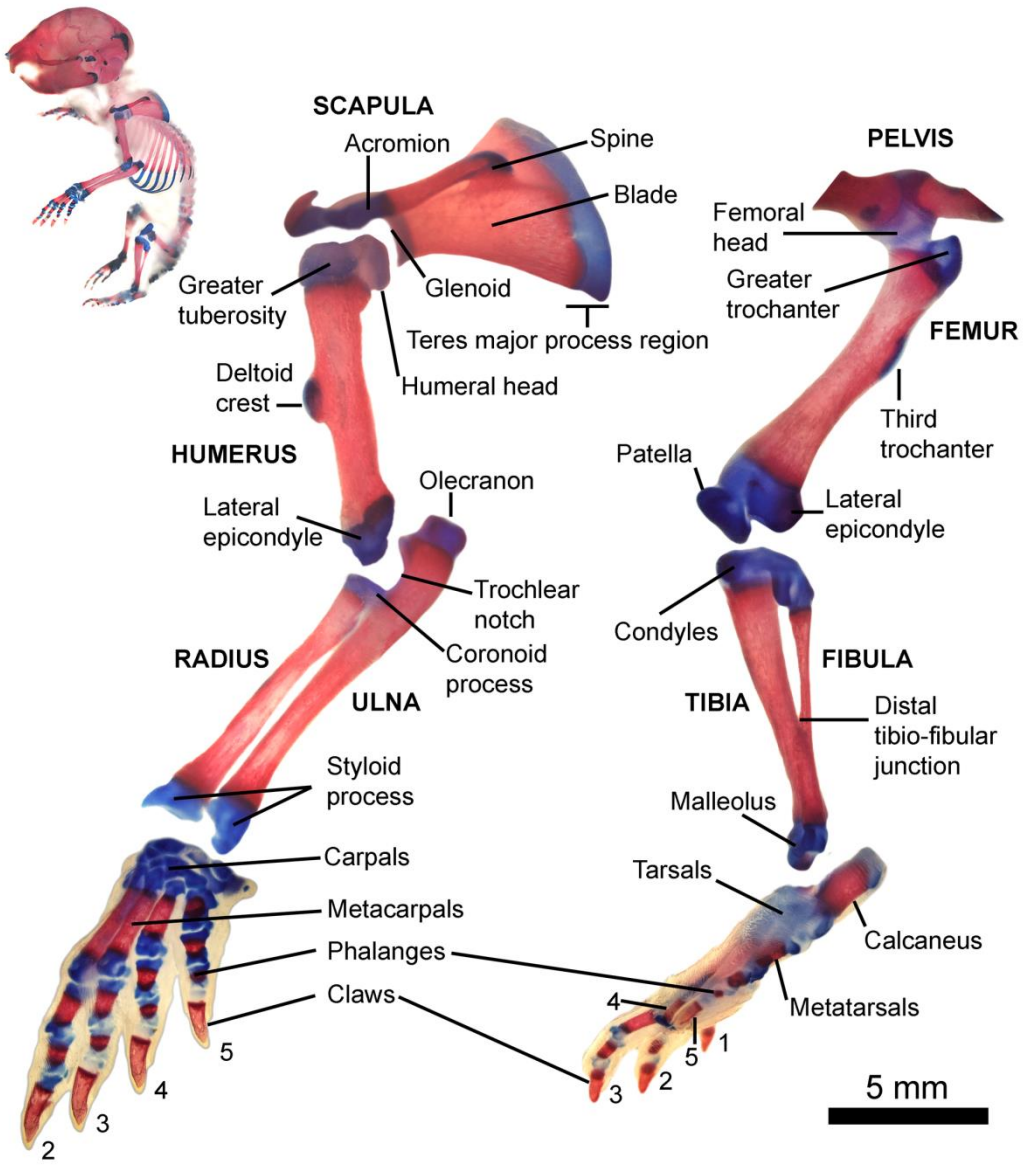

FIGURE 3.6. Cleared and double stained (alcian blue/alizarin red) skeleton of *Bathyergus janetta* (newborn, two days old) showing the early postnatal development of the appendicular skeleton (cartilage appears blue and bone matrix appears pink). This specimen showed wide extension of primary ossification centers and well-developed chondroepiphyses. Note the relatively well-developed teres major process, deltoid tubercle and olecranon in the forelimb, as well as a well-developed third trochanter and distal tibio-fibular junction in the hindlimb.

3.4 DISCUSSION

3.4.1 Development of the Skeletal Phenotype in *B. suillus*

Our results showed that juveniles of *B. suillus* have a highly specialized scratch-digging skeletal phenotype in forelimbs and hindlimbs. This phenotype is characterized by a set of external features associated with the improvement of digging ability, particularly by increasing the surface area available for muscle attachment at (epi)condyles and olecranon (e.g. Lessa & Stein, 1992; Vizcaíno *et al.*, 2016). This contrasts with the observed external morphology of adults (Fig. 3.4).

Juveniles have more robust humeri (higher HRI), a relatively enlarged (epi)condylar area in both the humerus (EIh) and femur (EIf), and a relatively larger olecranon process (IFA) (Table 3.2; Fig. 3.4). Bone superstructures associated with increased functional ability such as a more developed teres major process and a distal development of the deltoid tubercle (e.g. Elissamburu & De Santis, 2011; Echeverría *et al.*, 2014; Vizcaíno *et al.*, 2016) were also observed in juveniles, as well as in the newborn and juvenile of the closely related species *B. janetta* (Table 3.2, Fig. 3.6). Given the close haplotypic affinities within *Bathyergus* (Visser *et al.*, 2014), it is expected that the newborns of *B. suillus* would also show an early development of such bone superstructures. These features are generally absent or have a later development in cursorial and semifossorial mammals (Elissamburu & De Santis, 2011; Echeverría *et al.*, 2014). Thus, these findings support the particularity of the scratch-digging phenotype in *Bathyergus,* as well as its more precocial development as compared to other mammals. Later in life, an ontogenetic shift in bone morphology is observed (Fig. 3.7). The adults become more gracile in external shape, although they showed more robust ulnae in the anteroposterior direction (URI*), much more developed humeral (CDIh) and femoral (CDIf) cortical walls, and more developed tibial spines (TSI) (Table 3.2; Fig. 3.4, 3.7). Subadults showed an intermediate transitional stage of bone growth (Table 3.2, Fig. 3.3, 3.2, 3.4).

The features that contributed the most to morphological differentiation were found in the femur (Table 3.3; Fig. 3.3, 3.2, 3.4). In adults, the femur underwent a considerable condylar reduction, reaching a more gracile design with reduced relative area for muscles associated with the extension of the knee and plantar flexion of the pes. Comparatively, the forelimb varied relatively less during ontogeny, indicating that the phenotype of the humerus and ulna were reached earlier than in the femur and tibia-fibula. This can be related to the premature fusion of epiphyses in the forelimb, specifically the distal epiphysis of the humerus (Table 3.6), which clearly limits further growth at the epicondyles. These observations corroborate our initial hypothesis of an earlier development for the forelimb, probably associated with functional requirements for digging in this genus. Within the forelimb, the humerus showed lower morphological variation (Table 3.3), while the ulna underwent more modifications, especially in terms of the index of fossorial ability (IFA). Allometric trends also supported a faster relative development (in length) of the forelimb as compared to the hindlimb (Table 3.5). A similar pattern of skeletal development is observed in other rodents, where forelimbs reach adult size before hindlimbs, and the humerus before the ulna (Green & Fekete, 1933; Munyer, 1964; Patton & Kauffman, 1995). The faster maturity of the humerus among zeugopodial and stylopodial elements seems to be a generalized pattern in mammals (Sánchez-Villagra, 2002; Bennett & Goswami, 2011), most probably due to its earlier embryological development (Hill & Lettice, 2016), but also because of its biomechanical implications (Sánchez-Villagra, 2002) and/or early growth plate closure (e.g. Geiger *et al.*, 2014).

In general, our results are similar to those found by Hart *et al.* (2007) for cranial features of *B. suillus* from the same population. These authors used multivariate analyses of craniometric data of 187 individuals, and found clear differentiation between juveniles and adults, with subadults representing a

transitional stage (more closely related to adults), where a hypothetical growth curve for body size begins to stabilize. Similarly, our study also showed that subadults and adults are more similar (Fig. 3.2, 3.4), and that growth stabilization (depicted from morpho-functional trends, Fig. 3.2) would also occur during the subadult-adult transition, at least for some traits (Fig. 3.2). Thus, several postcranial elements followed similar growth trends as body size parameters, which is further supported by the fact that most linear measurements scaled isometrically with body size (Table 3.5). Despite the finding of significant morphological changes in *B. suillus*, the main features of their postcranial skeleton were already expressed in the newborn, and therefore the subsequent changes observed later in ontogeny are rather related to modifications in growth trends (heterochronic patterns) than to development, which does not differ from the typical mammalian growth pattern (e.g. Atchley & Hall, 1991; Smith, 1996).

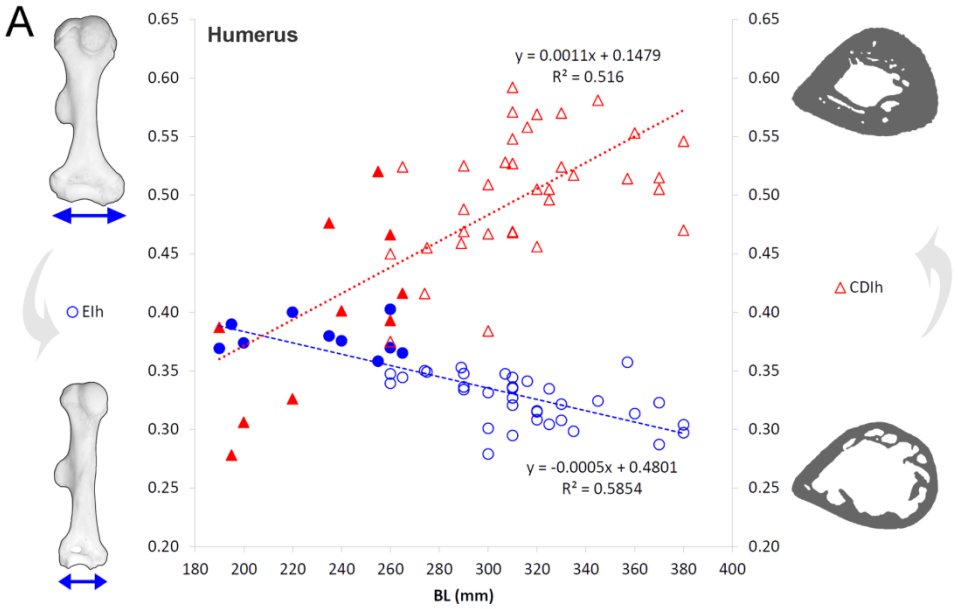

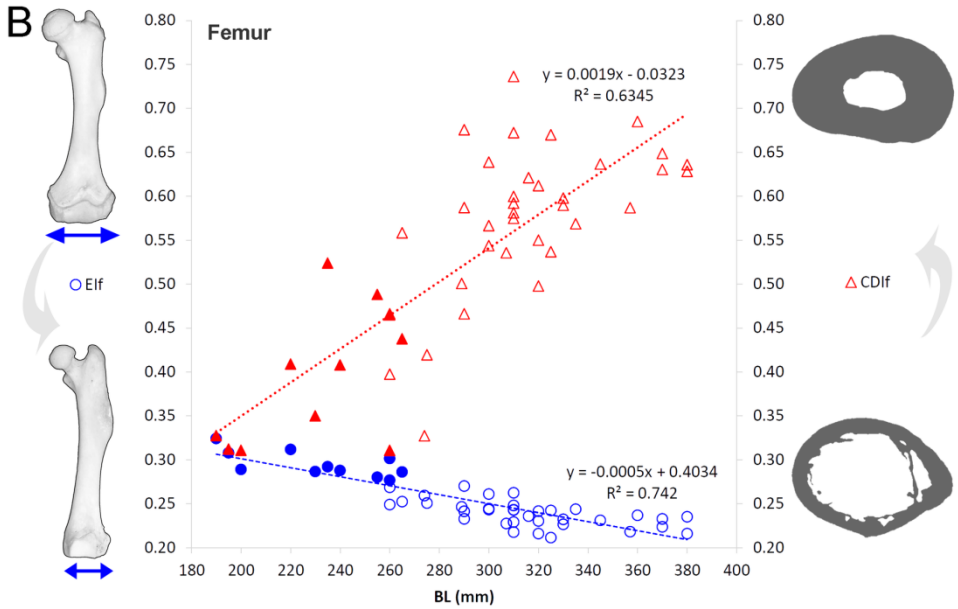

FIGURE 3.7 *(previous page).* Morphological shift during the ontogeny of *Bathyergus suillus*. Linear ordinary least–square (OLS) regressions show the relationship between morpho-functional indices and microanatomical parameters. The juvenile-subadult transition represents a period of morphological change where long bones become externally slender but internally thicker during ontogeny. A) Humeral epicondylar index (EIh, circles) and cortico-diaphyseal index of the humerus (CDIh, triangles). B) Femoral condylar index (EIf, circles) and cortico-diaphyseal index of the femur (CDIf, triangles). Data are plotted against body length (BL). Filled symbols indicate juveniles. The blue arrow below bones indicates magnitude of (epi)condylar growth in relation to bone length.

3.4.2 Timing and Causes of Ontogenetic Shifts in Bone Morphology

By using a multiscale approach, we observed how *Bathyergus* despite having slender bones with age (decreased HRI, EIh, EIf), also had thicker bone cortices (CDIh, CDIf; Fig. 3.7). Previously, Montoya-Sanhueza & Chinsamy (2017) described the thin cortical walls of juveniles, as well as the considerable amounts of periosteal and endosteal bone apposition of adults, which is also observed in *B. janetta* (e.g. G. Montoya-Sanhueza, unpubl. data, 2018). The cortical bone of juvenile mammals is generally composed of woven bone and/or fibrolamellar bone (Klevezal, 1996; Chinsamy, 2005; Chinsamy-Turan, 2012). The higher proportion of vascularized areas (Martin, 2003), as well as high bone turnover resulting from metaphyseal relocation during early ontogeny result in increased endosteal and intracortical porosity of the diaphysis, which contribute to decreased bone strength of young bone (Enlow, 1963; Altman *et al*, 2015; Montoya-Sanhueza & Chinsamy, 2018). The ossified matrix of these tissues also have lower biomechanical material properties as compared to lamellar or secondary bone tissues developed later in ontogeny (Currey, 2002). For these reasons, it has been hypothesized that mammalian juveniles have better built bones in external morphology as a strategy to increase geometric robusticity and hence reduce the risk of fractures of "weaker" young bone matrix, as well as to increase their effective force by altering muscles' line of action and thus compensating for their lower muscular development (Carrier, 1983; Young *et al.*, 2010; Echeverría *et al.*, 2014). This may explain the more robust external anatomy of newborns and juveniles of *Bathyergus*, while thicker cortical walls in adults (with higher bone mass) will provide higher bending resistance to increased muscle loading due to higher digging demands (Casinos *et al.*, 1993; Echeverría *et al.*, 2014). Interestingly, these morphologies develop at different ontogenetic stages in *Bathyergus* (Fig. 3.7, 8), suggesting that their causes also differ.

It has been traditionally suggested that the onset of particular behaviors and locomotor activities directly stimulate the genetic expression of the external morphology of subterranean rodents, and that features established early in ontogeny would have a direct genotypic regulation (e.g. Cubo *et al.*, 2006; Echeverría *et al.* 2014). The latter authors suggested that the early digging behavior of the solitary subterranean rodent *Ctenomys talarum* (Caviomorpha, Ctenomyidae), appearing at ~15-20 days may influence their external morphology (Echeverría *et al.*, 2014, 2016). In *Bathyergus*, newborns of *B. janetta* showed a highly specialized phenotype, indicating that this condition is prenatally acquired and that other –intrinsic– factors may explain the formation of its main design (e.g. Hall, 1978). In fact, experimental observations in other mammals have shown how

embryonic rudiments of bone and cartilage exhibiting many of their morphological features are developed even when allowed to grow in organ cultures, subcutaneously, intramuscularly, intracerebrally, or on the chorioallantoic membrane (Hall, 1978; and references therein). The differences between *Bathyergus* and *C. talarum* suggest that subterranean species may vary in terms of the adaptive processes responsible for their adult skeletal phenotype. However, there is increasing evidence showing that a variety of molecular, physiological and mechanical stimuli play important roles on morphogenesis and prenatal ossification (Sharir *et al.*, 2011; Felsenthal & Zelzer, 2017). Thus, the assumption that perinatally developed traits are principally controlled by genetic factors, assuming a lower exposure to mechanical stimuli is inaccurate. The attainment of the fundamental form of the skeleton, as well as the presence of bone superstructures such as condyles, articular surfaces, tuberosities, and grooves are independent of both functional demand and biomechanical factors, while the position of structures associated with muscle and ligament attachment (e.g. deltoid tubercle) may depend relatively more upon the functional demands to which the skeleton is subjected (Murray, 1936; Hall, 1978) and requires further study. The effects of prenatal muscle kinesis in *Bathyergus*, as well as in many other subterranean species are almost completely unknown and it may have an important impact on the normal development of epiphyses and joints such as the (epi)condylar breadth, even when these regions are still chondroepiphyses (e.g. Carter *et al.*, 1998; Cairns *et al.*, 2010). Similarly, (epi)condyles are regions directly associated with sites for muscle and tendon attachment, thus receiving direct biomechanical stimulation as compared to regions without it (e.g. diaphysis).

Differences in load bearing stresses experienced at early perinatal stages also may contribute to the development of such features. Both epicondylar and condylar growth start to decrease when individuals are 260-280 mm in body length (BL) and ~600 g in body mass (BM), which seems to coincide with increments in cortical bone thickness (Fig. 3.7). It appears that newborns and juveniles are exposed to several stimuli before the onset of digging behaviors and dispersal. A set of behaviors that could impose special selective mechanical pressures for an adequate bone growth are agonistic displays. In general, agonistic behaviors in rodents involve considerable stimulation of the musculoskeletal system (e.g. Carrier, 1983, 1996). Intersibling sparring in *B. suillus* begins quite early in ontogeny, at day 12 (Bennett *et al.*, 2009), when individuals weigh approximately 50 g (Bennett *et al.*, 1991). This activity usually involves incisor-locking and bracing themselves with the forefeet to pull one another. The intensity of this display increases with age, until injury is inflicted, or the individuals disperse (Bennett & Faulkes, 2000). Our smaller specimens weighed approximately 250 g, so it is assumed that they already went through sparring behavior. Sparring in bathyergids is developed more precocially in solitary molerats as compared to social species (Bennett *et al.*, 1991; Bennett & Faulkes, 2000). This behavior is also quite specialized as compared to the simpler "playful" fight documented for laboratory rats, in which it starts later in life (20 days old) and only becomes more aggressive at 6 months old, but rarely ending with bites among conspecifics (Scott, 1966). In *C. talarum*, pups express play fighting (rough-and-tumble play) early in ontogeny (8 days old), although this behavior does not involve aggression till later in

ontogeny (after weaning, ~31-58 days old) where strong mutual bites are observed in the snout (Zenuto *et al.*, 2002; Echeverría, 2011).

Although *B. suillus* and *C. talarum* are solitary species with a considerable degree of intraspecific aggressiveness and territoriality (Bennett & Faulkes 2000; Echeverría, 2011), *B. suillus* has a more robust body, especially males, which show body size-related sexual dimorphism and a thick skin layer on the ventral surface of the neck, suggesting that fighting represents an important aspect for prime burrow positions neighboring those of females (Davies & Jarvis, 1986; Hart *et al.*, 2007). *Ctenomys talarum* seems not to show conspicuous sexual dimorphism (Vassallo & Mora, 2007; Echeverría *et al.*, 2014), and its body appearance is more stylized (Nevo, 1999), probably allowing better agility (both above and belowground) to escape from predators (e.g. Luna & Antinuchi, 2003). Field observations of adult *B. suillus* show that they move quite slowly aboveground and lack fast escaping abilities (e.g. G. Montoya-Sanhueza, pers. obs., 2018). For these reasons, the earlier development of agonistic behaviors in *B. suillus* may play important roles for the attainment of their external morphology, suggesting that its body shape is apparently selected for a better built body phenotype to assist with multiple functions such as fighting, defense and digging.

Similar trade-offs in skeletal phenotypes have been documented in dog breeds selected for fighting as compared to runner breeds, with the former having relatively larger second moments of area at midshaft of their long bones and more circular cross-sectional shape (Kemp *et al.*, 2005). A better built skeleton composed of short, stout limbs and muscles specialized for high force production would also result in heavier bones, thus having a negative impact on locomotor performance (e.g. Kemp *et al.*, 2005). This would probably explain why *B. suillus* apparently has slower movements as compared to other subterranean species with higher levels of mobility. Nevertheless, additional studies are needed to test hypotheses related to locomotor performance and speed in bathyergids.

As mentioned before, the cortical bone thickening in *B. suillus* occurs when individuals are 260-280 mm in BL (Fig. 3.7, 8), so just before the juvenile-subadult transition (age class 4; Hart *et al.*, 2007). Based on Hart *et al.* (2007), this transition occurs in specimens of ~290 mm (BL) and 670 g (BM) (Fig. 3.8). Similarly, the first histological signs of cortical bone thickening are observed in older juveniles (Montoya-Sanhueza & Chinsamy, 2017), when individuals weigh ~450 g (Fig. 3.8). The femoral bone compactness of these juveniles is already higher than that of other adult cursorial mammals (see Montoya-Sanhueza & Chinsamy, 2018), thus indicating a relatively early onset of cortical bone adaptation. Since juveniles start digging at ~60 days and disperse when they are 60-65 days old, when they weigh ~300 g (Bennett *et al.*, 1991, 2009), modifications in bone microstructure occurs after their dispersal, and evidently after the onset of the digging activities. For this reason, it is difficult to associate the gains in bone mass with increased digging activities in this species. Other factors such as attainment of sexual maturity and/or genetic control could play a role in its development. The attainment of sexual maturity has been found to follow dispersion in social African molerats (Bennett & Faulkes 2000). In *B. suillus*, sexual maturity is hypothesized to happen when individuals are between 494-529 g, so after dispersion and before they reach subadult stages (Bennett *et al.*, 1991, 2009; Hart *et al.*, 2007) (Fig. 3.8). This

coincides with the beginning of deceleration of somatic growth in *B. suillus* (Hart *et al.*, 2007; Bray *et al.*, 2012), most probably resulting from different factors such as increasing digging demands and reproduction-related energy allocation. Although our juveniles did not show signs of sexual maturity, some subadults already show them (Montoya-Sanhueza & Chinsamy, 2017). In general, the attainment of sexual maturity and the consequent action of sex steroid has been associated with significant modifications in skeletal shape (e.g. Moss-Salentijn, 1991; Taylor, 1991; Callewaert *et al.*, 2009). In this study, some morpho-functional traits showed sexual differences (Table 3.2), while other traits tended to be higher in males (Table 3.4), indicating sexual dimorphism in *B. suillus*, which are not necessarily related to attainment of sexual maturity. Despite femora reaching higher bone compactness than the humerus, a systemic genetic regulation for bone thickening is more plausible rather than mechanical stimulation of a single limb (forelimb). Additionally, non-reproductive colony members born in captivity of the eusocial *Heterocephalus glaber*, still develop thick cortical bone walls before reaching sexual maturity (Pinto *et al.*, 2010). This information suggests that genetic factors are more likely to influence the development of cortical bone thickening in *Bathyergus* and other bathyergids. In this sense, genetic and gender factors are known to be strong regulators of peak bone mass and bone mineral density (BMD) in rodents and other mammals (Beamer *et al.*, 1996; Klein *et al.*, 1998). Additional studies are needed to assess the processes underlying the regulation of cortical bone thickening in bathyergids. For now, it is not possible to make any strict link between such events and cortical bone adaptation, although the interaction of different behaviors at different ontogenetic stages (sparring and digging activities) may represent two separated sets of factors relevant for the normal development of the postcranial phenotype of *Bathyergus*. Furthermore, the ontogenetic morphological shift described here also explain the larger morphological differences found between juveniles and subadult-adults, and it may represent an important process for the maintenance of safety factors in these mammals that undergo significant strain regimes of their long bones during life (e.g. Blob *et al.*, 2014).

To our knowledge, no previous studies have analyzed both internal and external anatomy simultaneously to understand the interrelationship between functional aspects and aging in subterranean/fossorial mammals. The complexity of these processes highlights the importance of defining the factors influencing specific bone architectures, especially identifying what traits are more susceptible to fluctuate under environmental conditions.

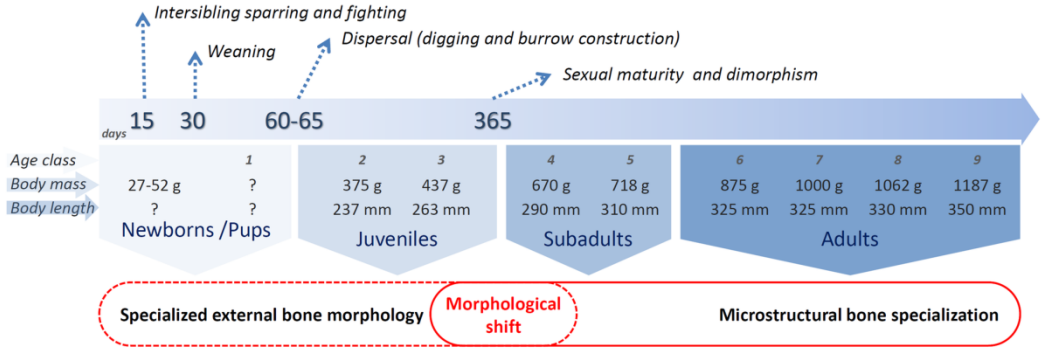

FIGURE 3.8. Appearance of most notorious morphological specializations in *Bathyergus suillus* and the onset of relevant behaviors during ontogeny. The morphological shift is marked by decreased (epi)condylar growth and increased periosteal-endosteal bone appositions. Body mas and body length are represented by average values. Data based on Bennett *et al.* (1991, 2009), Hart *et al.* (2007), and Montoya-Sanhueza & Chinsamy (2017).

3.4.3 Allometry and Modular Patterns of Long Bone Ossification

Phenotypic modifications in the skeleton of *B. suillus* resulted from different growth trends of the periosteal and endochondral bone modules (Table 3.5, 3.6). The use of linear measurements and allometric relationships to quantify those patterns allowed us to understand how these relatively independent processes interact to attain the adult phenotype, as well as to hypothesize about the main adaptive processes occurring in this and other species. The allometric growth trajectories of *B. suillus* were mostly isometric in relation to body mass (BM) and body length (BL), and more variable when skull length (SKL) was used as a proxy of body size (Table 3.5). Although SKL seems to be relatively large in subterranean mammals, especially in chisel-tooth diggers (Nevo, 1999; Stein, 2000), our allometric analyses showed that relative skull size of *B. suillus* rather stabilizes its growth during ontogeny in relation to postcranial elements, making the growth trajectories of postcranial elements appear incremental when plotted against SKL, and thus resulting in a higher number of positive allometric trends (Table 3.5). For this reason, the use of SKL does not reflect appropriately the relationship between body size and the appendicular system in this species, since this cranial parameter rather overestimates the growth of the limbs. Similar results for SKL have been found in other subterranean species like *C. talarum* (Echeverría *et al.*, 2014), although these authors did not assess other estimators of body size.

The main contributors of the observed morphological changes are related to the relative reduction in size of secondary centers and (epi)condylar breaths. These structures are primarily determined by endochondral ossification, and later in life by a dual process of endochondral and appositional (periosteal) bone formation which extend to metaphyses and diaphysis (Hall, 1978; Moss-Salentijn, 1991; Taylor, 1991). These traits showed negative allometries and therefore had little contribution to increased external skeletal robusticity in adulthood (Table 3.5). However, these features showed a more relevant contribution in perinatal and juvenile stages, where cartilaginous epiphyses and endochondral ossification played a fundamental role in developing anatomical structures (Fig. 3.6). Thus, the increased gracility of the long bones observed in adults (Table 3.2; Fig. 3.2, 3.3, 3.4)

can be explained not only by the relatively stable bone elongation observed throughout ontogeny, but also by the low osteogenic contribution of epiphyseal bone modules (Table 3.5). Epiphyseal fusion also contributed to this matter, especially in the forelimb, which showed higher frequency of fused epiphyses (Table 3.6), indicating the cease of longitudinal growth at that particular end very early in ontogeny. The distal portion of the humerus fused quite early in ontogeny, while the olecranon (OL) in the ulna fused before than the distal epiphysis (Table 3.6). This implies that the main growth directions for humerus and ulna are proximally and distally oriented, respectively. This is further supported by the lower rate of growth of the OL in the ulna as compared to the higher growth rate of the functional ulnar length (FUL) (Table 3.5). It is for this reason that the IFA index (relative size of the olecranon) decreases considerably during ontogeny (Fig. 3.2). A different pattern has been observed in *C. talarum* (Echeverría *et al.*, 2014), with the IFA increasing during ontogeny, most likely indicating a more balanced contribution of both epiphyses, and also suggesting a higher degree (or more time) of local bone adaptation. Such differences in intra-element growth dynamics provide the first insights on the modularity of a single long bone, and also explains the heterochronic differences observed between species, which suggest differential adaptive patterns due to phylogenetic and/or developmental constraints. Further research is required to solidify these conclusions, in particular the ossification sequences for the postcranial skeleton requires detailed examination for diverse subterranean species, which will enable comparison with comparative studies of heterochronic shifts in the postcranial skeleton among marsupials and placentals (Weisbecker *et al.*, 2008; Wilson *et al.*, 2010; Hautier *et al.*, 2011; López-Aguirre *et al.*, 2019).

Other results obtained in this study are the tendency of periosteal modules (bone thickening) to show higher slopes (Table 3.5), and that endochondral modules (bone lengthening) showed higher coefficients of determination in comparison to the periosteal modules (Table 3.5). It is known that bone length and bone thickness (mineral density) in mammals are regulated by different genes (Beamer *et al.*, 1996; Klein *et al.*, 1998; Sarges *et al* 2011; Wongdee *et al.*, 2012). These observations indicate that bone thickening is a fundamental process occurring in the long bones of *B. suillus,* and probably affected by several factors during early ontogenetic stages. These results also contrast with the reports for *C. talarum* where it seems that the endochondral modules are prioritized and elongate faster (Echeverría *et al.*, 2014). In the mammalian skeleton, endochondral features such as cartilage morphology and limb length are also known to have a substantial genetic control which seems to be less affected by external influences as compared to intramembranous ossification (cortical thickening) (e.g. Eckstein *et al.*, 2006; Sarges *et al* 2011). This suggests a stronger phylogenetic signal for the regulation of bathyergid limb length. Periosteal bone modules tended to be more variable during subadults stages (Table 3.2), probably related to several individual-level causes, including size at birth, variations in diet consumption, amount of digging activity, and variable hormonal effects associated to the attainment of sexual maturity (Hall, 1978; Moss-Salentijn, 1991; Taylor, 1991; Callewaert *et al.*, 2009).

Our analysis provides evidence of the decoupled nature of the bone modeling process within *B. suillus.* This is not unexpected since similar decoupled

patterns have been independently described for the modeling process of other rodents, as well as for the decoupled anabolic and catabolic activity within single bones (Lanyon, 1980; Wongdee *et al.* 2012; Rolian, 2008; Ausk *et al.*, 2013). Modifications in the patterns of bone modeling represent the most likely phenomenon explaining the intraspecific variation in body and skull shape found in other bathyergid species (e.g. Klein 1991; Barčiová *et al.*, 2009). For example, the skull morphology of African molerats exposed to different ecological and geographical factors, such as rainfall fluctuations and consequent changes in soil hardness will most likely result in phenotypic changes mediated by bone modeling, e.g. skull variation in *Heliophobius argenteocinereus* (Barčiová *et al.*, 2009). Nevertheless, additional studies are needed to understand processes associated to local bone adaptation and mechanobiological stimulation and its effects on bone modeling (e.g. Carter & Beaupré, 2001; Robling *et al.*, 2014). Besides providing a mechanistic explanation for the morphological modifications found in *Bathyergus* during ontogeny, the dynamics of the differential regulation of these bone modules could have important relevance for understanding the adaptive processes regulating the skeletal phenotype in subterranean mammals. As such, thick cortical bone walls represent a widespread adaptation of fossorial and subterranean mammals (see Montoya-Sanhueza & Chinsamy, 2017 and references therein), as well as their nonmammalian therapsid ancestors (Botha & Chinsamy, 2004; Ray & Chinsamy, 2004), so understanding its variation could shed light on patterns of bone adaptation and speciation among these vertebrates.

3.4.4 Limb Ratios in Subterranean Mammals: Implications for Locomotion

Life in burrows imposes morphological constraints in animals, typically resulting in phenotypes with elongated cylindrical body shapes and short limbs (Eilam *et al.*, 1995; Eilam, 1997; Nevo, 1999, Stein, 2000). Behavioral experiments have also shown important modifications in their locomotor pattern due to postural challenges (Eilam *et al.*, 1995; Horner *et al.*, 2016). Many subterranean mammals have implemented backward locomotion as a recurrent behavior to principally remove soil out of the burrow (Stein, 2000). Thus, locomotion and soil transport are closely related activities that can be considered as a locomotor pattern in a dense medium (McNab, 2002). Although *B. suillus* expels soil primarily using their forelimbs (Hickman, 1985), they also move backwards inside burrows. Our results suggest a close relationship between locomotion and appendicular morphology.

Eilam *et al.* (1995) studied the uphill locomotion of the head lift digger, *Spalax leucodon ehrenbergi*, and observed that, when moving backwards, they modify their gaits to a more lateral sequence (relative to the direction of progression). Lateral sequence gaits enable a more stable gait during locomotion (e.g., Gray, 1968), but this type of locomotion is not usually observed when terrestrial mammals walk backwards, because they do not re-accommodate their gaits. For this reason, when *S. l. ehrenbergi* performs backward lateral sequence gaits, it switches its hindlimb function, whereby these act as “forelimbs”. This kind of locomotion helps with the changes in weight distribution between the hind and forelimbs associated with moving the soil out of the burrow, either back or forward (Eilam *et al.*, 1995). In this way, they avoid modifying the footfall pattern relative to

the new direction of progression, by keeping it the same (Eilam *et al.*, 1995). Anatomically, this is facilitated by having symmetric limb proportions (IMI ~ 1) and elongated bodies, allowing equal bidirectional locomotion of the animal within burrows and emphasizing equal propulsive action of the fore and hindlimbs (Novacek, 1980). Although Eilam *et al* (1995) did not provide data on limb proportions for *S. l. ehrenbergi,* this species shows relatively high IMI (0.826) and intralimb ratios (BI = 0.809; CI = 0.979), as inferred from the anatomical descriptions made for this species elsewhere (Özkan, 2002a, b). In this sense, more symmetrical intermembral indices (IMI) seems to represent an advantage for mammals living in burrows. Howell (1965) reported an IMI of 0.75 as the generalized condition for surface-dwelling (terrestrial) mammals, so that they generally have larger hindlegs than forelegs, with bipedal jumpers showing the lowest ratios (0.32-0.50). Adult individuals of *B. suillus* have on average 0.874 (♀ = 0.857; ♂ = 0.891), with juveniles having a lower value (Table 3.2; Fig. 3.2), so that forelimbs are longer (or hindlimbs shorter) as compared to the hypothetical normal condition of other surface-dwelling mammals. This is also accompanied by having relatively similar adult BI (0.898) and CI (0.914) values, so that the stylopodial to zeugopodial ratio is also relatively equal. A relatively symmetrical intermembral index has also been observed in adults of other semifossorial mammals that build and spend considerable time in burrows such as the cricetid voles *Microtus socialis* (0.85) (Eilam, 1997), the small eulipotyphlan *Solenodon* (≈ 0.88) (Novacek, 1980), and canids, where the index varies from 0.83 to 0.94, with *Speothos venaticus* showing the maximum value (Howell, 1965). Although *Speothos venaticus* has a semifossorial lifestyle, they do not excavate their own burrows (Beisiegel & Zuercher, 2005). Other mammals with more cursorial locomotor patterns also show high IMI at birth, but their adults show a drastic divergence in their proportions (Eilam *et al.*, 1997). Consequently, the high IMI found in *B. suillus* and other fossorial mammals may not represent a fossorial adaptation for excavation *per se*, but an additional morphological specialization for bidirectional locomotion in burrows and narrow spaces. This phenotype probably appeared several times in mammalian lineages due to different causes, as has been hypothesized for the primitive condition of eutherians with a "unspecialized" ambulatory mode of locomotion (Novacek, 1980). This adaptation has also been observed in the fossil record, i.e. among early (Triassic) cynodonts such as *Galesaurus planiceps* and *Thrinaxodon liorhinus,* which have been found associated with burrow systems (Jasinoski & Abdala, 2017). Thus, our results provide novel information on the development of this fossorial adaptation in a truly subterranean mammal, which has further implications for understanding the paleobiology and biomechanical interpretations of nonmammalian therapsids and basal mammaliaforms.

3.5 CONCLUSIONS

Bathyergus show two different skeletal phenotypes associated with the increased ability to dig, but also to fight and for defense. An overexpressed external phenotype in early life may compensate for a less skilled digging ability, as well as

incompletely ossified epiphyses in juveniles. A slender but better built bone microanatomy may increase bending resistance for extensive burrow building during adulthood. This morphological shift during ontogeny reveals for the first time the developmental interaction between external anatomy and bone microanatomy. Thus, postnatal skeletal development in *Bathyergus*, and probably other subterranean vertebrates, involves a complex interaction between bone design, function and behavior, which are mediated by modular patterns of bone modeling. Intrinsic factors regulating the onset and direction of such processes are probably determining both endochondral and periosteal modules, although other factors such as gender, growth factors, hormones and environmental cues seems to have an important impact on intramembranous ossification. Local adaptation through mechanobiological sensing is most likely a secondary aspect of bone phenotyping in *Bathyergus*, mainly to give form to smaller features of the skeleton. This study also showed that changes in morpho-functional indices can be explained by modifications in growth trends of different bone modules (endochondral vs periosteal), as well as to the differential effects of epiphyseal closure, thus providing new adaptive interpretations for understanding morphological variation among species. Nevertheless, additional studies including a wider taxonomic sampling are needed to assess the magnitude of these observations. Ontogenetic analysis of natural populations and the inclusion of multiple levels of structural organization are thus demonstrated to be essential to answer complex questions about functional skeletal development and adaptation in mammals. Allometric trajectories also represent a powerful tool to quantify such complex processes, and suggest that certain proxies of body size based on cranial features (i.e. SKL) may overestimate growth trajectories of postcranial elements in this and other fossorial and subterranean species. Since skull length is widely used in studies of comparative anatomy and paleobiology, interpretations of postcranial growth patterns based on cranial features must be taken cautiously.

ACKNOWLEDGEMENTS

We thank Tamara Franz-Odendaal for inviting us to contribute to this special issue. We also thank Jennifer Jarvis and Justin O'Riain for access to *Bathyergus* specimens, as well as to Jan Okrouhlik and Nigel Bennett (University of Pretoria, South Africa) for giving access to live *Bathyergus* specimens. Aaron Armstrong is acknowledged for having selected and skeletonized part of the material used in this study. Thanks to René Navarro (Animal Demography Unit, UCT) for assistance with the statistical analyses, and to Marcelo Sánchez-Villagra, for his useful comments that helped improve this manuscript. We acknowledge the constructive reviews of Alejandra Echeverría and Andrew McIntosh which have considerably improved the quality of this manuscript. GM-S is supported by Becas Chile, Government of Chile (CONICYT, 73113757). LABW is supported by the Australian Research Council, Discovery Program (DE150100862). AC is funded through the National Research Foundation, South Africa AOP Programme (Grant number, 117716).

CHAPTER 4

Functional Anatomy and Disparity of the Postcranial Skeleton of African Mole-Rats

and the special case of naked mole-rats

"To-day the natives brought into camp a curious little creature, a sort of Mole, length 4 ½ inches, skin bare, with a few stiff hairs. Tail like that of a Hippo. Its toes armed with bristles, and its teeth like those of a Walrus. On being placed on the ground it commenced to dig furiously, using its teeth to loosen the earth with; its eyes were tiny, and its ears simply holes in the sides of its head."

E. Lort Phillips, 1885
FIRST WESTERN SIGHTS OF FARUMFERS (NAKED MOLE-RATS)

4.1 INTRODUCTION

Most studies in ecomorphology and diversity of the mammalian postcranial skeleton have focused on terrestrial cursorial groups, and have usually been based on only a few specimens. In general, these studies have shown that disparity (i.e. morphological diversity) in mammals is highly variable (e.g. Vianey-Liaud *et al.*, 2015); López-Aguirre *et al.* 2018; Sansalone *et al.*, 2019), even when comparing at intraspecific levels (e.g. Wayne, 1986). These studies have mainly tried to reveal the macroevolutionary patterns and causes of morphological variation such as speciation and radiation (e.g. see Jones & Safi, 2011 and references therein; Cox & Hautier, 2015). However, little is known about the phenotypic variation within more constrained phylogenetic brackets such as within families (e.g. Sansalone *et al.*, 2018). The integration of different levels of structural organization (i.e. cellular, tissular, organs) at which these morphological changes occur (see Enlow, 1969; Shea, 1993; Zelditch, 2005; Minelli, 2015) can provide novel insights. For example, recent studies assessing skeletal homeostasis and bone growth dynamics of some mammal species have shown that there is a wide variation in the patterns of bone modeling among them (e.g. Doherty *et al.*, 2016; Montoya-Sanhueza & Chinsamy, 2017). This indicates that certain physiological regulators of bone development can vary at species-specific level, and most probably also within families and orders. Moreover, it is not completely known how certain environmental (e.g. sunlight exposure or hypercapnic - high CO_2 conditions) and behavioral factors (e.g. locomotor modes) affect the growth of skeletal elements, and whether those factors have the same effects in all organisms (e.g. cursorial vs. subterranean species). Thus, the analysis of closely related taxa with a wide range of ecological,

reproductive and social strategies will contribute significantly to understanding the causes and mechanisms of morphological change.

There is an extensive literature reporting the morphological adaptations of fossorial and subterranean taxa, such as in the South American ctenomyids rodents (Vassallo, 1998; Stein, 2000; Elissamburu & Vizcaíno, 2004, and references therein) and dasypodid armadillos (Vizcaíno *et al.*, 1999; Vizcaíno & Milne, 2002, and references therein). These studies have demonstrated a strong correlation between anatomical structures and specific digging strategies (Lindstedt & Swain, 1988; Lessa & Thaeler, 1989), although it is unknown how different ecological settings (e.g. solitary or social life) affects the selection of certain structures, especially considering the different burrowing efforts performed by individuals in colonies. The study of bathyergid anatomical adaptations and fossoriality are fundamental to understand such aspects.

Since African mole-rats show a wide range of social systems and use different anatomical structures to dig soils, it is expected that their skeletal morphology will differ among species. The main objective of this study is to determine such morphological diversity (disparity) in adults, specifically aiming to determine which anatomical features of the appendicular system are shared between species, and how these are related to their specific social behaviors, digging strategies and locomotor ability. In this study, it is hypothesized that the type of social strategy observed in bathyergids influence the morphology of their appendicular skeleton, since a cooperative lifestyle would compensate for individual optimization of anatomical structures for burrow construction. Thus, it is expected that solitary species (*Heliophobius, Georychus* and *Bathyergus*) will show a more specialized ("morphologically divergent") appendicular anatomy as compared to social species (*Heterocephalus, Fukomys* spp. and *Cryptomys*), which will have a more generalized or simplified limb morphology. Additionally, it is expected that scratch-digging species like *Bathyergus* will show a higher degree of morphological specialization in their limbs as compared to chisel tooth digging taxa (*Heterocephalus, Fukomys* spp., *Cryptomys, Heliophobius* and *Georychus*), due to higher anatomical specialization to maximize scratch-digging behavior (i.e. soil breakup).

4.2 MATERIAL AND METHODS

4.2.1 Specimens, Maturity and Samples

A total of 244 specimens pertaining to seven species and six bathyergid genera (*Bathyergus, Heliophobius, Georychus, Cryptomys* and *Fukomys*) were analyzed (Appendix 4.1). The sample comprises only adult specimens of both sexes. It has been reported that bathyergids show a delayed tooth eruption sequence, and the last cheek teeth do not erupt until after sexual maturity (Gomes Rodrigues *et al.*, 2011; Berkovitz & Shellis, 2018). Thus, in this study maturity was defined as individuals having full -alveolar- eruption of all upper or lower molars. Almost all genera have four molars, although *Heterocephalus* has three (sometimes two) and *Heliophobius* has supernumerary molars (4-6) with continuous horizontal replacement during life (Hamilton, 1928; Taylor *et al.*, 1985; Bennett *et al.*, 1990; Jarvis & Sherman, 2002; Hart *et al.*, 2007; Gomes Rodrigues *et al.*, 2011; Gomes

Rodrigues & Šumbera, 2015). Unfortunately, no comprehensive descriptions of the eruption sequence for these taxa are published. For this reason, in *H. glaber*, only specimens with three fully erupted molars were selected and analyzed. In *H. argenteocinereus,* the third molar erupts after the second month of life and the full check teeth (four molars) are already developed at two years old (Gomes Rodrigues *et al.*, 2011). Additionally, specimens were also selected based on gross morphological features indicating a mature body size, like well-developed limbs showing at least fully developed secondary centres of ossification at epiphyses and a fused distal epiphysis of the humerus (see fused epiphysis in long bones in Fig. 4.2.2 of Ch. 2,). The majority of the specimens were wild-caught, although some individuals of *F. damarensis,* and all individuals of *H. glaber* are from captive colonies (Appendix 4.1). These aspects are addressed in the discussion.

4.2.2 Limb Bones, Measurements and Morpho-Functional Indices

Stylopodial (femur and humerus) and zeugopodial (ulna and tibia-fibula) elements from either the right or left side of the individual were dissected and skeletonized (see Ch. 2). The general anatomy of each bone was compared among species following the anatomical nomenclature provided in previous works (e.g. Salton & Sargis, 2008; Dagosto *et al.*, 2008; cites). The main features of the limb bone anatomy of African mole-rats are schematized in Figures 4.1-4.4.

A total of 16 linear measurements including lengths and midshaft diameters of limb bones were taken (Echeverría *et al.*, 2014; Montoya-Sanhueza *et al.*, 2019). All measurements were recorded to the nearest 0.01 mm using a digital calliper. From linear measurements, 17 functionally important indices were calculated following previous studies (e.g. Echeverría *et al.*, 2014; Wilson & Geiger, 2015), in particular the one in Ch. 3 (Montoya-Sanhueza *et al.*, 2019), which presented a corrected version of several functional indices to appropriately assess adaptations to fossoriality. These functional indices represent the main aspects of bone shape at the diaphyseal, proximal and distal portions of the bone, as well as represent the mechanical advantages of the principal muscles related to limb function. Some of these indices like BI, CI and IMI represent limb proportions and therefore reflect locomotor advantage. Except for one index (TJI, see below), all other indices are fully described in Ch. 3 (Montoya-Sanhueza *et al.*, 2019).

The tibio-fibular junction index (TJI) is an additional index developed in this chapter, and represents the distance of the proximal articular surface to the distal tibio-fibular junction (Fig. 4.4). This feature is described as percentage in the Ch. 3 (Montoya-Sanhueza *et al.*, 2019), and modified herein so that lower values (i.e. a more proximal fusion of the tibia and fibula) would suggest a longer bony base for the muscles acting on the paws. This would increase resistance for bending and torsional loads in animals that sustain relatively higher biomechanical activity against the substrates, for example during soil excavation (Carleton, 1941; Stein, 2000; Silva *et al.*, 2005).

Although Hill *et al.* (1957, p. 482) mention that "*There is a strong deltoid crest*" in *H. glaber*, in this study the deltoid tubercle in *H. glaber* is considered to be poorly developed and almost indistinguishable from the shaft. The reason for such discrepancies stem from the various definitions used for the "deltoid tubercle" and

it is briefly addressed here. The "official" term used for this feature is "deltoid tuberosity", as for humans (Terminologia Anatomica, FCAT, 1998) and other mammals (Nomina Anatomica Veterinaria, ICVGAN, 2017), although additional information about the morphological variation of this feature among different taxa is not provided. Several studies refer to this feature as tubercle, crest, ridge or process, without proper definition of the terms and the differences among them (K. Rose 2019, pers. comm.). Considering the variation found among bathyergids, as well as the wide variation of deltoid characteristics in mammals (e.g. Davis, 1964; Sargis & Dagosto, 2008), from presence to absence, or from local development to extensive occurrence through the diaphysis, in the current study distinction is made between a deltoid tubercle/process and a deltoid crest/ridge. Here, a tubercle or process represents a conspicuous protrusion of bone extending from the diaphysis, as observed in most bathyergids (Fig. 4.1) and many other fossorial rodents (Hildebrand, 1985; Stein, 2000). In comparison, a crest or ridge represents a line or extended surface in the diaphysis of the bone associated with an extended muscular insertion but does not form a localized protuberance from the diaphysis, e.g. as seen in some tubulidentates, mustelids, tenrecids and solenodontids (Lehmann *et al.*, 2006; Rose *et al.*, 2014; Sargis & Dagosto, 2008). These features are not mutually exclusive and a deltoid ridge would also be noticed at the proximal origin of a deltoid tubercle, and it can be more marked in some species than in others (Fig. 4.1). Armadillos show an intermediate level of development of this feature since its protrusion is quite conspicuous but also proximally extended throughout the diaphysis due to an extended deltoid ridge, making it difficult to determine its proximal origin. In this sense, *H. glaber* rather shows a deltoid ridge and lacks a developed deltoid tubercle, although some specimens show a small protuberance in the midshaft, which is considerably undifferentiated, not permitting a clear measurement of its extension (Fig. 4.5). The deltoid ridge of *H. glaber* is very similar to that described by Davis (1964) for the giant panda (*Ailuropoda melanoleuca*), which begins immediately below the posterior end of the greater tubercle in the posterolateral surface of the shaft, and near the midshaft it arches across the anterior surface. Because *H. glaber* lack a DP, the RDP index was not calculated for this species. Moreover, since this species does not fuse the tibia and fibula, the TRI, TRI* and TJI were also not calculated for this taxon. All specimens analyzed here are housed in the Department of Biological Sciences at the University of Cape Town (UCT), South Africa.

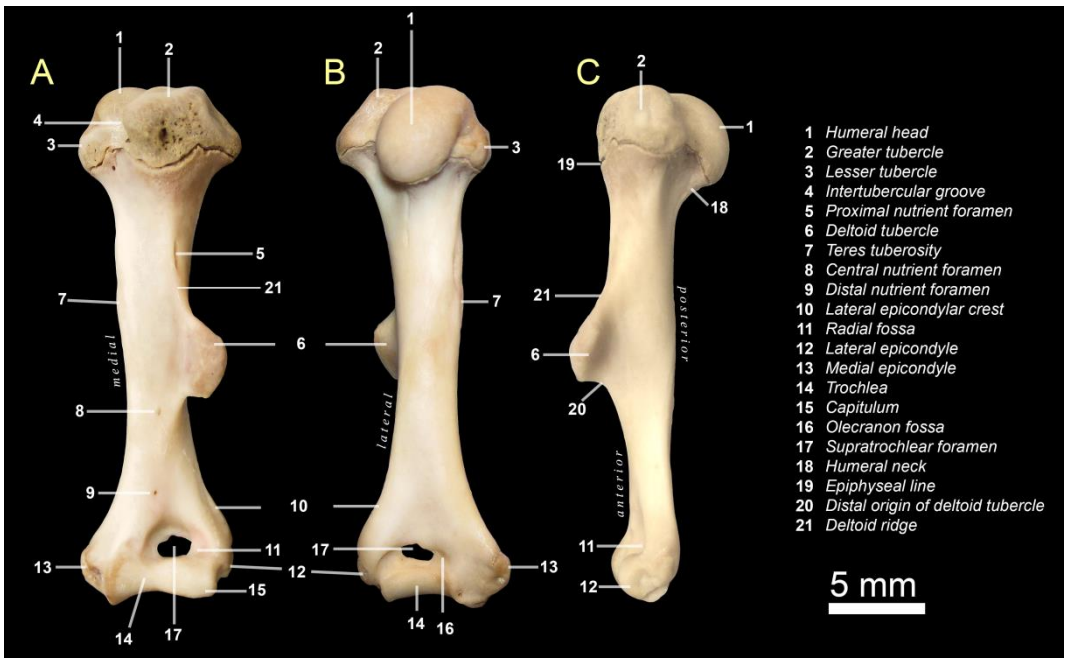

FIGURE 4.1. Humeral anatomy of *Georychus capensis*. Left humerus of a large male specimen #290 in anterior (A), posterior (B) and lateral (C) view.

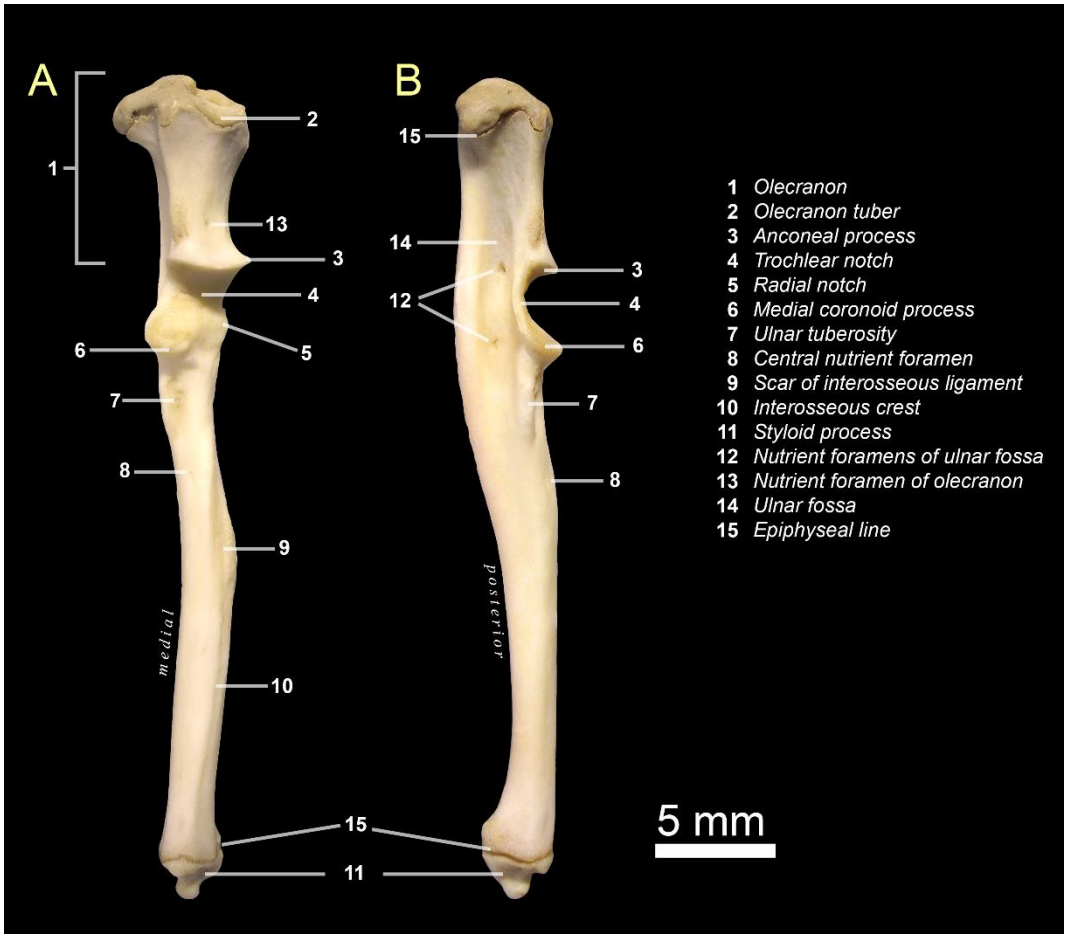

FIGURE 4.2. Ulnar anatomy of *Georychus capensis*. Left ulna in anterior (A) and lateral (B) view. See specimen details in Fig. 4.1.

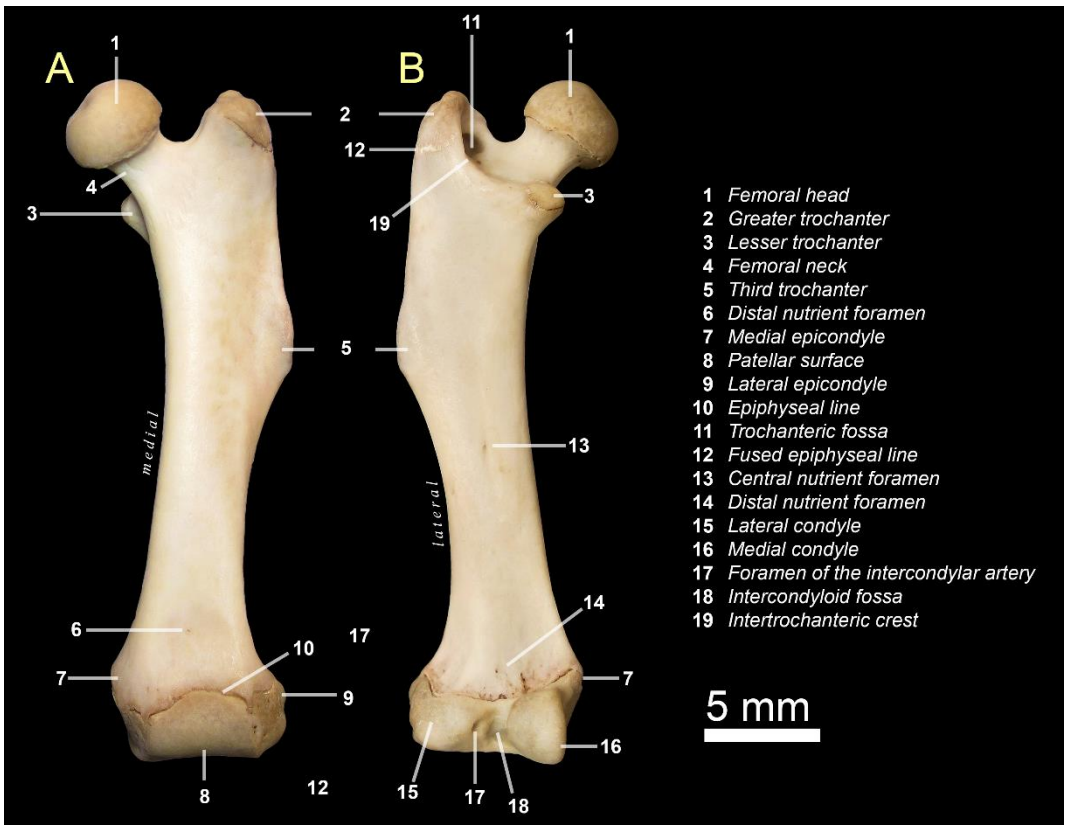

FIGURE 4.3. Femoral anatomy of *Georychus capensis*. Left femur in anterior (A) and posterior (B) view. See specimen details in Fig. 4.1.

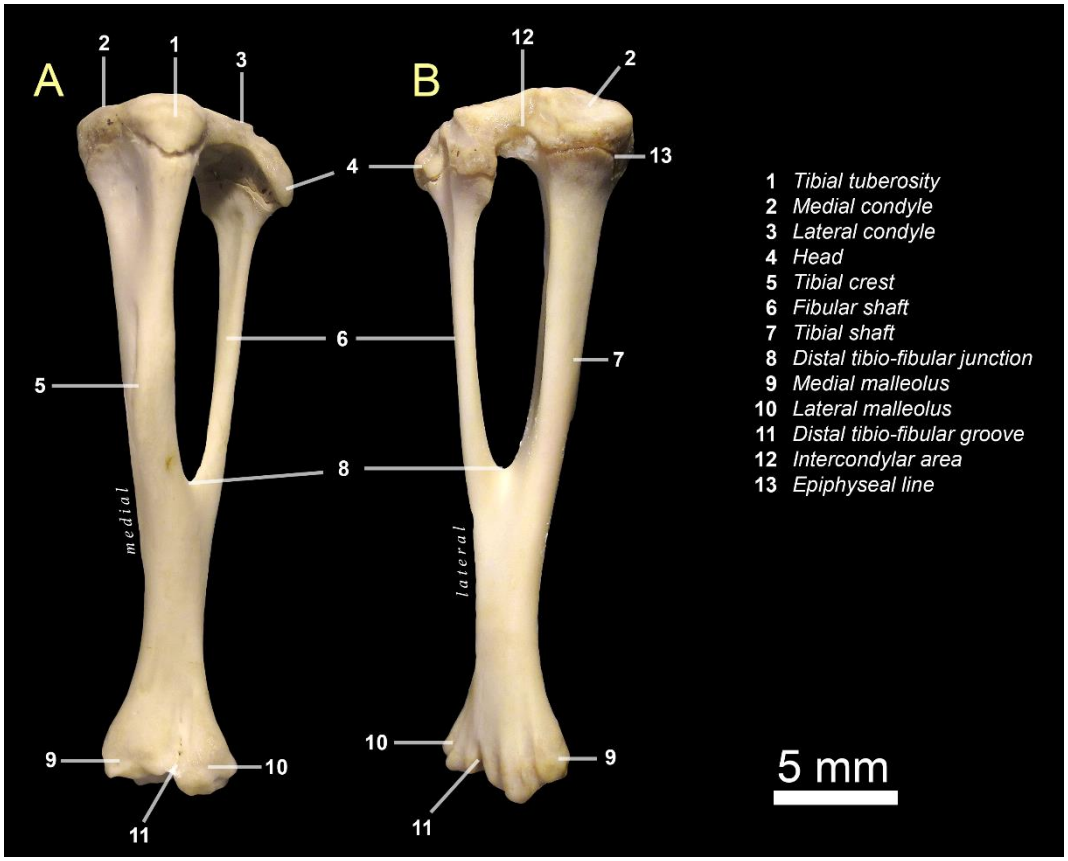

FIGURE 4.4. Tibio-fibular anatomy of *Georychus capensis*. Left tibia-fibula in anterior (A) and medial (B) view. See specimen details in Fig. 4.1.

4.2.3 Ecomorphological Groups

In order to assess the effects of a specific subterranean lifestyle on bone phenotype, three ecomorphological groups that account for the main ecological and behavioral features of different bathyergid species were created in this study. These groups are based on a combination of their social organization (solitary vs. social species) and digging strategy (scratch-diggers vs. chisel-tooth diggers) (Sherman *et al.*, 1991; Bennett & Faulkes, 2000; Begall *et al.*, 2007), and are classified as: i) solitary scratch-diggers, ii) solitary chisel-tooth diggers, and iii) social chisel-tooth diggers (Appendix 4.1). Note that the hypothetical group of "social scratch-diggers" was not defined since there are no bathyergid species reported with such combination of traits.

4.2.4 Sexual Dimorphism

Since sex differences are known to affect the growth trajectories and morphology of species (e.g. Klingenberg 1996, pp. 34), sexual dimorphism in body mass and morpho-functional indices were also assessed. Bathyergids show different levels of body size sexual dimorphism. Among solitary species, *B. suillus* and *H. argenteocinereus* exhibit male-biased sexual dimorphism (Šumbera *et al.*, 2003; Hart *et al.*, 2007), with the former showing the most remarkable degree of sexual dimorphism (Hart *et al.*, 2007), while *G. capensis* is monomorphic (Taylor *et al.*, 1985; Bennett & Faulkes, 2000). The social genera, *C. hottentotus*, *F. damarensis* and *F. mechowii* also show male-biased sexual dimorphism (Davies & Jarvis, 1986; Burda & Kawalika, 1993; Scharff *et al.*, 1999; Bennett & Jarvis, 2004; Bennett & Burda, 2013; Thomas, 2013), although Bennett (2013) mentions that there is no (or very little) dimorphism for *C. hottentotus*. Naked mole-rats are considered monomorphic, although it is known that sexual maturity and reproduction have strong effects on females, which result differing from the rest of the colony members by developing elongated bodies (O'Riain *et al.* 2000; Dengler-Crish & Catania, 2007, 2009). This does not necessarily mean that queens weigh more (O'Riain, 1996; Bennett & Faulkes, 2000).

4.2.5 Statistical procedures

Sex differences. Considering that some species have been reported to show subtle differences between sexes (e.g. Bennett & Faulkes, 2000; Šumbera *et al.*, 2003; Bennett (Happold, 2013), and that only *Bathyergus* has a marked dimorphism (Bennett & Faulkes, 2000; Hart *et al.*, 2007), it is likely that the pattern of sexual dimorphism in bathyergids may be obscured by different reasons, including their particular status within the colony and the cohort (Bennett & Faulkes, 2000). Additionally, this pattern can be biased and represented by only few specimens within the population, especially in reproductively skewed species like social mole-rats (Faulkes & Bennett, 2009). For this reason, intraspecific comparisons to assess sexual dimorphism in body mass (BM) were carried out by using the median as the measure of central tendency. This measure emphasizes the common tendency among individuals without being influenced by the extreme tendencies of one or few individuals. Sex differences in both BM and morpho-

functional indices were assessed by non-parametric two-tailed (Wilcoxon) Mann-Whitney *U* tests for equality of medians. Descriptive statistics of BM (mean ± SD) are presented in Table 4.1 for all species, as well as box plots (median ± 25-75% quartiles) of only statistically significant functional indices are also presented (Fig. 4.8; Appendix 4.2).

TABLE 4.1. Descriptive statistics and Mann-Whitney *U-test* of sexual dimorphism in body mass (BM) for bathyergid species analysed in this study. Species with male-biased sexual dimorphism are indicated with a male ♂ symbol (see references in text). Significant results ($p < 0.05$) are indicated with an asterisk.

Species	*N*	Mean ± SD (BM)	*N*	Mean ± SD (BM)	Mann-Whitney	
		Females		Males	*U-test*	*p*
B. suillus ♂	23	798.870 ± 282.637	16	1141.81 ± 370.43	91.0	**0.008***
H. argenteocinereus ♂	16	173.16 ± 51.31	12	177.453 ± 55.965	93.0	0.908
G. capensis	33	179.559 ± 61.777	15	152.90 ± 60.07	170.5	0.089
F. mechowi ♂	8	157.075 ± 93.280	5	270.12 ± 117.35	10.0	0.164
F. damarensis ♂	9	86.549 ± 33.590	10	140.00 ± 47.90	13.5	**0.011***
C. hottentotus ♂	13	58.550 ± 13.115	19	74.63 ± 23.55	73.0	0.055
H. glaber	28	30.690 ± 9.895	24	31.70 ± 11.32	335.0	0.993
Total	130		101			

Multivariate analysis. A series of multivariate analysis of variance (MANOVA) coupled with Tamhane *post hoc* tests were carried out to assess interspecific differences in morpho-functional indices. Forelimb and hindlimb morphologies were assessed separately to reduce issues concerned with multiple testing and high number of variables in the MANOVAs. This also helped to determine specific differences associated with one limb only. All MANOVA showed violations of the assumption of equal variances between samples. For this reason, both Wilks' lambda and Pillai trace statistics are provided, because the latter test is more robust under violations of homoscedastic covariance (Quinn & Keough, 2002). Nevertheless, to test if homoscedasticity of the sample could be recuperated, the data were $\log_{10}$ transformed without improvement. For this reason, the MANOVAs were carried out using the indices without transformation. Graphs (bar charts) were prepared for all indices and show mean (central point), standard error (shorter whiskers) and standard deviation (longer whiskers). Whisker length was calculated with one-sigma (Hammer *et al.*, 2001). The results of the *post hoc* tests are included in Figure 4.9.

Ordination analysis of morpho-functional indices. Both Principal Component Analysis (PCA) and Discriminant Analysis (DA) were performed to identify the major components of variation among the seven species and three ecomorphological groups, respectively (Wilson & Geiger 2015, and references therein). One important aspect implemented in this study is the introduction of novel ecomorphological categories for the analysis of the effects of different fossorial lifestyles on the appendicular phenotype. These were assessed by DA, which produces linear combinations of variables (canonical variates) that best separate *a priori* defined groups, based on maximizing differences between those groups and reducing their within-group differences. The DA was also used to estimate whether specimens could be classified into a defined ecomorphological

group. As no considerable sex-related differences were found among the morpho-functional indices (Appendix 4.2), the ordination analyses (PCA and DA) were carried out combining males, females and specimens of unknown sex.

The main questions addressed by the PCA and DA are: i) what variables contribute most to species differentiation for the forelimbs and hindlimbs independently, and ii) can bathyergid species be correctly classified *a priori* into defined ecomorphological groups, respectively. The PCA used separated datasets for forelimbs (n = 244) and hindlimbs (n = 217), and only specimens with a complete set of measurements (for forelimb or for hindlimb) were considered in the analyses. For the DA, a combined dataset of specimens with a full record of both forelimb and hindlimb indices (n = 216) was carried out. This reduced considerably the total number of individuals analyzed, although still showed a good representation of individuals per species.

Because some indices were lacking for *H. glaber*, separated PCAs and DAs were performed: i) a dataset including all species, but excluding the indices not present in *H. glaber* (i.e. RDP, TRI, TRI* and TJI), and ii) a dataset including all indices, but excluding *H. glaber*. All analyses and plots were performed in Microsoft Excel (2010), PAST version 2.17c and IBM SPSS version 25 (IBM, 2017) Statistical Package for Social Sciences. The algorithm to assess the correlation matrix for the PCA was the "variance-covariance", since all the linear measurements used to build the indices were originally measured in the same unit (mm). Variables were analyzed to highlight between group (species) differences.

4.3 RESULTS

4.3.1 Functional Morphology

The general anatomy of all limb bones in bathyergids showed typical features associated with fossoriality, i.e. presence of a well-defined deltoid tubercle, wide epicondyles, elongated olecranon processes and distal fusion of the tibia and fibula. However, the phenotype of the humerus, tibia and fibula of naked mole-rats (*H. glaber*) differed from that of other bathyergids. The following anatomical comparisons focused mostly on such bones. At intraspecific level, *H. glaber* also showed differences in the femur, tibia and fibula. For these reasons, the anatomical description of *H. glaber* is relatively more exhaustive, and directly discussed in this section considering early descriptive works made on wild-caught specimens of this species (e.g. Hill *et al.*, 1957).

4.3.1.1 Humerus *(Fig. 4.5)*

All bathyergid humeri showed typical adaptations to scratch-digging habits. In general, the shape of the humerus is stouter in comparison to surface-dwelling rodents (Samuels & Van Valkenburgh, 2008). In the proximal region, the humeral head is quite large and hemispherical (ellipsoid) with its longer proximo-distal axis oriented slightly distally towards the lateral aspect of the bone. In lateral/medial view, the humeral head is highly convex in all species, although *H. glaber* showed a more flattened humeral head. This feature has also been observed in wild-caught naked mole-rats (Hill *et al.*, 1957). The humeral head is generally slightly higher in position as compared to the greater and lesser tubercles, although sometimes it is

at similar height to the greater tubercle. The greater tubercle is always larger than the lesser tubercle. The intertubercular groove is well developed in all species.

The diaphysis is relatively straight in both anteroposterior and mediolateral views, and thickens towards the proximal and distal parts of the bone. In anterior view, a very well-developed deltoid tubercle appears relatively far from the shoulder joint, except in *H. glaber* where this trait is absent. The proximal origin of the deltoid tubercle starts under the greater tubercle and extends downwards through the diaphysis creating a marked deltoid crest ("ridge" in Holliger, 1916). Hill *et al.* (1957) also mentioned a strong deltoid crest in *H. glaber*, but there is not detailed description of this feature. In *H. glaber*, a pectoral crest is also observed running all the way down through the lateral side of the shaft, and joining with the deltoid crest at the midshaft. In the rest of the bathyergids, the deltoid tubercle is latero-distally oriented, which differs from other fossorial species such as ctenomyids in which the process appears to be oriented at right angles to the longitudinal axis of the bone (e.g. Lessa *et al.*, 2008; Morgan *et al.*, 2015). In the posteromedial side, at the level of the proximal origin of the deltoid tubercle, the teres tuberosity (tuberositas teres major) appears in all species, although seems to be less conspicuous in *G. capensis*. The marked humeral torsion of this bone is clearly observed in posterior view. This is defined by a line that diagonally crosses the midshaft, from the humeral head to the lateral area of the bone, giving rise to the lateral epicondylar crest (crista supracondylaris lateralis). Despite some interspecific and intraspecific differences, this crest is poorly developed in bathyergids as compared to other fossorial mammals such as armadillos (Hildebrand, 1985; Stein, 2000). The mediolateral diameter of the distal diaphysis (below the deltoid tubercle) is quite thick in all species, except in *H. glaber* where it is rather the narrowest point of the diaphysis. As described for wild-caught specimens of *H. glaber*, this region and its articular extremity are relatively weak (Hill *et al.*, 1957). Nevertheless, all species showed a relatively thick development of the epicondyles, especially the medial epicondyle, which is sometimes oriented downwards in some species and individuals (*F. damarensis* and *H. glaber*). The lateral epicondyle is well developed and associated with the lateral epicondylar crest, although *B. suillus* showed a smaller development of this crest. All species showed a well-developed supratrochlear fossa, which is sometimes resorbed and forms the supratrochlear foramen. The topography of the distal humerus of *H. glaber* is less marked and shows a more even surface, probably as a result of a lesser degree of muscular and tendon attachments. Hill *et al.* (1957) mentioned that the olecranon (trochlea) and coronoid fossa are distinct and that there is an additional small, rounded but deep (capitellar) fossa on the posterior surface of the medial epicondyle. In this study, it was observed that the trochlea and capitulum of all species were well-defined and similar in form and size, although it was less defined in *H. glaber*. As noted in previous studies (e.g. De Graaff, 1979, 1981), none of the specimens studied here showed an entepicondylar foramen in the distal humerus.

As mentioned previously, in *H. glaber* the most conspicuous difference with the rest of the bathyergids was the lack of the protuberant deltoid tubercle. Other mammals that exhibit a marked difference in the development of the deltoid tubercle at family level is found in the orycteropodids (Tubulidentata). The only extant orycteropodid species, the aardvark *Orycteropus afer* is a highly fossorial

mammal with a marked deltopectoral tuberosity, although some fossil relatives have a superficial development of this feature (Lehmann *et al.*, 2006). Lehmann *et al.* (2006) described the postcranial anatomy of the extinct *O. abundulafus* and emphasized the rather slender humerus in comparison to *O. afer,* and noted the absence of a projected deltoid tubercle with a thinner midshaft. These observations show that despite the strong developmental regulation of diaphyseal tuberosities and superstructures suggested for long bones (Hall, 1978; Stern *et al.*, 2015), marked interspecific differences within some mammalian clades can also be observed.

Another difference of *H. glaber* was the cross-sectional shape of the humerus at the midshaft. In most bathyergids, the diaphyseal bone geometry at the midshaft is triangular, with the anterolateral region showing a pointy projection due to the presence of the distal origin of the deltoid tubercle. In *H. glaber*, the diaphysis is highly compressed, forming a rather semi-triangular (ellipsoidal) diaphyseal cross-sectional shape (see Fig. 6.1 in Ch. 6). Thus, the cross-sectional morphology of the humerus in naked mole-rats is rather ellipsoidal when compared to other bathyergids and this is most likely a result of the lack of a deltoid tubercle, although the major axis of the bone is still oriented anterolaterally in all bathyergids.

4.3.1.2 Ulna *(Fig. 4.5)*

The anatomy of the ulna in bathyergids is also typical of a fossorial mammal, i.e. it is relatively robust and larger than the humerus, but not to the same extent as other terrestrial and cursorial mammals (Howell, 1965). The most distinctive feature is the elongated olecranon. In lateral/medial side view, below the olecranon, the diaphysis reaches its major anteroposterior thickness, which decreases distally. Both the anconeal process and the medial coronoid process are well-developed. The former rises perpendicularly to the longitudinal axis of the bone, while the latter orientates diagonally to the distal portion of the bone forming a ~45° angle with the longitudinal axis of the bone. This probably facilitates a maximal flexion and extension of this bone with the humerus. In the lateral view, there is a conspicuous sulcus beginning just below the trochlear notch and extending to the midshaft. At this point of the diaphysis, a conspicuous scar for the interosseous ligament appears in the anterior region. The midshaft region seems to be wider in *H. glaber* as compared to other species.

In anterior view, the ulna appears relatively straight in some specimens, although a slight curvature can appear in others, thus forming a concave medial side. This is accentuated when the tip of the proximal epiphysis tends to project internally (medially). Many specimens of *H. glaber* showed a very curved ulna. In anterior view, the olecranon also shows a wide surface behind the anconeal process, where a nutrient foramen is sometimes observed (Fig. 4.2). This surface is considerably larger in *B. suillus* as compared to other species. A conspicuous aspect observed in all bathyergids is that the anteroposterior diameter of the midshaft is thicker as compared to the mediolateral diameter, which probably accounts for a higher anteroposterior sectional area to withstand higher magnitudes of bone strain associated with bending loads (Montoya-Sanhueza *et al.*, 2019).

FIGURE 4.5. Humeri (A) and ulnae (B) of bathyergids studied here. The bones showed here are from the largest elements for each species. All bones are scaled to the same size to show differences in gross morphology. The bones in grey show the real relative size of bones with respect to other species. The humeri are aligned to the distal origin of the deltoid tubercle (except *H. glaber*), while the ulnae are aligned to the centre of the trochlear notch.

4.3.1.3 Femur *(Fig. 4.6)*

All species showed similar femoral shape, although some differences in diaphyseal robusticity were observed. In the proximal portion of the bone, all species showed a circular femoral head with a conspicuous femoral neck, so the neck and trochanters were clearly demarcated. However, *H. glaber* had a more hemispherical femoral head (Hill *et al.*, 1957) and a shorter femoral neck. Some specimens even showed fused ossification centers of the greater trochanter and the femoral head. This is probably the result of a reduced femoral neck, which reduces considerably the area between the femoral head and the greater trochanter (but see below). The greater trochanter is located at similar height as the femoral head in all species. The lesser trochanter is quite similar in position and size in all species, and it is located lower than the femoral head. Larger species showed a deeper trochanteric fossa, whereas smaller species showed a more superficial fossa. However, all species have a similar development of the intertrochanteric crest in terms of shape and size. The shape of the third trochanter varies between species: it covers a wider surface in solitary species, and tends to be more localized in social species, making it appear less differentiated. This results in solitary species having a longer extended third trochanter, which originates from the bottom part of the greater trochanter and results in the formation of the gluteal crest (ridge). The midshaft is considerably wider (mediolaterally) in all species and flattened in the anteroposterior direction, although some interspecific/intraspecific variation can be observed. In *H. glaber,* the anteroposterior section is highly compressed, which was also reported for wild-caught specimens (Hill *et al.*, 1957). The diaphysis is also straight when observed in lateral/medial view. In anterior view, the diaphysis is internally (medially) curved with respect to the proximal epiphysis. This is probably related to the internalization of the limbs of subterranean mammals with respect to the middle line of the body, i.e. the limbs tend to be closer to the mid-plane of the body in burrowing animals, so the limbs do not become an obstacle when locomoting within burrows. This is also observed in the position of the fore- and hindfeet which are internally oriented to reduce contact with the walls of the burrow, thus enhancing locomotor performance (see Ch. 3, Montoya-Sanhueza *et al.*, 2019). The distal femur shows a wide epicondylar region and a wide patellar surface without showing the typical femoral patellar groove observed in other surface-dwelling mammals (e.g. Szalay & Sargis, 2001). In general, both epicondyles project externally at a similar degree. In posterior view, some differences between species can be observed for the distal region of the femur. Both condyles are similar in size and shape (circular) in social species, whilst solitary species show a more irregular or ellipsoidal medial condyle, which is also slightly bigger than the lateral one. All species showed a well-developed intercondyloid fossa.

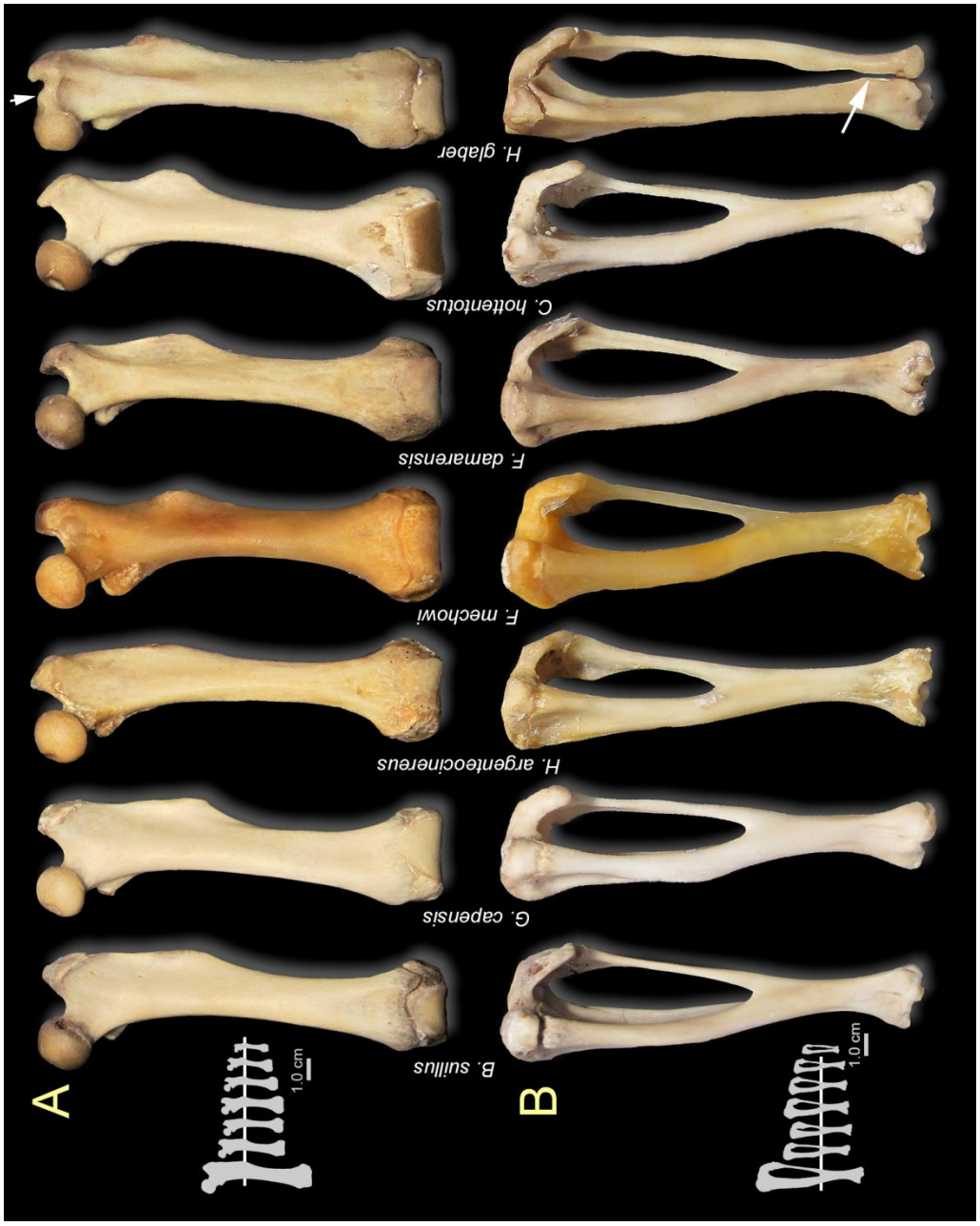

FIGURE 4.6. Femora and tibia-fibulae of bathyergids studied here. These bones are from the largest individuals of each species. All bones are scaled to the same size to show differences in gross morphology. The bones in grey show the real relative size of bones with respect to other species. All femora are aligned to the distal origin of the third trochanter, and the tibia-fibulae are aligned to the distal tibio-fibular junction, except *H. glaber*, which does not fuse the fibula to the tibia (arrow). The arrow head in the femur of *H. glaber* indicates the coalesced condition of the proximal epiphysis.

4.3.1.4 Tibia-fibula *(Fig. 4.6)*

All bathyergids showed a proximal and distal fusion of the tibia and fibula, except *H. glaber* in which the bones are not fused distally, but proximally. Previous studies have noted the fused condition of the proximal tibial and fibular epiphyses in bathyergids (Patterson & Upham, 2014 and references therein). However, although the latter authors mention that the general condition among Bathyergoidea is a distal fusion of the tibia and fibula (see also De Graaff, 1971), the present study shows for first time that this feature in naked mole-rats differs from the generalized –fused– condition found in other bathyergids. Hill *et al.* (1957) reported the individuality of tibia and fibula in *H. glaber*, but they did not mention that such condition differs from other bathyergids. In *H. glaber*, the fibula approaches to the tibia but without fusing to it, although there is a syndesmotic joint in the lowermost region of these bones (Fig. 4.7). Thus, the joint is sustained by connective tissue most likely similar to an interosseous ligament which also allows mobility (Carleton, 1941). The soft tissue nature of this connection was evidenced after dissection and skeletonization of both elements by bacterial activity which resulted in the separation of both elements. Extraordinarily, some specimens of *H. glaber* (3) in this study did show distal fusion of such bones (Fig. 4.7). The fusion was not evidently related to any pathology, although the individual #072 had an extremely thick tibia and fibula, and showed extreme resorption of the humeral midshaft, as well as epiphyseal femoral bone resorption. Similar osteopetrotic condition was observed in the tibia of one specimen of *F. mechowii* (#218, Fig. 4.7), although the rest of the long bones of the same individual did not show any apparent external abnormality.

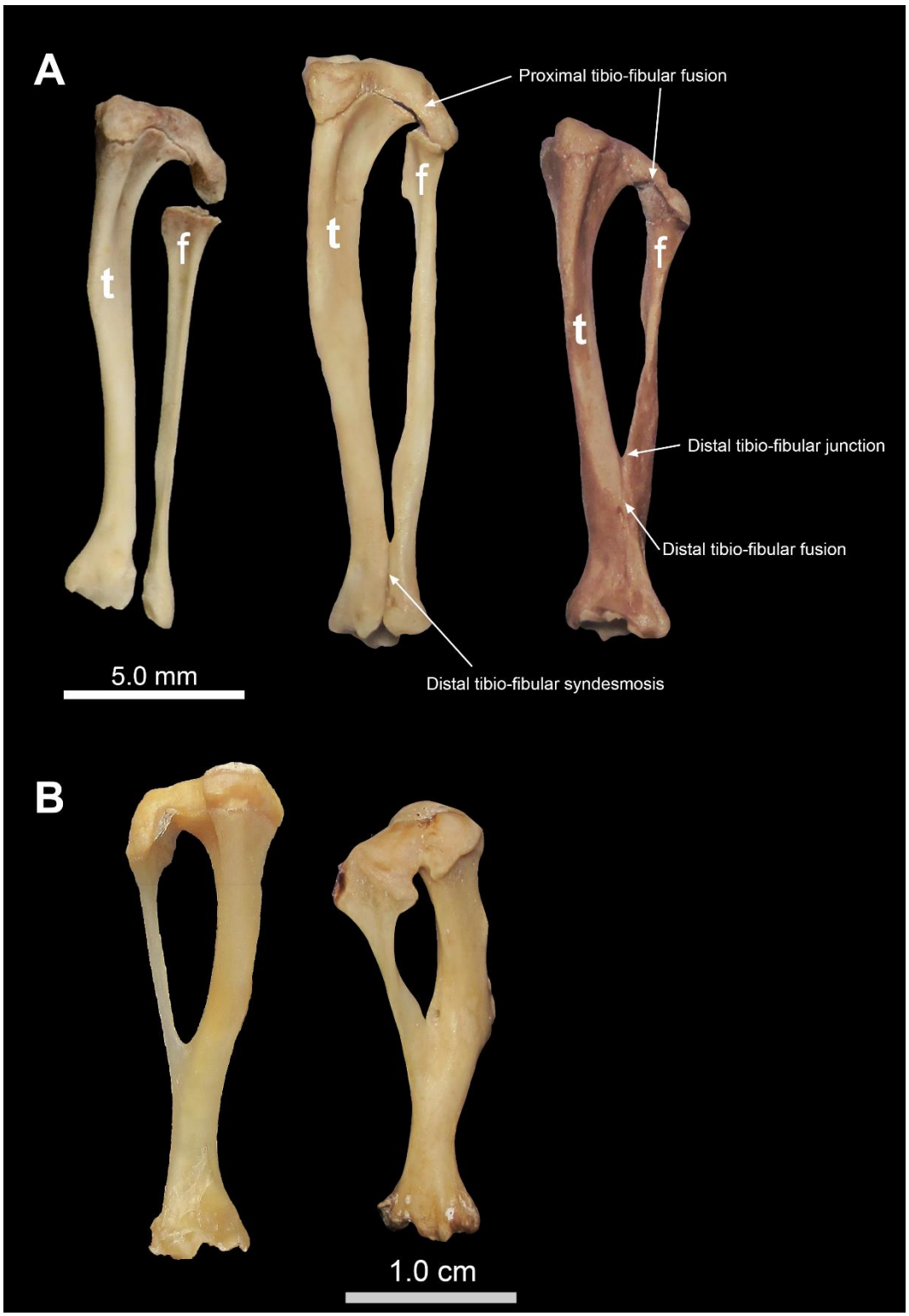

FIGURE 4.7. Tibial and fibular anatomy in Bathyergidae. A) Detail of the tibia and fibula of naked mole-rats (*Heterocephalus glaber*) and intraspecific variation showing fusion of these bones. The specimen on the left shows unfused (normal) condition, with post-skeletonization separation of bones. In the middle, a second specimen with normal condition showing both bones in anatomical position where a distal tibio-fibular syndesmosis (non-ossified) maintain the bones together. On the right, an individual showing non-pathological distal fusion of tibia and fibula. B) Two specimens of *Fukomys mechowii* showing a normal (left) and a pathological condition (right), probably related to some kind of localized intralimb osteopetrosis.

4.3.2 Sex Differences of Morpho-Functional Traits

Few significant differences were found between sexes for morpho-functional indices (Fig. 4.8). Solitary species (i.e. *B. suillus*, *G. capensis*) and *H. glaber* showed differences principally in the forelimb, while social species showed differences in the hindlimb (tibia) (Fig. 4.8). In this study, only *H. argenteocinereus* did not show sex differences in any functional traits. Despite the sexual dimorphism reported for social species in previous studies (e.g. *F. mechowii*, *F. damarensis, C. hottentotus*), the results obtained here were non-significant for such species. This means that the sample used in this study is biased or too small to show such differences.

The females of *B. suillus* have higher HRI and EIh as compared to males, although this could be an artefact of the non-normally distributed EIh. The females of *G. capensis* showed a lower HHI as compared to males. The females of *F. mechowii* have higher TRI* as compared to males. The species with most of the differences were *B. suillus* and *H. glaber*: In *H. glaber*, the females showed higher HRI, HHI and URI as compared to males. The variation in *H. glaber* is probably the result of the non-normal distribution of HRI in both sexes, as well as of HHI and URI in females.

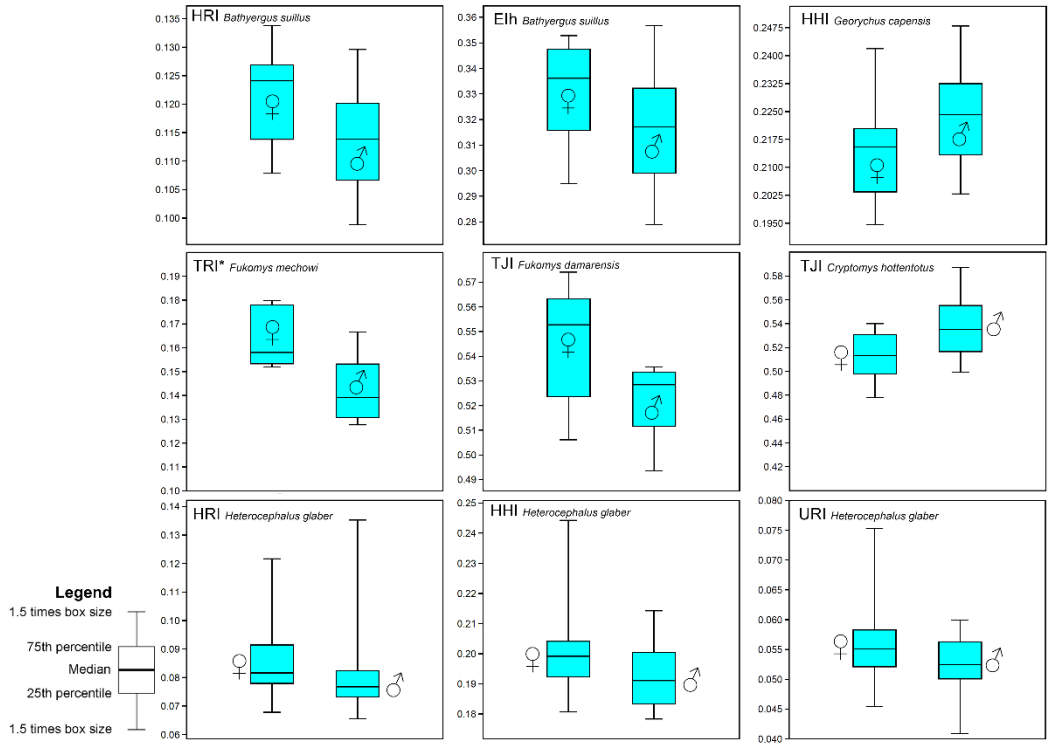

FIGURE 4.8. Box-whisker plots showing statistically significant sex differences for morpho-functional indices.

4.3.3 Multivariate and Ordination Analyses

4.3.3.1 MANOVA (Forelimb) *(Tables 4.2-4.4)*

The MANOVA showed significant differences for all species (Wilks' λ = 0.013; $F_{42, 1086}$ = 38.961; p << 0.001) (Table 4.2). Almost all the values accounting for the proportion of variance (partial eta squared) explaining the differences between

species were high (>0.50), with a maximum in BI (0.697) and a minimum in URI (0.207) (Table 4.3). The MANOVA for all indices also showed significant differences (Wilks' λ = 0.029; $F_{40, 726}$ = 22.823; p << 0.001). The partial eta squared was higher in IFA (0.588), URI* (0.499) and RDP (0.409), while the rest of the variables showed lower values (<0.35). The combined results of the Tamhane *post hoc* test are summarized in Figure 4.9. The brachial index (BI) showed the lowest scores among all indices (0.14) in the analysis of all the indices, whereas it was one of the highest (0.697) in the analysis including all species. This indicated that when *H. glaber* is included in the analysis, BI had a higher explanatory power to ordinate species, since this species has a smaller ulna among bathyergids relative to the humerus (Fig. 4.9). Most pair-wise *post hoc* tests showed significant differences between *H. glaber* and all other species for almost all indices except for ulnar features such as IFA, URI and URI* (Fig. 4.9).

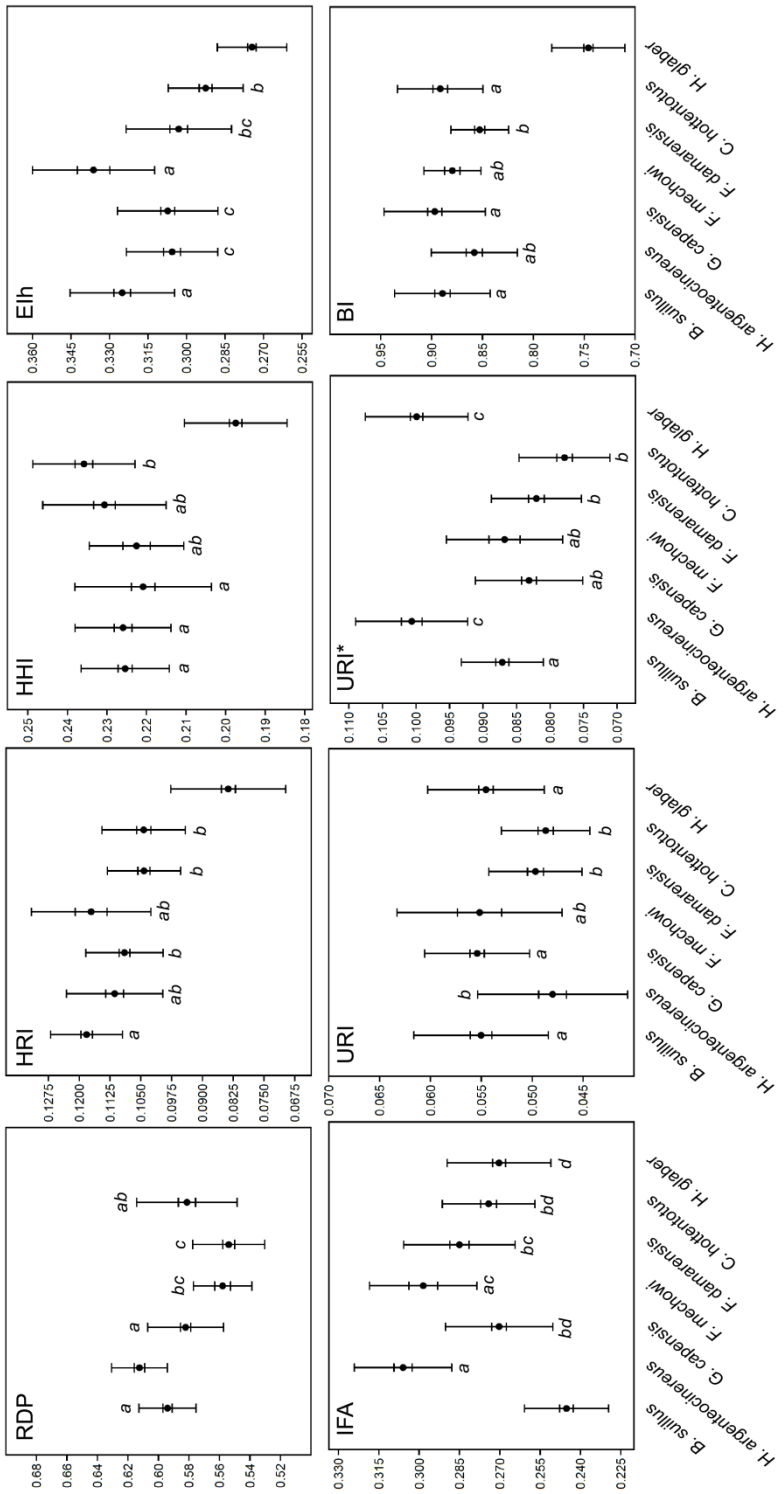

FIGURE 4.9. Box plots of each index (forelimb) in the seven bathyergid species, showing mean value (central point), standard error (shorter whiskers) and standard deviation (longer whiskers). Species that share the same letter represent homogeneous subsets, as identified by *post hoc* (Tamhane) tests.

TABLE 4.2. Descriptive statistics of morpho-functional indices of both fore and hindlimb datasets.

FORELIMB

Species	RDP ± SD	HRI ± SD	HHI ± SD	EIh ± SD	IFA ± SD	URI ± SD	URI* ± SD	BI ± SD
B. suillus (*n* = 39)	0.5940 ± *0.0187*	0.1182 ± *0.0087*	0.2254 ± *0.0112*	0.3251 ± *0.0203*	0.2452 ± *0.0156*	0.0550 ± *0.0066*	0.0871 ± *0.0061*	0.8893 ± *0.0469*
H. argenteocinereus (*n* = 29)	0.6125 ± *0.0183*	0.1113 ± *0.0117*	0.2259 ± *0.0121*	0.3057 ± *0.0178*	0.3060 ± *0.0181*	0.0480 ± *0.0074*	0.1006 ± *0.0084*	0.8581 ± *0.0423*
G. capensis (*n* = 33)	0.5868 ± *0.0203*	0.1109 ± *0.0092*	0.2203 ± *0.0172*	0.3076 ± *0.0197*	0.2757 ± *0.0187*	0.0552 ± *0.0056*	0.0832 ± *0.0091*	0.8886 ± *0.0465*
F. mechowi (*n* = 12)	0.5594 ± *0.0168*	0.1139 ± *0.0128*	0.2225 ± *0.0119*	0.3293 ± *0.0163*	0.3025 ± *0.0184*	0.0527 ± *0.0057*	0.0844 ± *0.0059*	0.8805 ± *0.0300*
F. damarensis (*n* = 32)	0.5540 ± *0.0239*	0.1048 ± *0.0090*	0.2314 ± *0.0151*	0.3017 ± *0.0209*	0.2878 ± *0.0178*	0.0498 ± *0.0046*	0.0821 ± *0.0067*	0.8521 ± *0.0285*
C. hottentotus (*n* = 34)	0.5813 ± *0.0329*	0.1043 ± *0.0101*	0.2358 ± *0.0129*	0.2926 ± *0.0146*	0.2741 ± *0.0172*	0.0487 ± *0.0043*	0.0778 ± *0.0068*	0.8916 ± *0.0421*
H. glaber (*n* = 65)	- -	0.0837 ± *0.0141*	0.1974 ± *0.0131*	0.2744 ± *0.0136*	0.2703 ± 0.0193	0.0545 ± *0.0057*	0.0999 ± *0.0077*	0.7458 ± *0.0360*
Total (*N* = 244)	- -	0.1067 ± *0.0113*	0.2227 ± *0.0123*	0.3052 ± *0.0187*	0.2802 ± *0.0208*	0.0520 ± *0.0031*	0.0879 ± *0.0089*	0.8580 ± *0.0519*
Total (*N* = 180)	0.5813 ± *0.0218*	0.1106 ± *0.0053*	0.2269 ± *0.0058*	0.3103 ± *0.0141*	0.2819 ± *0.0223*	0.0516 ± *0.0032*	0.0859 ± *0.0078*	0.8767 ± *0.0173*

HINDLIMB

Species	FRI ± SD	EIf ± SD	FHI ± SD	TSI ± SD	TRI ± SD	TRI* ± SD	TJI ± SD	CI ± SD	IMI ± SD
B. suillus (*n* = 39)	0.1190 ± *0.0089*	0.239 ± *0.0155*	0.136 ± *0.0095*	0.491 ± *0.0201*	0.094 ± *0.0063*	0.127 ± *0.0117*	0.599 ± *0.0184*	0.927 ± *0.0273*	0.862 ± *0.0299*
H. argenteocinereus (*n* = 29)	0.1273 ± *0.0136*	0.262 ± *0.0139*	0.144 ± *0.0072*	0.483 ± *0.0324*	0.081 ± *0.0081*	0.149 ± *0.0185*	0.531 ± *0.0363*	0.987 ± *0.0389*	0.875 ± *0.0241*
G. capensis (*n* = 23)	0.1291 ± *0.0126*	0.257 ± *0.0125*	0.139 ± *0.0071*	0.456 ± *0.0282*	0.094 ± *0.0101*	0.144 ± *0.0088*	0.517 ± *0.0248*	0.979 ± *0.0271*	0.884 ± *0.0258*
F. mechowi (*n* = 11)	0.1338 ± *0.0126*	0.300 ± *0.0206*	0.146 ± *0.0111*	0.468 ± *0.0233*	0.080 ± *0.0070*	0.153 ± *0.0178*	0.547 ± *0.0253*	1.035 ± *0.0335*	0.910 ± *0.0298*
F. damarensis (*n* = 18)	0.1197 ± *0.0125*	0.279 ± *0.0217*	0.144 ± *0.0077*	0.445 ± *0.0423*	0.073 ± *0.0077*	0.130 ± *0.0142*	0.533 ± *0.0231*	1.059 ± *0.0278*	0.851 ± *0.0230*
C. hottentotus (*n* = 33)	0.1239 ± *0.0169*	0.264 ± *0.0179*	0.132 ± *0.0070*	0.425 ± *0.0324*	0.079 ± *0.0095*	0.128 ± *0.0132*	0.529 ± *0.0245*	1.067 ± *0.0330*	0.844 ± *0.0189*
H. glaber (*n* = 64)	0.1098 ± *0.0098*	0.240 ± *0.0121*	0.138 ± *0.0116*	0.388 ± *0.0268*	- -	- -	- -	1.028 ± *0.0345*	0.856 ± *0.0194*
Total (*N* = 217)	0.1232 ± *0.0079*	0.2630 ± *0.0214*	0.1400 ± *0.0052*	0.4509 ± *0.0358*	- -	- -	- -	1.0118 ± *0.0500*	0.8688 ± *0.0228*
Total (*N* = 153)	0.1255 ± *0.0057*	0.2668 ± *0.0206*	0.1402 ± *0.0057*	0.4615 ± *0.0246*	0.0834 ± *0.0087*	0.1386 ± *0.0115*	0.5426 ± *0.0291*	1.0091 ± *0.0541*	0.8709 ± *0.0241*

TABLE 4.3. Details of the MANOVAs of morpho-functional indices for datasets with all species and all indices.

		Value	*F*	Hypothesis df	Error df	Sig.	Partial Eta Squared (PES)	PES (indices) > 0.50
Forelimb	*Pillai's Trace*	2.251	17.396	40	850	<< 0.0001	0.450	IFA
(all indices)	*Wilks' Lambda*	0.029	22.823	40	726	<< 0.0001	0.508	
Forelimb	*Pillai's Trace*	2.469	23.580	42	1416	<< 0.0001	0.412	All except URI
(all spp)	*Wilks' Lambda*	0.013	38.961	42	1087	<< 0.0001	0.512	
Hindlimb	*Pillai's Trace*	2.304	13.575	45	715	<< 0.0001	0.461	CI, TJI, EIf
(all indices)	*Wilks' Lambda*	0.023	18.534	45	625	<< 0.0001	0.532	
Hindlimb	*Pillai's Trace*	1.942	16.745	36	1260	<< 0.0001	0.324	CI, TSI, EIf
(all spp)	*Wilks' Lambda*	0.041	26.799	36	903	<< 0.0001	0.413	

TABLE 4.4. Details of the MANOVAs of morpho-functional indices for both fore- and hindlimb datasets.

Index	df	Mean Square	*F*	*p*	Partial Eta Squared
All indices (FORELIMB)					
RDP	5	0.013	23.959	<< 0.0001	0.409
HRI	5	0.001	9.744	<< 0.0001	0.220
HHI	5	0.001	5.412	<< 0.0001	0.135
EIh	5	0.005	15.016	<< 0.0001	0.303
IFA	5	0.015	49.380	<< 0.0001	0.588
URI	5	0.000	9.890	<< 0.0001	0.222
URI*	5	0.002	34.454	<< 0.0001	0.499
BI	5	0.010	5.596	<< 0.0001	0.139
All species (FORELIMB)					
HRI	6	0.006	51.457	<< 0.0001	0.566
HHI	6	0.008	43.678	<< 0.0001	0.525
EIh	6	0.014	44.822	<< 0.0001	0.532
IFA	6	0.013	40.206	<< 0.0001	0.504
URI	6	0.000	10.319	<< 0.0001	0.207
URI*	6	0.003	56.907	<< 0.0001	0.590
BI	6	0.145	90.806	<< 0.0001	0.697
All indices (HINDLIMB)					
FRI	5	0.001	3.815	0.0028	0.115
EIf	5	0.008	30.219	<< 0.0001	0.507
FHI	5	0.001	11.819	<< 0.0001	0.287
TSI	5	0.020	21.848	<< 0.0001	0.426
TRI	5	0.002	29.108	<< 0.0001	0.498
TRI*	5	0.003	15.947	<< 0.0001	0.352
TJI	5	0.029	43.891	<< 0.0001	0.599
CI	5	0.089	90.036	<< 0.0001	0.754
IMI	5	0.010	16.221	<< 0.0001	0.356
All species (HINDLIMB)					
FRI	6	0.0021	14.380	<< 0.0001	0.291
EIf	6	0.0101	42.751	<< 0.0001	0.550
FHI	6	0.0007	7.564	<< 0.0001	0.178
TSI	6	0.0590	70.142	<< 0.0001	0.667
CI	6	0.0806	76.605	<< 0.0001	0.686
IMI	6	0.0094	16.781	<< 0.0001	0.324

4.3.3.2 MANOVA (Hindlimb) *(Tables 4.2-4.3)*

This analysis showed significant differences between species for all indices (Wilks' λ = 0.041; $F_{36,\ 902}$ = 26.799; p << 0.001). The proportion of variance (partial eta squared) accounting for the differences between species was higher (>0.55) in CI and TJI. The Tamhane *post hoc* tests are shown in Figure 4.10. The MANOVA including *H. glaber* (but excluding RDP) also showed clear differences between species. The highest (>0.50) partial eta squared values were EIf, TSI and CI. The Tamhane *post hoc* tests showed significant differences between *H. glaber* and some species (Fig. 4.10).

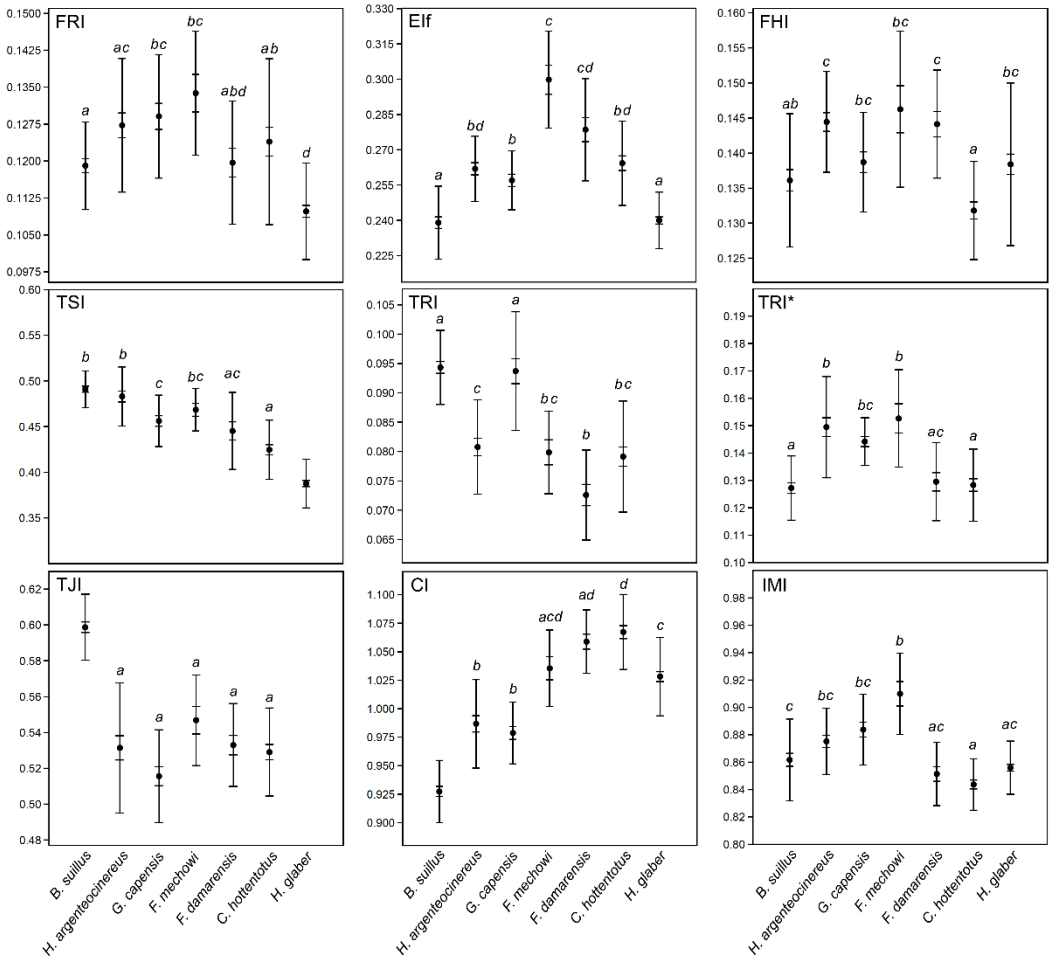

FIGURE 4.10. Box plots of each index (hindlimb) in seven bathyergid species, showing mean value (central point), standard error (shorter whiskers) and standard deviation (longer whiskers). For each index, species that share the same letter represent homogeneous subsets, as identified by *post hoc* (Tamhane) tests.

4.3.3.3 PCA (Forelimb)

Two PCAs (PCA[i] and PCA[ii]) were performed for the forelimb dataset including all specimens (of known and unknown sex): i) one considering all 7 species but excluding one index (RDP), and another ii) considering all 8 indices but excluding *H. glaber*.

The PCA[i] with all species generated six components although most of the variation found in the forelimb was contained in the three first components (98.28%) (Table 4.5; Fig. 4.11). Most of this variation was explained by PC1, which contained 81.75% of the total variance. This analysis showed significant separation among species for the two first components (Wilks' λ= 0.085; $F_{12, 472}$ = 95.66; p << 0.0001), especially showing differences between the morphospace occupied by *H. glaber* and most bathyergids along PC1. The indices that contributed most to the variation in PC1, following the criterion defined by Wilson & Geiger (2015) (as r^2 > 0.60), were BI (r^2 = 0.72) and HRI (r^2 = 0.62). Most specimens were distributed in the positive side of PC1, showing both higher brachial index (BI) and epicondylar index (EIh) (Table 4.5). The specimens of *H. glaber* were distributed in the negative side and showed higher robusticity of the ulna (high URI and URI*). The PC2 represented only 11.56% of the total variation. The index that contributed most to the variation in this axis was the index of fossorial ability (IFA; r^2 = 0.82). Most specimens distribute equally along the positive and negative sides of the axis, although the solitary species *B. suillus* and *H. argenteocinereus* tended to associate to the extremes of the negative and positive sides, respectively; *B. suillus* tended to show low IFA values, *H. argenteocinereus* higher values, and the rest of the species showed intermediate IFA values.

TABLE 4.5. Table showing the results of the PCA analysis for the forelimb.

All species (PCA[i]) - Forelimb

Variables	PC 1	PC 2	PC 3	PC 4	PC 5	PC 6
HRI	0.185	0.028	0.277	0.294	0.136	0.765
HHI	0.184	0.068	-0.336	0.094	0.859	0.068
EIh	0.258	0.076	0.834	-0.274	0.284	-0.262
IFA	0.013	0.985	-0.070	-0.090	-0.113	0.057
URI	-0.010	-0.085	0.129	-0.149	-0.253	0.518
URI*	-0.106	0.098	0.238	0.888	-0.070	-0.236
BI	0.924	-0.044	-0.192	0.101	-0.287	-0.116
Eigenvalue	0.003143	0.000444	0.000191	0.000036	0.000029	0.000001
% Variance	81.758	11.560	4.959	0.938	0.758	0.027

All indices (PCA[ii]) - Forelimb

Variables	PC 1	PC 2	PC 3	PC 4	PC 5
RDP	0.326	0.899	-0.010	0.059	0.026
HRI	0.094	0.048	0.283	-0.097	0.027
HHI	-0.020	-0.043	-0.290	-0.018	0.858
EIh	0.100	-0.110	0.846	-0.219	0.290
IFA	-0.772	0.224	0.240	0.531	0.041
URI	0.072	-0.047	0.108	-0.022	-0.399
URI*	-0.067	0.305	0.172	-0.180	0.101
BI	0.519	-0.175	0.145	0.790	0.086
Eigenvalue	0.00070	0.00050	0.00025	0.00014	0.00001
% Variance	43.773	31.050	15.510	8.745	0.923

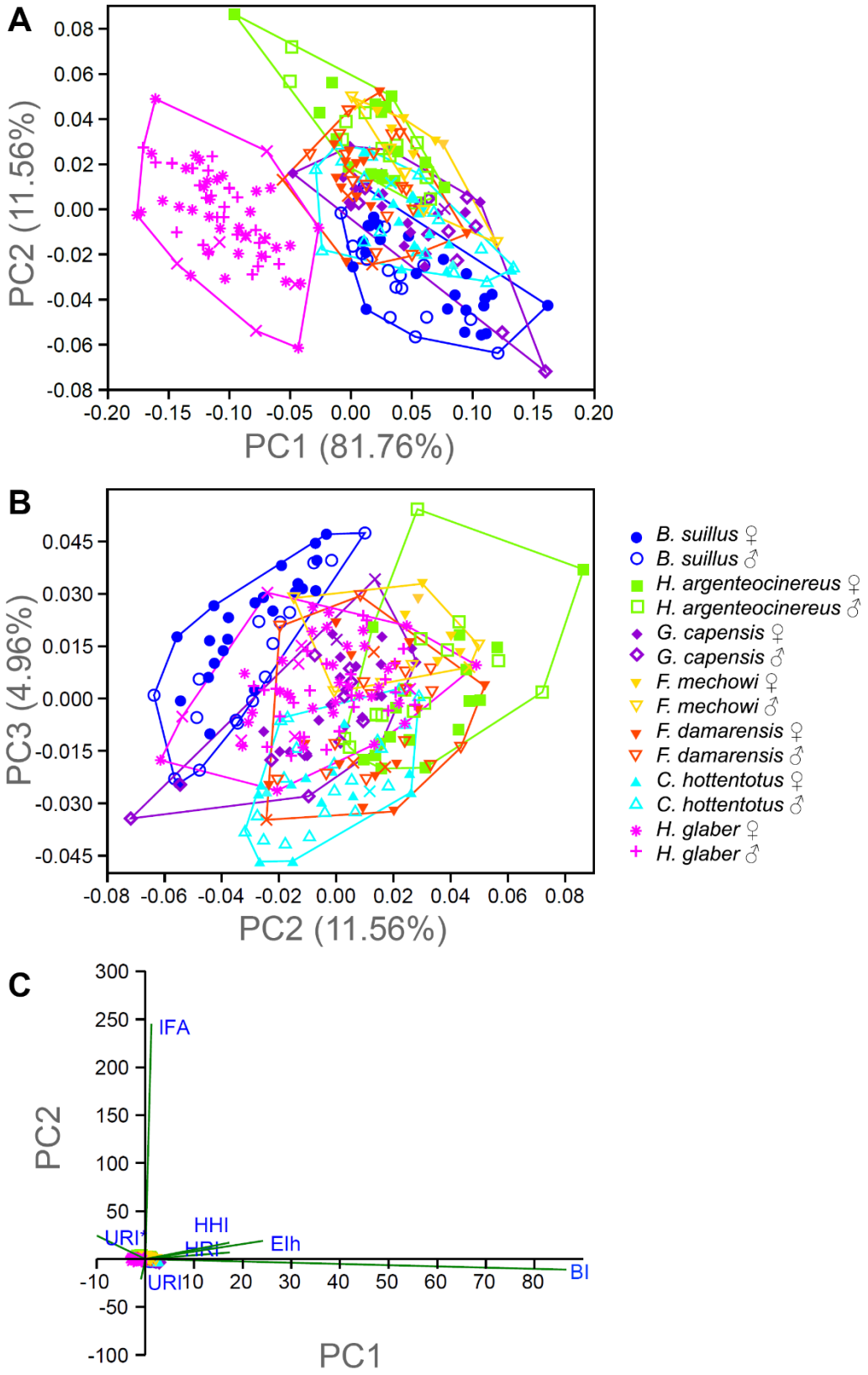

FIGURE 4.11. Results of PCA performed on all bathyergid species including forelimb indices (except RDP), and showing PC1 and PC2 (A), PC2 and PC3 (B) and and biplot for the two first axes (C).

The second PCA[ii] excluding *H. glaber* generated five components, although most of the variance was contained in the four first components (99.08%) (Table

4.5; Fig. 4.12). This analysis also showed significant differences for the three first components, although such differences were less evident (Wilks' λ= 0.224; $F_{15, 472}$ = 22.69; p << 0.0001). Species distribute almost evenly in the center of the two first components. The main contributor to the PC1 is the IFA index (IFA; r^2 = 0.76), where most species share both positive and negative values indicating intermediate IFA values and only *B. suillus* positioning mostly in the positive side thus indicating a relatively lower IFA. *Fukomys* spp. and *H. argenteocinereus* tended to have higher IFA values. The main contributors in PC2 were RDP (r^2 = 0.68) and URI* (r^2 = 0.67) which were mostly associated with the positive side of the axis, where only *F. mechowii* distributed in this region, whereas all the other species showed a variable distribution in the morphospace. *C. hottentotus* tended to be associated with the negative side, showing higher but not significant values of URI. The main contributor of the PC3 was EIh, which showed a relatively high correlation (r^2 = 0.60).

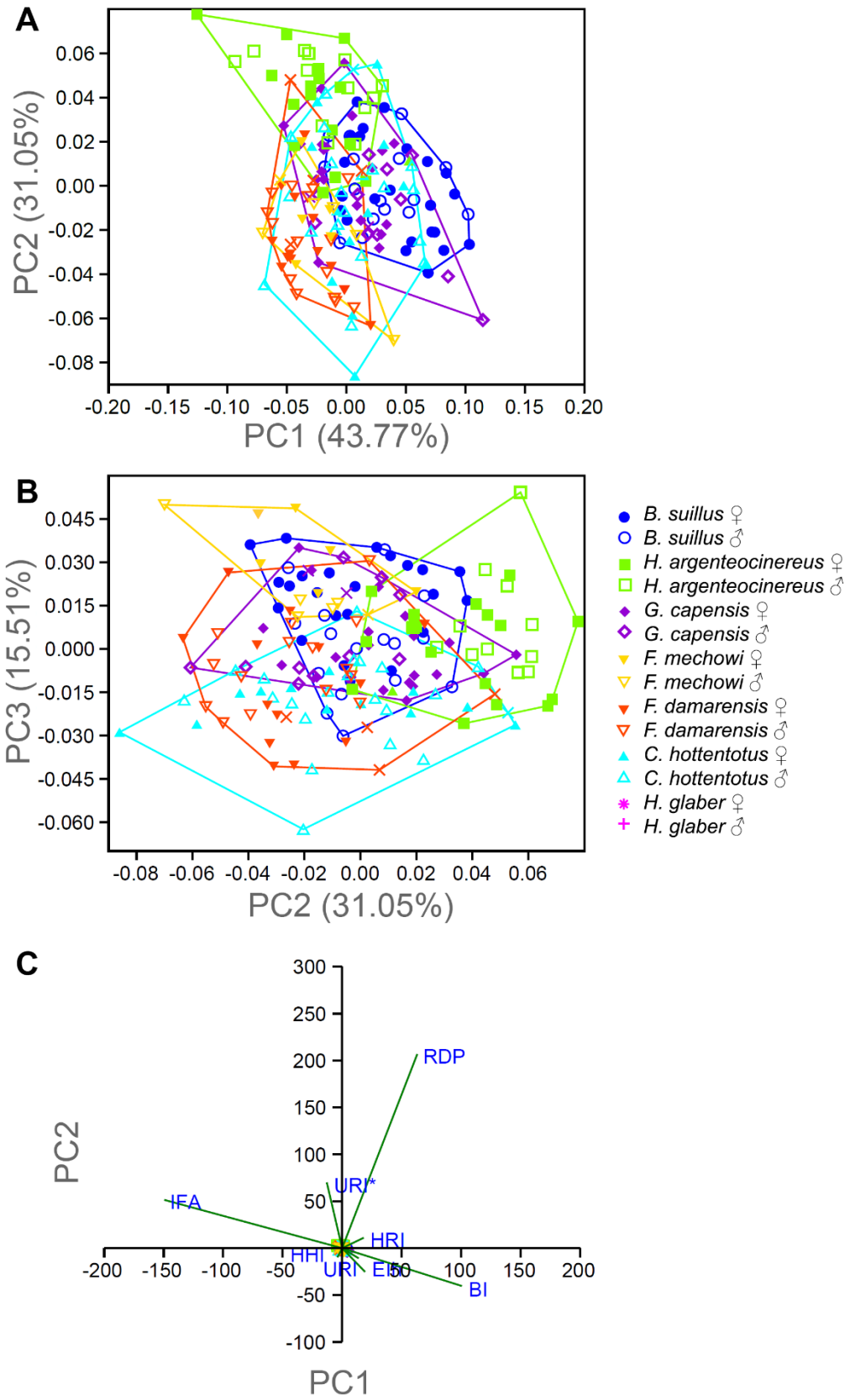

FIGURE 4.12. Results of PCA performed on all forelimb indices but excluding *H. glaber*, and showing PC1 and PC2 (A), PC2 and PC3 (B) and biplot for two first axes (C).

4.3.3.4 PCA (Hindlimb)

For the hindlimb, two PCAs (PCA[i] and PCA[ii]) were also performed; one considering all species (7) but excluding several indices (TRI, TRI* and TJI), and another considering all indices (9) but excluding one species (*H. glaber*). This analysis included the intermembral index (IMI) which is associated with locomotion. Since the comparatively lower number of specimens available for this limb as compared to the forelimb, specimens with an incomplete data set of indices were still included but performing the *"iterative imputation"* method as an estimation for the missing values.

TABLE 4.6. Table showing the results of the PCA analysis for the hindlimb.

All species (PCA[i]) - Hindlimb

Variables	PC 1	PC 2	PC 3	PC 4	PC 5	PC 6
FRI	-0.029	0.196	0.038	-0.697	0.280	0.629
EIf	0.136	0.569	0.025	0.230	-0.675	0.384
FHI	-0.005	0.101	0.066	0.672	0.574	0.453
TSI	-0.493	0.560	-0.578	-0.017	0.194	-0.267
CI	0.848	0.314	-0.215	-0.076	0.261	-0.248
IMI	-0.134	0.463	0.783	-0.064	0.174	-0.346
Eigenvalue	0.003280	0.001206	0.000326	0.000024	0.000006	0.000002
% Variance	67.706	24.902	6.727	0.491	0.134	0.040

All indices (PCA[ii]) - Hindlimb

Variables	PC 1	PC 2	PC 3	PC 4	PC 5
FRI	0.016	0.161	-0.044	0.134	0.385
EIf	0.223	0.408	0.318	-0.028	-0.488
FHI	0.007	0.135	0.050	-0.277	-0.446
TSI	-0.335	0.274	0.223	-0.689	0.193
TRI	-0.319	-0.232	0.847	0.252	0.146
TRI*	-0.070	0.735	0.066	0.435	-0.002
TJI	0.847	-0.030	0.314	-0.083	0.258
CI	-0.003	0.347	-0.099	-0.130	0.538
IMI	-0.112	-0.007	-0.119	0.393	0.000
Eigenvalue	0.00400	0.00100	0.00054	0.00011	0.00002
% Variance	70.527	17.618	9.536	2.014	0.305

The PCA[i] including all species generated six components where the three first components explain 99.33%) of the variance in the hindlimb (Table 4.5; Fig. 4.12). This analysis showed significant separation among species for the two first components (Wilks' λ= 0.098; $F_{12,\ 418}$ = 76.43; p << 0.0001). The PC1 represented 67.71% of the total variance, and it was able to separate *B. suillus* from all solitary and social species, although not *H. argenteocinereus* from *G. capensis*, which rather showed some degree of overlap between each other (Fig. 4.12). The indices the contributed most to differentiation in this axis were CI and TSI, although only CI showed a significant correlation (r^2 = 0.85). The species distributed in the negative side of the PC1 were associated with higher TSI index (solitary species, specially *B. suillus*), while the social species occupied the positive side of the axis and were

associated with higher CI indices. The PC2 contributed with 25.90% of the total variance and it was able to differentiate between the largest social species (*F. mechowii*) in the positive side and the smallest one in the negative side (*H. glaber*) (Fig. 4.12). The positive side of this axis is mostly associated with increased EIf, TSI and IMI, although only EIf showed a significant correlation (r^2 = 0.87). Most species distributed on both sides of the axis, although the largest social species *F. mechowii* distributed only on the positive side, whereas the smallest social species *H. glaber* distributed almost completely on the negative side (except some few specimens). Thus, *F. mechowii* showed higher EIf, TSI and IMI as compared to *H. glaber*. The largest species, *B. suillus* distributed evenly on both sides of the axis, being intermediate between *F. mechowii* and *H. glaber*.

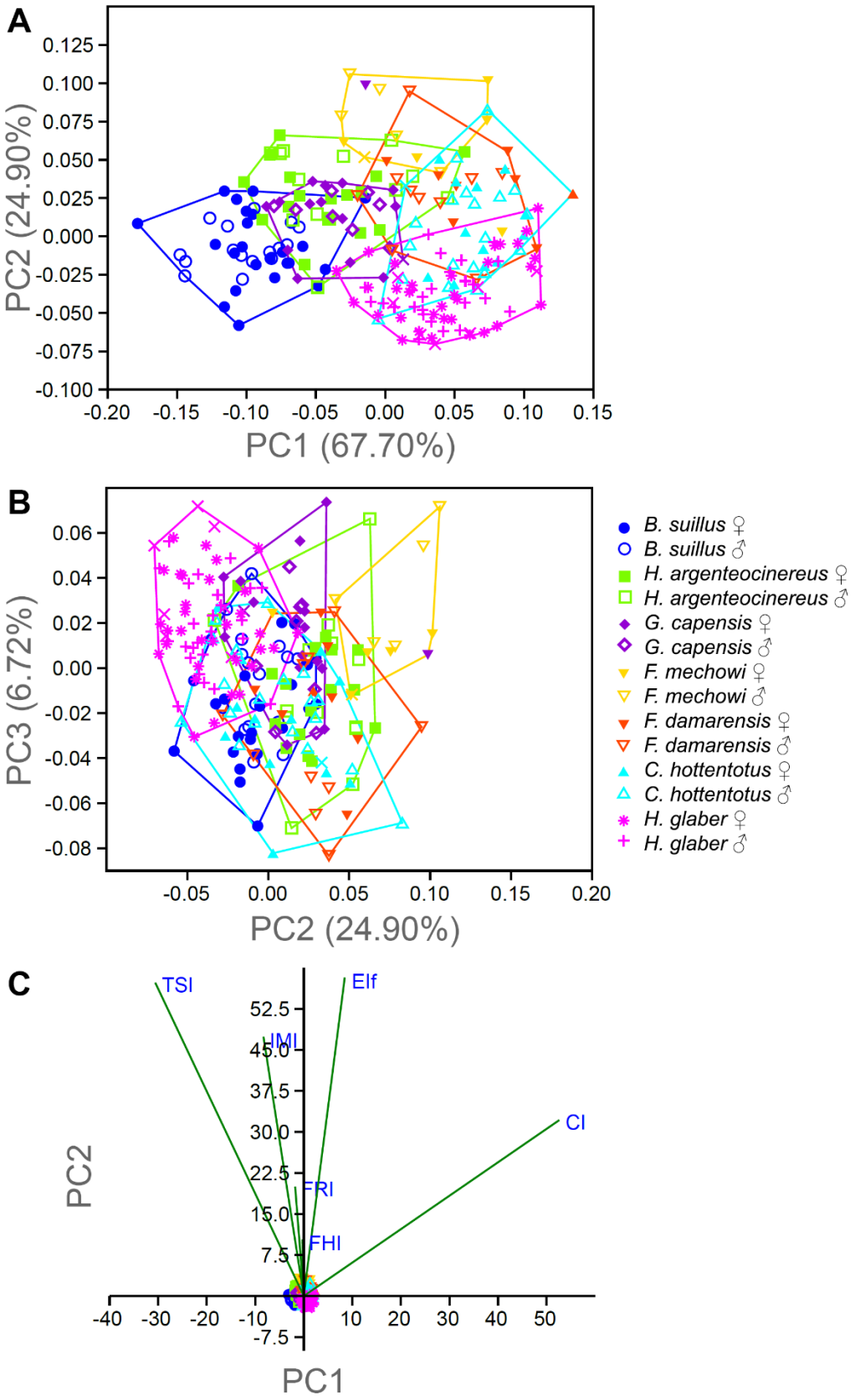

FIGURE 4.13. Results of PCA performed on all bathyergid species including hindlimb indices (except RDP), and showing PC1 and PC2 (A), PC2 and PC3 (B), and biplot for the two first axes (C).

The second PCA[ii] generated five components where the three first components explained 97.68% of the total variance (Table 4.6; Fig. 4.14). Significant differences among species were found for the two first components (Wilks′ λ= 0.102; $F_{10, 292}$ = 61.82; p << 0.0001). The PC1 contributed with 70.53% of the total variance and was positively correlated with CI (r^2 = 0.86) and EIf (r^2 = 0.61), and negatively correlated with TRI (r^2 = 0.62). The positive side of this axis was mostly occupied by social species while the negative side by the solitary *B. suillus,* so the latter species showed higher TSI and TJI as compared to social species. The other solitary species (*H. argenteocinereus* and *G. capensis*) occupied an intermediate location between *B. suillus* and social species (Fig. 4.14). The PC2 contributed only with 17.62% of the variance and the greatest positive correlations were obtained from IMI (r^2 = 0.75) and TRI* (r^2 = 0.64). In this axis, the largest social mole-rat *F. mechowii* occupied the positive sector while most individuals of *C. hottentotus* (the second smaller species in this study) occupied the negative sector. In this sense, *F. mechowii* showed higher IMI and TRI* as compared to *C. hottentotus* and the largest bathyergid *B. suillus*.

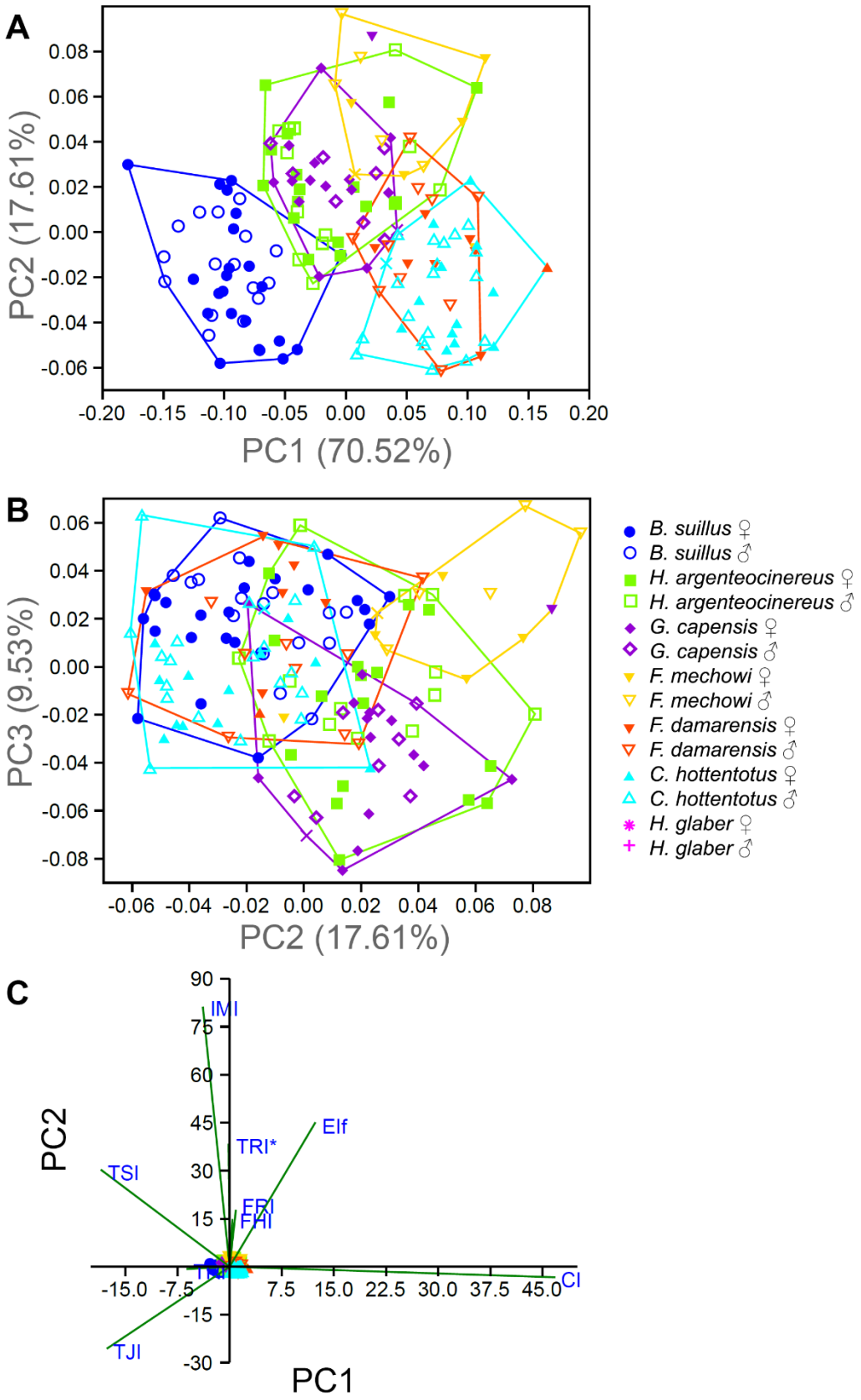

FIGURE 4.14. Results of PCA performed on all forelimb indices but excluding *H. glaber*, and showing PC1 and PC2 (A), PC2 and PC3 (B) and biplot for two first axes (C).

4.3.3.5 DA (Forelimb + Hindlimb)

To know whether bathyergid species could be correctly classified into *a priori* defined ecomorphological groups, a series of DAs were performed using all indices and all species. Here, both fore- and hindlimb data were combined in the analysis to have a more integrated view of the whole appendicular phenotype characterizing each ecomorphological group.

The first discriminant analysis (DA[i]) included all species and yielded two canonical functions, from which the first function accounted for 86.81% of the variance in the sample (Table 4.7; Fig. 4.15). The MANOVA of DF1 and DF2 scores showed significant separation between ecomorphological groups (Wilks′ λ= 0.063; $F_{4, 424}$ = 313.4; p << 0.0001). Most of this separation between groups was accounted by the variation on EIf, EIh and HRI in DF1, while IFA contributed most in the DF2 (Table 4.7). All individuals in the scratch-digging group and most of the solitary chisel-tooth digger group were on the positive side of the DF1, whereas the negative side was composed of most of the social chisel-tooth digger group (Fig. 4.15). The DF2 separated mostly solitary chisel-tooth diggers on the positive side with the social chisel tooth diggers on the negative side, while most scratch-diggers were related to the negative side (Fig. 4.15). Jackknifed cross-validation of group assignments produced a 93.06% of correctly classified individuals. In the scratch-digging group (containing only *B. suillus*), all individuals were correctly classified (Appendix 4.3). The solitary chisel-tooth diggers and social chisel-tooth diggers groups were not completely separated by the analysis; 15 individuals (6.94%) were misclassified (Appendix 4.3). Most misclassifications (11) were found among the social chisel-tooth digger group, where mostly specimens of *F. mechowii* were classified as being solitary chisel-tooth diggers. None of the individuals in the analysis were misclassified as scratch-diggers and none of the naked mole-rat individuals were misclassified.

TABLE 4.7. Tables showing the results of the DA analysis. Indices of the forelimb and hindlimb are analysed together. On the left, the loadings of the analysis included all species, and to the right the analysis included all indices. RDP, TRI, TRI* and TJI were not assessed when all species were compared.

All species

Loadings	DF1	DF2
HRI	32.555	1.564
HHI	-0.069	-14.316
EIh	39.250	-21.578
IFA	-25.404	52.713
URI	-27.326	14.961
URI*	17.591	40.070
BI	3.799	20.380
CI	-19.187	-8.105
IMI	-7.965	9.263
FRI	-11.049	3.388
EIf	-40.133	-4.540
FHI	23.022	36.098
TSI	11.116	-5.465
Eigval	6.737	1.024
%	86.810	13.190

All indices

	Loadings	DF1	DF2
1	RDP	-6.280	12.595
2	HRI	-31.797	13.908
3	HHI	9.433	-14.700
4	EIh	-40.159	-18.942
5	IFA	52.712	36.691
6	URI	17.597	8.433
7	URI*	-33.044	34.425
8	BI	10.076	15.153
9	FRI	19.414	0.427
10	EIf	47.882	-11.748
11	FHI	-31.999	86.971
12	TSI	-7.540	-0.727
13	TRI	-1.809	-0.580
14	TRI*	-7.128	-31.353
15	TJI	-8.965	-34.811
16	CI	10.419	-22.708
17	IMI	4.092	6.615
	Eigval	9.266	2.569
	%	78.290	21.710

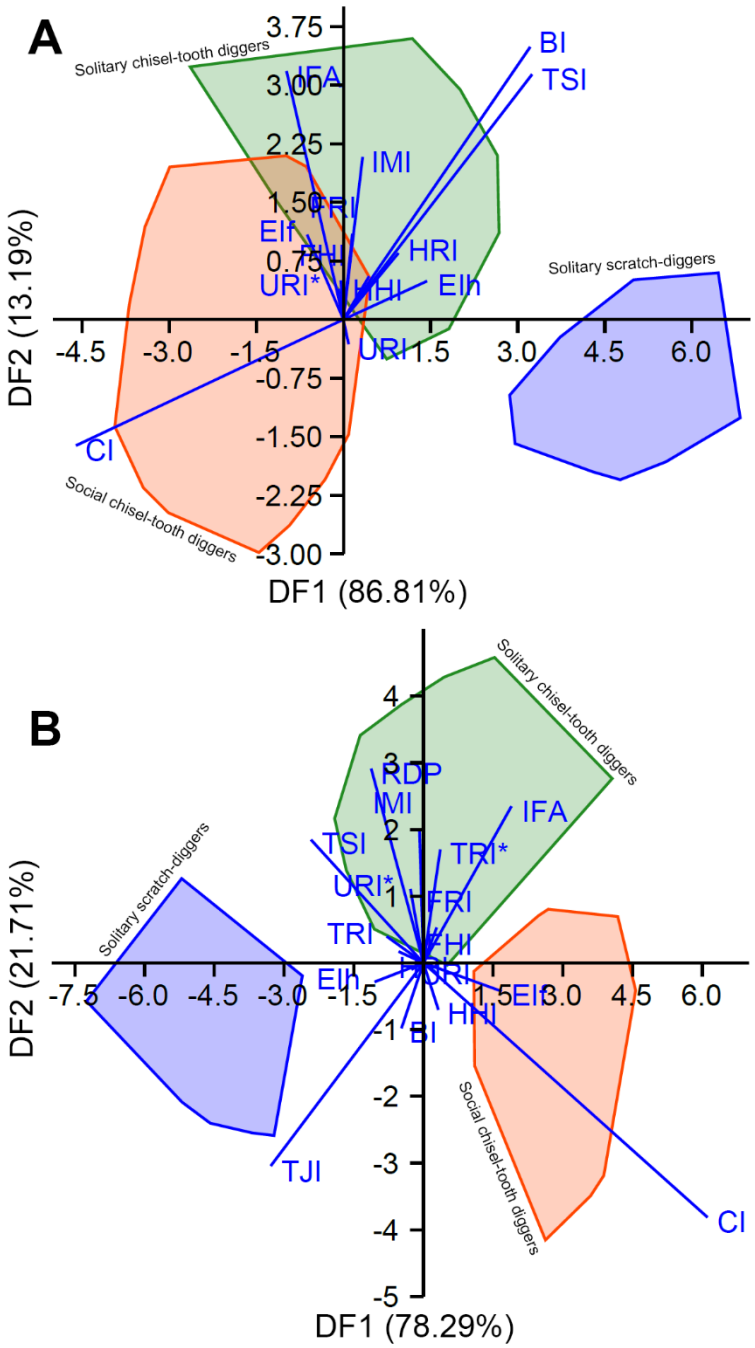

FIGURE 4.15. Results of DA performed on all species but excluding four indices (A) and on all forelimb indices but excluding *H. glaber* (B). Canonical functions (DF1 and DF2) are ploted and biplots superimpossed to show the main factors (eigenvectors) contributing to group discrimination.

The second DA[ii] included all indices and also yielded two functions, from which the first one contained most of the variance (78.29%). Groups were significantly separated (Wilks' λ= 0.037; $F_{4,\ 330}$ = 346.2; p << 0.0001), and showed higher discriminant power than the first analysis (DA[i]) that included a reduced number of indices and an extra species, *H. glaber*. The variables that most contributed to species discrimination were IFA, EIf and EIh in the DF1, and FHI in

the DF2 (Table 4.5). In this DA, the specimens took different locations in the morphospace as compared to the previous DA. However, within a DA, the direction of the sign for each variable is arbitrary and will not affect its interpretation (Quinn & Keough, 2002). All individuals of the scratch-digging group and few specimens of the solitary chisel-tooth digger group were associated with the negative side of the DF1, whereas the positive side was composed mostly by individuals of the solitary chisel-tooth digger group and all the individuals of the social chisel-tooth digger group (Fig. 4.15). The DF2 also separated solitary chisel-tooth diggers on the positive side with the social chisel tooth-diggers on the negative side, while most scratch-digger individuals were related to the negative side (Fig. 4.15). Jackknifed cross-validation produced a 97.37% of correctly classified individuals. As in the previous analysis DA^{i}, all specimens in the first group were correctly classified, although only 4 individuals (0.97%) (mostly from the solitary chisel-tooth digger group) were misclassified (Appendix 4.4). This represents a considerably lower number of misclassifications, probably related to the inclusion of RDP, TRI, TRI* and TJI, which showed significant explanatory power in previous multivariate analyses (Table 4.5). Thus, the inclusion of humeral and tibio-fibular indices represents a 4.31% increment in discriminant power respect to the previous DA^{i}. It is likely that the exclusion of *H. glaber* also contributed to a better discrimination between groups, since this species showed a highly variable component and therefore a large morphospace.

4.4 DISCUSSION

The goal of this study was to investigate the phenotypic variation of fore- and hindlimbs of Bathyergidae, specifically to: i) determine which are the main differences and similitudes between species, and how they are related to specific social behaviors, digging strategies and locomotor ability. The comparative analysis of the functional anatomy of all bathyergid species revealed clear differences, especially between naked mole-rats (*H. glaber*) and the other bathyergids (*Bathyergus, Heliophobius, Georychus, Cryptomys* and *Fukomys*). Additionally, an important aspect implemented in this study is the introduction of three novel ecomorphological categories for analyzing the effects of different fossorial and social strategies by combining fore- and hindlimb phenotypes, which resulted in a clear separation between groups. Moreover, non-significant differences between sexes in almost all morpho-functional indices, for each species, indicates that the appendicular morphology of mole-rats is strongly correlated with function regardless of sex, even among species with marked sexual dimorphism like *B. suillus*. Nevertheless, the few sex differences found in some species are also briefly discussed. The following discussion addresses the main differences and similarities in the forelimb and hindlimbs of bathyergids (mostly excluding naked mole-rats), as well as the main features characterizing each ecomorphological group. Due to the unique features of *H. glaber* among African mole-rats, a detailed discussion of its phenotype is also presented separately. Since this study represents the first comprehensive contribution to analyze the appendicular anatomy of African mole-rats, the implications of such features among hystricognath rodents are also briefly commented upon.

4.4.1 The Morphology of the Forelimb

Differences Among Bathyergids. The multivariate analyses showed clear differences among species (Table 4.3-4.4; Fig. 4.9). Most of these differences were explained by the index of fossorial ability (IFA) in the ulna, the anteroposterior robustness of the forearm (URI*) and the relative position of the deltoid tubercle (RDP) in the humerus (Table 4.4). Similar results were obtained from the PCA, where IFA, brachial index (BI) and RDP contributed most to the total variance (Table 4.5). Thus, in the forelimb, the zeugopod contained the highest amount of differences among species (IFA and URI*), followed by the differences in the stylopodial bone (RDP) and the ratio between the zeugopods and stylopods (BI).

The highest IFA, RDP and URI* values were found in the large solitary chisel-tooth digger *H. argenteocinereus* (Table 4.4). High IFA values indicate a relatively larger olecranon process in the ulna, thus reflecting an improved mechanical advantage of the m. triceps brachii and m. tensor fasciae antebrachii for elbow extension, which is usually considered a good estimator of the fossorial ability in mammals (Vizcaíno *et al.*, 2016). The largest social bathyergid, *F. mechowii* also showed similar values (Fig. 4.9). However, both species are primarily chisel-tooth diggers and live in environments with different soil properties (Bennett & Faulkes, 2000; Šumbera et al., 2004). However, Šumbera et al. (2012) analyzed habitat characteristics of both species and found that the soil parameters of such species were comparable, thus suggesting that there are no strong ecological constraints on mole-rats to occupy a diverse range of habitats and soil conditions.

An interesting result of this study was that the largest bathyergid and highly specialized scratch-digger, *Bathyergus suillus,* showed the lowest IFA among bathyergids, having a relatively smaller olecranon process as compared to other species. If compared to chisel-tooth diggers, *B. suillus* is considered to undergo higher mechanical strains in their forelimb bones due to increased efforts to break the soil during scratch-digging burrowing, so a higher IFA was expected. A possible explanation for these contradictory results may be because *B. suillus* lives in soft sandy soils and has long claws in fore- and hindfeet, which in combination would reduce the efforts required for "breaking up" the soil excavated. Thus, the biomechanical interaction between building burrows in less compacted soils and having a highly specialized set of appendicular structures to break up the soil (i.e. claws), may account for a reduction in the ulnar specialization of the elbow. In contrast, species that dig more compacted soils, primarily with their incisors, and which have comparatively poorly developed claws may require bigger attachment sites for stronger forearm muscles to move the soil out of the burrow, especially in wet conditions where the soils get highly compacted and heavier. This indicates that chisel-tooth diggers have a more specialized humero-ulnar joint to enable more effective scratch-digging, which also involves pushing the soil out of the burrow.

The high URI* values found in *H. argenteocinereus* (and also in *H. glaber*) indicate a thicker anteroposterior cross-sectional shape of the ulna, reflecting a more robust ulna in sagittal section which provides increased resistance to

bending and torsional loads in that axis. This would enable them to sustain higher strains during parasagittal scratch-digging movements to reduce fracture risks. The lowest URI values were found in the smaller social *C . hottentotus* (Fig. 4.9).

The high RDP found in *H. argenteocinereus* indicated a more distally located deltoid tubercle, and therefore an increased in-lever ability of the forelimb for the action of the deltoid and pectoral muscles. This implies a stronger flexion of the humerus on the scapula, and therefore a stronger ability of the forelimb for pulling the substrate against the body. In general, all solitary species showed higher RDP as compared to social species, although *C. hottentotus* also showed similar high values (Table 4.4). The lowest values were found in the social *Fukomys* (Fig. 4.9).

Similar values were found by Samuels & Van Valkenburgh (2008), in which they assessed the locomotor modes of 67 rodent species including four species of bathyergids: *G. capensis* (n = 1), *H. argenteocinereus* (n = 2), *C. hottentotus* (n = 3) and *H. glaber* (n = 4). Most mean values for those species showed differences with the values obtained in this study. This may be due to the reduced sample size these authors used (n = 10), although intraspecific differences cannot be ruled out. In the case of IFA and URI, these authors used a different calculation for those indices, so the final estimations are not comparable. Despite the limited number of specimens they used, they also found that *H. argenteocinereus* showed higher values for indices as compared to the other bathyergids. Overall, the presence of strong humeral and ulnar specializations in *H. argenteocinereus* suggest that this species has a set of features to maximize scratch-digging behaviour, which are structurally more specialized as compared to truly scratch-digging species.

Similarities Among Bathyergids. The indices that showed a lower contribution to species differentiation in the multivariate analyses were the humeral head (HHI) and brachial index (BI). In the ordination analyses, the least relevant variables explaining variation in the PC2 were the humeral head (HHI), mediolateral diameter of the ulna (URI), the humeral robustness (HRI), humeral epicondylar index (EIh) and brachial index (BI). In general, these features were similar among all bathyergids, and were higher as compared to other non-subterranean terrestrial mammals including the semifossorial ones reported by Samuels & Van Valkenburgh (2008). Only the HHI was not possible to compare since it has not been assessed previously.

On the basis of the present results, it appears that all bathyergids share i) enlarged humeral heads (high HHI), which increases the articular surface of the glenohumeral joint thus providing higher extensiveness for anteroposterior (and likely mediolateral) movements of the humerus; ii) relatively short functional length of the ulna (low BI), which indicates that humerus and ulna are functionally similar in length; iii) relatively thick mediolateral diameters in the ulna (high URI), which reflects increased sectional areas to resist bending in the mediolateral axis of the bone, and also indicating higher relative surface available for the insertion of muscles involved in pronation and supination of the forearm and flexion of the manus and digits which help during digging behaviour; iv) more robust humeri (high HRI), which indicates increased ability to resist bending stresses in the anteroposterior axis; and v) wider epicondylar width (EIh), which is associated with larger relative areas available for the origin of the forearm flexors, pronators,

and supinators, thus improving their degree of development and robustness for stronger hand and forearm flexion. These features have also been recognized as common for fossorial species in previous ecomorphological assessments (Lehmann, 1963; Echeverría *et al.*, 2014; Samuels & Van Valkenburgh, 2008).

Intraspecific Comparisons with Non-Bathyergids. The forelimb of bathyergids showed clear specializations associated with fossoriality. However, bathyergids did not show necessarily a more specialized morphology for these traits when compared to other fossorial mammals. The fossorial mammals analyzed in previous studies (e.g. Samuels & Van Valkenburgh, 2008) showed higher mean values for EIh, IFA and URI as compared to bathyergids. Within Rodentia, the EIh is higher in non-bathyergid fossorial forms (0.368), although semiaquatic and ricochetal forms showed similar values to bathyergids (0.307 and 0.310, respectively) (Table 4.x). The IFA in bathyergids (0.281) is also lower as compared to other fossorial rodents (i.e. 0.328), but higher than most non-fossorial species (Samuels & Van Valkenburgh, 2008). However, this parameter could be biased because these latter authors used a different calculation. In the case of URI (0.051), these values are lower than semiaquatic (0.057), semifossorial (0.055) and fossorial (0.067) rodents, although were higher as compared to terrestrial, arboreal ricochetal and gliding rodents (Samuels & Van Valkenburgh, 2008). Only the RDP (0.581) showed to be higher as compared to other fossorial rodents (0.539: Samuels & Van Valkenburgh, 2008), although these authors considered the length of the deltopectoral crest and not the deltoid tubercle, so some bases are also expected for those features. In general, these data indicate that bathyergids are not as functionally specialized to fossoriality as other solitary taxa (e.g. armadillos), and that these morphological features are not exclusive of digging species only, but also to swimmers, ricochetal and semifossorial species that also need to increase robusticity of such structures for activities that involve similar biomechanical regimes (Samuels & Van Valkenburgh, 2008). The interplay between different lifestyles, niche occupancies and functional anatomy clearly do not follow a linear ecomorphological continuum, so its analysis and interpretations become complicated when they are based on independent assessment of morphological features. More integrated studies assessing the ecomorphological variation among mammals is needed.

4.4.2 The Morphology of the Hindlimb

The hindlimb of bathyergids showed clear specializations associated with fossoriality. Most indices (EIf, TSI, TRI, TRI*, TJI, CI) showed increased hindlimb robusticity and digging ability as compared to other non-subterranean mammals (Samuels & Van Valkenburgh, 2008).

Differences Among Bathyergids. The multivariate analyses showed clear differences among species (Table 4.3-4.4; Fig. 4.10). Most of these differences were explained by the crural index (CI), tibio-fibula junction index (TJI) and femoral epicondylar index (EIf) (Table 4.4). Similar results were obtained from the PCA, where the TJI, tibial spine index (TSI) and the robustness of the tibia (TRI) contributed most to the total variance among species (Table 4.6). Thus, the

hindlimb showed a similar pattern of variation as the forelimb, where differences in the zeugopodial bones explained most of the variance among species.

The crural index (CI) showed the highest amount of variation among species (Table 4.4; Fig. 4.10). This index indicates the relative proportions of proximal (femur) and middle (tibia) elements of the hindlimb (foreleg) and gives an indication of how well the hindlimbs are adapted for speed (Howell, 1965). The lower values were found in solitary species, while the higher values were found in social species, especially in the smaller ones (*F. damarensis* and *C. hottentotus*), indicating that these species have a proportionally longer tibio-fibula in relation to the femur (Fig. 4.10). This tendency is typically found in cursorial and terrestrial mammals, although bathyergids still show lower values as compared to surface-dwelling species (Samuels & Van Valkenburgh, 2008; Wilson & Geiger, 2015). These results suggest that social species may have a tendency to develop a more "cursorial" phenotype, and this would allow them to have faster propulsive forces as compared to solitary species. Unfortunately, the locomotory dynamics of bathyergids have not been assessed, although previous works have suggested apparent differences in the locomotor speed of the largest bathyergids and other subterranean mammals (Ch. 3; Montoya-Sanhueza & Chinsamy, 2019). It is evident that further research is needed to understand the locomotory dynamics among bathyergids and other subterranean mammals.

The fused condition of the tibia and fibula of most bathyergids contrasts with that found in most arboreal/scansorial mammals where the fibula remains separated and is relatively mobile to increase agility and the range of limb motion (Carleton, 1941; Moss, 1977). The TJI index developed in this study showed in part the level of tibio-fibular fusion, and was usually associated with high values (Table 4.2). Higher values indicated longer bony bases for the muscles acting on the feet, thus increasing resistance for bending and torsional loads in animals that sustain relatively higher biomechanical activity against the substrates such as soil excavation (Carleton, 1941; Stein, 2000; Silva *et al.*, 2005). Among solitary species, *B. suillus* had the highest TJI values, while *G. capensis* had the lowest values (Fig. 4.10). The discriminant power of this index successfully differentiated scratch-digger species from chisel-tooth diggers, thus showing that this index can be used in future ecomorphological analyses of mammals.

The TSI was also an important index differentiating species. The TSI reflects the strength of the leg and the relative width available for the insertion of the semitendinosus and semimembranosus muscles. Higher values were found in the largest bathyergids, while the lowest values in the smaller species (Table 4.2). Wide surface areas for the attachment of these muscles increase the in-lever of hindlimb retracting muscles and hence increase the strength of the knee (Samuels & Van Valkenburgh, 2008). Thus, this index showed a clear positive trend with increased body size (Fig. 4.10), which has been also observed in other taxa including fossorial and non-fossorial forms (Samuels & Van Valkenburgh, 2008).

With respect to the EIf, this index indicates the relative area available for the origin of the gastrocnemius and soleus muscles used in extension of the knee and plantar-flexion of the pes. The EIf was higher in *Fukomys*, especially in *F. mechowii* (Fig. 4.10), indicating that this species has enlarged epicondylar areas. Similar qualitative observations have been reported by Sahd *et al.* (2019) in a social

species, *C. h. natalensis* (*n* = 8), where the epicondyles appeared more robust and prominent in this non-drumming species as compared with drumming species such as *B. suillus* and *G. capensis*. In the present study, non-significant differences were found between *C. hottentotus* and *G. capensis* for this trait (Fig. 4.10), indicating that intraspecific variation in epicondylar width can be found in *Cryptomys*. The lowest values for this index were found in the largest and smallest bathyergid species, *B. suillus* and *H. glaber*, respectively (Fig. 4.10). Additionally, such values were statistically non-significant for those species. The latter taxon is a non-drumming species, thus the differences between drumming and non-drumming species seems unrelated to the epicondylar width, contrasting with recent suggestions made on bathyergids (Sahd *et al.*, 2019).

Three indices associated with the hindlimb have been shown to be high in semifossorial and fossorial rodents, the epicondylar index of the femur (EIf), the tibial spine index (TSI) and the gluteal index (Samuels & Van Valkenburgh, 2008). The latter not assessed in this study. These indices are related to enlarged gluteus medius, gastrocnemius and hamstrings, respectively (Sahd *et al.*, 2019), all of which have been hypothesized to help to resist the tendency to move rearward during digging activities (Samuels & Van Valkenburgh, 2008). Since bodies of fossorial rodents tend to be pushed backwards as the soil resists digging, enlargement of these muscles aids in maintaining a stable position (Samuels & Van Valkenburgh, 2008). In addition to these features, the mediolateral femoral robustness (FRI) is also increased in fossorial forms (Samuels & Van Valkenburgh, 2008), although there are no detailed examinations of its development and functionality. It is likely, that the increased loads exerted during limb stabilization by the gluteal muscles (attached to the third trochanter in the lateral region of the bone), have a significant effect on stimulating periosteal bone formation along the mediolateral axis of the diaphysis. In this regard, *B. suillus* has an enlarged third trochanter with a wide surface area for the attachment of the gluteal muscles. Montoya-Sanhueza & Chinsamy (2017) described the bone histology of this species and showed that the ontogenetic pattern of bone modelling in the femoral mid-diaphysis has extensive mediolateral bone formation and the pattern of cortical drift and bone growth occurs in posterolateral direction of the bone (also see Ch. 6). This supports the idea that tensional loading exerted by the gluteus muscles is associated to the extension of the third trochanter along the diaphysis, and therefore osteogenesis has also been affected (Montoya-Sanhueza & Chinsamy, 2017). This process may provide a mechanobiological model for the development of the extended trochanter in fossorial and subterranean mammals. In other bathyergids, the third trochanter is less extensively developed and rather restricted to a certain region in the proximal area of the diaphysis where slightly sharpens (Fig. 4.3, 4.7). Thus, the third trochanter seems to protrude more in social species, while solitary species show a more proximo-distally extended trochanter, which originates from the greater trochanter. Sahd *et al.* (2019) described that the third trochanter in three species of bathyergids (*B. suillus, G. capensis* and *C. hottentotus natalensis*) extended to a third of the length of the femur in all three species, and suggest that the position and size of the trochanters of the femur are unlikely to play a role in hind foot drumming or fossoriality. However, these authors did not find differences in morphology, although the extension of the third trochanter was

clearly different among those species in the present study, and most likely has a functional correlation with stabilization and retraction of the femur during locomotion within burrows and/or digging behaviours (Samuels & Van Valkenburgh, 2008). Further research must focus on the effect of specific digging, locomotory and/or communicational behaviours on the development of bone superstructures.

Similarities Among Bathyergids. The indices that showed the lowest contribution to species differentiation in the multivariate and ordination analyses were the femoral head (FHI), femoral robustness index (FRI) and intermembral index (IMI) (Table 4.6). In general, these features were similar among all bathyergids, and differed from other non-subterranean terrestrial mammals including semifossorial ones (Samuels & Van Valkenburgh, 2008). Consequently, all bathyergids share: i) similar sized spherical shaped femoral heads (except for *H. glaber*, where is rather ellipsoidal); ii) relatively thick femoral diaphysis in its mediolateral axis; and iii) relatively symmetrical limb proportions. Unfortunately, the FHI could not be compared with other mammals since this feature was calculated differently or its mean values were not reported in previous studies (e.g. Wilson & Geiger, 2015). These latter authors calculated the dimension of the femoral head in a wide range of adult ctenohystrican rodents using a similar approach as the used here (i.e. based on diameters), and found that higher values were associated with larger femoral heads, which are characteristic of arboreal and fossorial rodents, while lower values were seen in cursorial species (Wilson & Geiger, 2015). In the latter study, only four bathyergid individuals from *B. suillus, G. capensis* and *C. hottentotus,* were analysed. Although their index cannot be directly compared to the one calculated here, both of them represent the magnitude of surface area available of the femoral head, so it is highly probable that the FHI observed in the present study does not vary considerably from the general pattern found by Wilson & Geiger (2015). For this reason, it would be pertinent to suggest that bathyergids show relatively enlarged femoral sizes as compared to other non-fossorial rodents, although further assessment of this feature is needed. The circular shape of the femoral head in such species was also recently described elsewhere (Montoya-Sanhueza *et al.*, 2019; Sahd *et al.*, 2019).

The FRI was relatively high among all bathyergids, indicative of high femoral robusticity to resist bending and shearing stresses associated in the mediolateral plane of the bone (Leppänen *et al.*, 2006). This feature is common to fossorial mammals relative to other cursorial/terrestrial species (Samuels & Van Valkenburgh, 2008; Wilson & Geiger, 2015), although previous studies used a different calculation for this index (e.g., Samuels and van Valkenburg, 2008; Wilson and Geiger, 2015), so comparisons must be done cautiously. Previous studies calculated the FRI with the anteroposterior diameter of the femur, thus indicating rather the resistance of the diaphysis to bending and shear stresses during walking and high speed movements, as well as a measure of the capacity to support compressive forces due to body mass (Samuels & Van Valkenburgh, 2008; Wilson & Geiger, 2015; Vizcaíno *et al.*, 2016). It is likely that varied repertoire of behaviors performed by the hindlimb of fossorial and subterranean mammals (e.g. body anchoring during digging, expelling soil out of the burrow and foot drumming) all contribute differentially to optimize bone designs. As mentioned

above, the extensive proximo-distal development of the third trochanter could also be involved in increased mediolateral growth. More in-deep ethological examination of species' behaviors would help to understand these variations in bone design.

The IMI showed relatively symmetrical limb proportions, although the hindlimb was still longer than the functional length of the forelimb (Fig. 4.10). Apart from indicating leaping ability, the IMI has not shown clear functional correlates in mammals, especially those associated with either higher speed or lack of it (Howell, 1965). Howell (1965) reported an IMI of 0.75 as the generalized condition for large surface-dwelling (terrestrial) mammals (i.e. the hindlegs are longer than the forelegs), with bipedal jumpers showing the lowest ratios (0.32-0.50). Adult bathyergids have higher (0.87) values as compared to the hypothetical normal condition of other surface-dwelling mammals. Lehmann (1963) found that the length of the hindlimbs of *Geomys*, *Ctenomys*, and *Tachyoryctes* are more nearly equal to the length of the forelimbs and differs from the non-fossorial forms and *Rattus* in which there is a tendency for the hindlimbs to be longer. In Ch. 3 (Montoya-Sanhueza *et al.,* 2019), the limb development of the largest bathyergid species was described and the function of symmetric limb proportions in mammals was discussed. It is suggested that symmetrical limb proportions may be related to maximizing equal bidirectional locomotion within burrows by emphasizing equal propulsive action of the fore- and hindlimbs. Consequently, the high IMI found in bathyergids and other fossorial mammals may not represent a fossorial adaptation for excavation *per se*, but an additional morphological specialization for bidirectional locomotion in burrows and narrow spaces (Montoya-Sanhueza *et al.*, 2019).

4.4.3 Ecomorphological Groups

The discriminant analysis of the three main ecomorphological groups (i.e. solitary scratch-diggers, solitary chisel-tooth diggers and social chisel-tooth diggers) showed that all of them were clearly differentiated (Fig. 4.15). The features that better discriminate between solitary scratch-diggers and chisel-tooth diggers are related to the forelimb in the first group and mostly to the hindlimb in the second (Table 4.7). The DF2 mostly separates solitary chisel-tooth diggers from social ones, with solitary scratch-diggers showing an intermediate position among them, but also tending to share more features with social chisel-tooth diggers. The main variables contributing to differentiation were the increased FHI, and an equal combination of IFA, TRI*, URI* and TJI (Table 4.7). However, the combined data (biplot) showed that the most relevant features that finally separate ecomorphological groups were: TJI, TRI and EIh for scratch digging species; IFA, RDP, TRI* and TSI for solitary chisel-tooth diggers; and CI, Eif and HHI for social chisel-tooth diggers (Fig. 4.15).

This indicates that solitary chisel-tooth diggers are mainly characterized by having a more proximally located distal junction of the tibio-fibula (high TJI), a more robust tibio-fibula in its mediolateral axis (high TRI) and wider epicondylar epiphyses in the humerus (high EIh). Morphological specializations in the tibia of the only scratch digger *B. suillus* indicate a more robust tibia-fibula, probably

related to the ability to resist higher bending and shearing stresses in the anterolateral axis. The humerus also showed better specialization in EIh associated with larger relative areas available for the origin of the forearm flexors, pronators, and supinators, thus improving their degree of development and robustness for stronger hand and forearm flexion. These features match with the primary digging strategy of *B. suillus* (Jarvis & Sales 1971).

Solitary chisel-tooth diggers are characterized by having a longer olecranon process (high IFA), a more distal extension of the deltoid tubercle (high RDP), a more robust tibio-fibular diaphysis in its anteroposterior axis (high TRI*) and a larger tibial spine surface (high TSI). Despite *H. argenteocinereus* and *G. capensis* are primarily chisel-tooth diggers, they showed highly specialized forelimbs associated with scratch-digging ability. These features allow an improved mechanical advantage of the triceps and dorsoepitrochlearis muscles during elbow extension (IFA) and a stronger ability of the arm for pulling the substrate against the body (RDP). The tibia in these species was also robust (TRI*). It is likely that their solitary condition makes them to increase their scratch-digging skills even when this is not their primary mode of excavation.

Social chisel-tooth diggers are characterized by longer tibio-fibulae in relation to the femur (high CI), wider epicondylar epiphyses in the femur (high EIf) and larger humeral heads (high HHI). These features suggest increased speed and locomotory capabilities in this group, as well as higher surface area in the glenohumeral joint thus providing wider range of anteroposterior (and likely mediolateral) movements of the humerus (HHI). A more robust distal femur was also characteristic of this group and can be related to the need of transporting and expelling soil out of the burrows.

4.4.4 The Phenotype of *Heterocephalus glaber*

The species with most differences in morpho-functional traits was *H. glaber* (Fig. 4.9-4.10). This species showed a wider morphospace as compared to other species (Fig. 4.11-4.15). This could be related to the wide phenotypic variation of this species (Jarvis et al., 1991; O'Riain et al., 2000; Dengler-Crish & Catania, 2007, 2009), and probably correlated to sex differences (Fig. 4.8), but also to cohort, role within the colony, and captivity conditions of course. Indeed, wide phenotypic variation (including skeletal variation) was previously suggested for *Heterocepahlus* by Hamilton (1928). In this study, several lines of evidence were presented to show that the considerable intraspecific variation found in this species, as well as its differences with the rest of the bathyergids are at least, unlikely to be due to prolongated life in captivity.

It is known that life in captivity has strong effects on the skeleton (O'Regan & Kitchener, 2005). Although the specimens analyzed here were kept under high inbreeding and captive conditions for more than 20 years, especially without real substrates to dig, they show clear and strong behaviors associated with digging activities (see Appendix 4.5). The Appendix 4.5 shows video recordings of active digging behavior in different members of the naked mole-rat colony at the University of Cape Town (now relocated to the University of Pretoria, South Africa). Despite the extended time that this colony has been inbred and have not

been supplied with soil to dig, the members of the colony still maintain a clear digging behavior even though the tunnels are made of glass and does not have substrate to dig. In the video is possible to observe that both chisel-tooth digging, and scratch-digging are performed simultaneously. The second part of the video also shows the process of expelling soils out of the burrow, where the --imaginary-- material is pushed out of the tunnel using backward locomotion and through potent synchronized kicks of both hindlimbs. The constant digging activity in colonies deprived of soil substrates, is hypothesized to act as a fundamental factor stimulating the adequate attainment of skeletal shape and size in captive colonies of mole-rats. This represents one of the clearest lines of evidence supporting the observation that the phenotype of the specimens of this study has been scarcely affected by being held in captivity, at least by disuse conditions (e.g. Burger & Veldhuijzen, 1993). To attain the normal size, shape and architecture of bones, it is known that muscle activity plays a major role in stimulation of bone formation (Burger & Veldhuijzen, 1993; Whedon & Heaney, 1993; Hillam & Skerry, 1995; Carter et al. 1996; Carter & Beaupré, 2001). Several experimental studies have demonstrated that the lack of muscle activity (muscle extirpation) results in deformed bones and isometric bone geometries in cross sectional shape, even from prenatal stages (e.g. Sharir et al., 2011). For this reason, it is assumed that despite the captivity condition of the specimens analyzed in this study, the presence of persistent digging behaviors in the colonies have had a positive impact on the normal development of their bone size and shape (i.e. reduced negative effects on normal bone modeling). For this reason, the final phenotype observed in *H. glaber* is expected to not vary considerably from that of wild specimens. Nevertheless, the specific effect of different load magnitudes and frequencies of muscular activity on bone architecture and geometry in this taxon must still be considered in further research.

No effects of captivity on features such as atrophied development of the deltoid tubercle and fusion of the tibia and fibula have been reported (O'Regan & Kitchener, 2005). Indeed, it is most likely that these features do not result from life in captivity, and may instead have a strong genetic component (Hall, 1978). Early descriptions of the skeletal anatomy of wild specimens of *H. glaber* have reported no development of deltoid tubercle and no fusion of their zeugopodial hindlimb bones (Hamilton, 1928; Hill, 1957). As mentioned before, most of the subordinate individuals showed individual tibia and fibula, and only few specimens exhibited distal fusion, which is most likely associated with the onset of sexual maturity and/or reproductive activity (Fig. 4.7). Only the proximal fusion of the tibiae and fibulae represents a character clearly observed in the majority of the individuals and species analyzed here (Fig. 4.6-4.7), and therefore this represents a character for the lineage including all extant and fossil mole-rat relatives, the Bathyergoidea. In this sense, it has been proposed that one of the anatomical features of Bathyergoidea is the distal fusion of the tibiae and fibulae (De Graaff, 1971; Patterson & Upham, 2014). The results of this study do not support this statement for *H. glaber* anymore, although it corroborates the previous observations made for the proximal tibia and fibula (e.g. Patterson & Upham, 2015 and references therein).

It is remarkable that sociality may have an effect on morphology, especially those taxa where physical labor such as digging behavior represents a fundamental part of their foraging strategies and life history (Sherman et al., 1991; Bennett & Faulkes, 2000). One hypothesis that could explain the simplification of such phenotype in species with high levels of sociality (eusociality), is the comparatively lower individual effort during burrow excavation as a product of the decreased physical activity that the members of the colony must perform when living in colonies. In this sense, the rise of large number of colony members in *H. glaber*, which reaches a maximum of 300 individuals per colony, with a mean of 75 (Jarvis et al., 1994), may have facilitated the reduction of selective pressures on individuals due to cooperative behavior. The fact that digging is not a compulsory task for all individuals within the colony, especially in ontogenetic terms (Sherman et al., 1991), may also have facilitated the evolution of simplified phenotypes within colonies. It is also likely that the ancestors of *H. glaber* may have had a less specialized phenotype, so the evolutionary history of this taxon cannot be ruled out as a potential explanation. Although *F. damarensis* is also eusocial, their colonies reach lower number of individuals; 41 per colony, with a mean of 16 (Jarvis et al., 1994).

The particularities of the skeletal system reported here for *H. glaber* are concordant with other aspects of their skeletal biology, such as the variable presence of molars, which can vary from 2 to 3, and which represents a lower number as compared to most bathyergids (4), as well as the vertebral elongation observed in sexually mature females. These data suggest a considerably high level of skeletal plasticity for this rodent and its study deserves more attention.

Forelimb morphology in H. glaber. Due to the extreme reduction of morphological adaptations observed in the appendicular skeleton of *H. glaber* in comparison to other fossorial mammals, this taxon was removed from the ordination analysis in order to observe more clearly the morphological differences between groups, thus allowing the conspicuous functional adaptations associated with the skeleton to be visible. In general, the limb anatomy and morpho-functional indices indicate that the morphology of *H. glaber* more closely resembles that of non-specialized mammals. For example, the proximal humerus of *H. glaber* resembles the general aspect of more surface-dwelling mammals such as the tenrecid *Setifer* and *Tenrec*, while the distal humerus of *H. glaber* is similar to that of the erinaceid *Echinosorex,* all of which have a terrestrial lifestyle (Salton & Sargis, 2008).

When *H. glaber* is included in the multivariate analysis, the strongest components of variation were associated with the brachial index (BI), anteroposterior robustness of the forearm (URI*) and robustness of the humerus (HRI) (Table 4.3). This indicates that the variables differentiating *H. glaber* from other bathyergids are associated with the humeral and ulnar proportions (longer humerus), which are substantially lower in *H. glaber* (BI = 0.74), as well as to the relatively higher robustness of the ulna (URI* = 0.09) and considerably decreased humeral robusticity (HRI = 0.83). The cross-sectional shape of the humerus is very distinct in *H. glaber* (see chapters 5 and 6), and this difference may explain the differences as compared to the other bathyergids. In this sense, it is true that the lower portion of the diaphysis of *H. glaber* is considerably thinner than its

proximal region, although it is also true that the anteroposterior diameter of the humerus is almost ~33% wider than its mediolateral diameter. This contrasts with other bathyergids where anteroposterior and mediolateral diameters are relatively equal. Thus, the small diameter of the mediolateral aspect of the humerus in *H. glaber* is compensated by a longer cross-section in its anteroposterior axis (Fig. 6.1 in Ch. 6). Actually, the cross-sectional shape of the humerus is more ellipsoidal in *H. glaber*, similar to the shape of the femur (Montoya-Sanhueza & Chinsamy, 2016; and see Ch. 6). It is likely that the longer diameter of the anteroposterior axis in *H. glaber* increases the cross-sectional area of the humerus, as the deltoid tubercle does in the rest of the species.

Additionally, the HRI in *H. glaber* was taken at a different location as compared to the other bathyergids, at 50% of the bone length, which is a slightly higher position as compared to the other bathyergids which was at around 60% of the bone length due to the presence of the deltoid tubercle at the 58%. For this reason, the HRI index may indicate a different aspect of the bone morphology in *H. glaber*, but actually because of the even thinner shape of the humerus in this species below the 60% of the bone, even lower values of the index are to be expected if measured from a more distal position.

4.4.5 The Skeletal Anatomy of Bathyergids: Implications for Systematics

The systematic position of Bathyergidae was subject to wide scientific debate before the development of the molecular era (Hamilton, 1928; Hill *et al.*, 1957; Lavocat, 1978; De Graaff, 1979, 1981). Cranial traits and aspects of their biology and reproduction were the main features used to group them into a coherent phylogenetic framework. Although its systematic position was in part resolved by using musculoskeletal features of the cranial region, some appendicular traits were also used to define its taxonomic status within hystricognaths. The absence of the entepicondylar foramen on the distal part of the humerus is a shared feature between hystricomorph rodents, and only present in early rodents (aplodontoids) and some sciuromorphs which tend to retain it (De Graaff, 1979). This feature is also lacking in all bathyergids (Fig. 4.1). Another feature that characterizes histricines (and sciurines) is the fact that the tibia and fibula are generally free, and "only" fuses in murines (De Graaff, 1979, 1981). The unequivocally fusion of the tibia and fibula observed in bathyergids was taken as an exception to the histricine condition because of their digging habits (De Graaff, 1979). The unfused condition is clearly observed in the two sister groups of Bathyergidae within Phiomorpha (Upham & Patterson, 2015), Petromuridae and Thryonomyidae, as well as in Hystricidae, which is the basal taxon within hystricognath rodents (Upham & Patterson, 2015). Thus, the fact that only naked mole-rats presents an unfused fibula (Hamilton, 1928; Hill *et al.*, 1957, and this study) it is most likely related to its basal position within Bathyergidae (e.g. Faulkes *et al.*, 2004; Upham & Patterson, 2015), and would represent the plesiomorphic state for this family, while its fusion among other genera would represent a synapomorphy. The discovery of some specimens of *H. glaber* having their fibula fused to the tibia (Fig. 4.7) could help to explain the mechanisms of how this feature develops among mammals, as well as what the selective pressures are that allow for this process to happen. Further

research should focus on how this process occurs from a developmental point of view.

4.5 CONCLUSIONS

Most species showed similar appendicular anatomy and the inclusion of naked mole-rats increased considerably morphological disparity among bathyergids. Despite general anatomical similarities, multivariate analyses showed differentiation among some species. When such differences are grouped into ecomorphological categories including the simultaneous analysis of fore- and hindlimb phenotypes (for each individual), they resulted in clear differentiation among groups, mostly indicating that some differences exist in their limb ratios and proportions. With the exception of *H. glaber*, social species appeared to have a more specialized fossorial phenotype (i.e. to increase digging ability), as well as more "cursorial" locomotor features. On the other hand, solitary species showed a relatively less specialized fossorial phenotype, and a more ambulatorial locomotor system (except for *G. capensis*). Other relevant aspect obtained in this study were: i) the most variable bones in bathyergids were the zeugopodial elements, and ii) gender seems to have a small effect on the external morphology of bathyergids. It is concluded that the type of social strategy, as well as the type of excavation had an effect on the appendicular system of bathyergids, most probably affecting the growth of certain areas of the bone, either their endochondral or intramembranous module, or both (see Ch. 3; Montoya-Sanhueza et al., 2019). These features seem to affect their activity patterns, although little effort has been put on the determination of their locomotor abilities. Due to the wide diversity of social strategies in bathyergids, more attention should be placed on these aspects in future research. The results of this study suggest that morphological adaptations in subterranean organisms are not as homogenous as previously thought, but instead they constitute a wide variety of morphological specializations that vary in terms of the particular ecological and biological context of the species, and they can sometimes result in a complex combination of phenotypes.

4.6 APPENDIX

APPENDIX 4.1 (*next page*). Specimens of seven bathyergid species analyzed in this study (N = 244), indicating ID code, sex and origin (Wild/Captivity). All species were classified into one of the three ecomorphological groups. Additionally, the reported body mass (BM) for the species (in g) and presence/absence of sexual dimorphism, based on BM of previous reports, are also included (see text for references). Solitary scratch-diggers: *Bathyergus suillus* (>2000 g; Male-biased sexual dimorphism). Solitary chisel-tooth diggers: *Heliophobius argenteocinereus* (260 g; Male-biased sexual dimorphism) and *Georychus capensis* (350 g; No sexual dimorphism). Social chisel-tooth diggers: *Fukomys mechowii* (345 g; Male-biased sexual dimorphism), *Fukomys damarensis* (234 g; Male-biased sexual dimorphism), *Cryptomys hottentotus* (79 g; Male-biased sexual dimorphism) and *Heterocephalus glaber* (25-80 g; No sexual dimorphism).

	Genus	Species	ID	Sex	Origin
1	*Bathyergus*	*suillus*	314a	F	Wild
2	*Bathyergus*	*suillus*	365a	F	Wild
3	*Bathyergus*	*suillus*	366a	F	Wild
4	*Bathyergus*	*suillus*	377a	F	Wild
5	*Bathyergus*	*suillus*	717a	F	Wild
6	*Bathyergus*	*suillus*	721a	F	Wild
7	*Bathyergus*	*suillus*	911a	F	Wild
8	*Bathyergus*	*suillus*	913a	F	Wild
9	*Bathyergus*	*suillus*	938a	F	Wild
10	*Bathyergus*	*suillus*	982a	F	Wild
11	*Bathyergus*	*suillus*	1085a	F	Wild
12	*Bathyergus*	*suillus*	1138a	F	Wild
13	*Bathyergus*	*suillus*	1144a	F	Wild
14	*Bathyergus*	*suillus*	1153a	F	Wild
15	*Bathyergus*	*suillus*	1155a	F	Wild
16	*Bathyergus*	*suillus*	1163a	F	Wild
17	*Bathyergus*	*suillus*	1169a	F	Wild
18	*Bathyergus*	*suillus*	1171a	F	Wild
19	*Bathyergus*	*suillus*	1332a	F	Wild
20	*Bathyergus*	*suillus*	1336a	F	Wild
21	*Bathyergus*	*suillus*	217a	M	Wild
22	*Bathyergus*	*suillus*	220a	M	Wild
23	*Bathyergus*	*suillus*	313a	M	Wild
24	*Bathyergus*	*suillus*	713a	M	Wild
25	*Bathyergus*	*suillus*	765a	M	Wild
26	*Bathyergus*	*suillus*	861a	M	Wild
27	*Bathyergus*	*suillus*	910a	M	Wild
28	*Bathyergus*	*suillus*	964a	M	Wild
29	*Bathyergus*	*suillus*	965a	M	Wild
30	*Bathyergus*	*suillus*	1039a	M	Wild
31	*Bathyergus*	*suillus*	1050a	M	Wild
32	*Bathyergus*	*suillus*	1139a	M	Wild
33	*Bathyergus*	*suillus*	1154a	M	Wild
34	*Bathyergus*	*suillus*	1338a	M	Wild
35	*Bathyergus*	*suillus*	1339a	M	Wild
36	*Bathyergus*	*suillus*	282	F	Wild
37	*Bathyergus*	*suillus*	283	F	Wild
38	*Bathyergus*	*suillus*	284	M	Wild
39	*Bathyergus*	*suillus*	285	F	Wild
40	*Heliophobius*	*argenteocinereus*	526	M	Wild
41	*Heliophobius*	*argenteocinereus*	26	F	Wild
42	*Heliophobius*	*argenteocinereus*	11	F	Wild
43	*Heliophobius*	*argenteocinereus*	387	F	Wild
44	*Heliophobius*	*argenteocinereus*	27	F	Wild
45	*Heliophobius*	*argenteocinereus*	386	M	Wild
46	*Heliophobius*	*argenteocinereus*	8	M	Wild
47	*Heliophobius*	*argenteocinereus*	6	F	Wild
48	*Heliophobius*	*argenteocinereus*	516	M	Wild
49	*Heliophobius*	*argenteocinereus*	361	F	Wild
50	*Heliophobius*	*argenteocinereus*	517	M	Wild
51	*Heliophobius*	*argenteocinereus*	585	M	Wild
52	*Heliophobius*	*argenteocinereus*	377	M	Wild
53	*Heliophobius*	*argenteocinereus*	451	F	Wild
54	*Heliophobius*	*argenteocinereus*	5	F	Wild
55	*Heliophobius*	*argenteocinereus*	18	M	Wild
56	*Heliophobius*	*argenteocinereus*	393	M	Wild
57	*Heliophobius*	*argenteocinereus*	473	F	Wild
58	*Heliophobius*	*argenteocinereus*	476	M	Wild
59	*Heliophobius*	*argenteocinereus*	508	F	Wild
60	*Heliophobius*	*argenteocinereus*	525	F	Wild
61	*Heliophobius*	*argenteocinereus*	492	F	Wild

	Genus	Species	ID	Sex	Origin
62	*Heliophobius*	*argenteocinereus*	479	F	Wild
63	*Heliophobius*	*argenteocinereus*	244	M	Wild
64	*Heliophobius*	*argenteocinereus*	590	F	Wild
65	*Heliophobius*	*argenteocinereus*	241	M	Wild
66	*Heliophobius*	*argenteocinereus*	242	F	Wild
67	*Heliophobius*	*argenteocinereus*	243	M	Wild
68	*Heliophobius*	*argenteocinereus*	244	F	Wild
69	*Georychus*	*capensis*	289	M	Wild
70	*Georychus*	*capensis*	290	M	Wild
71	*Georychus*	*capensis*	295	-	Wild
72	*Georychus*	*capensis*	297	F	Wild
73	*Georychus*	*capensis*	298	F	Wild
74	*Georychus*	*capensis*	346	M	Wild
75	*Georychus*	*capensis*	347	F	Wild
76	*Georychus*	*capensis*	351	F	Wild
77	*Georychus*	*capensis*	352	F	Wild
78	*Georychus*	*capensis*	355	F	Wild
79	*Georychus*	*capensis*	357	M	Wild
80	*Georychus*	*capensis*	358	F	Wild
81	*Georychus*	*capensis*	360	F	Wild
82	*Georychus*	*capensis*	361	F	Wild
83	*Georychus*	*capensis*	369	M	Wild
84	*Georychus*	*capensis*	380	F	Wild
85	*Georychus*	*capensis*	381	F	Wild
86	*Georychus*	*capensis*	382	M	Wild
87	*Georychus*	*capensis*	383	M	Wild
88	*Georychus*	*capensis*	384	F	Wild
89	*Georychus*	*capensis*	385	M	Wild
90	*Georychus*	*capensis*	386	F	Wild
91	*Georychus*	*capensis*	387	F	Wild
92	*Georychus*	*capensis*	388	F	Wild
93	*Georychus*	*capensis*	389	F	Wild
94	*Georychus*	*capensis*	390	F	Wild
95	*Georychus*	*capensis*	391	F	Wild
96	*Georychus*	*capensis*	392	M	Wild
97	*Georychus*	*capensis*	393	M	Wild
98	*Georychus*	*capensis*	394	F	Wild
99	*Georychus*	*capensis*	395	F	Wild
100	*Georychus*	*capensis*	396	F	Wild
101	*Georychus*	*capensis*	397	M	Wild
102	*Fukomys*	*mechowi*	213	F	Wild
103	*Fukomys*	*mechowi*	214	M	Wild
104	*Fukomys*	*mechowi*	215	F	Wild
105	*Fukomys*	*mechowi*	216	F	Wild
106	*Fukomys*	*mechowi*	217	M	Wild
107	*Fukomys*	*mechowi*	218	F	Wild
108	*Fukomys*	*mechowi*	219	M	Wild
109	*Fukomys*	*mechowi*	220	F	Wild
110	*Fukomys*	*mechowi*	221	F	Wild
111	*Fukomys*	*mechowi*	222	M	Wild
112	*Fukomys*	*mechowi*	223	M	Wild
113	*Fukomys*	*mechowi*	224	-	Wild
114	*Fukomys*	*damarensis*	305	F	Captivity
115	*Fukomys*	*damarensis*	306	M	Captivity
116	*Fukomys*	*damarensis*	308	M	Captivity
117	*Fukomys*	*damarensis*	310	M	Captivity
118	*Fukomys*	*damarensis*	311	M	Captivity
119	*Fukomys*	*damarensis*	316	F	Wild
120	*Fukomys*	*damarensis*	317	M	Wild
121	*Fukomys*	*damarensis*	318	F	Wild
122	*Fukomys*	*damarensis*	319	F	Wild

... continuation.

	Genus	Species	ID	Sex	Origin
123	*Fukomys*	*damarensis*	326	F	Wild
124	*Fukomys*	*damarensis*	320	F	Wild
125	*Fukomys*	*damarensis*	321	M	Wild
126	*Fukomys*	*damarensis*	322	M	Wild
127	*Fukomys*	*damarensis*	323	M	Wild
128	*Fukomys*	*damarensis*	325	M	Wild
129	*Fukomys*	*damarensis*	324	M	Wild
130	*Fukomys*	*damarensis*	227	F	Captivity
131	*Fukomys*	*damarensis*	228	F	Captivity
132	*Fukomys*	*damarensis*	238	-	Captivity
133	*Fukomys*	*damarensis*	11	F	Wild
134	*Fukomys*	*damarensis*	327	M	Captivity
135	*Fukomys*	*damarensis*	328	M	Captivity
136	*Fukomys*	*damarensis*	329	F	Captivity
137	*Fukomys*	*damarensis*	330	M	Captivity
138	*Fukomys*	*damarensis*	331	F	Captivity
139	*Fukomys*	*damarensis*	332	M	Captivity
140	*Fukomys*	*damarensis*	333	M	Captivity
141	*Fukomys*	*damarensis*	334	F	Captivity
142	*Fukomys*	*damarensis*	335	F	Captivity
143	*Fukomys*	*damarensis*	338	-	Captivity
144	*Fukomys*	*damarensis*	342	-	Captivity
145	*Fukomys*	*damarensis*	343	-	Captivity
146	*Cryptomys*	*hottentotus*	102	F	Wild
147	*Cryptomys*	*hottentotus*	103	M	Wild
148	*Cryptomys*	*hottentotus*	104	M	Wild
149	*Cryptomys*	*hottentotus*	105	M	Wild
150	*Cryptomys*	*hottentotus*	106	M	Wild
151	*Cryptomys*	*hottentotus*	108	F	Wild
152	*Cryptomys*	*hottentotus*	109	M	Wild
153	*Cryptomys*	*hottentotus*	110	M	Wild
154	*Cryptomys*	*hottentotus*	111	F	Wild
155	*Cryptomys*	*hottentotus*	112	F	Wild
156	*Cryptomys*	*hottentotus*	115	M	Wild
157	*Cryptomys*	*hottentotus*	116	-	Wild
158	*Cryptomys*	*hottentotus*	117	M	Wild
159	*Cryptomys*	*hottentotus*	123	M	Wild
160	*Cryptomys*	*hottentotus*	125	F	Wild
161	*Cryptomys*	*hottentotus*	126	M	Wild
162	*Cryptomys*	*hottentotus*	127	M	Wild
163	*Cryptomys*	*hottentotus*	128	F	Wild
164	*Cryptomys*	*hottentotus*	129	M	Wild
165	*Cryptomys*	*hottentotus*	132	M	Wild
166	*Cryptomys*	*hottentotus*	133	F	Wild
167	*Cryptomys*	*hottentotus*	135	M	Wild
168	*Cryptomys*	*hottentotus*	138	M	Wild
169	*Cryptomys*	*hottentotus*	140	M	Wild
170	*Cryptomys*	*hottentotus*	141	F	Wild
171	*Cryptomys*	*hottentotus*	142	M	Wild
172	*Cryptomys*	*hottentotus*	143	F	Wild
173	*Cryptomys*	*hottentotus*	144	F	Wild
174	*Cryptomys*	*hottentotus*	145	M	Wild
175	*Cryptomys*	*hottentotus*	146	F	Wild
176	*Cryptomys*	*hottentotus*	147	F	Wild
177	*Cryptomys*	*hottentotus*	150	M	Wild
178	*Cryptomys*	*hottentotus*	151	F	Wild
179	*Cryptomys*	*hottentotus*	152	M	Wild
180	*Heterocephalus*	*glaber*	1	F	Captivity
181	*Heterocephalus*	*glaber*	2	-	Captivity
182	*Heterocephalus*	*glaber*	8	F	Captivity
183	*Heterocephalus*	*glaber*	9	M	Captivity

	Genus	Species	ID	Sex	Origin
184	*Heterocephalus*	*glaber*	45	M	Captivity
185	*Heterocephalus*	*glaber*	46	F	Captivity
186	*Heterocephalus*	*glaber*	47	-	Captivity
187	*Heterocephalus*	*glaber*	48	M	Captivity
188	*Heterocephalus*	*glaber*	49	F	Captivity
189	*Heterocephalus*	*glaber*	50	M	Captivity
190	*Heterocephalus*	*glaber*	51	F	Captivity
191	*Heterocephalus*	*glaber*	52	M	Captivity
192	*Heterocephalus*	*glaber*	53	M	Captivity
193	*Heterocephalus*	*glaber*	54	F	Captivity
194	*Heterocephalus*	*glaber*	55	M	Captivity
195	*Heterocephalus*	*glaber*	56	-	Captivity
196	*Heterocephalus*	*glaber*	57	M	Captivity
197	*Heterocephalus*	*glaber*	58	M	Captivity
198	*Heterocephalus*	*glaber*	59	F	Captivity
199	*Heterocephalus*	*glaber*	60	M	Captivity
200	*Heterocephalus*	*glaber*	61	M	Captivity
201	*Heterocephalus*	*glaber*	63	F	Captivity
202	*Heterocephalus*	*glaber*	64	F	Captivity
203	*Heterocephalus*	*glaber*	65	F	Captivity
204	*Heterocephalus*	*glaber*	66	-	Captivity
205	*Heterocephalus*	*glaber*	67	F	Captivity
206	*Heterocephalus*	*glaber*	69	-	Captivity
207	*Heterocephalus*	*glaber*	70	F	Captivity
208	*Heterocephalus*	*glaber*	71	F	Captivity
209	*Heterocephalus*	*glaber*	73	M	Captivity
210	*Heterocephalus*	*glaber*	74	M	Captivity
211	*Heterocephalus*	*glaber*	75	-	Captivity
212	*Heterocephalus*	*glaber*	76	F	Captivity
213	*Heterocephalus*	*glaber*	77	F	Captivity
214	*Heterocephalus*	*glaber*	78	F	Captivity
215	*Heterocephalus*	*glaber*	79	F	Captivity
216	*Heterocephalus*	*glaber*	80	F	Captivity
217	*Heterocephalus*	*glaber*	81	M	Captivity
218	*Heterocephalus*	*glaber*	82	M	Captivity
219	*Heterocephalus*	*glaber*	83	F	Captivity
220	*Heterocephalus*	*glaber*	84	F	Captivity
221	*Heterocephalus*	*glaber*	85	M	Captivity
222	*Heterocephalus*	*glaber*	87	M	Captivity
223	*Heterocephalus*	*glaber*	88	M	Captivity
224	*Heterocephalus*	*glaber*	90	F	Captivity
225	*Heterocephalus*	*glaber*	91	F	Captivity
226	*Heterocephalus*	*glaber*	92	M	Captivity
227	*Heterocephalus*	*glaber*	93	F	Captivity
228	*Heterocephalus*	*glaber*	94	M	Captivity
229	*Heterocephalus*	*glaber*	96	F	Captivity
230	*Heterocephalus*	*glaber*	97	F	Captivity
231	*Heterocephalus*	*glaber*	98	F	Captivity
232	*Heterocephalus*	*glaber*	99	M	Captivity
233	*Heterocephalus*	*glaber*	101	M	Captivity
234	*Heterocephalus*	*glaber*	420	M	Captivity
235	*Heterocephalus*	*glaber*	498	F	Captivity
236	*Heterocephalus*	*glaber*	499	M	Captivity
237	*Heterocephalus*	*glaber*	500	-	Captivity
238	*Heterocephalus*	*glaber*	501	F	Captivity
239	*Heterocephalus*	*glaber*	505	M	Captivity
240	*Heterocephalus*	*glaber*	507	F	Captivity
241	*Heterocephalus*	*glaber*	508	F	Captivity
242	*Heterocephalus*	*glaber*	509	F	Captivity
243	*Heterocephalus*	*glaber*	510	F	Captivity
244	*Heterocephalus*	*glaber*	511	F	Captivity

APPENDIX 4.2. Table showing the results of the Mann-Whitney U-test for sex differences between sexes. Species with male-biased sexual dimorphism (based on literature) are indicated by ♂. Significance ($p < 0.05$) is indicated with asterisk (*).

Morpho-functional	*B. suillus* ♂		*H. argenteocinereus* ♂		*G. capensis*		*F. mechowi* ♂		*F. damarensis* ♂		*C. hottentotus* ♂		*H. glaber*	
index	*U-test*	*p*	*U-test*	*p*	*U-test*	*p*	*U-test*	*p*	*U-test*	*p*	*U-test*	*p*	*U-test*	*p*
RDP	177	0.842	65	0.087	235	0.646	19	0.884	97	0.982	122	0.768	-	-
HRI	98	**0.014***	97	0.759	239	0.710	8	0.079	95	0.908	111	0.484	271.5	**0.019***
HHI	148	0.304	103	0.965	67	**0.039***	9	0.273	68	0.174	82	0.077	280.5	**0.027***
EIh	100	**0.016***	73	0.174	251	0.913	9	0.107	74	0.279	102	0.302	413	0.854
IFA	182	0.954	89	0.511	189	0.193	15	0.464	91	0.765	115	0.580	381	0.621
URI	178	0.864	103	0.965	232	0.730	18	0.770	79	0.394	94	0.185	281	**0.039***
URI*	155	0.408	103	0.965	220	0.541	11	0.188	92	0.800	127	0.912	406	0.919
BI	144	0.253	96	0.726	160	0.068	15	0.464	77	0.345	100	0.269	393	0.759
CI	143	0.242	95	0.693	40	0.275	13	0.465	23	0.131	97	0.224	402	0.724
IMI	141	0.220	101	0.895	52	0.785	6	0.062	28	0.286	119	0.685	407	0.931
FRI	143	0.242	89.5	0.525	53	0.838	16	0.558	35	0.657	116.5	0.619	362	0.334
EIf	182	0.954	82	0.335	54	0.891	9	0.273	24	0.155	123	0.796	422	0.963
FHI	162	0.530	78	0.254	46	0.495	14	0.855	23	0.131	108.5	0.428	385	0.666
TSI	178	0.864	97	0.759	55	0.946	12	0.917	27	0.248	128	0.941	373	0.425
TRI*	176	0.819	102	0.930	39.5	0.260	5	**0.042***	29	0.328	110	0.461	-	-
TRI	156	0.424	96	0.726	54.5	0.918	13	0.465	20	0.076	104	0.338	-	-
TJI	135	0.162	91	0.569	51	0.942	8	0.123	16	**0.033***	68	**0.022***	-	-

APPENDIX 4.3. Jackknifed cross-validations of group assignments obtained from the discriminant analysis including all species (*N* = 216), excluding the morpho-functional indices RDP, TRI, TRI* and TJI. A total of 93.06% correctly classified individuals were obtained. The misclassified individuals are indicated with an asterisk (*) and pertained to the solitary chisel-tooth digger and social chisel-tooth digger groups, accumulating 6.94% (15 individuals).

Point	Given group	Classification	Jackknifed	Species
314a	1	1	1	*B. suillus*
365a	1	1	1	*B. suillus*
366a	1	1	1	*B. suillus*
377a	1	1	1	*B. suillus*
717a	1	1	1	*B. suillus*
721a	1	1	1	*B. suillus*
911a	1	1	1	*B. suillus*
913a	1	1	1	*B. suillus*
938a	1	1	1	*B. suillus*
982a	1	1	1	*B. suillus*
1085a	1	1	1	*B. suillus*
1138a	1	1	1	*B. suillus*
1144a	1	1	1	*B. suillus*
1153a	1	1	1	*B. suillus*
1155a	1	1	1	*B. suillus*
1163a	1	1	1	*B. suillus*
1169a	1	1	1	*B. suillus*
1171a	1	1	1	*B. suillus*
1332a	1	1	1	*B. suillus*
1336a	1	1	1	*B. suillus*
217a	1	1	1	*B. suillus*
220a	1	1	1	*B. suillus*
313a	1	1	1	*B. suillus*
713a	1	1	1	*B. suillus*
765a	1	1	1	*B. suillus*
861a	1	1	1	*B. suillus*
910a	1	1	1	*B. suillus*
964a	1	1	1	*B. suillus*
965a	1	1	1	*B. suillus*
1039a	1	1	1	*B. suillus*
1050a	1	1	1	*B. suillus*
1139a	1	1	1	*B. suillus*
1154a	1	1	1	*B. suillus*
1338a	1	1	1	*B. suillus*
1339a	1	1	1	*B. suillus*
282	1	1	1	*B. suillus*
283	1	1	1	*B. suillus*
284	1	1	1	*B. suillus*
285	1	1	1	*B. suillus*
169	2	2	2	*H.argenteocinereus*
170	2	2	2	*H.argenteocinereus*
171	2	2	2	*H.argenteocinereus*
172	2	2	2	*H.argenteocinereus*
173	2	2	2	*H.argenteocinereus*
174	2	2	2	*H.argenteocinereus*
175	2	2	2	*H.argenteocinereus*
176	2	2	2	*H.argenteocinereus*
177	2	2	2	*H.argenteocinereus*
178	2	2	2	*H.argenteocinereus*
179	2	2	2	*H.argenteocinereus*
180	2	2	2	*H.argenteocinereus*
181	2	2	2	*H.argenteocinereus*
182	2	2	2	*H.argenteocinereus*

Point	Given group	Classification	Jackknifed	Species
183	2	2	2	*H.argenteocinereus*
184	2	2	2	*H.argenteocinereus*
185	2	2	2	*H.argenteocinereus*
186	2	2	2	*H.argenteocinereus*
187	2	2	2	*H.argenteocinereus*
188	2	2	2	*H.argenteocinereus*
189	2	2	2	*H.argenteocinereus*
190	2	2	2	*H.argenteocinereus*
192	2	2	2	*H.argenteocinereus*
193	2	2	2	*H.argenteocinereus*
194	2	2	2	*H.argenteocinereus*
241	2	2	3*	*H.argenteocinereus*
242	2	2	2	*H.argenteocinereus*
243	2	2	3*	*H.argenteocinereus*
244	2	2	3*	*H.argenteocinereus*
289	2	2	2	*G.capensis*
290	2	2	2	*G.capensis*
295	2	2	2	*G.capensis*
297	2	2	2	*G.capensis*
298	2	2	2	*G.capensis*
380	2	2	2	*G.capensis*
381	2	2	3*	*G.capensis*
382	2	2	2	*G.capensis*
383	2	2	2	*G.capensis*
384	2	2	2	*G.capensis*
385	2	2	2	*G.capensis*
386	2	2	2	*G.capensis*
388	2	2	2	*G.capensis*
389	2	2	2	*G.capensis*
390	2	2	2	*G.capensis*
391	2	2	2	*G.capensis*
392	2	2	2	*G.capensis*
393	2	2	2	*G.capensis*
394	2	2	2	*G.capensis*
395	2	2	2	*G.capensis*
396	2	2	2	*G.capensis*
397	2	2	2	*G.capensis*
213	3	3	2*	*F.mechowii*
214	3	3	3	*F.mechowii*
215	3	3	3	*F.mechowii*
216	3	2	2*	*F.mechowii*
217	3	3	3	*F.mechowii*
219	3	3	3	*F.mechowii*
220	3	3	3	*F.mechowii*
221	3	2	2*	*F.mechowii*
222	3	2	2*	*F.mechowii*
223	3	2	2*	*F.mechowii*
224	3	2	2*	*F.mechowii*
305	3	3	3	*F.damarensis*
306	3	3	3	*F.damarensis*
308	3	3	3	*F.damarensis*
310	3	3	3	*F.damarensis*
311	3	3	3	*F.damarensis*

...continuation

Point	Given group	Classification	Jackknifed	Species
316	3	3	3	*F.damarensis*
317	3	3	3	*F.damarensis*
318	3	3	3	*F.damarensis*
319	3	3	3	*F.damarensis*
326	3	3	3	*F.damarensis*
320	3	3	3	*F.damarensis*
321	3	3	3	*F.damarensis*
322	3	3	3	*F.damarensis*
323	3	3	3	*F.damarensis*
325	3	2	2*	*F.damarensis*
324	3	2	2*	*F.damarensis*
227	3	3	3	*F.damarensis*
228	3	3	3	*F.damarensis*
102	3	3	3	*C.hottentotus*
103	3	3	3	*C.hottentotus*
104	3	3	3	*C.hottentotus*
105	3	3	3	*C.hottentotus*
106	3	3	3	*C.hottentotus*
108	3	3	3	*C.hottentotus*
109	3	3	3	*C.hottentotus*
110	3	3	3	*C.hottentotus*
111	3	3	3	*C.hottentotus*
112	3	3	3	*C.hottentotus*
115	3	3	3	*C.hottentotus*
116	3	3	3	*C.hottentotus*
117	3	3	3	*C.hottentotus*
123	3	3	3	*C.hottentotus*
125	3	3	3	*C.hottentotus*
126	3	3	3	*C.hottentotus*
127	3	3	3	*C.hottentotus*
128	3	3	3	*C.hottentotus*
129	3	2	2*	*C.hottentotus*
132	3	3	3	*C.hottentotus*
133	3	3	3	*C.hottentotus*
138	3	3	3	*C.hottentotus*
140	3	3	3	*C.hottentotus*
141	3	3	3	*C.hottentotus*
142	3	3	3	*C.hottentotus*
143	3	2	2*	*C.hottentotus*
144	3	3	3	*C.hottentotus*
145	3	3	3	*C.hottentotus*
146	3	3	3	*C.hottentotus*
147	3	3	3	*C.hottentotus*
150	3	3	2*	*C.hottentotus*
151	3	3	3	*C.hottentotus*
152	3	3	3	*C.hottentotus*
1	3	3	3	*H.glaber*
2	3	3	3	*H.glaber*
8	3	3	3	*H.glaber*
9	3	3	3	*H.glaber*
45	3	3	3	*H.glaber*
46	3	3	3	*H.glaber*
47	3	3	3	*H.glaber*
48	3	3	3	*H.glaber*
49	3	3	3	*H.glaber*

Point	Given group	Classification	Jackknifed	Species
50	3	3	3	*H.glaber*
51	3	3	3	*H.glaber*
52	3	3	3	*H.glaber*
53	3	3	3	*H.glaber*
54	3	3	3	*H.glaber*
55	3	3	3	*H.glaber*
56	3	3	3	*H.glaber*
57	3	3	3	*H.glaber*
58	3	3	3	*H.glaber*
59	3	3	3	*H.glaber*
60	3	3	3	*H.glaber*
61	3	3	3	*H.glaber*
63	3	3	3	*H.glaber*
64	3	3	3	*H.glaber*
65	3	3	3	*H.glaber*
66	3	3	3	*H.glaber*
67	3	3	3	*H.glaber*
69	3	3	3	*H.glaber*
70	3	3	3	*H.glaber*
71	3	3	3	*H.glaber*
73	3	3	3	*H.glaber*
74	3	3	3	*H.glaber*
75	3	3	3	*H.glaber*
76	3	3	3	*H.glaber*
77	3	3	3	*H.glaber*
78	3	3	3	*H.glaber*
79	3	3	3	*H.glaber*
80	3	3	3	*H.glaber*
81	3	3	3	*H.glaber*
82	3	3	3	*H.glaber*
83	3	3	3	*H.glaber*
84	3	3	3	*H.glaber*
85	3	3	3	*H.glaber*
87	3	3	3	*H.glaber*
88	3	3	3	*H.glaber*
90	3	3	3	*H.glaber*
91	3	3	3	*H.glaber*
92	3	3	3	*H.glaber*
93	3	3	3	*H.glaber*
94	3	3	3	*H.glaber*
96	3	3	3	*H.glaber*
97	3	3	3	*H.glaber*
99	3	3	3	*H.glaber*
101	3	3	3	*H.glaber*
420	3	3	3	*H.glaber*
498	3	3	3	*H.glaber*
499	3	3	3	*H.glaber*
500	3	3	3	*H.glaber*
501	3	3	3	*H.glaber*
505	3	3	3	*H.glaber*
507	3	3	3	*H.glaber*
508	3	3	3	*H.glaber*
509	3	3	3	*H.glaber*
510	3	3	3	*H.glaber*
511	3	3	3	*H.glaber*

APPENDIX 4.4. Jackknifed cross-validations of group assignments obtained from the discriminant analysis including all morpho-functional indices but excluding one species, *Heterocephalus glaber* (*N* = 152). A total of 97.37% correctly classified individuals were obtained. The misclassified individuals are indicated with an asterisk (*) and pertained mostly to the solitary chisel-tooth digger, accumulating only 0.97% (4 individuals).

Point	Given group	Classification	Jackknifed	Species
314a	1	1	1	*B. suillus*
365a	1	1	1	*B. suillus*
366a	1	1	1	*B. suillus*
377a	1	1	1	*B. suillus*
717a	1	1	1	*B. suillus*
721a	1	1	1	*B. suillus*
911a	1	1	1	*B. suillus*
913a	1	1	1	*B. suillus*
938a	1	1	1	*B. suillus*
982a	1	1	1	*B. suillus*
1085a	1	1	1	*B. suillus*
1138a	1	1	1	*B. suillus*
1144a	1	1	1	*B. suillus*
1153a	1	1	1	*B. suillus*
1155a	1	1	1	*B. suillus*
1163a	1	1	1	*B. suillus*
1169a	1	1	1	*B. suillus*
1171a	1	1	1	*B. suillus*
1332a	1	1	1	*B. suillus*
1336a	1	1	1	*B. suillus*
217a	1	1	1	*B. suillus*
220a	1	1	1	*B. suillus*
313a	1	1	1	*B. suillus*
713a	1	1	1	*B. suillus*
765a	1	1	1	*B. suillus*
861a	1	1	1	*B. suillus*
910a	1	1	1	*B. suillus*
964a	1	1	1	*B. suillus*
965a	1	1	1	*B. suillus*
1039a	1	1	1	*B. suillus*
1050a	1	1	1	*B. suillus*
1139a	1	1	1	*B. suillus*
1154a	1	1	1	*B. suillus*
1338a	1	1	1	*B. suillus*
1339a	1	1	1	*B. suillus*
282	1	1	1	*B. suillus*
283	1	1	1	*B. suillus*
284	1	1	1	*B. suillus*
285	1	1	1	*B. suillus*
169	2	2	2	*H.argenteocinereus*
170	2	2	2	*H.argenteocinereus*
171	2	2	2	*H.argenteocinereus*
172	2	2	2	*H.argenteocinereus*
173	2	2	2	*H.argenteocinereus*
174	2	2	2	*H.argenteocinereus*
175	2	2	2	*H.argenteocinereus*
176	2	2	2	*H.argenteocinereus*
177	2	2	2	*H.argenteocinereus*
178	2	2	2	*H.argenteocinereus*
179	2	2	2	*H.argenteocinereus*
180	2	2	2	*H.argenteocinereus*
181	2	2	2	*H.argenteocinereus*
182	2	2	2	*H.argenteocinereus*

Point	Given group	Classification	Jackknifed	Species
183	2	2	2	*H.argenteocinereus*
184	2	2	2	*H.argenteocinereus*
185	2	2	2	*H.argenteocinereus*
186	2	2	2	*H.argenteocinereus*
187	2	2	2	*H.argenteocinereus*
188	2	2	2	*H.argenteocinereus*
189	2	2	2	*H.argenteocinereus*
190	2	2	2	*H.argenteocinereus*
192	2	2	2	*H.argenteocinereus*
193	2	2	2	*H.argenteocinereus*
194	2	2	2	*H.argenteocinereus*
241	2	2	2	*H.argenteocinereus*
242	2	2	2	*H.argenteocinereus*
243	2	2	3*	*H.argenteocinereus*
244	2	2	3*	*H.argenteocinereus*
289	2	2	2	*G.capensis*
290	2	2	2	*G.capensis*
295	2	2	2	*G.capensis*
297	2	2	2	*G.capensis*
298	2	2	2	*G.capensis*
380	2	2	2	*G.capensis*
381	2	2	3*	*G.capensis*
382	2	2	2	*G.capensis*
383	2	2	2	*G.capensis*
384	2	2	2	*G.capensis*
385	2	2	2	*G.capensis*
386	2	2	2	*G.capensis*
388	2	2	2	*G.capensis*
389	2	2	2	*G.capensis*
390	2	2	2	*G.capensis*
391	2	2	2	*G.capensis*
392	2	2	2	*G.capensis*
393	2	2	2	*G.capensis*
394	2	2	2	*G.capensis*
395	2	2	2	*G.capensis*
396	2	2	2	*G.capensis*
397	2	2	2	*G.capensis*
213	3	3	3	*F.mechowii*
214	3	3	3	*F.mechowii*
215	3	3	3	*F.mechowii*
216	3	3	3	*F.mechowii*
217	3	3	3	*F.mechowii*
219	3	3	3	*F.mechowii*
220	3	3	3	*F.mechowii*
221	3	3	3	*F.mechowii*
222	3	3	3	*F.mechowii*
223	3	3	3	*F.mechowii*
224	3	3	3	*F.mechowii*
305	3	3	3	*F.damarensis*
306	3	3	3	*F.damarensis*
308	3	3	3	*F.damarensis*
310	3	3	3	*F.damarensis*
311	3	3	3	*F.damarensis*

...continuation

Point	Given group	Classification	Jackknifed	Species
316	3	3	3	*F.damarensis*
317	3	3	3	*F.damarensis*
318	3	3	3	*F.damarensis*
319	3	3	3	*F.damarensis*
326	3	3	3	*F.damarensis*
320	3	3	3	*F.damarensis*
321	3	3	3	*F.damarensis*
322	3	3	3	*F.damarensis*
323	3	3	3	*F.damarensis*
325	3	3	3	*F.damarensis*
324	3	3	3	*F.damarensis*
227	3	3	3	*F.damarensis*
228	3	3	3	*F.damarensis*
102	3	3	3	*C.hottentotus*
103	3	3	3	*C.hottentotus*
104	3	3	3	*C.hottentotus*
105	3	3	3	*C.hottentotus*
106	3	3	3	*C.hottentotus*
108	3	3	3	*C.hottentotus*
109	3	3	3	*C.hottentotus*
110	3	3	3	*C.hottentotus*
111	3	3	3	*C.hottentotus*
112	3	3	3	*C.hottentotus*

Point	Given group	Classification	Jackknifed	Species
115	3	3	3	*C.hottentotus*
116	3	3	3	*C.hottentotus*
117	3	3	3	*C.hottentotus*
123	3	3	3	*C.hottentotus*
125	3	3	3	*C.hottentotus*
126	3	3	3	*C.hottentotus*
127	3	3	3	*C.hottentotus*
128	3	3	3	*C.hottentotus*
129	3	3	2*	*C.hottentotus*
132	3	3	3	*C.hottentotus*
133	3	3	3	*C.hottentotus*
138	3	3	3	*C.hottentotus*
140	3	3	3	*C.hottentotus*
141	3	3	3	*C.hottentotus*
142	3	3	3	*C.hottentotus*
143	3	3	3	*C.hottentotus*
144	3	3	3	*C.hottentotus*
145	3	3	3	*C.hottentotus*
146	3	3	3	*C.hottentotus*
147	3	3	3	*C.hottentotus*
150	3	3	3	*C.hottentotus*
151	3	3	3	*C.hottentotus*
152	3	3	3	*C.hottentotus*

APPENDIX 4.5. Video recordings showing individuals of *Heterocephalus glaber* performing digging behavior using forelimbs and hindlimbs in glass containers lacking any substrate. The first video (00:08-00:45) shows an old mature individual using a combination of chisel-tooth digging and scratch-digging. The second video (00:46-01:19) shows an individual performing hindlimb -backwards- digging, typically used to push the soil out of the burrow. This colony has been maintained without soil substrate and despite of this, both individuals perform intense and repetitive digging behavior, indicating its innate nature. This colony was established in the early 1980's by Emeritus Associate Professor Jenny Jarvis, and its animals have ended up in different laboratories in the USA, UK, Germany, France, Japan, South Korea, China and Israel (De Blocq, 2016). Videos were recorded in January 2014, in the Department of Biological Sciences at the University of Cape Town. Copyright © Germán Montoya-Sanhueza. Video Editing: Floriane Blanc Marquis. Acknowledgements: Professor Jenny Jarvis for allowing the recording of the specimens.

https://www.youtube.com/watch?v=YpvqOSp1KUU

CHAPTER 5

An Allometric Approach to Limb Bone Modularity and Osteogenesis in Subterranean Mammals

"But although at all levels there can be shown a relationship between structure and function … it cannot be assumed that the relationship is always one of cause and effect, for many different causes combine to produce the finished architecture (of bones)…"

Patrick Desmond Fitzgerald Murray, 1936
BONES: A STUDY OF THE DEVELOPMENT AND STRUCTURE OF THE VERTEBRATE SKELETON

"... a highly simplified, approximate formula which applies to an astonishingly broad range of phenomena, but is neither a dogma nor an explanation for everything. (...) Notwithstanding its simplified character and mathematical shortcomings, the principle of allometry is an expression of the interdependence, organization and harmonization of physiological processes."

Ludwig von Bertalanffy, 1968
On the biological meaning of allometric relationships
GENERAL SYSTEM THEORY

5.1 INTRODUCTION

Phenotypic variation is a central topic in evolution. The last decades have witnessed a considerable interconnectedness between the fields of evolutionary morphology and genetics to understand the genetic and developmental origins of phenotypic variation. However, the genetic changes that provide the raw material for evolution do not act directly on morphology or behavior, but on the course of development and the formation of new traits throughout the appearance of new pathways (Staddon, 1983; Hall, 2002; Alba, 2002). For this reason, to understand the dynamics and mechanisms of morphological evolution, it is crucial to know the developmental bases of morphological variation within and among species (Sanger *et al.* 2011; Percival & Richtsmeier, 2017; Franz-Odendaal & Dorit, 2019). The main goal of this chapter is to assess the growth patterns of different bathyergid species as well as their ossification patterns during postnatal ontogeny. Before doing so, it is necessary to frame a brief introduction around the traditional use of allometries

in evolutionary morphology and how this approach can be used to understand specific processes associated with aspects of skeletal morphogenesis. A brief summary of the processes of ossification and bone modeling in mammals, as well as a succinct compilation of the current understanding of somatic growth in bathyergids are also provided.

5.1.1 Allometry and Modularity

A large proportion of structural evolution can be described in terms of relative growth (and their allometric approaches), as well as to the development of different models of heterochrony (Thomas, 1917; Huxley, 1932; Gould, 1966; von Bertalanffy, 1968; Alberch *et al.*, 1979; Minugh-Purvis & McNamara 2002). Most morphological studies have focused on understanding the relative growth of certain structures, especially with the scaling of body size among species. Ontogenetic allometry has also been relatively well assessed (Dodson, 1975; Carrier, 1983; Sánchez-Villagra, 2002; Echeverría *et al.*, 2014; Moyano *et al.*, 2019), although less attention has been placed on understanding the more specific processes that generate such morphological diversity, such as the cellular and molecular bases of morphological heterochrony (Raff & Wray, 1989; Klingenberg, 2013; Cubo *et al.*, 2006; Spicer, 2006). Allometric approaches usually focus on the linear relationship between body size and either a simple or a more complex shape (based on linear measurements, morpho-functional indices, complex forms in 2D or 3D imaging). However, the quantification of complex structures usually implies that the measurements representing a shape are composed of different parts. For example, the mammalian skull length, usually measured from the tip of the snout to the posterior part of the skull, includes different bones within its range, e.g. nasals, frontals, parietals, and occipital. Thus, such analyses provide an indication of the relationship between two complex –multivariate and multifactorial— systems (e.g. Von Bertalanffy, 1969), the measured structure (e.g. skull shape) and the size of the organism (usually body mass). This kind of analysis is highly relevant to have an idea of the magnitude and type of changes between systems, and it has been widely used to reconstruct the trends of morphological diversity and evolution in several animal clades (see references above). However, such analysis does not provide information about the cell-tissue mediated mechanisms responsible of such morphological diversity. Complex structures in animals are formed by several components, having independently ‘’unique growing parts” (Raff & Raff, 1987; Raff & Wray, 1989; Atchley & Hall, 1991). The case of the skeletal system is not the exception, and rather represents a constant of “modularity” (e.g. Koyabu *et al.*, 2011; Esteve-Altava, 2017). Thus, even when a bone appears as a unique independent unit (e.g. the mammalian skull or dentary), it is actually composed of several parts, which have been defined as morphological modules (Atchley *et al.*, 1985; Atchley & Hall, 1991; Anthwal & Tucker, 2012). In the example of the mammalian skull, this is composed of around 29 bones, which have different ossification types (Enlow, 1963; Sperber, 2001). Even at this level, when we consider all modules formed by one type of ossification, there will be differences in the rates of formation for each of those modules (Enlow, 1963; Sperber, 2001). These processes have been established in the developmental pattern of mammals

(Atchley & Hall, 1991), even from early evolution of therapsid lineages (Jasinoski & Chinsamy, 2012). This means that the entire shape or form of a structure cannot be reduced or analogized to a unique process of growth, since a structure will be composed of different cell lineages (envelopes) with distinct growth dynamics. The following corollary is obtained: "the growth of a system is not necessarily homologous to the growth of its components". Thus, allometric coefficients of morphometric studies usually represent size or shape rates and not actual growth (e.g. appositional) rates (Simpson *et al.* 1960; Gould 1966; Nelson & Shump 1978; Abdala *et al.*, 2001). Additionally, bivariate ontogenetic allometry usually examines the relationship between localized (one part) versus global (one system) rates of growth (Klingenberg, 2013; Sanger *et al.*, 2011). Thus, to understand morphological change, it is important to identify the "independent" modules, its contribution to the final phenotype, and their interconnectedness with respect to other modules.

5.1.2 Bone Modules and Ossification in Mammals

Early work on the conceptualization of morphological modules derives from the research of Olson & Miller (1958) on morphological integration, which focused on phenotypic correlation within subsets of morphological traits. Nowadays, several definitions of "module" exist and not all of them represent developmental units (Klingenberg, 2013; Assis *et al.* 2016; Esteve-Altava, 2017). One definition of developmental modules corresponds to a set of cells, genes, or tissues that are relatively independent with respect to the pattern of formation and differentiation, or an autonomous regulatory control (Assis *et al.* 2016). In this study, a developmental unit will be the basis of the analysis, since its study will provide information on how an "independent" growth trajectory is responsible for producing key changes in the overall phenotype of an organism during morphogenesis (Enlow, 1963).

Two main ways of ossification take place in the mammalian skeleton, endochondral and intramembranous ossification (Enlow, 1963; Hall, 2015). Since these processes are regulated by different gene expression factors and are formed by different mesenchymal cells, they represent relatively "independent" developmental entities (Hall, 2015). Ossification types are distributed unequally within the skeleton. For instance, the morphogenesis of the skull and dentary bone includes the mandibular condyle, intramembranous sutures, the periodontal membrane, the alveolar margin, and synchondroses among others (Enlow, 1963). In comparison, the morphogenesis of a long bone is relatively simpler in complexity and occurs within one unique structural entity (e.g. the humerus), which involves primarily endochondral ossification but also intramembranous ossification (Enlow, 1963). In the appendicular system, endochondral ossification is responsible for main changes in bone elongation, while intramembranous ossification is responsible for changes in bone expansion (radial thickening), specifically in the diaphysis and secondarily in metaphyses (Fig. 5.1A). Thus, the independent quantification of such osteogenic process permits a simplified but a more realistic view of the individual contribution of bone modules to attain its final shape and morphology. This also provides an opportunity to test the

interrelationships between the independent developmental modules, i.e integration (e.g., Cubo *et al.*, 2006; Sanger *et al.*, 2011; Koyabu *et al.*, 2011).

This approach was recently applied (see Ch. 3) to an ontogenetic series of the largest subterranean mammal, the Cape dune mole-rat, *Bathyergus suillus,* and showed that endochondral modules were less variable than intramembranous modules when regressed against proxies of body size, thus indicating that fluctuating rates of intramembranous osteogenesis during postnatal life plays an important role in its ontogenetic variability and skeletal morphology (Montoya-Sanhueza *et al.* 2019). These authors compared their results with another convergent subterranean species, the tuco-tuco, *Ctenomys talarum* (Ctenomyidae) to demonstrate the presence of distinct developmental patterns in bone specialization between these taxa, probably associated with adaptive modifications of their bone growth rates (Montoya-Sanhueza *et al.* 2019). These data suggest that certain ossification types are probably more susceptible to local adaptation and environmental cues during ontogeny (Echeverría *et al.*, 2014; Montoya-Sanhueza *et al.* 2019), and therefore may be an important factor to consider for understanding bone adaptation.

A more sophisticated approach for the study of ossification of long bones involved the phylogenetic contrasts performed by Cubo (2000) and Cubo *et al.* (2002, 2006) in a group of subterranean species (Arvicolidae). Although the conceptualization of bone modularity was lacking in the latter studies, these authors identified the role of independent ossification mechanisms orchestrating bone phenotyping and speciation. They demonstrated that morphological specializations were already present in juvenile stages, suggesting that morphological differences (and speciation processes) are the direct expression of genetic changes (most likely expressed throughout development) rather than the outcome of epigenetic factors of mechanical origin (Cubo *et al.*, 2006). These authors showed that the analysis of linear regressions and allometries are important tools to understand the specific mechanisms acting on morphogenesis during ontogeny and evolutionary process.

5.1.3 Bone Modeling: An Interaction of Different Developmental Modules

Mammals have evolved in such extraordinary ways and have resulted in a wide diversity of skeletal sizes and shapes, in comparison to other vertebrates. Despite huge differences in size and shape between mammals, the process by which their skeletons attain their size and shape is the same, i.e. through bone modeling (Enlow, 1963; Frost, 1969). Bone modeling is the process involving formation and resorption of bone tissues (not necessarily coupled), which is principally associated with the growth of the bone and resulting in changes in its shape and size (Frost, 1969, 1987; Parfitt, 2010; Allen & Burr, 2014). This is equivalent to Enlow's term "growth remodeling" (Enlow, 1963). Bone modeling involves the interaction of different chondrification and ossification mechanisms as well as the differential local and systemic regulation of bone dynamics (throughout catabolism and anabolism) (Lanyon *et al.*, 2009; Parfitt, 2010). It differentiates from bone remodeling since the latter is the process of replacement of bone tissues (also often referred to as secondary reconstruction) and which usually involves coupled bone

resorption and formation mainly along endosteal, intracortical and trabecular envelopes (Frost, 1969, 1987; Parfitt, 2010; Allen & Burr, 2014). The lining of bone forming and resorbing cells on the outer and inner surfaces of the bones, gives rise to distinctive bone envelopes or membranes with distinct properties, receptors and expression mechanisms (Enlow, 1969; Frost, 1969; Biewener & Bertram, 1993; Morgan *et al.* 2010b; Stout & Crowder, 2012; Burr & Akkus, 2014). In long bones, bone modeling is initially carried out by endochondral ossification and growth plate activity at epiphyses, while intramembranous ossification takes place around the diaphysis and metaphysis by direct bone apposition (Fig. 5.1A) (Murray, 1936; Moss-Salentijn, 1991; Hall, 2015). In mammals, long bone growth is also completed by secondary centers of ossification at the epiphyses, which represents another endochondral module (see below). Intramembranous ossification involves both periosteal (centrifugal) and endosteal (centripetal) bone formation, which occurs in the external and internal layers of bone, respectively (Fig. 5.1B). The periosteum lines the outer surface of nearly the entire long bone and contributes to appositional bone growth during bone development and it is responsible for the expansion of the diameters of the long bones through ontogeny (Morgan *et al.* 2010). The endosteum lines the inner surfaces of bones and consists of bone surface cells, including osteoblasts and bone lining cells (Morgan *et al.* 2010). If this latter envelope is active (non-resorptive), it also contributes to appositional growth within the medullary cavity, resulting in bones with thick cortical walls, typical of fossorial and semiaquatic species (Wall, 1983; Biknevicius, 1993; Casinos *et al.*, 1993; Montoya-Sanhueza & Chinsamy, 2017). In many terrestrial mammals, trabecular components of endochondral origin become progressively removed by resorption during growth and are replaced by cancellous bone of an endosteal type (Enlow, 1963). This process initiates around the metaphyseal regions, closer to the (epi)condyles of stylopodial bones (humerus and femur) (Fig. 5.1A). Thus, this region represents the interface between endochondral and periosteal bone formations (Hall, 1978; Moss-Salentijn, 1992), and involves the interaction of two different developmental modules through a process that results in the incorporation of trabecular bone into cortical bone, traditionally denominated bone “compaction” (Enlow, 1963) or as recently termed “coalescence” (Cadet *et al.*, 2003).

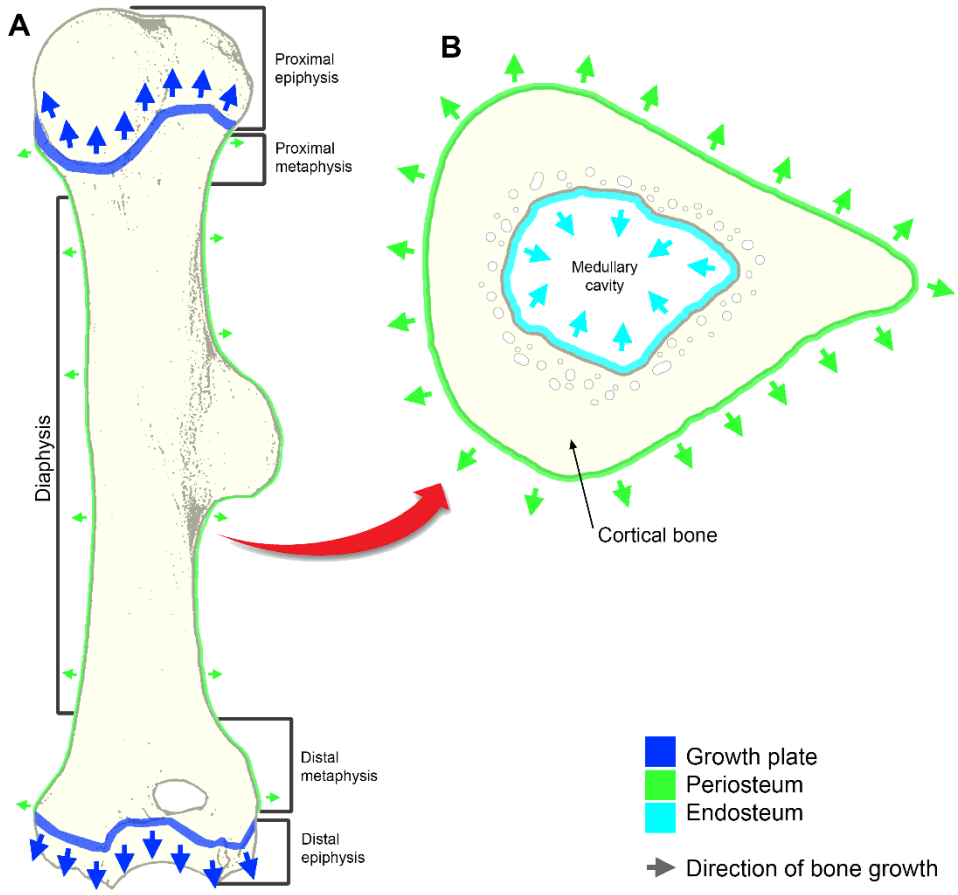

FIGURE 5.1. Ossification types and bone modularity. Generalized long bone anatomy and topographical distribution of endochondral and intramembranous ossification. A) Humerus showing (proximal and distal) epiphyses, metaphyses and diaphysis. Endochondral ossification (blue line) occurs in the growth plates and results in bone elongation. B) Mid-shaft cross-section showing cortical bone and the location of intramembranous ossification, specifically showing external (periosteal) and internal (endosteal) bone modules, which results in radial bone thickening.

5.1.4 Body Growth in African Mole-Rats

Numerous ecological studies have assessed the general growth trends of body mass in bathyergids (Taylor *et al.*, 1985; Bennett & Jarvis, 1988; Bennett, 1989; Burda, 1989; Bennett & Aguilar, 1995; O'Riain, 1996; Bennett & Navarro, 1997; O'Riain & Jarvis, 1998; Scharff *et al.*, 1999; O'Riain *et al.*, 2000; O'Connor *et al.* 2002; Malherbe *et al.*, 2003; Šumbera *et al.*, 2003; Herbst *et al.*, 2004; Janse Van Rensburg *et al.*, 2004; Hart *et al.*, 2007; Henry *et al.*, 2007; Young & Bennett, 2010; Zöttl *et al.*, 2016; Ruby *et al.*, 2018; Thorley *et al.*, 2018). Bennett *et al.* (1990, 1991) have the distinction of having studied the body growth of African mole-rats in a comparative way. However, only some of these studies measured skeletal parameters such as body length (Bennett *et al.*, 1990; O'Riain & Jarvis, 1998; Šumbera *et al.*, 2003; Henry *et al.*, 2007; Young & Bennett, 2010; Thorley *et al.*, 2018). In general, the body growth of bathyergids is represented by slow growth rates as compared to other non-subterranean mammals of similar size (Bennett *et al.*, 1991; Brett, 1991; Jarvis *et al.*, 1991; O'Riain, 1996; Bennett & Navarro, 1997;

O'Riain & Jarvis, 1998). Social bathyergids seem to show extremely low mean maximum growth rates when compared to solitary ones (Bennett *et al.*, 1991), especially naked mole-rats, which show the slowest growth rates among all bathyergids (O'Riain, 1996; O'Riain & Jarvis, 1998). It has been suggested (Bennett *et al.*, 1991; O'Riain, 1996) that the slow growth rates observed in naked mole-rats (and probably other social bathyergids) is related to their poor ability to regulate and sustain high body temperatures (poikilothermic thermoregulation) and low metabolic rates, as well as to a number of complex sociobiological factors acting upon them, including incorporation of pups into established hierarchies, overlap of litters, cooperative care of young and the strict socially-induced sterility imposed upon individuals in the colonies, i.e. delayed puberty (McNab 1966; Withers & Jarvis 1980; Lovegrove 1986; Buffenstein & Yahav, 1991; Bennett *et al.*, 1994, 1996; Bennett & Aguilar, 1995; Pinto *et al.*, 2010). Interestingly, sociality seems not to be a constraint for reaching high growth rates, since the highest growth rates among the social mole-rats have been found in *Fukomys mechowii*, which is the largest social mole-rat, and resembles that of the solitary species, *Georychus capensis* and *Bathyergus janetta* (Bennett & Aguilar, 1995; Scharff *et al.*, 1999). Some authors suggested higher growth rates in larger body-sized species (Scharff *et al.*, 1999).

Only one study has assessed the growth patterns of the appendicular skeleton in bathyergids (Ch. 3, Montoya-Sanhueza *et al.*, 2019). In the present chapter, the growth patterns of all bathyergid species are assessed to determine the rates of bone growth. Changes in the rate of growth can produce either *acceleration*, when the rate increases, or *neoteny*, when there is a retardation in the growth rate (McNamara, 1997). Acceleration implies fast growing and results in peramorphosis, that is, more shape change and an increase in structural/morphological complexity, while the contrary occurs under neoteny, which implies slow growth resulting in paedomorphosis, that is less shape change and decrease in complexity (McNamara, 1997).

In this study, two hypotheses are assessed. The first is related to the relative bone growth rates between fore- and hindlimbs (*Hypothesis B,* in Ch. 1). Previous studies on extant mammals with various locomotor modes, gaits, postures and sizes that included marsupials, lagomorphs, rodents, scandentians and primates, found that hindlimb elements generally grow much faster than the homologous forelimb elements (Carrier, 1983; Lammers & German, 2002; Schilling & Petrovitch, 2006; Young, Fernandez & Fleagle, 2010). Due to the importance of the pectoral girdle and forelimb bones for burrow construction in bathyergids (e.g. Genelly, 1965; Jarvis & Sale, 1971), the humerus, ulna and humerus+ulna will show faster growth rates as compared to their serial homologues, the femur, tibia-fibula, femur+tibia-fibula, respectively. It is expected that the forelimb elements will show higher slopes, thus indicating comparatively faster/earlier rates of maturity than hindlimb bones.

The second hypothesis (*Hypothesis C*, Ch. 1), explores the differences in growth rates between endochondral and intramembranous ossifications during ontogeny. It is expected that because of the differences in the timing of epithelial cell production and growth plate conservatism (predetermination), endochondral ossification will show a more stable pattern of bone growth, and therefore faster growth rates as compared to intramembranous ossification, which will be more

variable due to the constant *de novo* cell formation at periosteal surfaces. Additionally, based on the results of the Ch. 4, where external bone morphology was found to be similar among species (except for *H. glaber*), it is expected that there would be similar growth rates for all bathyergids, except for *H. glaber*, which is expected to have comparatively lower growth rates. The results obtained in this study are discussed in terms of general growth patterns in bathyergids, and especially in terms of differences between social and solitary species, but also with emphasis on the neotenic tendency suggested for naked mole rats (Skulachev *et al.*, 2017). Comparisons with terrestrial (surface-dwelling) mammals are also presented.

5.2 MATERIAL AND METHODS

5.2.1 Specimens

Postnatal ontogenetic series from seven bathyergid species (*Bathyergus suillus*, *Heliophobius argenteocinereus*, *Georychus capensis*, *Fukomys mechowii*, *F. damarensis*, *Cryptomys hottentotus* and *H. glaber*) involving 307 specimens from both sexes were analyzed. Ontogenetic series are based on age and body size of the individuals, as well as considering features of the skeletal development such as fused or unfused epiphyses and dental development (see Ch. 2 for more details). The specimens included representatives of early and late stages of ontogeny available for each species. Specimens were selected from either captive conditions or they were collected in the field by other researchers. A list of researchers that provided specimens and their associated institutions are presented in Ch. 2.

Fore- and hindlimbs were dissected from each specimen, although some specimens are represented by the forelimb only, and other specimens are represented by the hindlimb only. For this reason, the total number of specimens analyzed for the forelimb is higher than for the hindlimb (Table 5.1). Sample size, bone length and general descriptive statistics for each bone element and species are given in Table 5.1. Tables 5.2-5.4 show descriptive statistics for bone diameters and (epi)condyles.

Most specimens were skeletonized exclusively for this study, although some specimens were already skeletonized prior to this study (e.g. some specimens of *B. suillus, G. capensis* and *F. damarensis*). Other specimens like pups and juveniles, were already diaphanized at collection, so the measurements were obtained directly on such specimens or after photographing them. Small bones (especially from neonates and juveniles) were photographed using a stereomicroscope (Nikon SMZ 745T), and then analyzed in Image Pro-Plus version 4.5 (Media Cybernetics, Silver Spring, USA).

5.2.2 Proxies of Body Size

For all specimens, general data of body mass (BM) and body length (BL) were obtained (see Ch. 2). Most measurements of BM were taken by different researchers, so certain degree of measurement error is assumed to be present in the analyses. Additionally, almost all BM measurements were obtained at death, except for *H. glaber* which were done after defrosting the specimens. For this

reason, the body masses of this species may be underestimated and may affect the respective allometric estimations. However, the underestimation of body masses in allometric analysis should not have a strong effect on slope estimates, but on their elevation and/or intercept, since the equal lack of mass in the specimens along the ontogenetic sequence will result in a shift of the "*x*" axis (horizontal shift towards right side). Nevertheless, such results will be interpreted with caution, although it should be noted that elevation/intercept parameters are not assessed in this study.

However, to counteract these aspects, BL was also included in the comparisons, all of which were taken by the author of this thesis (see Ch. 2). The regressions of these two proxies would help to compare their results and thus reduce biases obtained from the fluctuations of BM. All specimens are housed in the Department of Biological Sciences at the University of Cape Town (UCT), South Africa.

5.2.3 Measurements

Fourteen linear measurements were recorded from forelimbs (humerus and ulna) and hindlimbs (femur and tibia-fibula) of each specimen. A total of 1132 bones were analyzed (Table 5.1). Linear measurements were recorded using a digital Mitutoyo caliper (0.01 mm) and are fully described in the Ch. 3 (Montoya-Sanhueza *et al.*, 2019). In this study, the anteroposterior diameter of the femur (APDF) is also added to the analysis. This parameter was measured at the 50% of the femoral length from its proximal epiphysis. All limb bone measurements were taken by the author of this thesis and followed standard linear measurements (e.g. Montoya-Sanhueza *et al.*, 2019; and references therein). In addition to the 14 linear measurements, two more measurements were calculated; the total length of the forelimb (HL+UL) and hindlimb (FL+TL) for each specimen, which represent the sum of the individual stylopodial and zeugopodial elements for each limb.

Some specimens lacked one or both of their epiphyses, especially the proximal epiphysis of the humerus and proximal and distal epiphyses of the ulna. In such cases, additional measurements of individual epiphyses from specimens with available epiphyses were taken and then regressed against the total length of the bone (the "*x*" variable). Ordinary least square (OLS) regressions were performed for this, since this type of regression works better for estimation and prediction of the "*y*" parameter (Warton *et al.* 2006). The estimated values obtained from the OLS regressions were added to the length of the bone lacking epiphyses.

Since *H. glaber* lacks a well-developed deltoid tubercle in the humerus (see Fig. 4.5 in Ch. 4), the anteroposterior (APDH) and mediolateral (TDH) diameters were taken at the 50% of the total length of the humerus, from the proximal epiphysis (see Fig. 6.1A in Ch. 6;). In general, in all other bathyergids, this point of the diaphysis is occupied by the deltoid tubercle (Fig. 4.5 in Ch. 4;), and it is of functional significance since it reflects the area of the diaphysis that is most affected by bending and torsion during digging behavior (Lepännen *et al.*, 2006; Montoya-Sanhueza *et al.*, 2019). For this reason, the anteroposterior and mediolateral aspects of the humeral diaphysis in all other bathyergid species were

measured more distally in relation to the proximal epiphysis (>50%) (see Fig. 6.1B in Ch. 6;).

5.2.4 Bone Modules and Osteogenesis

In this study, linear measurements associated with bone elongation (e.g. HL, UL, FL, TL, HL+UL and FL+TL) are considered as part of the endochondral bone module, while the measurements associated with radial bone thickening (e.g. TDH, TDU, TDF, TDT, APDH, APDU, APDF and APDT), are considered to reflect the intramembranous bone module (Ch. 4; Montoya-Sanhueza *et al.*, 2019). Since this study focusses on the external diameters of bones, the measurements associated with the intramembranous ossification are defined from here onwards as the periosteal bone module (Fig. 1B).

5.2.5 Bivariate Allometry and Statistical Design

Linear measurements were analyzed by standardized major axis (SMA) estimation (Model II regression, RMA) (Warton *et al.*, 2006). This type of regression was chosen over ordinary least square regressions (OLS) and major axis (MA) estimation types because the main goal of this study is to determine the relationship between two variables which are not necessarily independent in the strict sense, so it is assumed that both variables contain error to some extent (Warton *et al.*, 2006). In this study, the slope of the equation was used as an estimator of bone growth, and it was used to test common allometric patterns between species (e.g. Gould, 1977; Alba, 2002; Moyano *et al.* 2019). Coefficients of determination from each regression were also used to estimate the interrelatedness between linear measurements and body size as well as between ossification types.

Three main sets of bivariate regressions were done: i) the first accounted for independent determination of growth patterns in endochondral modules (for both fore- and hindlimbs), ii) the second for determination of growth patterns in periosteal modules (for both fore- and hindlimbs), and iii) the third for determination of growth patterns between endochondral and periosteal modules (its interaction). The first analysis included a series of regressions of all parameters regressed against BM and BL (e.g. HL vs BM). This analysis also included intra-limb (proximal vs distal elements) and inter-limb (serial homologues) comparisons. The second analysis for periosteal modules followed the same procedure as the first one (e.g. TDH vs BM). The third analysis tested the allometric trends of all periosteal and (epi)condylar modules against their respective bone lengths (e.g. TDH vs HL).

Those analyses consisted of two steps: i) the first to assess the significance of the deviations from isometry in the allometric coefficients, and ii) the second to test for a common interspecific coefficient of allometry between species for a given variable. Departures from isometry were assessed by inspection of slopes (b) and fitting to the 95% confidence intervals (CI) by testing the null hypothesis $b = 1.0$ when comparisons of the scalars are in the same unit (e.g. mm), and $b = 0.33$ when comparisons involve different units (e.g. mm or g). If the CI excluded a value of 1.0 (or 0.33), then allometry was considered significant, and significance p-value was also provided (see Warton *et al.* 2012). If the slope is <1.0 (or <0.33), there is

negative (-) allometry, and therefore a decrease in size of the "*y*" variable; if the slope is >1.0 (or >0.33), there will be positive (+) allometry and therefore an increase in size of the "*y*" variable. In this study, proxies of body size (BL and BM) are always plotted in the "*x*" axis, to highlight the effect on the "*y*" variable. Testing for common slopes between species was performed by likelihood ratio test (Warton *et al.*, 2006). This procedure is done through the argument *multcomp=T* (Warton *et al.*, 2012). Pairwise multiple comparisons were performed by using the argument *multcompmethod="adjust"*, which uses adjusted *p*-values via the Šidák (*post-hoc*) adjustment to counteract the problem of multiple comparisons in a conservative way (Warton *et al.*, 2012, and references therein). A *p*-value <0.05 (or equal) was used for all tests. All data were log_{10} transformed prior to analysis. Tests and plots were performed in PAST version 2.17c (Hammer *et al.*, 2001) and in R package smatr version 3.4-8 (Warton *et al.*, 2012).

5.3 RESULTS

A detailed description of long bone measurements of each species is given in Tables 5.1-5.4. Boxplots of bone lengths are shown in Figure 5.2.

Regression of body length and body mass. The likelihood ratio test showed that species have equal slopes (*p*-value: 0.095) and did not differ from a common isometric line (*p*-value: 0.106). Pairwise multiple comparisons also showed non-significant differences among species (Appendix 5.1). However, independent allometric estimations for each species showed that *F. mechowii* had negative allometry, i.e. body length grew relatively less than body mass (Table 5.5; Fig. 5.3).

TABLE 5.1. Total number of bones (*n* = 1132) and specimens (*N* = 303) analyzed, and descriptive statistics of bone lengths for *Bathyergus suillus*, *Heliophobius argenteocinereus*, *Georychus capensis*, *Fukomys mechowii*, *F. damarensis*, *Cryptomys hottentotus* and *H. glaber*.

Species				Humeral length (HL) (mm)	
	N	Min	Max	Mean ± SD	Median
B. suillus	51	24.63	49.19	36.94 ± 6.61	37.22
H. argenteocinereus	32	13.01	26.46	22.48 ± 2.90	23.11
G. capensis	58	10.81	29.67	22.18 ± 4.26	22.99
F. mechowii	13	7.12	28.54	23.57 ± 5.40	24.65
F. damarensis	33	7.74	23.03	16.22 ± 4.65	16.76
C. hottentotus	53	11.60	19.42	15.38 ± 1.85	15.05
H. glaber	63	11.46	16.19	14.12 ± 1.08	14.20
Total	303				
				Ulnar length (UL) (mm)	
B. suillus	51	28.72	57.44	43.63 ± 7.73	42.46
H. argenteocinereus	32	16.34	32.02	27.69 ± 3.75	28.73
G. capensis	58	12.25	35.78	27.51 ± 4.98	28.52
F. mechowii	13	8.96	35.96	29.74 ± 6.78	30.70
F. damarensis	33	9.30	28.49	19.26 ± 5.97	19.80
C. hottentotus	53	14.19	23.84	18.92 ± 2.24	18.60
H. glaber	62	11.09	16.30	14.47 ± 1.02	14.61
Total	302				
				Femoral length (FL) (mm)	
B. suillus	52	27.68	54.26	41.84 ± 7.46	42.34
H. argenteocinereus	32	14.27	28.14	24.06 ± 3.13	24.92
G. capensis	29	9.20	31.05	22.67 ± 5.57	23.78
F. mechowii	13	6.94	28.95	23.91 ± 5.59	24.74
F. damarensis	24	11.00	25.80	19.02 ± 4.31	18.92
C. hottentotus	53	12.28	21.38	16.71 ± 1.94	16.47
H. glaber	63	11.49	16.47	14.25 ± 1.16	14.27
Total	266				
				Tibio-fibular length (TL) (mm)	
B. suillus	52	28.45	49.51	39.03 ± 6.11	39.22
H. argenteocinereus	32	13.02	28.11	23.80 ± 2.96	24.33
G. capensis	27	12.79	29.91	22.99 ± 4.40	23.94
F. mechowii	12	7.04	30.04	24.59 ± 5.99	25.30
F. damarensis	22	13.74	26.37	20.67 ± 4.08	21.24
C. hottentotus	53	13.79	21.60	17.90 ± 1.86	17.57
H. glaber	63	11.59	16.71	14.58 ± 0.99	14.61
Total	261				

TABLE 5.2. Total number of specimens and descriptive statistics of mediolateral bone diameters for bathyergid species. See taxonomic abbreviations in Table 5.1.

Species	N	Min	Max	Mean ± SD	Median
			Mediolateral diameter of humerus (TDH) (mm)		
B. suillus	51	2.86	6.15	4.55 ± 0.80	4.64
H. argenteocinereus	32	1.96	3.70	3.04 ± 0.46	3.06
G. capensis	58	1.28	3.63	2.63 ± 0.53	2.69
F. mechowii	13	1.43	3.62	2.88 ± 0.56	2.95
F. damarensis	33	1.06	2.94	1.85 ± 0.51	1.76
C. hottentotus	53	1.17	2.54	1.81 ± 0.33	1.79
H. glaber	63	1.42	2.51	1.78 ± 0.19	1.79
Total	303				
			Mediolateral diameter of ulna (TDU) (mm)		
B. suillus	51	1.53	3.13	2.40 ± 0.39	2.41
H. argenteocinereus	32	0.89	1.91	1.35 ± 0.22	1.33
G. capensis	58	0.87	2.12	1.53 ± 0.26	1.56
F. mechowii	13	0.7	2.03	1.58 ± 0.33	1.58
F. damarensis	33	0.44	1.52	0.98 ± 0.30	0.89
C. hottentotus	53	0.65	1.23	0.92 ± 0.15	0.91
H. glaber	63	0.6	0.98	0.78 ± 0.07	0.78
Total	303				
			Mediolateral diameter of femur (TDF) (mm)		
B. suillus	51	2.8	6.7	4.95 ± 0.99	5.17
H. argenteocinereus	32	2.02	3.82	3.06 ± 0.42	3.12
G. capensis	28	1.38	4.24	2.89 ± 0.93	2.97
F. mechowii	13	1.52	4.04	3.22 ± 0.71	3.44
F. damarensis	24	1.58	3.39	2.32 ± 0.52	2.20
C. hottentotus	53	1.3	3.01	2.02 ± 0.46	2.02
H. glaber	63	1.27	2.05	1.55 ± 0.17	1.51
Total	264				
			Mediolateral diameter of tibio-fibula (TDT) (mm)		
B. suillus	51	2.35	4.99	3.67 ± 0.70	3.77
H. argenteocinereus	32	1.29	2.42	1.92 ± 0.30	1.96
G. capensis	26	1.11	3.16	2.15 ± 0.58	2.16
F. mechowii	12	0.85	2.84	2.00 ± 0.49	2.04
F. damarensis	22	1.02	2.21	1.52 ± 0.37	1.46
C. hottentotus	53	0.9	1.92	1.37 ± 0.28	1.34
Total	196				
Total	261				

TABLE 5.3. Total number of specimens and descriptive statistics of anteroposterior bone diameters for bathyergid species. See taxonomic abbreviations in Table 5.1.

Species	N	Min	Max	Mean ± SD	Median
				Anteroposterior diameter of humerus (APDH) (mm	
B. suillus	51	3.09	6.01	4.41 ± 0.72	4.37
H. argenteocinereus	32	1.35	3.36	2.51 ± 0.42	2.55
G. capensis	58	1.30	3.47	2.45 ± 0.46	2.46
F. mechowii	13	1.04	3.28	2.70 ± 0.61	2.75
F. damarensis	33	0.77	2.49	1.72 ± 0.49	1.71
C. hottentotus	53	0.94	2.11	1.61 ± 0.30	1.59
H. glaber	63	0.87	1.43	1.12 ± 0.11	1.14
Total	303				
				Anteroposterior diameter of ulna (APDU) (mm)	
B. suillus	51	2.26	5.07	3.75 ± 0.75	3.91
H. argenteocinereus	32	1.52	3.32	2.78 ± 0.44	2.88
G. capensis	58	1.02	3.18	2.30 ± 0.49	2.29
F. mechowii	13	1.07	3.28	2.54 ± 0.57	2.55
F. damarensis	33	0.67	2.59	1.55 ± 0.53	1.56
C. hottentotus	53	0.98	2.13	1.47 ± 0.28	1.47
H. glaber	63	1.13	1.83	1.45 ± 0.15	1.44
Total	303				
				Anteroposterior diameter of femur (APDF) (mm)	
B. suillus	51	2.33	4.67	3.40 ± 0.55	3.43
H. argenteocinereus	32	1.42	2.16	1.78 ± 0.19	1.74
G. capensis	28	1.34	2.88	2.01 ± 0.39	2.02
F. mechowii	13	1.07	2.84	2.23 ± 0.50	2.26
F. damarensis	24	1.24	2.77	1.86 ± 0.41	1.89
C. hottentotus	53	0.92	2.23	1.43 ± 0.31	1.40
H. glaber	63	0.77	1.27	0.98 ± 0.10	0.96
Total	264				
				Anteroposterior diameter of tibio-fibula (APDT) (mm)	
B. suillus	51	2.70	6.65	4.92 ± 1.01	4.87
H. argenteocinereus	32	2.10	4.73	3.52 ± 0.60	3.62
G. capensis	26	1.85	4.42	3.31 ± 0.74	3.37
F. mechowii	12	1.63	4.88	3.80 ± 0.89	4.08
F. damarensis	22	1.51	3.86	2.69 ± 0.70	2.68
C. hottentotus	53	1.33	3.10	2.26 ± 0.41	2.30
Total	196				
Total	261				

TABLE 5.4. Total number of specimens and descriptive statistics of (epi)condylar widths for bathyergid species. See taxonomic abbreviations in Table 5.1.

Species	N	Min	Max	Mean ± SD	Median
				Humeral epicondyles (EH) (mm)	
B. suillus	51	9.09	14.58	12.29 ± 1.39	12.50
H. argenteocinereus	32	4.64	8.51	6.94 ± 0.70	6.96
G. capensis	58	3.58	8.54	6.85 ± 1.03	6.95
F. mechowii	13	3.15	8.93	7.80 ± 1.48	8.24
F. damarensis	23	4.20	7.24	5.77 ± 0.90	6.02
C. hottentotus	53	3.39	5.77	4.56 ± 0.51	4.58
H. glaber	63	3.35	4.39	3.87 ± 0.23	3.90
Total	293				
				Femoral epicondyles (FH) (mm)	
B. suillus	51	8.31	12.52	10.39 ± 0.97	10.31
H. argenteocinereus	32	4.66	7.49	6.38 ± 0.61	6.42
G. capensis	28	2.58	7.58	5.97 ± 1.16	6.13
F. mechowii	12	6.25	8.18	7.59 ± 0.58	7.76
F. damarensis	23	3.83	6.69	5.43 ± 0.87	5.50
C. hottentotus	53	3.51	5.36	4.48 ± 0.49	4.47
H. glaber	63	2.81	3.97	3.41 ± 0.22	3.42
Total	262				

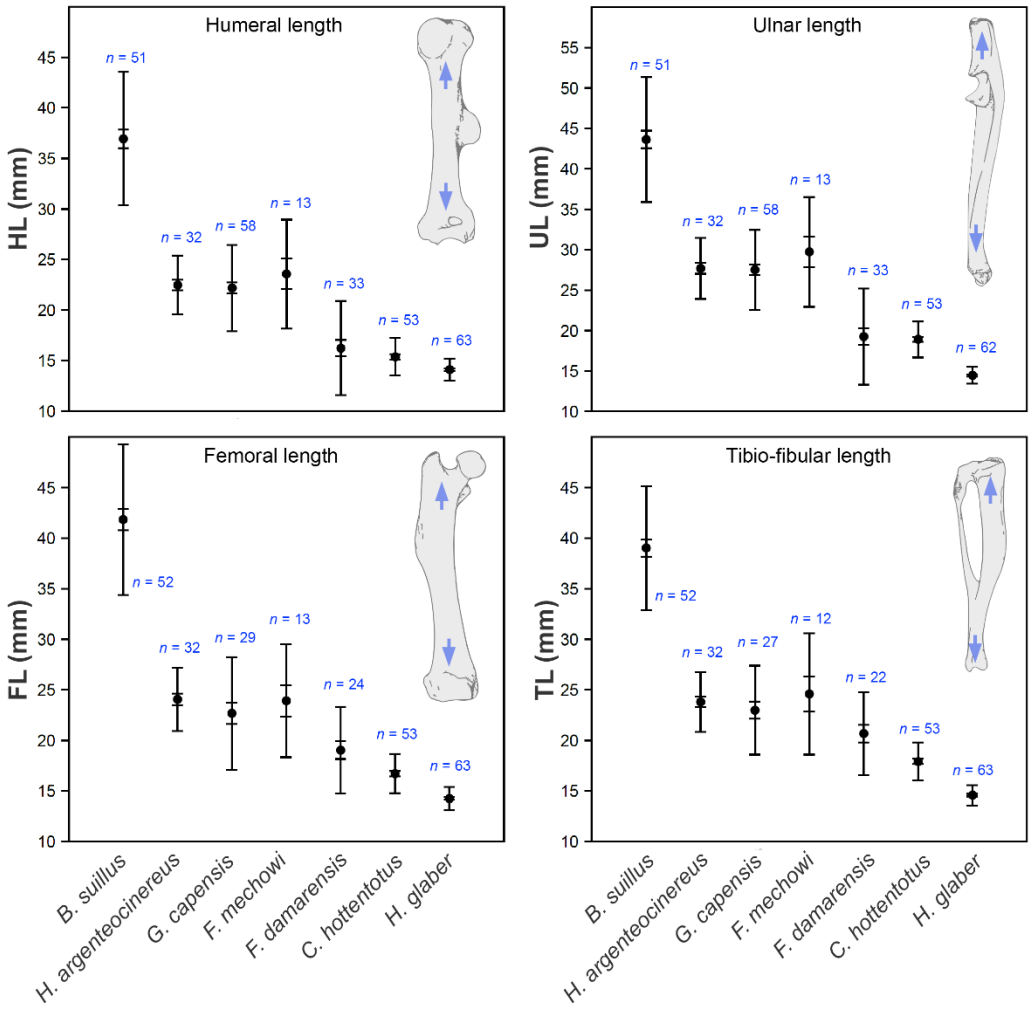

FIGURE 5.2. Boxplots of bone lengths (fore- and hindlimb bones) showing mean values for all specimens and species analyzed in this study. Associated descriptive data is presented in Table 1. *Legend*: mean (central black dot); standard error (shorter whiskers); standard deviation (longer whiskers). Arrows within bones indicate direction of endochondral ossification. See taxonomic abbreviations in Table 5.1.

TABLE 5.5. Results of the regressions between body length (BL) and body mass (BM) for all species of bathyergids analyzed here. Growth trend is indicated in parenthesis next to the slope: isometry *(I)*, negative *(-)* and positive *(+)* allometry. See taxonomic abbreviations in Table 5.1.

Species	Elevation	CI		Slope		CI		r^2	*P*-value
B. suillus (*N* = 50)	1.587	1.498	1.677	0.307	*(I)*	0.277	0.340	0.877	0.107
H. argenteocinereus (*N* = 29)	1.382	1.205	1.559	0.358	*(I)*	0.286	0.448	0.669	0.529
G. capensis (*N* = 49)	1.422	1.280	1.564	0.364	*(I)*	0.305	0.434	0.637	0.318
F. mechowii (*N* = 12)	1.592	1.510	1.674	0.272	*(-)*	0.238	0.311	0.964	**0.006**
F. damarensis (*N* = 8)	1.548	1.357	1.740	0.320	*(I)*	0.224	0.459	0.866	0.801
C. hottentotus (*N* = 51)	1.446	1.364	1.528	0.337	*(I)*	0.294	0.386	0.774	0.869
H. glaber (*N* = 50)	1.514	1.422	1.607	0.352	*(I)*	0.295	0.420	0.626	0.537

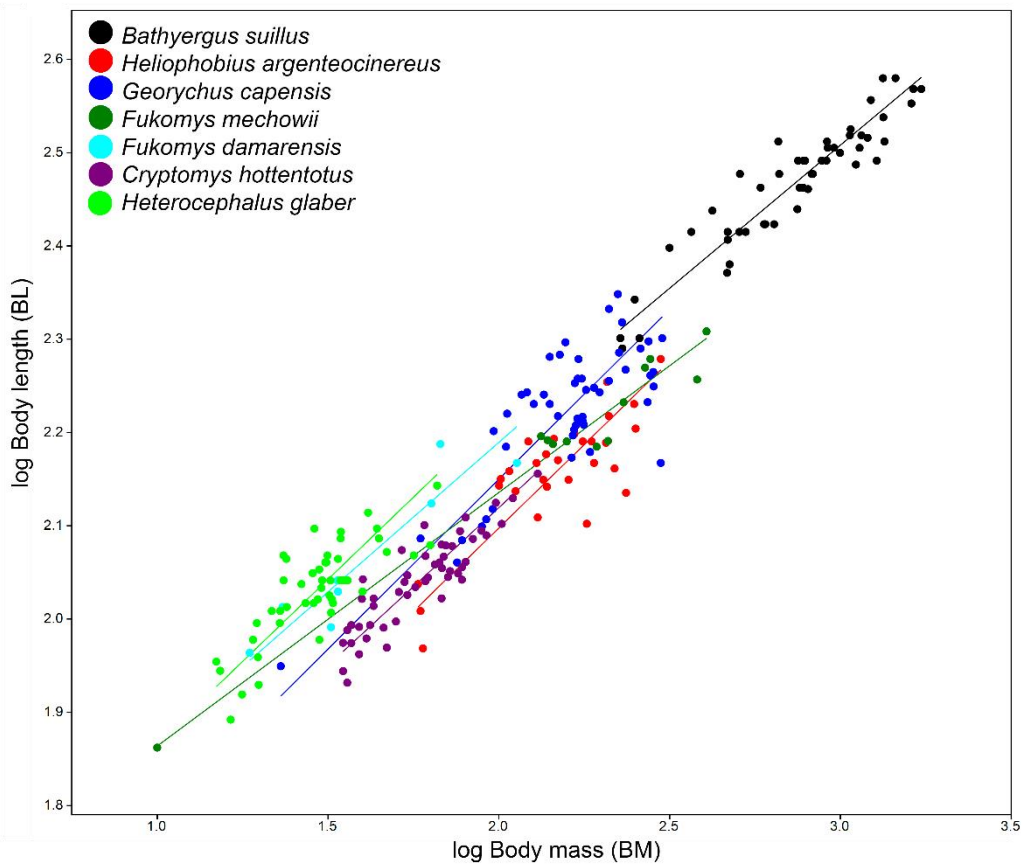

FIGURE 5.3. Bivariate scatterplot of regressions for proxies of body size; body length (BL) and body mass (BM). All species showed isometry, except *F. mechowii*, which showed negative allometry (Table 5.5).

5.3.1 Endochondral Ossification

Here, bone lengths are regressed against BM and BL. The coefficient of correlation (r^2) is used to estimate the variability of the ossification module with respect to the proxies of body size, while the regression analysis is performed to determine the general growth trend between the ossification module and the proxy of body size. In general, all the regressions using both proxies of body size showed the same pattern, i.e., the growth pattern of bone elongation was more variable when assessed against BL than for BM. Pairwise comparisons were performed and all of them showed significant differences (inequal slopes) among bathyergids, although these differences were principally due to the distinct growth trends of *H. glaber* (and sometimes *G. capensis*) (Appendix 5.2-5.3). Same procedures were used for the periosteal module and (epi)condylar growth in sections 5.3.2 and 5.3.3.

5.3.1.1 Endochondral Module: Forelimb

Regressions resulted in high coefficients of determination for almost all species (r^2 = 0.70 or higher) except for *H. argenteocinereus* and *H. glaber* (Table 5.6). Coefficients of determination were similar between BM and BL regressions, although quite variable among species. Two main trends were observed in the growth patterns: i) the pattern of bone elongation was more variable when

assessed against BL, and ii) *H. glaber* showed mostly negative allometry, which differs from other bathyergids. Test for equality of slopes showed significant differences (p<0.001) among species, although the pairwise comparisons showed that most of such significant differences were explained by *H. glaber* (and sometimes *G. capensis*) having lower slopes (Appendix 5.2).

5.3.1.2 Endochondral Module: Hindlimb

Regressions resulted in high determination coefficients for almost all species (r^2 = 0.70 or higher) except for *H. argenteocinereus*, *C. hottentotus* and *H. glaber*. In general, these values were slightly higher as compared to the forelimb (Table 5.6). Within *C. hottentotus,* the lowest value was found in the tibial length (TL) against BL (r^2 = 0.698; Table 5.7). Like in the forelimb, coefficients of determination were similar between BM and BL regressions, and regarding to growth patterns, bone elongation was more variable when assessed against BL. *H. glaber* showed mostly negative allometry, differing from most bathyergids. Test for equality of slopes showed significant differences (p<0.001) among species, although the pairwise comparisons showed that most of such significant differences were explained by *H. glaber* (and sometimes *F. mechowii*) having lower slopes (Appendix 5.3).

TABLE 5.6. Regressions of the endochondral modules of the forelimb showing coefficients of determination (r^2), allometric coefficients (slope), growth pattern and elevation. Bone traits assessed against body mass (BM) in the left and body length (BL) in the right. *Abbreviations*: humeral length (HL); ulnar length (UL). See additional abbreviations in Tables 5.1 and 5.5.

BM vs	Species	Elevation	CI		Slope		CI		r^2	*P*-value
	B. suillus	0.586	0.500	0.672	0.341	*(I)*	0.312	0.372	0.908	0.603
	H. argenteocinereus	0.556	0.348	0.764	0.363	*(I)*	0.280	0.470	0.526	0.507
	G. capensis	0.661	0.551	0.772	0.320	*(I)*	0.273	0.374	0.714	0.596
HL	*F. mechowii*	0.493	0.394	0.593	0.385	*(+)*	0.343	0.431	0.971	0.018
	F. damarensis	0.629	0.581	0.678	0.328	*(I)*	0.301	0.356	0.947	0.686
	C. hottentotus	0.552	0.480	0.624	0.358	*(I)*	0.320	0.401	0.844	0.207
	H. glaber	0.824	0.774	0.873	0.222	*(-)*	0.191	0.258	0.719	<0.001
	B. suillus	0.681	0.575	0.788	0.333	*(I)*	0.298	0.372	0.853	0.992
	H. argenteocinereus	0.596	0.377	0.815	0.386	*(I)*	0.299	0.499	0.533	0.254
	G. capensis	0.802	0.705	0.900	0.297	*(I)*	0.256	0.344	0.742	0.120
UL	*F. mechowii*	0.594	0.484	0.704	0.385	*(+)*	0.339	0.436	0.964	0.028
	F. damarensis	0.658	0.613	0.704	0.353	*(I)*	0.328	0.379	0.960	0.126
	C. hottentotus	0.650	0.571	0.728	0.354	*(I)*	0.313	0.401	0.810	0.333
	H. glaber	0.852	0.791	0.913	0.211	*(-)*	0.173	0.256	0.541	<0.001
	B. suillus	0.944	0.852	1.036	0.334	*(I)*	0.304	0.368	0.891	0.950
	H. argenteocinereus	0.885	0.675	1.095	0.372	*(I)*	0.288	0.480	0.539	0.387
	G. capensis	1.044	0.943	1.145	0.304	*(I)*	0.262	0.354	0.740	0.230
HL+UL	*F. mechowii*	0.848	0.743	0.953	0.385	*(+)*	0.341	0.434	0.967	0.023
	F. damarensis	0.945	0.900	0.991	0.341	*(I)*	0.316	0.368	0.957	0.559
	C. hottentotus	0.910	0.838	0.982	0.353	*(I)*	0.315	0.396	0.839	0.318
	H. glaber	1.148	1.096	1.200	0.210	*(-)*	0.178	0.248	0.667	<0.001

BL vs	Species	Elevation	CI		Slope		CI		r^2	*P*-value
	B. suillus	-1.121	-1.342	-0.900	1.088	*(+)*	1.002	1.182	0.918	0.044
	H. argenteocinereus	-0.902	-1.433	-0.370	1.041	*(I)*	0.824	1.316	0.627	0.728
	G. capensis	-0.351	-0.546	-0.157	0.773	*(-)*	0.690	0.867	0.830	<0.001
HL	*F. mechowii*	-1.757	-2.270	-1.244	1.414	*(+)*	1.200	1.666	0.945	0.001
	F. damarensis	-1.338	-2.204	-0.472	1.213	*(I)*	0.864	1.703	0.880	0.218
	C. hottentotus	-0.935	-1.214	-0.656	1.039	*(I)*	0.911	1.185	0.781	0.560
	H. glaber	-0.190	-0.406	0.026	0.659	*(-)*	0.561	0.774	0.610	<0.001
	B. suillus	-1.000	-1.290	-0.711	1.069	*(I)*	0.958	1.193	0.853	0.228
	H. argenteocinereus	-0.950	-1.508	-0.392	1.106	*(I)*	0.877	1.394	0.635	0.385
	G. capensis	-0.278	-0.476	-0.080	0.780	*(-)*	0.695	0.875	0.831	<0.001
UL	*F. mechowii*	-1.663	-2.202	-1.124	1.418	*(+)*	1.193	1.684	0.940	0.001
	F. damarensis	-1.307	-2.291	-0.324	1.232	*(I)*	0.845	1.797	0.851	0.231
	C. hottentotus	-0.820	-1.123	-0.518	1.027	*(I)*	0.889	1.186	0.736	0.712
	H. glaber	-0.102	-0.325	0.121	0.621	*(-)*	0.521	0.740	0.540	<0.001
	B. suillus	-0.739	-0.986	-0.492	1.071	*(I)*	0.975	1.176	0.894	0.148
	H. argenteocinereus	-0.611	-1.147	-0.075	1.068	*(I)*	0.849	1.345	0.640	0.565
	G. capensis	-0.011	-0.206	0.183	0.777	*(-)*	0.694	0.871	0.838	<0.001
HL+UL	*F. mechowii*	-1.406	-1.933	-0.880	1.416	*(+)*	1.196	1.675	0.942	0.001
	F. damarensis	-1.013	-1.923	-0.104	1.219	*(I)*	0.856	1.737	0.869	0.225
	C. hottentotus	-0.557	-0.839	-0.274	1.024	*(I)*	0.895	1.172	0.768	0.722
	H. glaber	0.189	-0.018	0.396	0.623	*(-)*	0.530	0.734	0.605	<0.001

TABLE 5.7. Regressions of the endochondral modules of the hindlimb showing coefficients of determination (r^2), allometric coefficients (slope), growth pattern and elevation. Bone traits assessed against body mass (BM) in the left and body length (BL) in the right. *Abbreviations*: femoral length (FL); tibial length (TL). See additional abbreviations in Tables 5.1 and 5.5.

BM vs	Species	Elevation	CI		Slope		CI		r^2	*P*-value
	B. suillus	0.669	0.588	0.750	0.332	*(I)*	0.305	0.361	0.912	0.922
	H. argenteocinereus	0.551	0.314	0.788	0.381	*(I)*	0.288	0.505	0.545	0.336
	G. capensis	0.782	0.677	0.887	0.284	*(I)*	0.239	0.338	0.855	0.068
FL	*F. mechowii*	0.470	0.349	0.591	0.397	*(I)*	0.348	0.454	0.959	0.151
	F. damarensis	0.645	0.572	0.717	0.332	*(I)*	0.296	0.373	0.932	0.954
	C. hottentotus	0.602	0.530	0.674	0.350	*(I)*	0.312	0.393	0.838	0.391
	H. glaber	0.798	0.742	0.854	0.243	*(-)*	0.208	0.284	0.704	<0.001
	B. suillus	0.751	0.670	0.832	0.293	*(-)*	0.266	0.323	0.888	0.010
	H. argenteocinereus	0.566	0.317	0.815	0.372	*(I)*	0.275	0.503	0.470	0.471
	G. capensis	0.825	0.727	0.922	0.260	*(-)*	0.218	0.309	0.851	0.007
TL	*F. mechowii*	0.471	0.323	0.620	0.404	*(+)*	0.344	0.475	0.947	0.024
	F. damarensis	0.665	0.572	0.757	0.333	*(I)*	0.289	0.384	0.906	0.999
	C. hottentotus	0.705	0.631	0.779	0.309	*(I)*	0.270	0.354	0.779	0.272
	H. glaber	0.876	0.826	0.927	0.197	*(-)*	0.165	0.234	0.632	<0.001
	B. suillus	1.013	0.934	1.091	0.312	*(I)*	0.286	0.340	0.907	0.134
	H. argenteocinereus	0.869	0.631	1.107	0.372	*(I)*	0.279	0.497	0.517	0.444
	G. capensis	1.106	1.006	1.205	0.271	*(-)*	0.229	0.322	0.857	0.020
FL+TL	*F. mechowii*	0.771	0.636	0.905	0.402	*(I)*	0.347	0.466	0.956	0.496
	F. damarensis	0.964	0.875	1.053	0.329	*(I)*	0.286	0.378	0.912	0.838
	C. hottentotus	0.962	0.893	1.032	0.326	*(I)*	0.289	0.367	0.826	0.697
	H. glaber	1.144	1.094	1.194	0.216	*(-)*	0.184	0.253	0.694	<0.001

BL vs	Species	Elevation	CI		Slope		CI		r^2	*P*-value
	B. suillus	-1.049	-1.280	-0.818	1.082	*(I)*	0.992	1.180	0.907	0.074
	H. argenteocinereus	-0.847	-1.383	-0.310	1.030	*(I)*	0.811	1.307	0.612	0.807
	G. capensis	-0.622	-0.748	-0.495	0.924	*(-)*	0.866	0.985	0.975	0.018
FL	*F. mechowii*	-1.849	-2.406	-1.292	1.458	*(+)*	1.226	1.733	0.939	0.001
	F. damarensis	-1.048	-2.037	-0.058	1.081	*(I)*	0.701	1.666	0.849	0.672
	C. hottentotus	-0.834	-1.095	-0.573	1.007	*(I)*	0.887	1.143	0.796	0.908
	H. glaber	-0.282	-0.499	-0.065	0.706	*(-)*	0.607	0.821	0.657	<0.001
	B. suillus	-0.726	-0.946	-0.506	0.939	*(I)*	0.854	1.033	0.887	0.192
	H. argenteocinereus	-0.782	-1.321	-0.243	0.998	*(I)*	0.779	1.278	0.583	0.988
	G. capensis	-0.452	-0.631	-0.273	0.841	*(-)*	0.762	0.928	0.947	0.001
TL	*F. mechowii*	-1.924	-2.602	-1.246	1.501	*(+)*	1.223	1.842	0.925	0.001
	F. damarensis	-0.887	-2.199	0.425	1.017	*(I)*	0.566	1.830	0.886	0.936
	C. hottentotus	-0.581	-0.864	-0.298	0.898	*(I)*	0.770	1.047	0.698	0.168
	H. glaber	-0.009	-0.218	0.200	0.577	*(-)*	0.483	0.689	0.523	<0.001
	B. suillus	-0.581	-0.799	-0.363	1.009	*(I)*	0.924	1.101	0.904	0.846
	H. argenteocinereus	-0.482	-1.003	0.038	0.999	*(I)*	0.787	1.269	0.612	0.997
	G. capensis	-0.181	-0.340	-0.023	0.857	*(-)*	0.786	0.934	0.960	0.001
FL+TL	*F. mechowii*	-1.607	-2.221	-0.994	1.490	*(+)*	1.237	1.796	0.938	0.001
	F. damarensis	-0.397	-1.596	0.802	0.922	*(I)*	0.510	1.666	0.884	0.707
	C. hottentotus	-0.381	-0.642	-0.119	0.940	*(I)*	0.821	1.077	0.764	0.369
	H. glaber	0.178	-0.029	0.384	0.631	*(-)*	0.537	0.740	0.612	<0.001

5.3.1.3 Intralimb Comparisons

Forelimb (UL vs HL). All regressions showed high coefficients of determination (r^2 = 0.80 or higher), although again *H. glaber* showed the lowest scores (Table 5.8). All species showed isometric growth, except *F. damarensis* which showed positive allometry of the ulna (i.e. ulna grows relatively more than the humerus). Test for equality of slopes showed significant differences (p = 0.02) among species, although the pairwise comparisons showed that such differences were explained by differences between *Fukomys* spp, where *F. damarensis* showed higher slopes (Table 5.8; Appendix 5.4). Although almost all species showed isometric growth between the humerus and ulna, the ulna was always longer than the humerus, and only *H. glaber* showed similar lengths for those bones (Table 5.1; Fig. 5.2). Although they have symmetric limb bone proportions (Table 5.1; Fig. 5.2; also see Ch. 4), *H. glaber* showed the lowest coefficients of determination among species (Table 5.8).

Hindlimb (TL vs FL). All regressions showed high determination coefficients (r^2 = 0.85 or higher). Four species showed isometric growth, except *B. suillus*, *C. hottentotus* and *H. glaber* that showed negative allometry (i.e. tibia grows relatively less than the femur) (Table 5.8). Test for equality of slopes showed significant differences (p<0.001) among species, and the pairwise comparisons showed that such differences were explained by *H. glaber* having significantly lower slopes as compared to *B. suillus* and *Fukomys* spp. (Table 5.8; Appendix 5.4). In the hindlimb of bathyergids, the tibia was always shorter than the femur, although *H. glaber* again showed similar lengths for these bones (Table 5.1; Fig. 5.2).

TABLE 5.8. Intralimb regressions showing independent comparisons of the endochondral module for fore- and hindlimbs (i.e. zeugopodial elements regressed against stylopodial elements). See abbreviations in Tables 5.1 and 5.5.

Intralimb	Species	Elevation	CI		Slope		CI		r^2	*P*-value
UL vs HL	*B. suillus*	0.100	0.003	0.198	0.982	(I)	0.922	1.046	0.951	0.570
	H. argenteocinereus	0.005	-0.130	0.141	1.063	(I)	0.967	1.168	0.936	0.196
	G. capensis	0.078	0.008	0.148	1.008	(I)	0.957	1.061	0.964	0.763
	F. mechowii	0.100	0.067	0.134	1.001	(I)	0.976	1.025	0.999	0.961
	F. damarensis	-0.019	-0.066	0.029	1.076	(+)	1.037	1.116	0.990	<0.001
	C. hottentotus	0.104	0.021	0.187	0.988	(I)	0.921	1.061	0.937	0.740
	H. glaber	0.087	-0.033	0.207	0.934	(I)	0.835	1.044	0.813	0.225
TL vs FL	*B. suillus*	0.184	0.116	0.252	0.868	(-)	0.827	0.911	0.971	<0.001
	H. argenteocinereus	0.035	-0.124	0.195	0.971	(I)	0.862	1.094	0.898	0.619
	G. capensis	0.046	-0.026	0.118	0.960	(I)	0.908	1.014	0.982	0.135
	F. mechowii	0.000	-0.077	0.077	1.011	(I)	0.956	1.069	0.994	0.682
	F. damarensis	-0.008	-0.097	0.082	1.023	(I)	0.955	1.095	0.979	0.501
	C. hottentotus	0.163	0.073	0.253	0.892	(-)	0.821	0.968	0.914	0.007
	H. glaber	0.203	0.118	0.289	0.833	(-)	0.762	0.910	0.880	<0.001

5.3.1.4 Interlimb Comparisons

Stylopod (HL vs FL). In general, the humerus is the shortest limb bone among all species, except in *G. capensis*, *F. mechowii* and *H. glaber* which showed similar lengths to the femur (Table 5.1; Fig. 5.2). Regressions between stylopodial

serial homologous (humerus and femur) showed high coefficients of determination (r^2 = 0.90 or higher). These were even higher than for the intralimb comparisons. Isometry was the main trend, although negative allometry of the humerus was also observed for *G. capensis*, *F. damarensis* and *H. glaber* (i.e. the humerus grew considerably less than the femur) (Table 5.9). Despite of this, test for equality of slopes and pairwise comparisons showed equal slopes for all species (Table 5.9; Appendix 5.4).

Zeugopod (UL vs TL). In general, the ulna is usually the longest bone of all limb bones, except in *F. damarensis* and *H. glaber,* where ulna (and tibia) showed similar lengths (Table 5.1; Fig. 5.2). The zeugopodial serial homologous showed slightly lower coefficients of determination (r^2 = 0.80 or higher) as compared to stylopodial elements but were similar to the intralimb comparisons (Table 5.9). Thus, zeugopodial elements seem relatively less correlated to each other than stylopodial elements. Isometry was predominant, although *B. suillus* and *C. hottentotus* showed positive allometry of the ulna (i.e. the ulna grew considerably more than the tibia). The test for equality of slopes showed significant differences (p<0.001) and pairwise comparisons showed differences among *B. suillus* and *C. hottentotus*, but also for *Fukomys* (Table 5.9; Appendix 5.4).

Forelimb versus Hindlimb (HL+UL vs FL+TL). In terms of whole limb growth, regressions also showed high determination coefficients (r^2 = 0.90 or higher), and mostly isometric growth trends, although *B. suillus* and *C. hottentotus* showed positive allometry, and *F. damarensis* showed negative allometry (Table 5.9). The test for equality of slopes showed significant differences (p<0.001) and pairwise comparisons also showed differences among *B. suillus* and *C. hottentotus*, but also for *Fukomys* (Table 5.9; Appendix 5.4).

TABLE 5.9. Interlimb regressions showing independent comparisons of the endochondral module for stylopodial and zeugopodial elements (i.e. forelimb elements regressed against hindlimb elements). See abbreviations in Tables 5.1 and 5.5.

Interlimb	Species	Elevation	CI		Slope		CI		r^2	*P*-value
HL vs FL	*B. suillus*	-0.075	-0.140	-0.010	1.011	(I)	0.972	1.052	0.981	0.574
	H. argenteocinereus	-0.045	-0.141	0.050	1.012	(I)	0.945	1.083	0.966	0.735
	G. capensis	0.087	-0.001	0.175	0.914	(-)	0.851	0.982	0.968	0.016
	F. mechowii	0.039	-0.026	0.103	0.968	(I)	0.921	1.016	0.995	0.169
	F. damarensis	0.044	-0.020	0.107	0.946	(-)	0.897	0.997	0.986	0.038
	C. hottentotus	-0.075	-0.146	-0.003	1.032	(I)	0.975	1.092	0.959	0.275
	H. glaber	0.071	0.005	0.138	0.935	(-)	0.879	0.994	0.942	0.033
UL vs TL	*B. suillus*	-0.192	-0.324	-0.059	1.149	(+)	1.068	1.235	0.936	<0.001
	H. argenteocinereus	-0.082	-0.313	0.149	1.107	(I)	0.952	1.288	0.834	0.180
	G. capensis	0.000	-0.088	0.088	1.048	(I)	0.985	1.115	0.978	0.129
	F. mechowii	0.069	-0.010	0.147	0.972	(I)	0.914	1.034	0.983	0.346
	F. damarensis	0.140	0.067	0.213	0.957	(I)	0.906	1.011	0.994	0.106
	C. hottentotus	-0.156	-0.262	-0.050	1.144	(+)	1.062	1.232	0.930	0.001
	H. glaber	-0.059	-0.190	0.071	1.048	(I)	0.942	1.166	0.828	0.382
HLUL x FLTL	*B. suillus*	-0.137	-0.228	-0.046	1.069	(+)	1.023	1.118	0.976	0.004
	H. argenteocinereus	-0.094	-0.263	0.076	1.068	(I)	0.971	1.174	0.935	0.168
	G. capensis	-0.031	-0.113	0.051	1.030	(I)	0.982	1.080	0.987	0.219
	F. mechowii	0.103	0.034	0.173	0.962	(I)	0.921	1.005	0.996	0.075
	F. damarensis	0.080	0.012	0.147	0.953	(-)	0.912	0.997	0.991	0.036
	C. hottentotus	-0.142	-0.222	-0.062	1.090	(+)	1.039	1.143	0.971	0.001
	H. glaber	0.030	-0.065	0.125	0.977	(I)	0.914	1.044	0.934	0.486

5.3.2 Periosteal Ossification

5.3.2.1 Periosteal Module: Forelimb

Coefficients of determination for periosteal modules were highly variable, ranging from very low values in *G. capensis* (0.135) to high values in *F. damarensis* (0.929) (Table 5.10). In general, this module was much less correlated to body size as compared to the endochondral modules of the same limb (Table 5.6). The coefficients of determination for BL and BM were relatively similar. Periosteal modules also showed variable growth patterns, although the pairwise comparisons showed less significant differences for those patterns (Table 5.10). Contrary to the endochondral module where most interspecific differences were associated to *H. glaber*, the differences of the periosteal module were associated to different species. Thus, *H. glaber* did not differ considerably in periosteal growth patterns as compared to other species. The variance observed in the periosteal module contrasts considerably with the variance of the endochondral module of the forelimb. Test for equality of slopes showed significant differences (p<0.001) among species, and the pairwise comparisons showed some differences between species, not associated uniquely to *H. glaber* (Appendix 5.5-5.6).

5.3.2.2 Periosteal module: hindlimb

Periosteal ossification in the hindlimb also showed highly variable coefficients of determination, ranging from extremely low values in *G. capensis* (0.012) to high

values in *F. damarensis* (0.928) (Table 5.11). The coefficients of determination for the BL were slightly lower than for BM, thus indicating the higher variability of the hindlimb bones. The variance observed in the periosteal module contrasts considerably with the variance of the endochondral module of the hindlimb (Table 5.1). Test for equality of slopes showed significant differences (p<0.001) among species, and the pairwise comparisons showed some differences between species, again not associated uniquely to *H. glaber* (Appendix 5.7-5.8)

5.3.2.3 Intralimb Comparisons

(TDU vs TDH). Coefficients of determination for TDU and TDH ranged from 0.266 (*H. argenteocinereus*) and 0.923 (*F. damarensis*) (Table 5.12). Test for equality of slopes showed significant differences (p<0.001) among species, and the pairwise comparisons showed that almost all species showed equal slopes, except *F. damarensis* which showed higher slopes as compared to *G. capensis* and *C. hottentotus* (Table 5.12; Appendix 5.9).

(APDU vs APDH). Coefficients of determination for APDU and APDH were higher as compared to mediolateral diameters in humerus and ulna and ranged from 0.418 (*H. glaber*) and 0.932 (*F. damarensis*) (Table 5.12). The APDU showed always isometry or positive allometry respect to APDH, i.e. the anteroposterior diameter of the ulna grows more or equally to the anteroposterior diameter of the humerus. However, pairwise comparisons showed that all species showed equal slopes (Appendix 5.9).

(TDT vs TDF). Coefficients of determination for TDT and TDF ranged from 0.441 (*H. argenteocinereus*) and 0.916 (*F. damarensis*) (Table 5.12). All species showed isometry, except *G. capensis* that showed negative allometry. However, pairwise comparisons showed that all species have equal slopes (Appendix 5.9).

(APDT vs APDF). Coefficients of determination for APDT and APDF were relatively lower as compared to mediolateral diameters of the femur and tibia-fibula, and ranged from 0.309 (*H. argenteocinereus*) and 0.798 (*G. capensis*) (Table 5.12). This indicates more variation in the anteroposterior periosteal module of the hindlimb as compared to the mediolateral diameter. The APDT showed mostly positive allometry and isometry respect to APDF, which is like the observations of the ulna and humerus. This indicates that the anteroposterior diameter of the tibia-fibula grew more or equally to the anteroposterior diameter of the femur. Only *C. hottentotus* showed a statistically significant lower slope than *H. argenteocinereus* and *B. suillus*. Pairwise comparisons showed that almost all species showed equal slopes, except *C. hottentotus* that showed the lowest slopes for this trait (Appendix 5.9).

TABLE 5.10. Regressions of the periosteal module of the forelimb showing coefficients of determination (r^2), allometric coefficients (slope), growth pattern and elevation. Bone traits assessed against body mass (BM) in the left and body length (BL) in the right. *Abbreviations*: humeral length (HL); ulnar length (UL). See additional abbreviations in Tables 5.1, 5.2, 5.3 and 5.5.

BM vs	Species	Elevation	CI		Slope		CI		r^2	*P*-value
TDH	*B. suillus*	-0.292	-0.427	-0.158	0.330	(I)	0.287	0.380	0.764	0.899
	H. argenteocinereus	-0.371	-0.631	-0.110	0.388	(I)	0.287	0.525	0.348	0.314
	G. capensis	-0.288	-0.429	-0.147	0.329	(I)	0.271	0.399	0.561	0.893
	F. mechowii	-0.123	-0.272	0.026	0.256	(-)	0.199	0.330	0.851	0.043
	F. damarensis	-0.254	-0.315	-0.192	0.295	(-)	0.262	0.331	0.896	0.041
	C. hottentotus	-0.721	-0.903	-0.538	0.551	(+)	0.457	0.663	0.576	<0.001
	H. glaber	-0.194	-0.309	-0.078	0.300	(I)	0.232	0.388	0.179	0.423
APDH	*B. suillus*	-0.223	-0.369	-0.077	0.302	(I)	0.255	0.356	0.664	0.236
	H. argenteocinereus	-0.553	-0.820	-0.285	0.434	(I)	0.328	0.573	0.448	0.063
	G. capensis	-0.459	-0.621	-0.297	0.389	(I)	0.323	0.470	0.585	0.104
	F. mechowii	-0.320	-0.529	-0.111	0.329	(I)	0.250	0.434	0.823	0.924
	F. damarensis	-0.336	-0.392	-0.281	0.324	(I)	0.294	0.357	0.929	0.537
	C. hottentotus	-0.800	-1.003	-0.598	0.568	(+)	0.465	0.693	0.510	<0.001
	H. glaber	-0.394	-0.496	-0.292	0.299	(I)	0.238	0.376	0.347	0.352
TDU	*B. suillus*	-0.556	-0.723	-0.390	0.325	(I)	0.272	0.388	0.624	0.779
	H. argenteocinereus	-0.717	-1.016	-0.418	0.386	(I)	0.273	0.546	0.135	0.400
	G. capensis	-0.525	-0.651	-0.399	0.327	(I)	0.275	0.389	0.643	0.826
	F. mechowii	-0.447	-0.599	-0.296	0.284	(I)	0.225	0.358	0.875	0.160
	F. damarensis	-0.613	-0.681	-0.544	0.340	(I)	0.303	0.381	0.902	0.726
	C. hottentotus	-0.886	-1.036	-0.736	0.479	(+)	0.402	0.571	0.623	<0.001
	H. glaber	-0.502	-0.598	-0.405	0.267	(I)	0.210	0.340	0.278	0.072
APDU	*B. suillus*	-0.541	-0.672	-0.410	0.387	(+)	0.345	0.436	0.836	0.013
	H. argenteocinereus	-0.524	-0.780	-0.268	0.440	(+)	0.339	0.572	0.511	0.038
	G. capensis	-0.525	-0.683	-0.368	0.409	(+)	0.343	0.486	0.645	0.022
	F. mechowii	-0.293	-0.418	-0.169	0.306	(I)	0.256	0.366	0.928	0.318
	F. damarensis	-0.501	-0.570	-0.432	0.388	(+)	0.351	0.429	0.924	0.004
	C. hottentotus	-0.807	-0.952	-0.662	0.548	(+)	0.473	0.636	0.730	<0.001
	H. glaber	-0.262	-0.331	-0.192	0.288	(I)	0.245	0.339	0.676	0.079

BL vs	Species	Elevation	CI		Slope		CI		r^2	*P*-value
TDH	*B. suillus*	-1.994	-2.295	-1.693	1.074	(I)	0.959	1.202	0.843	0.215
	H. argenteocinereus	-1.903	-2.608	-1.199	1.103	(I)	0.824	1.476	0.416	0.504
	G. capensis	-1.416	-1.629	-1.203	0.834	(-)	0.743	0.937	0.825	0.003
	F. mechowii	-1.633	-2.366	-0.901	0.948	(I)	0.671	1.338	0.751	0.740
	F. damarensis	-1.336	-2.647	-0.026	0.756	(I)	0.353	1.621	0.295	0.440
	C. hottentotus	-3.065	-3.641	-2.488	1.625	(+)	1.367	1.932	0.617	<0.001
	H. glaber	-1.568	-2.000	-1.135	0.894	(I)	0.706	1.132	0.150	0.348
APDH	*B. suillus*	-1.731	-2.097	-1.365	0.962	(I)	0.825	1.122	0.710	0.615
	H. argenteocinereus	-2.236	-2.999	-1.472	1.215	(I)	0.912	1.619	0.435	0.178
	G. capensis	-1.167	-1.460	-0.874	0.708	(-)	0.587	0.854	0.541	<0.001
	F. mechowii	-2.269	-3.180	-1.358	1.222	(I)	0.876	1.705	0.768	0.214
	F. damarensis	-1.682	-2.500	-0.865	0.911	(I)	0.597	1.389	0.811	0.617
	C. hottentotus	-3.172	-3.851	-2.493	1.653	(+)	1.354	2.019	0.487	<0.001
	H. glaber	-1.643	-2.046	-1.240	0.833	(I)	0.658	1.054	0.150	0.127
TDU	*B. suillus*	-2.112	-2.527	-1.698	1.009	(I)	0.855	1.191	0.663	0.913
	H. argenteocinereus	-2.232	-3.056	-1.408	1.093	(I)	0.776	1.539	0.188	0.604
	G. capensis	-1.250	-1.476	-1.025	0.653	(-)	0.559	0.764	0.688	<0.001
	F. mechowii	-2.127	-2.789	-1.465	1.054	(I)	0.795	1.397	0.836	0.692
	F. damarensis	-1.985	-3.480	-0.490	0.930	(I)	0.455	1.902	0.394	0.828
	C. hottentotus	-2.865	-3.329	-2.401	1.385	(+)	1.176	1.631	0.659	<0.001
	H. glaber	-1.684	-2.071	-1.297	0.775	(-)	0.608	0.988	0.097	0.040
APDU	*B. suillus*	-2.509	-2.799	-2.219	1.248	(+)	1.136	1.371	0.892	<0.001
	H. argenteocinereus	-2.288	-2.939	-1.637	1.261	(I)	0.996	1.598	0.619	0.054
	G. capensis	-1.532	-1.818	-1.247	0.860	(I)	0.740	1.000	0.712	0.050
	F. mechowii	-2.074	-2.590	-1.558	1.120	(I)	0.910	1.379	0.912	0.254
	F. damarensis	-2.113	-3.169	-1.057	1.094	(I)	0.697	1.718	0.781	0.654
	C. hottentotus	-3.137	-3.643	-2.630	1.616	(+)	1.386	1.883	0.701	<0.001
	H. glaber	-1.628	-1.975	-1.282	0.880	(I)	0.726	1.067	0.438	0.191

TABLE 5.11. Regressions of the periosteal module of the hindlimb showing coefficients of determination (r^2), allometric coefficients (slope), growth pattern and elevation. Bone traits assessed against body mass (BM) in the left and body length (BL) in the right. *Abbreviations*: humeral length (HL); ulnar length (UL). See additional abbreviations in Tables 5.1, 5.2, 5.3 and 5.5.

BM vs	Species	Elevation	CI		Slope		CI		r^2	*P*-value
TDF	*B. suillus*	-0.420	-0.563	-0.277	0.387	(+)	0.341	0.440	0.798	0.023
	H. argenteocinereus	-0.298	-0.549	-0.046	0.355	(I)	0.258	0.488	0.408	0.692
	G. capensis	-0.485	-0.710	-0.259	0.457	(+)	0.364	0.574	0.744	0.008
	F. mechowii	-0.151	-0.345	0.042	0.289	(I)	0.216	0.387	0.802	0.310
	F. damarensis	-0.226	-0.342	-0.110	0.310	(I)	0.255	0.376	0.803	0.444
	C. hottentotus	-0.882	-1.108	-0.657	0.668	(+)	0.553	0.807	0.562	<0.001
	H. glaber	-0.267	-0.377	-0.158	0.313	(I)	0.247	0.396	0.281	0.597
APDF	*B. suillus*	-0.340	-0.478	-0.203	0.303	(I)	0.259	0.355	0.697	0.233
	H. argenteocinereus	-0.319	-0.535	-0.103	0.259	(I)	0.179	0.376	0.182	0.181
	G. capensis	-0.254	-0.385	-0.124	0.270	(I)	0.216	0.338	0.754	0.065
	F. mechowii	-0.302	-0.495	-0.110	0.285	(I)	0.212	0.382	0.799	0.268
	F. damarensis	-0.306	-0.429	-0.184	0.302	(I)	0.244	0.373	0.767	0.347
	C. hottentotus	-0.971	-1.197	-0.745	0.633	(+)	0.518	0.773	0.508	<0.001
	H. glaber	-0.427	-0.521	-0.334	0.286	(I)	0.229	0.356	0.372	0.169
TDT	*B. suillus*	-0.482	-0.603	-0.361	0.364	(I)	0.324	0.408	0.837	0.138
	H. argenteocinereus	-0.571	-0.839	-0.303	0.394	(I)	0.290	0.536	0.453	0.274
	G. capensis	-0.558	-0.725	-0.390	0.423	(+)	0.352	0.508	0.834	0.013
	F. mechowii	-0.405	-0.537	-0.272	0.311	(I)	0.257	0.375	0.928	0.424
	F. damarensis	-0.566	-0.705	-0.426	0.381	(I)	0.316	0.460	0.838	0.150
	C. hottentotus	-0.917	-1.115	-0.719	0.594	(+)	0.493	0.716	0.573	<0.001
APDT	*B. suillus*	-0.451	-0.594	-0.309	0.397	(+)	0.350	0.450	0.810	0.007
	H. argenteocinereus	-0.419	-0.704	-0.133	0.434	(I)	0.323	0.585	0.488	0.079
	G. capensis	-0.157	-0.310	-0.004	0.325	(I)	0.261	0.404	0.765	0.813
	F. mechowii	-0.120	-0.365	0.126	0.308	(I)	0.218	0.436	0.750	0.634
	F. damarensis	-0.410	-0.576	-0.244	0.428	(+)	0.351	0.521	0.818	0.015
	C. hottentotus	-0.645	-0.802	-0.487	0.562	(+)	0.481	0.658	0.699	<0.001

BL vs	Species	Elevation	CI		Slope		CI		r^2	*P*-value
TDF	*B. suillus*	-1.732	-2.394	-1.070	1.025	(I)	0.764	1.376	0.404	0.866
	H. argenteocinereus	-1.939	-2.321	-1.556	1.118	(I)	0.953	1.312	0.847	0.165
	G. capensis	-0.784	-1.584	0.017	0.515	(I)	0.256	1.036	0.565	0.060
	F. mechowii	-1.569	-1.980	-1.158	0.865	(I)	0.686	1.091	0.181	0.219
	F. damarensis	-3.726	-4.474	-2.978	1.971	(+)	1.638	2.372	0.562	<0.001
	C. hottentotus	-1.832	-2.717	-0.946	1.057	(I)	0.728	1.534	0.708	0.752
	H. glaber	-2.477	-2.829	-2.125	1.284	(+)	1.149	1.434	0.846	<0.001
APDF	*B. suillus*	-1.320	-1.848	-0.792	0.726	(I)	0.522	1.011	0.245	0.057
	H. argenteocinereus	-1.021	-1.282	-0.761	0.621	(-)	0.510	0.755	0.771	<0.001
	G. capensis	-0.854	-2.011	0.303	0.493	(I)	0.185	1.313	0.012	0.145
	F. mechowii	-1.717	-2.094	-1.340	0.840	(I)	0.675	1.045	0.269	0.117
	F. damarensis	-3.642	-4.399	-2.885	1.857	(+)	1.523	2.265	0.495	<0.001
	C. hottentotus	-1.968	-2.881	-1.054	1.047	(I)	0.711	1.541	0.683	0.804
	H. glaber	-1.872	-2.214	-1.531	0.973	(I)	0.844	1.122	0.748	0.705
TDT	*B. suillus*	-2.144	-2.807	-1.480	1.120	(I)	0.855	1.468	0.499	0.402
	H. argenteocinereus	-2.075	-2.493	-1.657	1.115	(I)	0.937	1.327	0.836	0.209
	G. capensis	-1.074	-2.593	0.444	0.548	(I)	0.183	1.646	0.473	0.225
	F. mechowii	-3.458	-4.141	-2.776	1.759	(+)	1.456	2.125	0.542	<0.001
	F. damarensis	-2.234	-2.841	-1.627	1.148	(I)	0.904	1.458	0.898	0.227
	C. hottentotus	-2.321	-2.655	-1.987	1.168	(+)	1.040	1.312	0.833	<0.001
APDT	*B. suillus*	-2.144	-2.807	-1.480	1.120	(I)	0.855	1.468	0.554	0.051
	H. argenteocinereus	-2.075	-2.493	-1.657	1.115	(I)	0.937	1.327	0.903	0.474
	G. capensis	-1.074	-2.593	0.444	0.548	(I)	0.183	1.646	0.546	0.354
	F. mechowii	-3.458	-4.141	-2.776	1.759	(+)	1.456	2.125	0.723	<0.001
	F. damarensis	-2.234	-2.841	-1.627	1.148	(I)	0.904	1.458	0.766	0.394
	C. hottentotus	-2.321	-2.655	-1.987	1.168	(+)	1.040	1.312	0.803	<0.001

TABLE 5.12. Intralimb regressions showing independent comparisons of the periosteal module for fore- and hindlimbs (i.e. zeugopodial elements regressed against stylopodial elements). See abbreviations in Tables 5.1 and 5.5.

Intralimb	Species	Elevation	CI		Slope		CI		r^2	*P*-value
TDU vs TDH	*B. suillus*	-0.238	-0.345	-0.131	0.940	(I)	0.791	1.117	0.637	0.475
	H. argenteocinereus	-0.348	-0.501	-0.194	0.992	(I)	0.725	1.358	0.266	0.959
	G. capensis	-0.167	-0.221	-0.114	0.832	(-)	0.715	0.967	0.693	0.017
	F. mechowii	-0.311	-0.474	-0.148	1.109	(I)	0.810	1.516	0.770	0.490
	F. damarensis	-0.320	-0.353	-0.287	1.154	(+)	1.043	1.277	0.923	0.007
	C. hottentotus	-0.253	-0.286	-0.219	0.852	(-)	0.734	0.990	0.715	0.037
	H. glaber	-0.324	-0.378	-0.270	0.863	(I)	0.677	1.102	0.076	0.235
APDU vs APDH	*B. suillus*	-0.263	-0.377	-0.149	1.298	(+)	1.132	1.487	0.774	<0.001
	H. argenteocinereus	0.036	-0.057	0.128	1.022	(I)	0.817	1.278	0.634	0.848
	G. capensis	-0.112	-0.179	-0.044	1.205	(+)	1.045	1.389	0.727	0.011
	F. mechowii	0.004	-0.100	0.109	0.930	(I)	0.721	1.201	0.849	0.549
	F. damarensis	-0.098	-0.127	-0.069	1.199	(+)	1.090	1.319	0.932	0.001
	C. hottentotus	-0.037	-0.063	-0.010	0.977	(I)	0.863	1.107	0.803	0.714
	H. glaber	0.110	0.097	0.124	1.031	(I)	0.849	1.252	0.418	0.752
TDT vs TDF	*B. suillus*	-0.067	-0.136	0.003	0.910	(I)	0.815	1.016	0.848	0.093
	H. argenteocinereus	-0.256	-0.406	-0.105	1.108	(I)	0.842	1.460	0.441	0.456
	G. capensis	-0.071	-0.122	-0.020	0.852	(-)	0.752	0.965	0.907	0.014
	F. mechowii	-0.245	-0.390	-0.099	1.065	(I)	0.818	1.387	0.856	0.610
	F. damarensis	-0.242	-0.300	-0.185	1.123	(I)	0.981	1.285	0.916	0.090
	C. hottentotus	-0.133	-0.174	-0.093	0.892	(I)	0.771	1.033	0.728	0.124
APDT vs APDF	*B. suillus*	-0.016	-0.116	0.085	1.327	(+)	1.150	1.532	0.744	<0.001
	H. argenteocinereus	0.102	-0.037	0.241	1.772	(+)	1.306	2.405	0.309	<0.001
	G. capensis	0.114	0.038	0.189	1.305	(+)	1.086	1.569	0.798	0.006
	F. mechowii	0.207	0.055	0.360	1.073	(I)	0.726	1.585	0.677	0.704
	F. damarensis	0.050	-0.038	0.138	1.337	(+)	1.065	1.678	0.758	0.014
	C. hottentotus	0.218	0.187	0.249	0.885	(I)	0.727	1.077	0.504	0.219

5.3.2.4 Interlimb Comparisons

Stylopod (TDH vs TDF). Coefficients of determination ranged from 0.314 (*H. glaber*) and 0.924 (*F. mechowii*). Most growth trends showed isometry, and the rest showed negative allometry (Table 5.13).

Zeugopod (TDU vs TDT). Coefficients of determination ranged from 0.363 (*H. argenteocinereus*) and 0.912 (*F. damarensis*). Most growth trends showed isometry, and only two species showed negative allometry (*G. capensis* and *C. hottentotus*) (Table 5.13).

Stylopod (APDH vs APDF). Coefficients of determination ranged from 0.341 (*H. glaber*) and 0.871 (*F. mechowii*). All species showed isometry, except *H. argenteocinereus* which showed positive allometry (Table 5.13).

Zeugopod (APDU vs APDT). Coefficients of determination were relatively higher as compared to the regressions of the stylopods, ranging from 0.566 (*C. hottentotus*) to 0.899 (*F. damarensis*). All species showed isometry, i.e. the ulna and tibia showed similar growth trends in this aspect (Table 5.13).

TABLE 5.13. Interlimb regressions showing independent comparisons of the periosteal module for stylopodial and zeugopodial elements (i.e. forelimb traits regressed against hindlimb traits). See abbreviations in Tables 5.1 and 5.5.

Interlimb	Species	Elevation	CI		Slope		CI		r^2	*P*-value
TDH vs TDF	*B. suillus*	0.074	0.013	0.135	0.842	(-)	0.758	0.935	0.866	0.002
	H. argenteocinereus	-0.048	-0.164	0.067	1.093	(I)	0.881	1.356	0.660	0.410
	G. capensis	0.025	-0.019	0.070	0.817	(-)	0.726	0.920	0.914	0.002
	F. mechowii	0.011	-0.071	0.094	0.886	(I)	0.739	1.063	0.924	0.172
	F. damarensis	-0.035	-0.087	0.017	0.941	(I)	0.810	1.093	0.885	0.410
	C. hottentotus	0.007	-0.023	0.037	0.824	(-)	0.732	0.928	0.821	0.002
	H. glaber	0.058	0.016	0.100	1.010	(I)	0.818	1.247	0.314	0.926
TDU vs TDT	*B. suillus*	-0.106	-0.197	-0.015	0.863	(I)	0.716	1.039	0.575	0.118
	H. argenteocinereus	-0.146	-0.230	-0.061	0.978	(I)	0.730	1.312	0.363	0.881
	G. capensis	-0.022	-0.058	0.015	0.577	(-)	0.479	0.694	0.804	<0.001
	F. mechowii	-0.076	-0.161	0.008	0.923	(I)	0.691	1.234	0.826	0.559
	F. damarensis	-0.132	-0.158	-0.105	0.976	(I)	0.850	1.120	0.912	0.716
	C. hottentotus	-0.142	-0.157	-0.126	0.788	(-)	0.694	0.894	0.797	<0.001
APDH vs APDF	*B. suillus*	0.112	0.035	0.190	1.000	(I)	0.865	1.156	0.743	0.999
	H. argenteocinereus	-0.029	-0.144	0.087	1.705	(+)	1.306	2.225	0.477	<0.001
	G. capensis	0.032	-0.026	0.090	1.145	(I)	0.971	1.349	0.832	0.103
	F. mechowii	0.029	-0.068	0.126	1.156	(I)	0.913	1.464	0.871	0.207
	F. damarensis	0.029	-0.025	0.084	0.941	(I)	0.764	1.159	0.776	0.553
	C. hottentotus	0.071	0.050	0.092	0.890	(I)	0.778	1.019	0.769	0.090
	H. glaber	0.059	0.048	0.069	1.027	(I)	0.835	1.262	0.341	0.800
APDU vs APDT	*B. suillus*	-0.097	-0.172	-0.021	0.970	(I)	0.867	1.085	0.846	0.588
	H. argenteocinereus	-0.093	-0.214	0.027	0.983	(I)	0.787	1.227	0.639	0.874
	G. capensis	-0.170	-0.267	-0.074	1.002	(I)	0.834	1.204	0.808	0.986
	F. mechowii	-0.173	-0.313	-0.033	0.987	(I)	0.774	1.258	0.879	0.906
	F. damarensis	-0.124	-0.180	-0.067	0.881	(I)	0.760	1.021	0.899	0.088
	C. hottentotus	-0.182	-0.247	-0.117	0.983	(I)	0.818	1.182	0.566	0.856

5.3.3 Epicondylar and condylar bone growth

5.3.3.1 Humerus (EH)

Humeral epicondyles showed coefficients of determination ranging from 0.395 in *G. capensis* to 0.931 in *F. mechowii* (Table 5.14). BM and BL regressions showed relatively similar values and negative allometry predominates.

5.3.3.2 Femur (FH)

Femoral condyles showed lower coefficients of determination as compared to the humeral epicondyles, and ranged between 0.141 in *C. hottentotus* and 0.873 in *H. argenteocinereus* (Table 5.14). BM regressions showed slightly higher coefficients of determination than BL regressions. Growth patterns were identical as for the epicondyles of the humerus for each species (i.e., negative allometry predominates), thus indicating similar growth trends.

5.3.3.3 Interlimb comparison (EH vs EF)

As mentioned above, EH and EF showed the same growth trends for BM, although slightly different for BL. Regression of EH vs EF showed strong coefficients of determination (i.e., 0.80 or higher), although those were lower in *H. glaber* (0.696). All species showed isometry, and only *B. suillus* showed positive allometry of the EH (i.e. the humeral epicondyles grew more than the femoral condyles).

5.3.4 Comparative Osteogenesis: growth pattern of endochondral and periosteal ossification

In this section, the comparisons are focused on diameters versus bone lengths for each bone, so both anteroposterior and mediolateral diameters are regressed against their respective bone length. The comparisons for the tibia-fibula do not include the tibia of *H. glaber*.

In the humerus, APDH showed relatively high coefficients of determination with HL in most species (r^2 = 0.7 or higher), although *H. glaber* and *H. argenteocinereus* showed low values (Table 5.15).

In the ulna, a similar pattern was observed for TDU and UL, although such values were considerably higher between APDU and UL, indicating that there is a stronger relationship between anteroposterior diameters of the ulna and ulnar length. Only *H. glaber* showed a low value (0.521) for these parameters. The pairwise comparisons showed similar slopes between APDH and TDH for each species, while the TDU and APDU showed some differences between species, suggesting higher slopes for anteroposterior diameters (Table 5.15).

In the femur, coefficients of determination and slopes were generally lower for APDF than for TDF (Table 5.15). The pairwise comparisons showed similar growth trends of APDF and TDF for each species. In the tibia, most species showed high coefficients of determination, and only *H. argenteocinereus* showed lower values (i.e. lower than 0.6). Pairwise comparisons showed that TDT accumulated more differences between species than APDT.

For (epi)condyles, most regressions showed high coefficients of determination (r^2 = 0.6 or higher), although negative allometry (Table 5.15). This indicates that despite the relatively lower rate of bone growth in these regions, such features are highly correlated with endochondral bone growth. The pairwise comparisons showed that almost all species have equal slopes, although *B. suillus* differed from *G. capensis, C. hottentotus* and *H. glaber* by having significantly lower slopes (Table 5.15).

TABLE 5.14. Regressions of the epicondylar region of humerus and femur showing coefficients of determination (r^2), allometric coefficients (slope), growth pattern and elevation. Bone traits assessed against body mass (BM) in the left and body length (BL) in the right. In the bottom right, interlimb regressions showing comparisons of the epicondylar widths (i.e. humeral epicondyles regressed against femoral condyles). See abbreviations in Tables 5.1, 5.4 and 5.5.

BM vs	Species	Elevation	CI		Slope		CI		r^2	*P*-value
EH	*B. suillus*	0.484	0.412	0.556	0.211	(-)	0.188	0.237	0.835	<0.001
	H. argenteocinereus	0.266	0.100	0.432	0.263	(I)	0.198	0.350	0.421	0.100
	G. capensis	0.238	0.138	0.339	0.277	(-)	0.235	0.327	0.685	0.028
	F. mechowii	0.227	0.111	0.343	0.292	(I)	0.246	0.348	0.931	0.124
	F. damarensis	0.291	0.204	0.377	0.242	(-)	0.202	0.291	0.835	0.001
	C. hottentotus	0.061	-0.055	0.177	0.338	(I)	0.279	0.409	0.546	0.893
	H. glaber	0.351	0.302	0.399	0.162	(-)	0.133	0.199	0.498	<0.001
EF	*B. suillus*	0.517	0.460	0.574	0.174	(-)	0.155	0.195	0.844	<0.001
	H. argenteocinereus	0.255	0.085	0.426	0.252	(I)	0.186	0.342	0.461	0.073
	G. capensis	0.272	0.165	0.380	0.246	(-)	0.201	0.302	0.797	0.005
	F. mechowii	0.381	0.098	0.663	0.213	(I)	0.124	0.365	0.356	0.098
	F. damarensis	0.259	0.176	0.343	0.247	(-)	0.207	0.294	0.851	0.002
	C. hottentotus	0.079	-0.043	0.201	0.323	(I)	0.262	0.400	0.451	0.778
	H. glaber	0.265	0.219	0.311	0.185	(-)	0.156	0.219	0.636	<0.001

BL vs	Species	Elevation	CI		Slope		CI		r^2	*P*-value
EH	*B. suillus*	-0.610	-0.801	-0.418	0.689	(-)	0.615	0.771	0.845	<0.001
	H. argenteocinereus	-0.782	-1.204	-0.359	0.750	(-)	0.579	0.971	0.545	0.030
	G. capensis	-0.489	-0.676	-0.303	0.604	(-)	0.525	0.695	0.744	<0.001
	F. mechowii	-1.487	-2.035	-0.939	1.076	(I)	0.855	1.354	0.892	0.495
	F. damarensis	-0.784	-1.932	0.364	0.710	(I)	0.347	1.451	0.543	0.300
	C. hottentotus	-1.341	-1.701	-0.981	0.979	(I)	0.818	1.172	0.588	0.817
	H. glaber	-0.417	-0.619	-0.216	0.495	(-)	0.405	0.604	0.395	<0.001
EF	*B. suillus*	-0.677	-1.090	-0.265	0.685	(-)	0.520	0.902	0.481	0.008
	H. argenteocinereus	-0.765	-0.991	-0.540	0.722	(-)	0.624	0.836	0.873	<0.001
	G. capensis	-0.890	-2.080	0.299	0.750	(I)	0.370	1.521	0.694	0.351
	F. mechowii	-0.558	-0.765	-0.350	0.537	(-)	0.444	0.649	0.458	<0.001
	F. damarensis	-1.285	-1.665	-0.904	0.948	(I)	0.779	1.153	0.509	0.588
	C. hottentotus	-0.938	-2.207	0.332	0.816	(I)	0.425	1.566	0.141	0.524
	H. glaber	-0.348	-0.506	-0.191	0.553	(-)	0.493	0.621	0.834	<0.001
EH vs EF	*B. suillus*	-0.185	-0.338	-0.032	1.253	(+)	1.111	1.412	0.825	<0.001
	H. argenteocinereus	-0.041	-0.171	0.088	1.096	(I)	0.947	1.269	0.845	0.210
	G. capensis	0.110	0.030	0.190	0.917	(I)	0.819	1.026	0.921	0.127
	F. mechowii	0.212	0.042	0.383	0.796	(I)	0.626	1.013	0.881	0.062
	F. damarensis	0.013	-0.103	0.128	1.007	(I)	0.863	1.176	0.895	0.923
	C. hottentotus	-0.014	-0.086	0.058	1.033	(I)	0.928	1.150	0.854	0.545
	H. glaber	0.108	0.040	0.176	0.900	(I)	0.782	1.036	0.696	0.139

TABLE 5.15. Regressions of the endochondral versus periosteal modules (including epicondyles and condyles) showing coefficients of determination (r^2), allometric coefficients (slope), growth pattern and elevation. See abbreviations in Tables 5.1-5.5.

	Species	Elevation	CI		Slope		CI		r^2	*P*-value
TDH x HL	*B. suillus*	-0.888	-1.044	-0.733	0.986	(I)	0.892	1.091	0.876	0.787
	H. argenteocinereus	-0.973	-1.322	-0.623	1.077	(I)	0.848	1.366	0.584	0.535
	G. capensis	-1.019	-1.168	-0.871	1.068	(I)	0.964	1.185	0.850	0.205
	F. mechowii	-0.451	-0.685	-0.218	0.666	(-)	0.516	0.859	0.850	0.004
	F. damarensis	-0.819	-0.965	-0.674	0.899	(I)	0.786	1.028	0.864	0.117
	C. hottentotus	-1.602	-1.865	-1.339	1.564	(+)	1.358	1.801	0.746	<0.001
	H. glaber	-1.302	-1.650	-0.954	1.350	(+)	1.081	1.686	0.233	0.009
APDH x HL	*B. suillus*	-0.741	-0.923	-0.558	0.884	(I)	0.775	1.008	0.789	0.065
	H. argenteocinereus	-1.214	-1.596	-0.832	1.192	(I)	0.942	1.509	0.594	0.139
	G. capensis	-0.828	-1.001	-0.656	0.904	(I)	0.785	1.042	0.717	0.162
	F. mechowii	-0.743	-1.019	-0.467	0.856	(I)	0.677	1.082	0.873	0.175
	F. damarensis	-0.957	-1.090	-0.825	0.987	(I)	0.883	1.104	0.907	0.815
	C. hottentotus	-1.684	-1.967	-1.401	1.591	(+)	1.370	1.847	0.715	<0.001
	H. glaber	-1.449	-1.771	-1.126	1.302	(+)	1.052	1.613	0.293	0.016
TDU x UL	*B. suillus*	-1.168	-1.457	-0.879	0.944	(I)	0.784	1.137	0.575	0.541
	H. argenteocinereus	-1.318	-1.812	-0.824	1.005	(I)	0.718	1.404	0.161	0.979
	G. capensis	-1.067	-1.240	-0.893	0.870	(-)	0.757	0.999	0.730	0.049
	F. mechowii	-0.886	-1.148	-0.623	0.738	(-)	0.580	0.939	0.866	0.017
	F. damarensis	-1.247	-1.381	-1.114	0.964	(I)	0.865	1.075	0.911	0.503
	C. hottentotus	-1.759	-2.012	-1.506	1.349	(+)	1.165	1.561	0.727	<0.001
	H. glaber	-1.548	-1.900	-1.196	1.241	(I)	0.974	1.581	0.102	0.080
APDU x UL	*B. suillus*	-1.342	-1.548	-1.135	1.168	(+)	1.048	1.301	0.858	0.006
	H. argenteocinereus	-1.210	-1.503	-0.916	1.146	(I)	0.960	1.368	0.772	0.127
	G. capensis	-1.220	-1.405	-1.035	1.098	(I)	0.977	1.235	0.808	0.115
	F. mechowii	-0.766	-0.990	-0.542	0.796	(-)	0.657	0.964	0.916	0.023
	F. damarensis	-1.225	-1.352	-1.098	1.100	(+)	1.005	1.204	0.939	0.040
	C. hottentotus	-1.846	-2.070	-1.622	1.573	(+)	1.407	1.759	0.842	<0.001
	H. glaber	-1.509	-1.807	-1.211	1.439	(+)	1.204	1.719	0.521	<0.001
TDF x FL	*B. suillus*	-1.230	-1.420	-1.041	1.185	(+)	1.074	1.308	0.881	0.001
	H. argenteocinereus	-0.890	-1.225	-0.555	0.996	(I)	0.783	1.268	0.573	0.975
	G. capensis	-1.188	-1.433	-0.942	1.213	(+)	1.045	1.410	0.861	0.013
	F. mechowii	-0.493	-0.779	-0.207	0.728	(-)	0.548	0.966	0.813	0.031
	F. damarensis	-0.827	-1.075	-0.578	0.932	(I)	0.757	1.148	0.775	0.492
	C. hottentotus	-2.094	-2.507	-1.680	1.957	(+)	1.647	2.324	0.621	<0.001
	H. glaber	-1.251	-1.560	-0.943	1.249	(+)	1.010	1.545	0.301	0.040

…continuation

APDF x FL	*B. suillus*	-0.919	-1.113	-0.725	0.894	*(I)*	0.782	1.021	0.782	0.097
	H. argenteocinereus	-0.727	-0.999	-0.455	0.708	*(-)*	0.537	0.932	0.442	0.015
	G. capensis	-0.608	-0.777	-0.439	0.674	*(-)*	0.560	0.812	0.787	<0.001
	F. mechowii	-0.639	-0.929	-0.349	0.717	*(-)*	0.535	0.960	0.801	0.028
	F. damarensis	-0.892	-1.146	-0.638	0.909	*(I)*	0.731	1.130	0.753	0.376
	C. hottentotus	-2.105	-2.492	-1.717	1.843	*(+)*	1.553	2.188	0.625	<0.001
	H. glaber	-1.377	-1.661	-1.094	1.186	*(I)*	0.965	1.457	0.344	0.104
TDT x TL	*B. suillus*	-1.441	-1.635	-1.247	1.258	*(+)*	1.142	1.386	0.886	<0.001
	H. argenteocinereus	-1.283	-1.654	-0.911	1.137	*(I)*	0.898	1.439	0.593	0.277
	G. capensis	-1.479	-1.768	-1.191	1.328	*(+)*	1.132	1.558	0.855	0.001
	F. mechowii	-0.767	-1.014	-0.520	0.768	*(-)*	0.610	0.968	0.891	0.029
	F. damarensis	-1.326	-1.630	-1.022	1.144	*(I)*	0.935	1.399	0.811	0.181
	C. hottentotus	-2.321	-2.674	-1.968	1.958	*(+)*	1.696	2.261	0.737	<0.001
APDT x TL	*B. suillus*	-1.514	-1.804	-1.225	1.383	*(+)*	1.213	1.577	0.789	<0.001
	H. argenteocinereus	-1.232	-1.672	-0.792	1.291	*(+)*	1.010	1.650	0.558	0.042
	G. capensis	-1.026	-1.179	-0.872	1.135	*(+)*	1.027	1.254	0.944	0.015
	F. mechowii	-0.479	-0.772	-0.186	0.763	*(I)*	0.580	1.004	0.844	0.053
	F. damarensis	-1.263	-1.560	-0.967	1.284	*(+)*	1.077	1.530	0.857	0.007
	C. hottentotus	-1.942	-2.327	-1.556	1.830	*(+)*	1.547	2.163	0.641	<0.001
EH x HL	*B. suillus*	0.099	0.001	0.198	0.633	*(-)*	0.572	0.699	0.879	<0.001
	H. argenteocinereus	-0.135	-0.301	0.030	0.723	*(-)*	0.610	0.856	0.793	<0.001
	G. capensis	-0.211	-0.308	-0.115	0.779	*(-)*	0.710	0.854	0.881	<0.001
	F. mechowii	-0.148	-0.236	-0.059	0.760	*(-)*	0.697	0.827	0.983	<0.001
	F. damarensis	-0.269	-0.450	-0.087	0.813	*(-)*	0.682	0.969	0.848	0.023
	C. hottentotus	-0.460	-0.610	-0.310	0.942	*(I)*	0.824	1.077	0.772	0.379
	H. glaber	-0.285	-0.424	-0.146	0.759	*(-)*	0.648	0.890	0.612	0.001
EF x FL	*B. suillus*	0.189	0.088	0.290	0.511	*(-)*	0.452	0.577	0.819	<0.001
	H. argenteocinereus	-0.116	-0.273	0.041	0.667	*(-)*	0.563	0.790	0.790	<0.001
	G. capensis	-0.282	-0.417	-0.146	0.783	*(-)*	0.689	0.890	0.898	0.001
	F. mechowii	-0.317	-0.897	0.263	0.853	*(I)*	0.535	1.361	0.527	0.480
	F. damarensis	-0.248	-0.378	-0.117	0.764	*(-)*	0.669	0.873	0.914	<0.001
	C. hottentotus	-0.500	-0.702	-0.297	0.941	*(I)*	0.790	1.121	0.607	0.491
	H. glaber	-0.377	-0.515	-0.238	0.789	*(-)*	0.678	0.918	0.646	0.003

5.4 DISCUSSION

Postnatal ontogenetic series of the humerus, ulna, femur and tibia-fibula of six bathyergid species were analyzed with RMA regressions to determine growth patterns associated with body size as well as differences in ossification modules. Although there are many studies reporting on patterns of long bone growth in mammals, they have used different approaches and methodologies, resulting in generalized interpretations about i) relative growth rates and ii) allometric/isomteric trends. Since relative growth rates (slope) and growth patterns (allometry/isometry) showed contrasting results for bathyergids, they are considered separately in the current study. Here, the relative growth rates are

discussed firstly to show the effects of analyzing several species simultaneously (by the estimation of equal slopes), and secondarily, it is discussed in terms of allometric trends (by the independent estimation of isometry and its deviations). The special case of naked mole-rats is also discussed to include a revision of their neotenic features and implications for the evolution of African mole-rats (Section 5.4.4).

5.4.1 Endochondral Bone Growth in Bathyergids

Although bathyergids show different growth patterns (isometry or positive/negative allometry) of their long bones, multiple *post hoc* analysis (equal slopes) showed that these growth trends do not represent statistically significant differences in slopes (at least for comparisons of BM) (Tables 5.6, 5.7). The following discussion explains these processes separately and includes explanations for such methodological discordances (Sections 5.4.1.1-5.4.1.3). Only some bones showed a lower but still non-significant difference in growth rates, and those are also discussed below (Section 5.4.1.4). For this reason, except for naked mole-rats (Section 5.4.1.5), it is assumed that most bathyergids showed similar slopes and therefore experience similar growth rates of bone elongation during ontogeny. In general, these findings show that most bathyergid species share similar postnatal growth dynamics of the endochondral module, thus suggesting a relatively conserved developmental pattern of growth plate ossification. Studies assessing the relationship between growth plate activity and allometric/isometric growth within a wide range of phylogenetically controlled group of species are lacking, so further research should focus on assessing such aspects of limb bone growth.

5.4.1.1 Intralimb and Interlimb Comparisons: Proximo-Distal Pattern

The intralimb (Table 5.8) and interlimb (Table 5.9) regressions generally showed high coefficients of determination, indicating a highly interrelated growth between bone elements. Multiple comparisons also showed non-significant differences within and between species for the growth rates of humerus and femur, and only few differences for the growth rates between the ulna and tibia among social species (Table 5.9; Appendix 5.4). The stylopodial interlimb comparison (humerus vs femur) appeared to be more correlated than the rest of the regressions (Table 5.9). This indicates that the stylopodial serial homologous pair represents a highly correlated system in bathyergids, which is also reflected in the correlations between the total length of the limbs (see comparison below for the forelimb vs hindlimb) (Table 5.9). Comparatively lower correlations (but still high) were found for the zeugopodial elements (UL vs TL). This suggests that the length of humerus and femur have a stronger developmental regulatory component during postnatal development as compared to ulna and tibia-fibula, also acting at the level of whole limb development. These findings preliminarily do not support the initial hypothesis of a functional prioritization of forelimb growth over hindlimb growth in bathyergids, since serial homologues showed similar growth rates (but see section 5.4.1.2). Despite such differences between stylopodial and zeugopodial elements are not strong, they still show a proximo-distal pattern of variation in

their growth, where proximal elements are more tightly correlated than distal ones.

Previously, it has been mentioned the existence of separate developmental processes acting in the proximal and distal parts of limb bones which implies a spatial "division of labor" in endochondral bone growth in the appendicular skeleton of mammals (Rolian, 2008). Rolian (2008, p. 25) suggests that "*the separation of developmental mechanisms into proximal and distal limb fields could have been selected, for example, because it allows morphological changes in the autopods to evolve independently of, and/or more rapidly, than changes in limb size and shape in the proximal appendicular skeleton*". This idea highlights the modular nature of bone elements and is further supported by other studies showing that that the autopodial skeleton of vertebrates is morphologically more diverse than the long limb bones (Rolian, 2008 and references therein, Shubin *et al.* 1997; Hildebrand & Goslow 2001). This diversity reflects, in part, that metapodials and/or phalanges are under strong selective pressures due to their direct interaction with the substrate, so they can evolve morphological adaptations for particular habitats and locomotor behaviors (Rolian, 2008). Several terrestrial mammals show these patterns, e.g., rodents, (Weisbecker & Schmid, 2007), primates (Jouffroy & Lessertisseur *et al.*, 1978; Chiu & Hamrick, 2002) and didelphid marsupials (Lemelin, 1999). Thus, the lower correlation observed in zeugopodial elements in bathyergids, can be explained by this generalized pattern of modularity observed along the proximo-distal axis of the mammalian limb. Additionally, since zeugopods are in direct contact with autopodial elements, they must also adapt and synchronize in response to the changes occurring in the autopodial modules. It is likely that this generates a bottom-up cascade of decreasing morphological changes (from distal to proximal appendages), where proximal structures are probably evolutionarily more stable than distal ones.

5.4.1.2 Forelimb and Hindlimb Growth

When the whole limb is considered, the pattern of similar growth rates was maintained in bathyergids (Table 5.6, 5.7). Previous studies on extant mammals showing various locomotor modes, gaits, postures and sizes that included marsupials, lagomorphs, rodents, scandentians and primates, found that hindlimb elements generally grow much faster than the homologous forelimb elements (Carrier, 1983; Lammers & German, 2002; Schilling & Petrovitch, 2006; Young, Fernandez & Fleagle, 2010). For this reason, some authors have suggested that this may be "*a common developmental bauplan among mammals*" (Lammers & German, 2002; Iijima & Kubo 2019). The present study does not support this hypothesis, since all bathyergids showed similar growth rates for each limb and limb bones (Table 5.6, 5.7). Thus, both fore- and hindlimbs elongates at similar rates in these subterranean rodents, and in fact these growth rates are slightly higher in the forelimb for some species (Table 5.6, 5.7, 5.9). Whether these similar growth rates between limbs in bathyergids are the product of increased growth rates in forelimb bones or a decrease in growth rates in hindlimbs is unknown and should be tested in future work. The determination of these features may shed light on the possibility that non-fossorial ancestors of bathyergids show higher hindlimb bone

growth rates, and consequent adaptations to fossoriality would have stimulated the increase in forelimb bone growth rates. In such case, the original hypothesis suggested in this study would have to be re-assessed.

In a functional sense, similar growth rates in fore- and hindlimbs may also explain the similar intermembral bone proportions (IMI) found in chapters 3 and 4 (Montoya-Sanhueza *et al.*, 2019). Similar growth rates may represent a systemic adaptation of growth plates to maintain similar bone proportions in order to maximize locomotor performance within burrows systems (Montoya-Sanhueza *et al.*, 2019). The fact that some species even showed higher bone growth rates for the forelimb supports the initial hypothesis of this study which supposes that the anterior limb represent an important structure in fossorial mammals for digging, so its growth may be prioritized or positively selected to attain somatic maturity earlier than the hindlimb. Nevertheless, the scratch-digging species *B. suillus* did not show necessarily higher growth rates as compared to chisel-tooth digger species. These observations also help to understand that it is unlikely that the development of the hindlimb *per se* constrains forelimb proportions, as suggested elsewhere (Schmidt & Fischer, 2009). The data presented here rather suggest an alternative hypothesis, where the functional aspects, habits and niche, like locomotion in narrow spaces (burrows) may have a stronger effect on the independent modulation and selection of forelimb and hindlimb proportions of subterranean mammals by modifications in their growth patterns. In this regard, a recent study assessing the external and internal morphology of stylopodial bones of a wide range of rodents with different locomotor strategies showed that subterranean and fossorial species were the only ecomorphological group to consistently show increased rates of humeral and femoral morphological evolution (Hedrick *et al.*, 2020). This study suggest that the subterranean niche imposes strong selective pressures in the phenotype of mammals, and therefore, that terrestrial –aboveground– locomotion may restrict the diversity of growth patterns in mammals, especially those associated with the forelimb.

It is known that life in burrows decreases the threats of predators and increases the chances of survival in subterranean mammals (Begall *et al.,* 2007). This may suggest that the appendicular skeleton of bathyergids has not being selected specifically for high-speed phenotypes or to increase escape capabilities, but rather locomotor capabilities have been considerably reduced (see below). This would be associated with the reduction in the patterns of kinetic ability in bathyergids, i.e. slow movements, which most likely also occurs in other subterranean mammals. Comparative studies on their behavior and locomotor dynamics are scarce, but they are needed to understand the relationship between morphological adaptation and kinematics. Interspecific differences between bathyergids and other subterranean mammals with less restricted subterranean habits like ctenomyids may help to understand such specific observations (Ch. 4, Montoya-Sanhueza *et al.*, 2019).

Generalizations about a common body plan in growth rates among mammals must be taken cautiously since growth rates are known to vary considerably in bones (Currey, 2002). It is most likely that such interpretations result from the small sample of organisms analyzed, which is composed mainly of species with a terrestrial (surface-dwelling) lifestyle.

Although surface-dwelling species may show differences in locomotor modes, they do not involve considerable changes in their general kinematic patterns, which is still under the main propulsion of the posterior part of the skeleton, specifically the pelvic girdle and hindlimbs (Howell, 1965; Schmidt & Fischer, 2009). In this respect, it is known that some subterranean mammals have changed their locomotor patterns to be functionally bidirectional (and thus include backward movements), so the propulsive regions are now located in both the pectoral and the pelvic girdles (Eilam *et al.*, 1995; Montoya-Sanhueza *et al.*, 2019). For this reason, when assessing common trends in mammals, it is imperative to consider not only the morphology but also studies of behavior, biomechanics and kinetics to assess the appropriateness of the taxonomic and ecomorphological comparisons. The study of these patterns in more phylogenetically constrained groups with different lifestyles would highly improve our understanding of what processes are driving growth dynamics and therefore phenotypic variation.

5.4.1.3 Ontogenetic Allometry and Bone Proportions of the Endochondral Module in Bathyergids and other Mammals

The analysis of the endochondral module of the fore- and hindlimbs showed that growth trends between bone lengths and BM were mostly consistent with isometry, while regressions against BL showed a more variable pattern of ontogenetic allometry, including isometry but also negative and positive allometry depending on the species (Tables 5.6 and 5.7). It is known that long bone scaling varies with changes in BM of the species (e.g. Jungers & Fleagle 1980; Roth, 1984; Wayne 1986), although comparisons with BL have been scarcely assessed. For this reason, the results observed in bathyergids showing a more variable growth pattern in relation to BL are unfortunately not comparable with other studies. However, variation of allometric ontogenetic patterns of long bones is known to occur in species of different body sizes (Jungers & Fleagle, 1980; Roth, 1984; Wayne, 1986; Turnquist & Wells 1994; Lammers & German, 2002; Schilling & Petrovitch, 2005; Schmidt & Fischer, 2009, and references therein).

Lammers & German (2002) reported the ontogenetic allometry of four small mammals, including two rodents (*Chinchilla lanigera* and *Rattus norvegicus*), one lagomorph (*Oryctolagus cuniculus*) and one marsupial (*Monodelphis domestica*). They performed RMA regressions of bone lengths against body mass and showed that such species have positive allometry of the hindlimb bones (femur and tibia) and humerus, although *C. lanigera* showed isometry for the humerus (Lammers & German, 2002). This indicates proportionally higher growth rates for the appendicular system in relation to body size, which is often associated with organisms with proportionally elongated limbs. Similar positive allometries were observed for the humerus and femur of the scansorial *Tupaia glis* (Scandentia, Tupaiidae), but an isometric pattern for the tibia (Schilling & Petrovitch, 2006). The domestic cat *Felis catus* also showed positive allometry of the humerus (Peters, 1983). Similarly, it has been suggested that positive allometry of postnatal limb bone growth is common for altricial organisms (Dodson, 1975), including birds (Huggins, 1940), rodents (Green & Fekete, 1933; MacArthur & Chiasson, 1946) and humans (Moss, 1955). Even different surface-dwelling species with different locomotor modes, like those possessing highly specialized half-

bounding gaits (e.g. *C. lanigera* and *O. cuniculus*) or a more generalized locomotor behavior and morphology (e.g. *R. norvegicus* and *M. domestica*), still show positive allometry (Lammers & German, 2002). Thus, the characteristic positive allometry (i.e. proportionally increased growth of limb bones with respect to body size) described for surface-dwelling organisms, is probably related to changes of the appendicular muscle mass closer to the centre of rotation (hip joint) thus decreasing the moment of inertia of the limb, and increasing the speed of both protraction and retraction of the limbs, allowing a more efficient terrestrial locomotion (Dodson, 1975). Based on these allometric estimations, some authors have suggested that small mammals may share strong developmental constraints that govern their relative growth rates regardless of their locomotor mode (Lammers & German, 2002). Although other authors have suggested that the apparent evolutionary stasis of the static allometric slope is not generated by internal (developmental) constraints but more likely results from external constraints imposed by selection (Pélabon, *et al.*, 2013). The results observed in bathyergids do not support the developmental constraint hypothesis, and rather provides additional evidence to the hypothesis of external factors and natural selection as drivers of appendicular modification in mammals. In this case, all genera within Bathyergidae showed marked isometry of their long bones, except for *Heterocephalus* which showed negative allometry and the species *F. mechowii* which showed positive allometry (Table 5.6-5.7). These taxa represent the smallest and the largest social species within this group, respectively.

Consequently, the mostly isometric growth pattern observed in long bones of bathyergids can be considered as a generalized reduction in limb bone size with respect to BM, to maximize locomotion in narrow spaces, but also implies slower locomotor performances as compared to surface-dwelling relatives of similar size (see Montoya-Sanhueza *et al.*, 2019). The fact that only *F. mechowii* showed positive allometry of all their long bones (Tables 5.6, 5.7), it resembles the condition found in surface-dwelling mammals, and could indicate higher locomotor capabilities. Based on allometric analysis of their long bones (Echeverría *et al.,* 2014), as well as aspects of their ecology and cranial anatomy (e.g. larger and functional eyes), higher locomotor capabilities have been suggested for the subterranean tuco-tucos (*Ctenomys*) (see Montoya-Sanhueza *et al.*, 2019).

In general, *F. mechowii* showed the longest bones among social species, which were also slightly longer than in solitary species of smaller body size like *H. argenteocinereus* and *G. capensis* (Fig. 5.2). Despite some bones are longer than others within a species (e.g. ulna vs tibia, Table 5.1, Fig. 5.2), such differences are not considerably big in comparison to the proportion found in surface-dwelling mammals. Larger zeugopodial elements of the hindlimb have been typically associated with specializations for increased speed (Howell, 1965). Limb proportions in bathyergids are quite symmetrical, especially for the intermembral index (forelimb vs hindlimb), ≈1.0 (see details in Ch. 4). In this respect, some differences in the hindlimb were found between solitary and social species (excluding *H. glaber*). Most solitary species showed longer femora than tibio-fibula, whereas social species showed a larger tibio-fibula (Table 5.1). The analysis of the crural and intermembral indices in Ch. 4 (and 3), also showed that the femur was longer than the tibia-fibula in solitary species, and that hindlimbs were

relatively longer than forelimbs. It is likely that social bathyergids have a more "cursorial" phenotype to increase locomotor performance within burrows to maximize foraging and connection between distantly located chambers. In fact, it has been reported that social bathyergid species have more complex and relatively longer burrow systems as compared to solitary species (Le Comber *et al.* 2002, 2006; Thomas *et al.*, 2009; Šumbera *et al.*, 2012). This aspect has not been assessed in subterranean mammals and needs further research.

The generalized isometric patterns found in bathyergids among mammals can be explained because of the lack of previous comparative studies including subterranean mammals, and because the study of adaptations associated with the subterranean niche have been principally focused on their digging mechanisms rather than their locomotor modes. Thus, it is likely that other subterranean mammals also show isometric or negative allometry of their appendicular system. From an energetic point of view, McNab (2002) already considered the locomotion of subterranean mammals as within a dense medium. The implications of living in a dense medium in the appendicular system have not been assessed in mammals, and its analysis could shed light on the selective pressures acting not only during digging, but also when moving underground. Eilam *et al.* (1995) studied the uphill locomotion of the head lift digger, *Spalax leucodon ehrenbergi*, and observed that these animals changed their locomotor patterns to be functionally bidirectional to thus include backward movements, so the propulsive regions of the body are now located in both the pectoral and the pelvic girdles (Eilam *et al.*, 1995). Similarly, the eastern mole *Scalopus aquaticus* (Talpidae) has highly specialized and reduced limb bones where the forelimb shows unusual kinematics during walking (Lin *et al.*, 2019). The study of their ontogenetic allometry in such species with distinct locomotor modes with respect to tetrapods, may help to understand the diversity of growth patterns in mammals.

The proposed shorter limbs observed in subterranean mammals has been scarcely studied, and its ontogeny was considerably neglected until the present study. This study points to the relevance of understanding locomotor modes and kinematics in subterranean species, which seems to play an important role for driving modifications of their appendicular system. However, this study also recognizes that the simplification of allometric approaches, which intend to determine the fitness of structures within or outside a linear isometric tendency, considerably limits our visualization of other growth patterns potentially involved in the growth and development of the skeletal system. Additionally, although growth patterns can relatively be identified as pertaining to one of the three main growth trends (i.e. isometry or positive/negative allometry), biological interpretations of their adaptations, origin, and mechanisms cannot be restricted to mere comparisons of such values. Allometric studies must be complemented with others such as comparative and functional anatomy, bone modularity, tissue identification, cell proliferation rates, locomotor function, and should ideally include multivariate analyses, so that the diversity of mammalian bone growth can be more comprehensively understood.

5.4.1.4 Foot Drumming and Slow Growth Rates in the Tibia-Fibula

Among the bones that showed the lowest growth rates and a marked negative allometry among solitary species such as *B. suillus* and *G. capensis,* was the tibia (including humerus and ulna in *G. capensis*). In solitary species, the mean bone length of the tibia-fibula was usually shorter than the femur, except in *G. capensis* where it is slightly larger than the femur (Table 5.1; Fig. 5.1). In Ch. 4, the crural index (CI) was calculated and showed that the femur of solitary species was longer than the tibio-fibula, while the tibia-fibula was longer in social species (Fig. 4.10 in Ch. 4). Thus, tibio-fibulas in solitary species are shorter and have also a lower growth rate (with respect to the femur and other bones). Since the slopes of the humerus, ulna and femur showed similar values among species, and are higher as compared to the growth rates of the tibio-fibula (Table 5.6-5.7), it is most likely that the slow growth rates of the tibia-fibula are related to a slowdown in endochondral ossification on growth plates ion this particular bone. One factor known to reduce long bone growth by affecting growth plate activity is compressive forces (Moss, 1977; Stokes *et al.*, 2006). The hindlimb of bathyergids assist during digging behavior, especially to expel the soil out of the burrow (Genelly, 1965; Jarvis & Sale, 1971). However, *B. suillus* and *G. capensis* are the only bathyergids that exhibit foot drumming (Bennett & Jarvis, 1988; van Sandwyk & Bennett, 2005; Sahd *et al.*, 2019). Foot drumming in bathyergids has been scarcely studied, and only more detailed descriptions have been done for *G. capensis*. Foot drumming occurs very fast and is repetitive with the simultaneous striking of both hind feet on the burrow floor, while the forelimbs support its body (Bennett & Jarvis, 1988). No detailed data of this process exist for *B. suillus* (Van Sandwyk & Bennett, 2005), although preliminary personal observations indicate that foot drumming is slower as compared to *G. capensis*.

Interestingly, the other solitary species *H. argenteocinereus* showed similar bone growth rates for all limb bones including the tibio-fibula (Table 5.6), although there are no reports of foot drumming for this species (Šumbera *et al.*, 2003). For this reason, the lower growth rates of the tibia-fibula in *B. suillus* and *G. capensis* seems to be related to this behavior. In these two species, the tibia-fibula seems to be maintained relatively vertical when beating the substrate, while the femur maintains a horizontal/diagonal position, with the femoral-pelvic joint being closer to the floor so that the animal takes a sitting/crouched posture (Fig. 2.1 in Ch. 2). Thus, during foot drumming, the tibia-fibula undergoes compression mainly due to direct muscular action which pushes the lower leg down. The higher values of the mediolateral robustness of tibia index (TRI) reported in the Ch. 4 (and 3) for these species in comparison to other AMs (e.g. Fig. 4.10), suggest an increased cross-sectional area to resist bending and shearing stresses, and therefore a stronger ability to slam the leg against the floor. In fact, biomechanical testing on tibias of other rodent models, using proximo-distal compression to assess changes in cross-sectional properties, has evidenced endosteal and periosteal bone formation (De Souza *et al.,* 2005; Brodt & Silva, 2010). Thus, drumming behavior might stimulate periosteal/endosteal growth. Further research is needed to fully describe how foot drumming is executed and what factors may affect growth plate activity and periosteal bone formation in the hindlimb of mole-rats.

5.4.1.5 Slow Bone Growth Rates in Naked Mole-Rats

The most marked differences in bone growth rates were found in naked mole-rats, *H. glaber*. Naked mole-rats showed negative allometry of all long bones and they have the lowest growth rates among all bathyergids (Tables 5.6-5.7). The differences in growth trends in this species are similar when using either BM or BL, and were statistically significant in terms of lower slopes as compared to the rest of the bathyergids (Table 5.6). Since most bones in bathyergids showed mainly isometric growth trends when assessed with BM, it is expected that the underestimated BM values of naked mole-rats (see section 5.2) had influenced the results, so the regressions estimated on body mass for this species must be treated with caution. Nevertheless, when data of BL regressions are compared among all bathyergids, *H. glaber* still showed negative allometry and most of the others either isometry or positive allometry (Tables 5.6-5.7).

The lengths of their long bones were basically the same for all bones (Table 5.1), thus contrasting with the pattern found in other bathyergids which showed some differences at intralimb and interlimb levels (Fig. 5.1). These features show that naked mole-rats have comparatively shorter limbs (and therefore relatively longer body lengths) as compared to other bathyergids. This also contrasts with the extreme case of the largest social mole-rat *F. mechowii,* which showed positive allometry of their limb bones (see above). Another small mammal with ontogenetic negative allometry on long bones with respect to body mass (humerus and tibia), is the cui, *Galea musteloides* (Rodentia, Caviidae) (Schilling & Petrovitch, 2006). Cuis are unspecialized mammals that live underground in open grasslands and which locomotor mode has been compared to the ancestral therian pattern (Schilling & Petrovitch, 2006, and references therein). Curiously, this species showed positive allometry for the femur (Schilling & Petrovitch, 2006). It is likely that the primitive therian locomotion is associated with reduced limbs, resembling more the reptilian generalized phenotype. An early study assessing the relative growth of *Alligator mississipiensis* showed negative allometry of limb bone lengths versus proxies of body size (Dodson, 1975). This author suggested that the strategy of limb growth has an interesting adaptive basis, and crocodilians show an ontogenetic decrease in importance of the limbs throughout life because in adult life they mostly preclude of terrestrial locomotion. A recent study of the limb bone growth of crocodilians showed similar generalized results (Iijima & Kubo, 2019). The data of this study supports the hypothesis of a reduction in locomotor performance in shortened-legged species, although no assessments of the kinetic patterns among bathyergids has been done.

5.4.2 The Growth Pattern of the Periosteal Module

5.4.2.1 Anteroposterior and Mediolateral Diameters in Bathyergids

A general pattern observed across bathyergid species is that anteroposterior diameters of the forelimb showed higher coefficients of determination, so were better correlated than mediolateral diameters (Table 5.10). In the forelimb, it seems that the degree of variability decreases towards the distal elements with the ulna having higher levels of correlation as compared to other limb bones. This is contrary to what was found in the endochondral module, where distal elements

(ulna and tibia) were more variable in length as compared to the proximal elements (humerus and femur) (Table 5.6). However, only the anteroposterior diameter of the ulna showed the highest correlations among all the periosteal modules of the forelimb. The mediolateral diameter (TDU) was not higher than the correlations found in the humerus (Table 5.10). Thus, the growth of the ulna in bathyergids occurs principally in the anteroposterior axis, resulting in a thicker structure probably to provide a larger surface for attachment of the flexor muscles involved during digging behavior, i.e. m. extensor carpi ulnaris, m. flexor carpi ulnaris, and m. flexor digitorum profundus (see Montoya-Sanhueza *et al.*, 2019). This would increase anteroposterior bending resistance of such bones, especially considering that the higher bending stresses in the forearm of mammals performing parasagittal movements during scratch-digging, are expected to occur in the anteroposterior axis of the bone (Biewener & Taylor, 1986; Carter & Beaupré, 2001; Leppänen *et al.*, 2006). Scratch-digging species did not show higher slopes for this feature, but the small social *C. hottentotus* showed the higher slopes among bathyergids for this feature (Table 5.10).

In the hindlimb, the correlations were also higher for the zeugopodial elements (Tables 5.11), and stylopodial elements showed the lowest coefficients of determination. Thus, it is apparent that the periosteal module is less variable in distal elements while proximal elements seems to be more variable. This again contrasts with the pattern observed in the endochondral ossification. In the hindlimb, periosteal ossification always showed isometry or positive allometry with respect to BM (Tables 5.11). The APDF showed the lowest coefficients of determination for the hindlimb.

5.4.2.2 Comparative Allometry of the Periosteal Module among Mammals

The analysis of the periosteal module showed a more variable pattern of bone ossification than that observed for the endochondral module, mainly evidenced by the coefficients of determination which were considerably more variable and lower for periosteal ossification (Tables 5.10, 5.11). Differences are not restricted to one species only (e.g. *H. glaber*) and rather include differences among different species. Nevertheless, there are some similarities between the endochondral module and periosteal module: BM regressions showed more stable growth trends (mostly isometry) as compared to BL (more variable growth trends) for both fore- and hindlimbs. With respect to these growth trends, most traits showed isometry and positive allometry, while negative allometry was observed only in a few cases, e.g. in the forelimb of the social *Fukomys* and in the solitary *G. capensis* (Table 5.10). Thus, although the periosteal module showed more variability than the endochondral module, it tended to have proportional growth with respect to body size and in many instances showed a proportionally higher growth (positive allometry) with respect to body size.

Similar results were found for the subterranean ctenomyid rodent *C. talarum* (Echeverría *et al.*, 2014), which mostly shows positive allometry of bone diameters, and presents only one isometric trend on the mediolateral diameter of the ulna. Although all coefficients of determination were extremely high for *C. talarum*, the lowest values reported for this species pertain to periosteal modules

(Echeveria *et al.*, 2014). Such observations were based on regressions of bone lengths and skull length (SKL), so the allometric patterns of such bones with BM and BL are unknown. In Ch. 3 (Montoya-Sanhueza *et al.*, 2019), it was demonstrated that regressions of bone lengths with SKL in *B. suillus* showed increased number of positive allometries, indicating that some postcranial elements have a distinct (higher) growth pattern in relation to SKL.

The observations in subterranean rodents contrast with other mammals, were widths (diameters) show negative allometry with respect to body size. The study of Lammers & German (2002) showed that all diameters in eutherian mammals (*C. lanigera*, *R. norvegicus*, and *O. cuniculus*) presented negative allometry, except in the didelphid marsupial *M. domestica* which showed positive allometry. Similar results have been described in primates with distinct developmental patterns (altricial and precocial) by Young *et al.* (2010). These estimations were based on linear measurements (diameter) of one axis of the diaphysis, either the anteroposterior or the mediolateral axis, so the entire periosteal bone tissue growth around the diaphysis was not really considered. A more precise measurement of periosteal bone formation in long bones is the midshaft circumference (or perimeter), which was previously quantified in a larger sample of mammals and showed that both "*isometry and positive allometry are the most widespread patterns of growth across mammals*" and that "*Negative allometry (i.e., bones growing more robust during ontogeny) occurs in mammals but is largely restricted to cetartiodactyls*" (Kilbourne & Makovicky, 2012, pp. 1111). These authors positioned the axes of the regressions inversely to the present study, so the periosteal parameters are set in the "*x*" axis, and the increments of the bone lengths and body sizes on the "*y*" variable. This results in growth trends appearing inverse to the ones used in this study. In any case, the main pattern reported by these authors for periosteal growth in mammals are i) proportional growth (isometry) and ii) proportionally lower periosteal growth during ontogeny (this study = negative allometry), resulting in slender bones in adulthood (Kilbourne & Makovicky, 2012).

Thus, the bone growth trends found in bathyergids resemble those observed in marsupials (Table 5.15). Maunz & German (1997) found that one of the smallest and one of the largest species within the Didelphidae (*Monodelphis domestica* and *Didelphis virginiana*) family exhibit the same length to width proportions in the scaling of limb bones throughout growth, despite variation in locomotion, i.e. limb bone isometry regardless of phylogenetic changes in body size. This suggests that both the periosteal and endochondral modules could have similar growth rates in marsupials. This would explain the typically more robust skeletons of quadrupedal marsupials.

Some authors have proposed that negative allometry of long bone diaphysis (growing slender) may represent a common pattern among mammals which is perhaps "preadaptive" for different purposes among different lineages (e.g. Young *et al.*, 2010; Kilbourne & Makovicky, 2012). As mentioned above, such interpretations are most likely the result of the limited size of the taxa compared, which is generally composed of terrestrial (surface-dwelling) species, which have relatively high-speed locomotion and agility, and live under "normal" gravitational terrestrial conditions (see section 5.4.1). In a terrestrial lifestyle, body mass imposes

physical constrains in the skeletal system, and as body size increases during ontogeny, it also yields increased bone strains (Biewener & Taylor, 1986). Consequently, these growth patterns indicate that terrestrial surface-dwelling mammals tend to show a slender (and thinner) diaphyseal long bone morphology, most likely related to functional and locomotor requirements to increase agility and speed by reducing bone mass (limited cortical thickening) (Currey, 2002). For this reason, the medullary cavities of long bones of terrestrial mammals expand considerably during ontogeny resulting in lighter bones (see Montoya-Sanhueza & Chinsamy, 2017, and references therein). However, fossorial species need to strengthen their limb bones due to digging demands, which explains the increments in periosteal and endosteal bone growth. Thus, negative allometry of cortical thickness/diameter is not a generalized growth pattern among mammals, and positive allometry is not only restricted to cetartiodactyls (Kilbourne & Makovicky, 2012), but also present in fossorial mammals (Montoya-Sanhueza & Chinsamy, 2017). Similarly, in crocodylians, the analysis of midshaft circumferences showed mostly positive allometries in the humerus and isometric and positive allometries in the femur (Iijima & Kubo 2019).

5.4.3 Implications of Differential Endochondral and Periosteal Ossification Rates on Bone Phenotypes

It is widely known that the growth and development of the skeleton are under regulation of both genetic (intrinsic) and environmental (extrinsic) factors (Murray, 1936; Hall, 1978, 2015; Moss-Salentijn, 1992). Genetic factors principally play a role on development, specifically in the ability of skeletogenic cells to differentiate, to undergo mitoses, and to produce specific components of the extracellular matrix, whereas environmental factors appear to determine the timing and the rates of such events (Moss-Salentijn, 1992). Therefore, it is expected that environmental factors may be responsible of heterochronic patterns observed in the skeletal system of mammals, specifically by modulating when and for how long those processes start and prolong. Long bone modeling is attained by the dual cellular process of formation and resorption of bone tissues, as well as by the differential osteogenic activity of endochondral and intramembranous (periosteal/endosteal) ossifications. Such processes have been studied independently, and in general, the analysis of intramembranous ossification and its growth patterns have not been so extensively assessed in comparison to studies of endochondral ossification (Hall, 2015). Importantly, no special efforts have been put on the determination and comparison of the interrelated contribution of such ossification types on the phenotyping of bones.

In general, in this study, the periosteal module showed relatively higher growth rates as compared to the endochondral module (Tables 6-7, 10-11). However, a more conspicuous pattern was identified, where the periosteal module showed a considerably higher degree of variation, thus appearing to be considerably less dependent on body size (and age) as compared to the endochondral module (Table 5.6-5.10). This does not necessarily agree with the original hypothesis that such modules will show different growth rates, but indicates a marked difference in their variance. This suggests that intramembranous ossification is probably more prone to external cues, and

therefore has a lower genetic regulation. These results provide important evidence to support the hypothesis that endochondral and periosteal ossification are under distinct regulatory factors (Moss-Salentijn, 1992). For example, the important role of environmental regulation on appositional bone growth has been well supported since early studies of bone adaptation (Moss-Salentijn, 1992). Similarly, based on *in vivo* and *in vitro* experimentation of long bone rudiments, the explants have shown the ability to grow to relatively normal lengths even in the absence of normal physiological loading conditions, thus suggesting a significant regulation of chondrocytic proliferation and hypertrophy (Moss-Salentijn, 1992). Thus, a much greater amount of intrinsic control has been claimed for the endochondral module (Moss-Salentijn, 1992). Additionally, it is possible to see how several studies assessing endochondral and intramembranous ossification separately or in the same study, have reported great differences in their coefficients of determination (or equivalent parameters of variance), usually showing higher values for bone elongation (e.g. Castanet *et al.*, 2004; Cubo *et al.*, 2006). However, this phenomenon has not received the necessary attention, most likely because the more reductionist approaches used to assess osteogenesis, principally focused on quantifying the general shape of a bone or because of the assumption that both undergo similar developmental processes.

In general, one of the main goals in evolutionary morphology is to measure the general shape of a structure, which is usually summarized as its total length, diameter or morphospace (Klingenberg, 2013). However, these assessments include both modules (endochondral and periosteal) indistinctively, but do not assess the relationship and implications osteogenic processes. Such studies contain the raw data to understand the interrelationship of those processes and are necessary to make some initial comparisons. For example, Gould (1967) described the independence of limb widths and lengths for pelycosaur species, and the poor relationship between body weight and limb and vertebral widths. This study is one of the few studies that deals directly with a comparison between ossification modules.

Finally, the results obtained in the current research suggest that periosteal ossification represents a process showing higher intraspecific variation, probably indicating different levels of local adaptation. In this sense, it seems that this module represents a more labile module that helps to counteract external fluctuations so occurs as the module that adapts during life, whilst the endochondral module acts as a more stable process (canalization), probably because its initial cell proliferation type is established in early ontogeny due to chondrocyte and growth plate formation, and which are genetically regulated features (Rolian, 2008). In comparison, the periosteal module is constantly depositing new cells, i.e. *de novo* bone formation (Hall, 2015), and it is known to have a more specialized mechanosensory function (Wallace *et al.*, 2017). This suggest that evolution of limb bones can be accomplished by the modular interplay of these two processes acting at different temporal scales, one at an ontogenetic scale, influencing more the periosteal module, and therefore selecting genotypes with higher mechanosensory adaptations, and another at an evolutionary scale by selecting the phenotype of growth plates. This information indicates that the study of bone modularity in long bones needs further assessment, specially to include

multivariate and multiscale approaches within an evolutionary framework of musculoskeletal adaptation.

5.4.4 Limb Bone Growth and Neoteny in *H. glaber*

The results obtained here clearly showed that *H. glaber* has the lowest postnatal growth rates among bathyergids (Tables 5.6, 5.7, 5.10, 5.11; Appendices 5.2-5.8). Both endochondral and periosteal modules are affected, but endochondral bone growth rates were slower than for periosteal growth rates. Among endochondral growth rates, the femur showed the highest and the tibia the lowest. The elongation of the humerus and tibia showed negative allometry with the femur, so the femur grows proportionally more. The thickening of long bones showed similar growth rates, with the lowest values found in the mediolateral diameter of the ulna, and the highest in the mediolateral diameter of the femur (Tables 5.10 and 5.11).

These data provides additional evidence to support the neotenic condition of the appendicular skeleton of naked mole-rats. As hypothesized for neotenic species (McNamara, 1997), structures showing slow growth rates result in more simplified morphologies, which is also observed for naked mole-rats (see Ch. 4), where the absence of the deltoid tubercle in the humerus and the lack of tibio-fibular fusion make their appendicular skeleton comparatively less specialized as compared to the rest of the bathyergids. In this sense, species with higher growth rates will show more morphological disparity, and may explain the case of most bathyergids. Based on this information, and given that naked mole-rats are basal and divergent within the family (Faulkes *et al.*, 2004), it is hypothesized that the descendants of this lineage have evolved larger body sizes and more complex phenotypes, most likely by increasing (accelerating) their skeletal growth (i.e. peramorphosis). Thus, these data suggests that peramorphosis is the most probable developmental phenomenon explaining the speciation process associated with the evolution of most bathyergids.

Neoteny in *H. glaber* has been reported since the earliest anatomical and embryological descriptions of this species. The descriptions of Hill (1955) and Ellerman (1956) pointed out that the general appearance of the mature *H. glaber* resembles the naked newborn stage of many other rodents, such as mice and rats, including the newborns of other social bathyergids like *Cryptomys*. Ellerman (1956, p. 13) specifically suggested a paedomorphic condition for *H. glaber*; "*it is a* Cryptomys*-like form that in some way does not develop but remains in a permanently subadult state.*" These features are based on i) their lack of pigmentation, ii) almost nude integument, iii) the vestigial condition of the eyes and ears, iv) to the comparatively feeble (week) limbs, and v) to the animal's wriggling movements (Hill, 1955). Ellerman (1956) also identifies that this species has only three upper/lower molars each side, or sometimes only two, which would be the case of young specimens of *Cryptomys*. Hill (1955) suggested that such observations clearly envisages the idea of a genetic trend towards "fetilization" (i.e. becoming morphologically similar to the fetus) or at least paedomorphy (neoteny) and gives some support by mentioning embryonic features of the female genital tract (Hill, 1955). Based on embryological data, Maier & Schrenk (1987) showed

that the development of the infraorbital foramen in bathyergids occurs rapidly in *H. glaber* and slowly in the rest of the species, although *H. glaber* retain a comparatively smaller infraorbital foramen during ontogeny. Maier & Schrenk (1987) suggests that such differences reflect varying degrees of development of the pars infraorbitalis of the zygomatico-mandibular muscle during ontogeny.

Another set of data supporting the neoteny of *H. glaber* is that the brain of naked mole-rats is resistant to low oxygen concentrations (hypoxic conditions), which is a main feature of neonatal mammals (Larson & Park, 2009). Larson & Park (2009) have suggested that naked mole-rats may represent a case of slowed or arrested brain development, perhaps to maintain brain function in a chronically hypoxic environment. Other studies have concluded that "*…naked mole rats show an extremely protracted period of brain maturation that may permit plasticity and resilience to neurodegenerative processes over their decades-long lifespan. This conclusion is consistent with the hypothesis that naked mole rats are neotenous, with retention of juvenile characteristics…*" (Penz *et al.*, 2015, p. 1).

Recently, Skulachev *et al.* (2017) provided a comprehensive review of the neotenic traits of these animals, which is mostly characterized by physiological features and a few morphological traits pertaining to soft tissues. Out of the 43 neotenic characters gathered by these authors, only three are associated with the musculoskeletal system (see Skulachev *et al.* 2017): i) no decline on cortical bone area and bone mineral density with age (Pinto *et al.*, 2010), ii) delayed maturation of the skeletal system (Henry *et al.*, 2007), and iii) absence of any decline in the state of articular cartilage with age (Pinto *et al.*, 2010). Apart from this, there is a complete lack of data regarding patterns of skeletal growth for these animals. This is curious since the extremities of fossorial and subterranean mammals have been relatively well-studied (e.g. Hildebrand, 1985: Kley & Kearney, 2007). In this study, the comprehensive analysis of ontogenetic series of their long bones supports the neotenic condition suggested for naked mole-rats. Moreover, the list of neotenic features presented by Skulachev *et al.* (2017), increases with the addition of the pattern of skeletal growth. The revelation of such features also provides important cues for understanding the evolutionary biology of bathyergids.

5.5 CONCLUSIONS

This study showed that bathyergids have relatively similar skeletal growth, irrespective of social behavior or digging strategy, although some differences can be seen in some bones. Furthermore, this study considerably improves our understanding of growth patterns in mammals and demystified previous hypothesis suggesting that mammals have developmental constrains in their appendicular system and that most mammals show isometric or positive allometric scaling of their long bones. Contrary to the initial hypothesis, it was demonstrated that the hindlimb exhibits similar growth rates as compared to the forelimb. However, it is likely that forelimb growth rates have increased in bathyergids as an adaptation to balance the growth of this limb with that of the hindlimb. The original hypotheses suggesting faster growth rates for hindlimbs, mostly stems from the scarce assessment of subterranean species, and from generalizations made on terrestrial (surface-dwelling) mammals. Naked mole-rats showed the

most distinct growth patterns among bathyergids, indicating neotenic features for the development of their appendicular system, and therefore suggesting a consequent increment of the bone growth rates for all other bathyergid species during their evolution. The lower growth rates observed in naked mole-rats are probably associated with the less specialized morphology of their appendicular system (i.e. humerus and tibia), which contrasts with the more specialized and more morphologically complex condition of the humerus and tibia of the other bathyergids (Ch. 4).

In this study, clear differences in the growth pattern between the periosteal and endochondral modules were observed. The periosteal module showed relatively higher growth rates and higher degree of variation as compared to the endochondral module, thus appearing to be considerably less dependent on body size (and age) and genetic factors. These results highlight the relevance of considering developmental modularity of long bones for further assessment of their bone adaptations, especially for understanding the differential effects of intrinsic and extrinsic factors regulating endochondral and periosteal (intramembranous) ossification and maturity.

5.6 APPENDIX

APPENDIX 5.1. Test for equality of slopes and pairwise comparisons of RMA regressions between proxies of body size including body mass (BM) and body length (BL) of all bathyergids.

Results of multiple comparisons among groups (BL x BM)				
Test for pair-wise difference in slope:			P-value : 0.095402	
	Species_1	**Species_2**	**p-value**	**TestStat**
1	*H. argenteocinereus*	*G. capensis*	1.000	0.016
2	*H. argenteocinereus*	*F. damarensis*	1.000	0.330
3	*H. argenteocinereus*	*H. glaber*	1.000	0.012
4	*H. argenteocinereus*	*C. hottentotus*	1.000	0.205
5	*H. argenteocinereus*	*F. mechowii*	0.531	4.423
6	*H. argenteocinereus*	*B. suillus*	0.994	1.537
7	*G. capensis*	*F. damarensis*	1.000	0.506
8	*G. capensis*	*H. glaber*	1.000	0.072
9	*G. capensis*	*C. hottentotus*	1.000	0.476
10	*G. capensis*	*F. mechowii*	0.161	6.968
11	*G. capensis*	*B. suillus*	0.877	2.787
12	*F. damarensis*	*H. glaber*	1.000	0.278
13	*F. damarensis*	*C. hottentotus*	1.000	0.090
14	*F. damarensis*	*F. mechowii*	1.000	0.909
15	*F. damarensis*	*B. suillus*	1.000	0.070
16	*H. glaber*	*C. hottentotus*	1.000	0.151
17	*H. glaber*	*F. mechowii*	0.331	5.505
18	*H. glaber*	*B. suillus*	0.985	1.796
19	*C. hottentotus*	*F. mechowii*	0.389	5.153
20	*C. hottentotus*	*B. suillus*	0.999	1.216
21	*F. mechowii*	*B. suillus*	0.953	2.225

APPENDIX 5.2 (*next page*). Test for equality of slopes and pairwise comparisons of RMA regressions between proxies of body size (BM and BL) and humeral length (HL), ulnar length (UL) and forelimb length (HLUL) for all bathyergids. Abbreviations: body mass (BM) and body length (BL).

Results of multiple comparisons among groups (HL x BM)				
Test for pair-wise difference in slope:			P-value : 1.8584e-05	
	Species_1	Species_2	p-value	TestStat
1	*H. argenteocinereus*	*G. capensis*	1.000	0.708
2	*H. argenteocinereus*	*F. damarensis*	1.000	0.569
3	*H. argenteocinereus*	*H. glaber*	**0.032**	10.032
4	*H. argenteocinereus*	*C. hottentotus*	1.000	0.009
5	*H. argenteocinereus*	*F. mechowii*	1.000	0.169
6	*H. argenteocinereus*	*B. suillus*	1.000	0.212
7	*G. capensis*	*F. damarensis*	1.000	0.078
8	*G. capensis*	*H. glaber*	**0.023**	10.633
9	*G. capensis*	*C. hottentotus*	0.997	1.372
10	*G. capensis*	*F. mechowii*	0.691	3.703
11	*G. capensis*	*B. suillus*	1.000	0.513
12	*F. damarensis*	*H. glaber*	**<0.001**	18.122
13	*F. damarensis*	*C. hottentotus*	0.993	1.586
14	*F. damarensis*	*F. mechowii*	0.407	5.053
15	*F. damarensis*	*B. suillus*	1.000	0.430
16	*H. glaber*	*C. hottentotus*	**<0.001**	22.785
17	*H. glaber*	*F. mechowii*	**<0.001**	23.929
18	*H. glaber*	*B. suillus*	**<0.001**	21.212
19	*C. hottentotus*	*F. mechowii*	1.000	0.827
20	*C. hottentotus*	*B. suillus*	1.000	0.471
21	*F. mechowii*	*B. suillus*	0.857	2.902

Results of multiple comparisons among groups (HL x BL)				
Test for pair-wise difference in slope:			P-value : 1.729e-10	
	Species_1	Species_2	p-value	TestStat
1	*H. argenteocinereus*	*G. capensis*	0.413	5.018
2	*H. argenteocinereus*	*F. damarensis*	1.000	0.660
3	*H. argenteocinereus*	*H. glaber*	**0.038**	9.721
4	*H. argenteocinereus*	*C. hottentotus*	1.000	0.000
5	*H. argenteocinereus*	*F. mechowii*	0.491	4.620
6	*H. argenteocinereus*	*B. suillus*	1.000	0.128
7	*G. capensis*	*F. damarensis*	0.333	5.491
8	*G. capensis*	*H. glaber*	0.911	2.571
9	*G. capensis*	*C. hottentotus*	**0.020**	10.902
10	*G. capensis*	*F. mechowii*	**<0.001**	19.517
11	*G. capensis*	*B. suillus*	**<0.001**	21.042
12	*F. damarensis*	*H. glaber*	0.096	7.951
13	*F. damarensis*	*C. hottentotus*	1.000	0.886
14	*F. damarensis*	*F. mechowii*	1.000	0.818
15	*F. damarensis*	*B. suillus*	1.000	0.489
16	*H. glaber*	*C. hottentotus*	**<0.001**	17.862
17	*H. glaber*	*F. mechowii*	**<0.001**	23.722
18	*H. glaber*	*B. suillus*	**<0.001**	27.082
19	*C. hottentotus*	*F. mechowii*	0.098	7.910
20	*C. hottentotus*	*B. suillus*	1.000	0.353
21	*F. mechowii*	*B. suillus*	0.149	7.109

Results of multiple comparisons among groups (HLUL x BM)				
Test for pair-wise difference in slope:			P-value : 8.6144e-06	
	Species_1	Species_2	p-value	TestStat
1	*H. argenteocinereus*	*G. capensis*	0.983	1.836
2	*H. argenteocinereus*	*F. damarensis*	1.000	0.443
3	*H. argenteocinereus*	*H. glaber*	**0.007**	12.912
4	*H. argenteocinereus*	*C. hottentotus*	1.000	0.142
5	*H. argenteocinereus*	*F. mechowii*	1.000	0.055
6	*H. argenteocinereus*	*B. suillus*	1.000	0.621
7	*G. capensis*	*F. damarensis*	0.985	1.784
8	*G. capensis*	*H. glaber*	**0.028**	10.295
9	*G. capensis*	*C. hottentotus*	0.929	2.436
10	*G. capensis*	*F. mechowii*	0.273	5.909
11	*G. capensis*	*B. suillus*	0.999	1.105
12	*F. damarensis*	*H. glaber*	**<0.001**	23.893
13	*F. damarensis*	*C. hottentotus*	1.000	0.271
14	*F. damarensis*	*F. mechowii*	0.836	3.015
15	*F. damarensis*	*B. suillus*	1.000	0.097
16	*H. glaber*	*C. hottentotus*	**<0.001**	23.333
17	*H. glaber*	*F. mechowii*	**<0.001**	24.849
18	*H. glaber*	*B. suillus*	**<0.001**	20.716
19	*C. hottentotus*	*F. mechowii*	0.999	1.123
20	*C. hottentotus*	*B. suillus*	1.000	0.533
21	*F. mechowii*	*B. suillus*	0.752	3.424

Results of multiple comparisons among groups (HLUL x BL)				
Test for pair-wise difference in slope:			P-value : 1.3841e-10	
	Species_1	Species_2	p-value	TestStat
1	*H. argenteocinereus*	*G. capensis*	0.280	5.855
2	*H. argenteocinereus*	*F. damarensis*	1.000	0.477
3	*H. argenteocinereus*	*H. glaber*	**0.006**	13.313
4	*H. argenteocinereus*	*C. hottentotus*	1.000	0.099
5	*H. argenteocinereus*	*F. mechowii*	0.629	3.976
6	*H. argenteocinereus*	*B. suillus*	1.000	0.000
7	*G. capensis*	*F. damarensis*	0.381	5.198
8	*G. capensis*	*H. glaber*	0.459	4.776
9	*G. capensis*	*C. hottentotus*	**0.047**	9.315
10	*G. capensis*	*F. mechowii*	**<0.001**	19.002
11	*G. capensis*	*B. suillus*	**0.001**	17.305
12	*F. damarensis*	*H. glaber*	0.071	8.525
13	*F. damarensis*	*C. hottentotus*	1.000	1.025
14	*F. damarensis*	*F. mechowii*	1.000	0.721
15	*F. damarensis*	*B. suillus*	1.000	0.629
16	*H. glaber*	*C. hottentotus*	**<0.001**	20.239
17	*H. glaber*	*F. mechowii*	**<0.001**	24.887
18	*H. glaber*	*B. suillus*	**<0.001**	28.973
19	*C. hottentotus*	*F. mechowii*	0.083	8.230
20	*C. hottentotus*	*B. suillus*	1.000	0.290
21	*F. mechowii*	*B. suillus*	0.129	7.397

Results of multiple comparisons among groups (UL x BM)				
Test for pair-wise difference in slope:			P-value : 3.8844e-05	
	Species_1	Species_2	p-value	TestStat
1	*H. argenteocinereus*	*G. capensis*	0.817	3.111
2	*H. argenteocinereus*	*F. damarensis*	1.000	0.466
3	*H. argenteocinereus*	*H. glaber*	**0.006**	13.047
4	*H. argenteocinereus*	*C. hottentotus*	1.000	0.367
5	*H. argenteocinereus*	*F. mechowii*	1.000	0.001
6	*H. argenteocinereus*	*B. suillus*	0.999	1.111
7	*G. capensis*	*F. damarensis*	0.566	4.263
8	*G. capensis*	*H. glaber*	0.126	7.442
9	*G. capensis*	*C. hottentotus*	0.780	3.293
10	*G. capensis*	*F. mechowii*	0.153	7.061
11	*G. capensis*	*B. suillus*	0.993	1.558
12	*F. damarensis*	*H. glaber*	**<0.001**	21.309
13	*F. damarensis*	*C. hottentotus*	1.000	0.004
14	*F. damarensis*	*F. mechowii*	0.993	1.557
15	*F. damarensis*	*B. suillus*	1.000	0.732
16	*H. glaber*	*C. hottentotus*	**<0.001**	18.316
17	*H. glaber*	*F. mechowii*	**<0.001**	22.840
18	*H. glaber*	*B. suillus*	**0.002**	15.297
19	*C. hottentotus*	*F. mechowii*	1.000	0.930
20	*C. hottentotus*	*B. suillus*	1.000	0.537
21	*F. mechowii*	*B. suillus*	0.826	3.065

Results of multiple comparisons among groups (UL x BL)				
Test for pair-wise difference in slope:			P-value : 1.1575e-09	
	Species_1	Species_2	p-value	TestStat
1	*H. argenteocinereus*	*G. capensis*	0.169	6.873
2	*H. argenteocinereus*	*F. damarensis*	1.000	0.293
3	*H. argenteocinereus*	*H. glaber*	**0.003**	14.337
4	*H. argenteocinereus*	*C. hottentotus*	1.000	0.294
5	*H. argenteocinereus*	*F. mechowii*	0.829	3.053
6	*H. argenteocinereus*	*B. suillus*	1.000	0.070
7	*G. capensis*	*F. damarensis*	0.442	4.867
8	*G. capensis*	*H. glaber*	0.502	4.563
9	*G. capensis*	*C. hottentotus*	0.072	8.492
10	*G. capensis*	*F. mechowii*	**<0.001**	18.539
11	*G. capensis*	*B. suillus*	**0.003**	14.580
12	*F. damarensis*	*H. glaber*	0.088	8.118
13	*F. damarensis*	*C. hottentotus*	1.000	0.983
14	*F. damarensis*	*F. mechowii*	1.000	0.568
15	*F. damarensis*	*B. suillus*	1.000	0.649
16	*H. glaber*	*C. hottentotus*	**<0.001**	18.147
17	*H. glaber*	*F. mechowii*	**<0.001**	24.426
18	*H. glaber*	*B. suillus*	**<0.001**	24.639
19	*C. hottentotus*	*F. mechowii*	0.109	7.712
20	*C. hottentotus*	*B. suillus*	1.000	0.193
21	*F. mechowii*	*B. suillus*	0.159	6.986

APPENDIX 5.3 (*next page*). Test for equality of slopes and pairwise comparisons of RMA regressions between proxies of body size (BM and BL) and femoral length (FL), tibio-fibular length (TL) and hindlimb length (FLTL) for all bathyergids. Abbreviations: body mass (BM) and body length (BL).

Results of multiple comparisons among groups (FL x BM)

Test for pair-wise difference in slope : P-value : 0.00029981

	Species_1	Species_2	p-value	TestStat
1	*H. argenteocinereus*	*G. capensis*	0.805	3.170
2	*H. argenteocinereus*	*F. damarensis*	1.000	0.838
3	*H. argenteocinereus*	*H. glaber*	0.125	7.455
4	*H. argenteocinereus*	*C. hottentotus*	1.000	0.318
5	*H. argenteocinereus*	*F. mechowii*	1.000	0.072
6	*H. argenteocinereus*	*B. suillus*	1.000	0.903
7	*G. capensis*	*F. damarensis*	0.945	2.305
8	*G. capensis*	*H. glaber*	0.982	1.842
9	*G. capensis*	*C. hottentotus*	0.624	3.999
10	*G. capensis*	*F. mechowii*	0.057	8.955
11	*G. capensis*	*B. suillus*	0.907	2.598
12	*F. damarensis*	*H. glaber*	0.033	9.948
13	*F. damarensis*	*C. hottentotus*	1.000	0.431
14	*F. damarensis*	*F. mechowii*	0.578	4.208
15	*F. damarensis*	*B. suillus*	1.000	0.000
16	*H. glaber*	*C. hottentotus*	0.006	13.314
17	*H. glaber*	*F. mechowii*	<0.001	18.284
18	*H. glaber*	*B. suillus*	0.014	11.529
19	*C. hottentotus*	*F. mechowii*	0.961	2.139
20	*C. hottentotus*	*B. suillus*	1.000	0.562
21	*F. mechowii*	*B. suillus*	0.411	5.033

Results of multiple comparisons among groups (FL x BL)

Test for pair-wise difference in slope : P-value : 1.1597e-06

	Species_1	Species_2	p-value	TestStat
1	*H. argenteocinereus*	*G. capensis*	1.000	0.773
2	*H. argenteocinereus*	*F. damarensis*	1.000	0.051
3	*H. argenteocinereus*	*H. glaber*	0.175	6.802
4	*H. argenteocinereus*	*C. hottentotus*	1.000	0.026
5	*H. argenteocinereus*	*F. mechowii*	0.322	5.562
6	*H. argenteocinereus*	*B. suillus*	1.000	0.154
7	*G. capensis*	*F. damarensis*	1.000	0.676
8	*G. capensis*	*H. glaber*	0.030	10.135
9	*G. capensis*	*C. hottentotus*	0.995	1.483
10	*G. capensis*	*F. mechowii*	0.003	14.336
11	*G. capensis*	*B. suillus*	0.083	8.239
12	*F. damarensis*	*H. glaber*	0.728	3.534
13	*F. damarensis*	*C. hottentotus*	1.000	0.134
14	*F. damarensis*	*F. mechowii*	0.976	1.943
15	*F. damarensis*	*B. suillus*	1.000	0.000
16	*H. glaber*	*C. hottentotus*	0.009	12.317
17	*H. glaber*	*F. mechowii*	<0.001	21.873
18	*H. glaber*	*B. suillus*	<0.001	21.710
19	*C. hottentotus*	*F. mechowii*	0.032	10.021
20	*C. hottentotus*	*B. suillus*	1.000	0.856
21	*F. mechowii*	*B. suillus*	0.093	8.013

Results of multiple comparisons among groups (TL x BM)

Test for pair-wise difference in slope : P-value : 1.9553e-06

	Species_1	Species_2	p-value	TestStat
1	*H. argenteocinereus*	*G. capensis*	0.993	4.138
2	*H. argenteocinereus*	*F. damarensis*	1.000	0.430
3	*H. argenteocinereus*	*H. glaber*	0.010	12.124
4	*H. argenteocinereus*	*C. hottentotus*	0.999	1.223
5	*H. argenteocinereus*	*F. mechowii*	1.000	0.252
6	*H. argenteocinereus*	*B. suillus*	0.955	2.209
7	*G. capensis*	*F. damarensis*	0.444	4.854
8	*G. capensis*	*H. glaber*	0.415	5.010
9	*G. capensis*	*C. hottentotus*	0.918	2.524
10	*G. capensis*	*F. mechowii*	0.010	12.162
11	*G. capensis*	*B. suillus*	0.995	1.491
12	*F. damarensis*	*H. glaber*	<0.001	19.597
13	*F. damarensis*	*C. hottentotus*	1.000	0.590
14	*F. damarensis*	*F. mechowii*	0.768	3.348
15	*F. damarensis*	*B. suillus*	0.950	2.261
16	*H. glaber*	*C. hottentotus*	0.001	15.793
17	*H. glaber*	*F. mechowii*	<0.001	22.425
18	*H. glaber*	*B. suillus*	0.002	14.876
19	*C. hottentotus*	*F. mechowii*	0.230	6.253
20	*C. hottentotus*	*B. suillus*	1.000	0.426
21	*F. mechowii*	*B. suillus*	0.042	9.498

Results of multiple comparisons among groups (TL x BL)

Test for pair-wise difference in slope : P-value : 1.078e-06

	Species_1	Species_2	p-value	TestStat
1	*H. argenteocinereus*	*G. capensis*	0.990	1.653
2	*H. argenteocinereus*	*F. damarensis*	1.000	0.006
3	*H. argenteocinereus*	*H. glaber*	0.011	11.978
4	*H. argenteocinereus*	*C. hottentotus*	1.000	0.525
5	*H. argenteocinereus*	*F. mechowii*	0.211	6.433
6	*H. argenteocinereus*	*B. suillus*	1.000	0.212
7	*G. capensis*	*F. damarensis*	1.000	0.687
8	*G. capensis*	*H. glaber*	0.007	12.905
9	*G. capensis*	*C. hottentotus*	1.000	0.523
10	*G. capensis*	*F. mechowii*	0.002	14.828
11	*G. capensis*	*B. suillus*	0.906	2.602
12	*F. damarensis*	*H. glaber*	0.729	3.531
13	*F. damarensis*	*C. hottentotus*	1.000	0.306
14	*F. damarensis*	*F. mechowii*	0.966	2.087
15	*F. damarensis*	*B. suillus*	1.000	0.134
16	*H. glaber*	*C. hottentotus*	0.005	13.386
17	*H. glaber*	*F. mechowii*	<0.001	23.387
18	*H. glaber*	*B. suillus*	<0.001	21.208
19	*C. hottentotus*	*F. mechowii*	0.010	12.197
20	*C. hottentotus*	*B. suillus*	1.000	0.242
21	*F. mechowii*	*B. suillus*	0.013	11.645

Results of multiple comparisons among groups (FLTL x BM)

Test for pair-wise difference in slope : P-value : 1.4312e-05

	Species_1	Species_2	p-value	TestStat
1	*H. argenteocinereus*	*G. capensis*	0.734	3.505
2	*H. argenteocinereus*	*F. damarensis*	1.000	0.610
3	*H. argenteocinereus*	*H. glaber*	0.031	10.089
4	*H. argenteocinereus*	*C. hottentotus*	1.000	0.734
5	*H. argenteocinereus*	*F. mechowii*	1.000	0.233
6	*H. argenteocinereus*	*B. suillus*	0.997	1.364
7	*G. capensis*	*F. damarensis*	0.823	3.080
8	*G. capensis*	*H. glaber*	0.658	3.849
9	*G. capensis*	*C. hottentotus*	0.880	3.047
10	*G. capensis*	*F. mechowii*	0.019	11.021
11	*G. capensis*	*B. suillus*	0.963	2.120
12	*F. damarensis*	*H. glaber*	0.003	14.679
13	*F. damarensis*	*C. hottentotus*	1.000	0.011
14	*F. damarensis*	*F. mechowii*	0.612	4.052
15	*F. damarensis*	*B. suillus*	1.000	0.425
16	*H. glaber*	*C. hottentotus*	0.001	15.918
17	*H. glaber*	*F. mechowii*	<0.001	21.043
18	*H. glaber*	*B. suillus*	0.002	15.199
19	*C. hottentotus*	*F. mechowii*	0.438	4.886
20	*C. hottentotus*	*B. suillus*	1.000	0.335
21	*F. mechowii*	*B. suillus*	0.114	7.623

Results of multiple comparisons among groups (FL+TL x BL)

Test for pair-wise difference in slope : P-value : 3.6081e-07

	Species_1	Species_2	p-value	TestStat
1	*H. argenteocinereus*	*G. capensis*	0.995	1.465
2	*H. argenteocinereus*	*F. damarensis*	1.000	0.116
3	*H. argenteocinereus*	*H. glaber*	0.040	9.602
4	*H. argenteocinereus*	*C. hottentotus*	1.000	0.199
5	*H. argenteocinereus*	*F. mechowii*	0.167	6.890
6	*H. argenteocinereus*	*B. suillus*	1.000	0.005
7	*G. capensis*	*F. damarensis*	1.000	0.110
8	*G. capensis*	*H. glaber*	0.021	10.781
9	*G. capensis*	*C. hottentotus*	0.998	1.320
10	*G. capensis*	*F. mechowii*	0.002	15.499
11	*G. capensis*	*B. suillus*	0.175	6.795
12	*F. damarensis*	*H. glaber*	0.968	2.063
13	*F. damarensis*	*C. hottentotus*	1.000	0.008
14	*F. damarensis*	*F. mechowii*	0.877	2.790
15	*F. damarensis*	*B. suillus*	1.000	0.167
16	*H. glaber*	*C. hottentotus*	0.005	13.577
17	*H. glaber*	*F. mechowii*	0.000	22.821
18	*H. glaber*	*B. suillus*	0.000	23.593
19	*C. hottentotus*	*F. mechowii*	0.011	11.974
20	*C. hottentotus*	*B. suillus*	1.000	0.744
21	*F. mechowii*	*B. suillus*	0.027	10.349

APPENDIX 5.4 (*next page*). Test for equality of slopes and pairwise comparisons of RMA regressions: Top, intralimb comparisons (UL vs HL and TL vs FL). Center, interlimb comparisons (HL vs FL and TL vs UL). Bottom, forelimb versus hindlimb comparisons (UL+HL vs TL+FL).

Results of multiple comparisons among groups (UL x HL)				
Test for pair-wise difference in slope :			P-value : 0.020008	
	Species_1	Species_2	p-value	TestStat
1	*H. argenteocinereus*	*G. capensis*	1.000	0.993
2	*H. argenteocinereus*	*F. damarensis*	1.000	0.056
3	*H. argenteocinereus*	*H. glaber*	0.819	3.103
4	*H. argenteocinereus*	*C. hottentotus*	0.994	1.534
5	*H. argenteocinereus*	*F. mechowii*	0.993	1.558
6	*H. argenteocinereus*	*B. suillus*	0.977	1.941
7	*G. capensis*	*F. damarensis*	0.589	4.156
8	*G. capensis*	*H. glaber*	0.995	1.508
9	*G. capensis*	*C. hottentotus*	1.000	0.199
10	*G. capensis*	*F. mechowii*	1.000	0.066
11	*G. capensis*	*B. suillus*	1.000	0.398
12	*F. damarensis*	*H. glaber*	0.324	5.554
13	*F. damarensis*	*C. hottentotus*	0.535	4.405
14	*F. damarensis*	*F. mechowii*	0.031	10.087
15	*F. damarensis*	*B. suillus*	0.266	5.963
16	*H. glaber*	*C. hottentotus*	1.000	0.725
17	*H. glaber*	*F. mechowii*	0.996	1.436
18	*H. glaber*	*B. suillus*	1.000	0.608
19	*C. hottentotus*	*F. mechowii*	1.000	0.110
20	*C. hottentotus*	*B. suillus*	1.000	0.017
21	*F. mechowii*	*B. suillus*	1.000	0.304

Results of multiple comparisons among groups (TL x FL)				
Test for pair-wise difference in slope :			P-value : 3.4409e-05	
	Species_1	Species_2	p-value	TestStat
1	*H. argenteocinereus*	*G. capensis*	1.000	0.034
2	*H. argenteocinereus*	*F. damarensis*	1.000	0.583
3	*H. argenteocinereus*	*H. glaber*	0.576	4.215
4	*H. argenteocinereus*	*C. hottentotus*	0.997	1.399
5	*H. argenteocinereus*	*F. mechowii*	1.000	0.385
6	*H. argenteocinereus*	*B. suillus*	0.889	3.001
7	*G. capensis*	*F. damarensis*	0.959	2.166
8	*G. capensis*	*H. glaber*	0.148	7.127
9	*G. capensis*	*C. hottentotus*	0.957	2.186
10	*G. capensis*	*F. mechowii*	0.980	1.880
11	*G. capensis*	*B. suillus*	0.144	7.179
12	*F. damarensis*	*H. glaber*	0.008	12.642
13	*F. damarensis*	*C. hottentotus*	0.213	6.412
14	*F. damarensis*	*F. mechowii*	1.000	0.079
15	*F. damarensis*	*B. suillus*	0.006	13.276
16	*H. glaber*	*C. hottentotus*	0.998	1.261
17	*H. glaber*	*F. mechowii*	0.007	12.896
18	*H. glaber*	*B. suillus*	1.000	0.675
19	*C. hottentotus*	*F. mechowii*	0.224	6.308
20	*C. hottentotus*	*B. suillus*	1.000	0.310
21	*F. mechowii*	*B. suillus*	0.006	13.150

Results of multiple comparisons among groups (HL x FL)				
Test for pair-wise difference in slope :			P-value : 0.024088	
	Species_1	Species_2	p-value	TestStat
1	*H. argenteocinereus*	*G. capensis*	0.994	4.133
2	*H. argenteocinereus*	*F. damarensis*	0.926	2.461
3	*H. argenteocinereus*	*H. glaber*	0.857	2.901
4	*H. argenteocinereus*	*C. hottentotus*	1.000	0.199
5	*H. argenteocinereus*	*F. mechowii*	0.999	1.166
6	*H. argenteocinereus*	*B. suillus*	1.000	0.000
7	*G. capensis*	*F. damarensis*	1.000	0.597
8	*G. capensis*	*H. glaber*	1.000	0.224
9	*G. capensis*	*C. hottentotus*	0.182	6.725
10	*G. capensis*	*F. mechowii*	0.984	1.798
11	*G. capensis*	*B. suillus*	0.288	5.799
12	*F. damarensis*	*H. glaber*	1.000	0.082
13	*F. damarensis*	*C. hottentotus*	0.418	4.994
14	*F. damarensis*	*F. mechowii*	1.000	0.451
15	*F. damarensis*	*B. suillus*	0.602	4.100
16	*H. glaber*	*C. hottentotus*	0.352	5.371
17	*H. glaber*	*F. mechowii*	1.000	0.809
18	*H. glaber*	*B. suillus*	0.524	4.458
19	*C. hottentotus*	*F. mechowii*	0.837	3.008
20	*C. hottentotus*	*B. suillus*	1.000	0.332
21	*F. mechowii*	*B. suillus*	0.968	2.056

Results of multiple comparisons among groups (UL x TL)				
Test for pair-wise difference in slope :			P-value : 0.00027407	
	Species_1	Species_2	p-value	TestStat
1	*H. argenteocinereus*	*G. capensis*	1.000	0.459
2	*H. argenteocinereus*	*F. damarensis*	0.917	2.532
3	*H. argenteocinereus*	*H. glaber*	1.000	0.352
4	*H. argenteocinereus*	*C. hottentotus*	1.000	0.148
5	*H. argenteocinereus*	*F. mechowii*	0.786	3.266
6	*H. argenteocinereus*	*B. suillus*	1.000	0.195
7	*G. capensis*	*F. damarensis*	0.831	3.041
8	*G. capensis*	*H. glaber*	1.000	0.000
9	*G. capensis*	*C. hottentotus*	0.792	3.236
10	*G. capensis*	*F. mechowii*	0.432	4.917
11	*G. capensis*	*B. suillus*	0.697	3.673
12	*F. damarensis*	*H. glaber*	0.995	1.497
13	*F. damarensis*	*C. hottentotus*	0.022	10.738
14	*F. damarensis*	*F. mechowii*	1.000	0.159
15	*F. damarensis*	*B. suillus*	0.014	11.557
16	*H. glaber*	*C. hottentotus*	0.986	1.759
17	*H. glaber*	*F. mechowii*	0.943	2.324
18	*H. glaber*	*B. suillus*	0.974	1.977
19	*C. hottentotus*	*F. mechowii*	0.005	13.599
20	*C. hottentotus*	*B. suillus*	1.000	0.008
21	*F. mechowii*	*B. suillus*	0.003	14.435

Results of multiple comparisons among groups (HLUL x FLTL)				
Test for pair-wise difference in slope :			P-value : 8.3075e-05	
	Species_1	Species_2	p-value	TestStat
1	*H. argenteocinereus*	*G. capensis*	1.000	0.474
2	*H. argenteocinereus*	*F. damarensis*	0.498	4.584
3	*H. argenteocinereus*	*H. glaber*	0.941	2.343
4	*H. argenteocinereus*	*C. hottentotus*	1.000	0.147
5	*H. argenteocinereus*	*F. mechowii*	0.626	3.991
6	*H. argenteocinereus*	*B. suillus*	1.000	0.001
7	*G. capensis*	*F. damarensis*	0.332	5.500
8	*G. capensis*	*H. glaber*	0.991	1.648
9	*G. capensis*	*C. hottentotus*	0.881	2.765
10	*G. capensis*	*F. mechowii*	0.508	4.537
11	*G. capensis*	*B. suillus*	0.997	1.341
12	*F. damarensis*	*H. glaber*	1.000	0.380
13	*F. damarensis*	*C. hottentotus*	0.002	15.096
14	*F. damarensis*	*F. mechowii*	1.000	0.100
15	*F. damarensis*	*B. suillus*	0.010	12.236
16	*H. glaber*	*C. hottentotus*	0.173	6.820
17	*H. glaber*	*F. mechowii*	1.000	0.155
18	*H. glaber*	*B. suillus*	0.428	4.940
19	*C. hottentotus*	*F. mechowii*	0.007	12.985
20	*C. hottentotus*	*B. suillus*	1.000	0.320
21	*F. mechowii*	*B. suillus*	0.025	10.514

APPENDIX 5.5. Test for equality of slopes and pairwise comparisons of RMA regressions for the periosteal module (diameters) of the humerus: Top, mediolateral diameter of the humerus (TDH). Bottom, anteroposterior diameter of the humerus (APDH). Abbreviations: body mass (BM) and body length (BL).

Results of multiple comparisons among groups (TDH x BM)				
Test for pair-wise difference in slope:			P-value : 6.4414e-06	
	Species_1	Species_2	p-value	TestStat
1	*H. argenteocinereus*	*G. capensis*	1.000	0.849
2	*H. argenteocinereus*	*F. damarensis*	0.868	2.841
3	*H. argenteocinereus*	*H. glaber*	0.990	1.653
4	*H. argenteocinereus*	*C. hottentotus*	0.675	3.772
5	*H. argenteocinereus*	*F. mechowii*	0.519	4.480
6	*H. argenteocinereus*	*B. suillus*	1.000	0.936
7	*G. capensis*	*F. damarensis*	1.000	0.942
8	*G. capensis*	*H. glaber*	1.000	0.316
9	*G. capensis*	*C. hottentotus*	0.004	13.854
10	*G. capensis*	*F. mechowii*	0.914	2.548
11	*G. capensis*	*B. suillus*	1.000	0.001
12	*F. damarensis*	*H. glaber*	1.000	0.018
13	*F. damarensis*	*C. hottentotus*	<0.001	28.005
14	*F. damarensis*	*F. mechowii*	0.999	1.081
15	*F. damarensis*	*B. suillus*	0.994	1.549
16	*H. glaber*	*C. hottentotus*	0.004	13.779
17	*H. glaber*	*F. mechowii*	1.000	0.810
18	*H. glaber*	*B. suillus*	1.000	0.415
19	*C. hottentotus*	*F. mechowii*	0.001	16.755
20	*C. hottentotus*	*B. suillus*	0.001	17.696
21	*F. mechowii*	*B. suillus*	0.814	3.128

Results of multiple comparisons among groups (TDH x BL)				
Test for pair-wise difference in slope:			P-value : 1.129e-06	
	Species_1	Species_2	p-value	TestStat
1	*H. argenteocinereus*	*G. capensis*	0.825	3.074
2	*H. argenteocinereus*	*F. damarensis*	1.000	0.933
3	*H. argenteocinereus*	*H. glaber*	0.999	1.235
4	*H. argenteocinereus*	*C. hottentotus*	0.407	5.052
5	*H. argenteocinereus*	*F. mechowii*	1.000	0.482
6	*H. argenteocinereus*	*B. suillus*	1.000	0.029
7	*G. capensis*	*F. damarensis*	1.000	0.074
8	*G. capensis*	*H. glaber*	1.000	0.267
9	*G. capensis*	*C. hottentotus*	<0.001	34.671
10	*G. capensis*	*F. mechowii*	1.000	0.539
11	*G. capensis*	*B. suillus*	0.050	9.194
12	*F. damarensis*	*H. glaber*	1.000	0.198
13	*F. damarensis*	*C. hottentotus*	0.689	3.712
14	*F. damarensis*	*F. mechowii*	1.000	0.328
15	*F. damarensis*	*B. suillus*	1.000	0.901
16	*H. glaber*	*C. hottentotus*	0.002	15.730
17	*H. glaber*	*F. mechowii*	1.000	0.085
18	*H. glaber*	*B. suillus*	0.978	1.909
19	*C. hottentotus*	*F. mechowii*	0.157	7.012
20	*C. hottentotus*	*B. suillus*	0.002	14.862
21	*F. mechowii*	*B. suillus*	1.000	0.521

Results of multiple comparisons among groups (APDH x BM)				
Test for pair-wise difference in slope:			P-value : 2.2259e-05	
	Species_1	Species_2	p-value	TestStat
1	*H. argenteocinereus*	*G. capensis*	1.000	0.411
2	*H. argenteocinereus*	*F. damarensis*	0.663	3.823
3	*H. argenteocinereus*	*H. glaber*	0.597	4.121
4	*H. argenteocinereus*	*C. hottentotus*	0.931	2.424
5	*H. argenteocinereus*	*F. mechowii*	0.969	2.051
6	*H. argenteocinereus*	*B. suillus*	0.447	4.839
7	*G. capensis*	*F. damarensis*	0.840	2.993
8	*G. capensis*	*H. glaber*	0.825	3.070
9	*G. capensis*	*C. hottentotus*	0.137	7.273
10	*G. capensis*	*F. mechowii*	0.999	1.073
11	*G. capensis*	*B. suillus*	0.621	4.013
12	*F. damarensis*	*H. glaber*	1.000	0.390
13	*F. damarensis*	*C. hottentotus*	<0.001	22.624
14	*F. damarensis*	*F. mechowii*	1.000	0.016
15	*F. damarensis*	*B. suillus*	1.000	0.527
16	*H. glaber*	*C. hottentotus*	0.001	16.520
17	*H. glaber*	*F. mechowii*	1.000	0.304
18	*H. glaber*	*B. suillus*	1.000	0.003
19	*C. hottentotus*	*F. mechowii*	0.052	9.120
20	*C. hottentotus*	*B. suillus*	<0.001	21.468
21	*F. mechowii*	*B. suillus*	1.000	0.322

Results of multiple comparisons among groups (APDH x BL)				
Test for pair-wise difference in slope:			P-value : 4.2286e-07	
	Species_1	Species_2	p-value	TestStat
1	*H. argenteocinereus*	*G. capensis*	0.046	9.354
2	*H. argenteocinereus*	*F. damarensis*	0.995	1.474
3	*H. argenteocinereus*	*H. glaber*	0.616	4.036
4	*H. argenteocinereus*	*C. hottentotus*	0.833	3.031
5	*H. argenteocinereus*	*F. mechowii*	1.000	0.001
6	*H. argenteocinereus*	*B. suillus*	0.970	2.037
7	*G. capensis*	*F. damarensis*	0.997	1.390
8	*G. capensis*	*H. glaber*	0.999	1.127
9	*G. capensis*	*C. hottentotus*	<0.001	33.747
10	*G. capensis*	*F. mechowii*	0.133	7.337
11	*G. capensis*	*B. suillus*	0.242	6.153
12	*F. damarensis*	*H. glaber*	1.000	0.169
13	*F. damarensis*	*C. hottentotus*	0.285	5.823
14	*F. damarensis*	*F. mechowii*	0.996	1.408
15	*F. damarensis*	*B. suillus*	1.000	0.074
16	*H. glaber*	*C. hottentotus*	<0.001	18.427
17	*H. glaber*	*F. mechowii*	0.717	3.585
18	*H. glaber*	*B. suillus*	1.000	1.024
19	*C. hottentotus*	*F. mechowii*	0.920	2.508
20	*C. hottentotus*	*B. suillus*	0.001	17.076
21	*F. mechowii*	*B. suillus*	0.984	1.803

APPENDIX 5.6. Test for equality of slopes and pairwise comparisons of RMA regressions for the periosteal module (diameters) of the ulna: Top, mediolateral diameter of the ulna (TDU). Bottom, anteroposterior diameter of the ulna (APDU). Abbreviations: body mass (BM) and body length (BL).

Results of multiple comparisons among groups (TDU x BM)				
Test for pair-wise difference in slope:			P-value : 0.0018976	
	Species_1	Species_2	p-value	TestStat
1	*H. argenteocinereus*	*G. capensis*	1.000	0.725
2	*H. argenteocinereus*	*F. damarensis*	1.000	0.481
3	*H. argenteocinereus*	*H. glaber*	0.845	2.967
4	*H. argenteocinereus*	*C. hottentotus*	0.999	1.218
5	*H. argenteocinereus*	*F. mechowii*	0.955	2.206
6	*H. argenteocinereus*	*B. suillus*	1.000	0.769
7	*G. capensis*	*F. damarensis*	1.000	0.140
8	*G. capensis*	*H. glaber*	0.984	1.801
9	*G. capensis*	*C. hottentotus*	0.051	9.136
10	*G. capensis*	*F. mechowii*	1.000	1.004
11	*G. capensis*	*B. suillus*	1.000	0.002
12	*F. damarensis*	*H. glaber*	0.804	3.175
13	*F. damarensis*	*C. hottentotus*	**0.029**	10.193
14	*F. damarensis*	*F. mechowii*	0.970	2.029
15	*F. damarensis*	*B. suillus*	1.000	0.179
16	*H. glaber*	*C. hottentotus*	**0.003**	14.407
17	*H. glaber*	*F. mechowii*	1.000	0.139
18	*H. glaber*	*B. suillus*	0.989	1.685
19	*C. hottentotus*	*F. mechowii*	**0.019**	10.955
20	*C. hottentotus*	*B. suillus*	0.048	9.256
21	*F. mechowii*	*B. suillus*	1.000	0.916

Results of multiple comparisons among groups (TDU x BL)				
Test for pair-wise difference in slope:			P-value : 1.6133e-07	
	Species_1	Species_2	p-value	TestStat
1	*H. argenteocinereus*	*G. capensis*	0.148	7.125
2	*H. argenteocinereus*	*F. damarensis*	1.000	0.188
3	*H. argenteocinereus*	*H. glaber*	0.904	2.622
4	*H. argenteocinereus*	*C. hottentotus*	0.994	1.531
5	*H. argenteocinereus*	*F. mechowii*	1.000	0.029
6	*H. argenteocinereus*	*B. suillus*	1.000	0.174
7	*G. capensis*	*F. damarensis*	1.000	1.031
8	*G. capensis*	*H. glaber*	0.997	1.365
9	*G. capensis*	*C. hottentotus*	**<0.001**	37.750
10	*G. capensis*	*F. mechowii*	0.108	7.733
11	*G. capensis*	*B. suillus*	**0.005**	13.668
12	*F. damarensis*	*H. glaber*	1.000	0.268
13	*F. damarensis*	*C. hottentotus*	0.998	1.283
14	*F. damarensis*	*F. mechowii*	1.000	0.121
15	*F. damarensis*	*B. suillus*	1.000	0.057
16	*H. glaber*	*C. hottentotus*	**0.002**	14.860
17	*H. glaber*	*F. mechowii*	0.873	2.814
18	*H. glaber*	*B. suillus*	0.813	3.134
19	*C. hottentotus*	*F. mechowii*	0.857	2.904
20	*C. hottentotus*	*B. suillus*	0.149	7.108
21	*F. mechowii*	*B. suillus*	1.000	0.076

Results of multiple comparisons among groups (APDU x BM)				
Test for pair-wise difference in slope:			P-value : 1.2292e-06	
	Species_1	Species_2	p-value	TestStat
1	*H. argenteocinereus*	*G. capensis*	1.000	0.221
2	*H. argenteocinereus*	*F. damarensis*	1.000	0.810
3	*H. argenteocinereus*	*H. glaber*	0.145	7.164
4	*H. argenteocinereus*	*C. hottentotus*	0.965	2.094
5	*H. argenteocinereus*	*F. mechowii*	0.377	5.223
6	*H. argenteocinereus*	*B. suillus*	1.000	0.783
7	*G. capensis*	*F. damarensis*	1.000	0.271
8	*G. capensis*	*H. glaber*	0.082	8.243
9	*G. capensis*	*C. hottentotus*	0.218	6.369
10	*G. capensis*	*F. mechowii*	0.352	5.373
11	*G. capensis*	*B. suillus*	1.000	0.256
12	*F. damarensis*	*H. glaber*	0.051	9.159
13	*F. damarensis*	*C. hottentotus*	**0.004**	13.814
14	*F. damarensis*	*F. mechowii*	0.388	5.162
15	*F. damarensis*	*B. suillus*	1.000	0.000
16	*H. glaber*	*C. hottentotus*	**<0.001**	29.856
17	*H. glaber*	*F. mechowii*	1.000	0.272
18	*H. glaber*	*B. suillus*	0.079	8.328
19	*C. hottentotus*	*F. mechowii*	**0.001**	17.583
20	*C. hottentotus*	*B. suillus*	**0.008**	12.614
21	*F. mechowii*	*B. suillus*	0.452	4.814

Results of multiple comparisons among groups (APDU x BL)				
Test for pair-wise difference in slope:			P-value : 2.814e-07	
	Species_1	Species_2	p-value	TestStat
1	*H. argenteocinereus*	*G. capensis*	0.151	7.088
2	*H. argenteocinereus*	*F. damarensis*	1.000	0.378
3	*H. argenteocinereus*	*H. glaber*	0.349	5.390
4	*H. argenteocinereus*	*C. hottentotus*	0.832	3.035
5	*H. argenteocinereus*	*F. mechowii*	1.000	0.606
6	*H. argenteocinereus*	*B. suillus*	1.000	0.007
7	*G. capensis*	*F. damarensis*	0.999	1.197
8	*G. capensis*	*H. glaber*	1.000	0.034
9	*G. capensis*	*C. hottentotus*	**<0.001**	30.271
10	*G. capensis*	*F. mechowii*	0.568	4.253
11	*G. capensis*	*B. suillus*	**0.001**	16.108
12	*F. damarensis*	*H. glaber*	1.000	0.935
13	*F. damarensis*	*C. hottentotus*	0.871	2.826
14	*F. damarensis*	*F. mechowii*	1.000	0.011
15	*F. damarensis*	*B. suillus*	1.000	0.406
16	*H. glaber*	*C. hottentotus*	**<0.001**	22.389
17	*H. glaber*	*F. mechowii*	0.839	3.001
18	*H. glaber*	*B. suillus*	**0.031**	10.071
19	*C. hottentotus*	*F. mechowii*	0.126	7.429
20	*C. hottentotus*	*B. suillus*	0.100	7.870
21	*F. mechowii*	*B. suillus*	1.000	0.989

APPENDIX 5.7. Test for equality of slopes and pairwise comparisons of RMA regressions for the periosteal module (diameters) of the femur: Top, mediolateral diameter of the femur (TDF). Bottom, anteroposterior diameter of the femur (APDF). Abbreviations: body mass (BM) and body length (BL).

Results of multiple comparisons among groups (TDF x BM)				
Test for pair-wise difference in slope :			P-value : 2.4359e-07	
	Species_1	Species_2	p-value	TestStat
1	*H. argenteocinereus*	*G. capensis*	0.989	1.679
2	*H. argenteocinereus*	*F. damarensis*	1.000	0.541
3	*H. argenteocinereus*	*H. glaber*	1.000	0.402
4	*H. argenteocinereus*	*C. hottentotus*	0.022	10.747
5	*H. argenteocinereus*	*F. mechowii*	1.000	0.948
6	*H. argenteocinereus*	*B. suillus*	1.000	0.258
7	*G. capensis*	*F. damarensis*	0.198	6.553
8	*G. capensis*	*H. glaber*	0.377	5.222
9	*G. capensis*	*C. hottentotus*	0.224	6.314
10	*G. capensis*	*F. mechowii*	0.263	5.986
11	*G. capensis*	*B. suillus*	0.991	1.626
12	*F. damarensis*	*H. glaber*	1.000	0.005
13	*F. damarensis*	*C. hottentotus*	<0.001	26.196
14	*F. damarensis*	*F. mechowii*	1.000	0.167
15	*F. damarensis*	*B. suillus*	0.710	3.617
16	*H. glaber*	*C. hottentotus*	<0.001	23.041
17	*H. glaber*	*F. mechowii*	1.000	0.190
18	*H. glaber*	*B. suillus*	0.928	2.450
19	*C. hottentotus*	*F. mechowii*	0.001	16.386
20	*C. hottentotus*	*B. suillus*	<0.001	20.560
21	*F. mechowii*	*B. suillus*	0.762	3.377

Results of multiple comparisons among groups (TDF x BL)				
Test for pair-wise difference in slope :			P-value : 4.091e-07	
	Species_1	Species_2	p-value	TestStat
1	*H. argenteocinereus*	*G. capensis*	1.000	0.270
2	*H. argenteocinereus*	*F. damarensis*	0.760	3.386
3	*H. argenteocinereus*	*H. glaber*	1.000	0.807
4	*H. argenteocinereus*	*C. hottentotus*	0.007	12.984
5	*H. argenteocinereus*	*F. mechowii*	1.000	0.018
6	*H. argenteocinereus*	*B. suillus*	0.972	2.006
7	*G. capensis*	*F. damarensis*	0.548	4.345
8	*G. capensis*	*H. glaber*	0.789	3.249
9	*G. capensis*	*C. hottentotus*	0.000	19.287
10	*G. capensis*	*F. mechowii*	1.000	0.085
11	*G. capensis*	*B. suillus*	0.972	2.005
12	*F. damarensis*	*H. glaber*	0.958	2.178
13	*F. damarensis*	*C. hottentotus*	0.045	9.395
14	*F. damarensis*	*F. mechowii*	0.748	3.443
15	*F. damarensis*	*B. suillus*	0.315	5.611
16	*H. glaber*	*C. hottentotus*	<0.001	28.182
17	*H. glaber*	*F. mechowii*	1.000	0.890
18	*H. glaber*	*B. suillus*	0.056	8.985
19	*C. hottentotus*	*F. mechowii*	0.101	7.860
20	*C. hottentotus*	*B. suillus*	0.003	14.626
21	*F. mechowii*	*B. suillus*	0.999	1.073

Results of multiple comparisons among groups (APDF x BM)				
Test for pair-wise difference in slope :			P-value : 1.838e-07	
	Species_1	Species_2	p-value	TestStat
1	*H. argenteocinereus*	*G. capensis*	1.000	0.038
2	*H. argenteocinereus*	*F. damarensis*	1.000	0.509
3	*H. argenteocinereus*	*H. glaber*	1.000	0.201
4	*H. argenteocinereus*	*C. hottentotus*	0.001	16.068
5	*H. argenteocinereus*	*F. mechowii*	1.000	0.165
6	*H. argenteocinereus*	*B. suillus*	1.000	0.596
7	*G. capensis*	*F. damarensis*	1.000	0.533
8	*G. capensis*	*H. glaber*	1.000	0.125
9	*G. capensis*	*C. hottentotus*	<0.001	25.936
10	*G. capensis*	*F. mechowii*	1.000	0.088
11	*G. capensis*	*B. suillus*	1.000	0.714
12	*F. damarensis*	*H. glaber*	1.000	0.132
13	*F. damarensis*	*C. hottentotus*	<0.001	21.983
14	*F. damarensis*	*F. mechowii*	1.000	0.114
15	*F. damarensis*	*B. suillus*	1.000	0.001
16	*H. glaber*	*C. hottentotus*	<0.001	25.858
17	*H. glaber*	*F. mechowii*	1.000	0.000
18	*H. glaber*	*B. suillus*	1.000	0.188
19	*C. hottentotus*	*F. mechowii*	0.002	15.090
20	*C. hottentotus*	*B. suillus*	<0.001	29.525
21	*F. mechowii*	*B. suillus*	1.000	0.153

Results of multiple comparisons among groups (APDF x BL)				
Test for pair-wise difference in slope :			P-value : 2.0822e-10	
	Species_1	Species_2	p-value	TestStat
1	*H. argenteocinereus*	*G. capensis*	1.000	0.666
2	*H. argenteocinereus*	*F. damarensis*	1.000	0.604
3	*H. argenteocinereus*	*H. glaber*	1.000	0.529
4	*H. argenteocinereus*	*C. hottentotus*	<0.001	21.023
5	*H. argenteocinereus*	*F. mechowii*	0.962	2.137
6	*H. argenteocinereus*	*B. suillus*	0.908	2.590
7	*G. capensis*	*F. damarensis*	1.000	0.230
8	*G. capensis*	*H. glaber*	0.593	4.139
9	*G. capensis*	*C. hottentotus*	<0.001	44.776
10	*G. capensis*	*F. mechowii*	0.334	5.488
11	*G. capensis*	*B. suillus*	0.008	12.528
12	*F. damarensis*	*H. glaber*	0.999	1.185
13	*F. damarensis*	*C. hottentotus*	0.233	6.229
14	*F. damarensis*	*F. mechowii*	0.964	2.113
15	*F. damarensis*	*B. suillus*	0.977	1.926
16	*H. glaber*	*C. hottentotus*	<0.001	26.383
17	*H. glaber*	*F. mechowii*	1.000	1.044
18	*H. glaber*	*B. suillus*	0.998	1.250
19	*C. hottentotus*	*F. mechowii*	0.214	6.401
20	*C. hottentotus*	*B. suillus*	<0.001	25.116
21	*F. mechowii*	*B. suillus*	1.000	0.137

APPENDIX 5.8. Test for equality of slopes and pairwise comparisons of RMA regressions for the periosteal module (diameters) of the tibio-fibula: Top, mediolateral diameter of the tibio-fibula (TDT). Bottom, anteroposterior diameter of the tibio-fibula (APDT). Abbreviations: body mass (BM) and body length (BL).

Results of multiple comparisons among groups (TDT x BM)				
Test for pair-wise difference in slope :			P-value : 0.00013146	
	Species_1	**Species_2**	**p-value**	**TestStat**
1	*H. argenteocinereus*	*G. capensis*	1.000	0.157
2	*H. argenteocinereus*	*F. damarensis*	1.000	0.036
3	*H. argenteocinereus*	*C. hottentotus*	0.314	5.039
4	*H. argenteocinereus*	*F. mechowii*	0.947	1.817
5	*H. argenteocinereus*	*B. suillus*	1.000	0.247
6	*G. capensis*	*F. damarensis*	1.000	0.651
7	*G. capensis*	*C. hottentotus*	0.149	6.515
8	*G. capensis*	*F. mechowii*	0.249	5.511
9	*G. capensis*	*B. suillus*	0.930	1.951
10	*F. damarensis*	*C. hottentotus*	0.017	10.582
11	*F. damarensis*	*F. mechowii*	0.830	2.533
12	*F. damarensis*	*B. suillus*	1.000	0.193
13	*C. hottentotus*	*F. mechowii*	<0.001	17.411
14	*C. hottentotus*	*B. suillus*	<0.001	18.197
15	*F. mechowii*	*B. suillus*	0.900	2.155

Results of multiple comparisons among groups (TDT x BL)				
Test for pair-wise difference in slope :			P-value : 0.0028005	
	Species_1	**Species_2**	**p-value**	**TestStat**
1	*H. argenteocinereus*	*G. capensis*	1.000	0.001
2	*H. argenteocinereus*	*F. damarensis*	0.940	1.878
3	*H. argenteocinereus*	*C. hottentotus*	0.107	7.138
4	*H. argenteocinereus*	*F. mechowii*	1.000	0.020
5	*H. argenteocinereus*	*B. suillus*	1.000	0.081
6	*G. capensis*	*F. damarensis*	0.940	1.874
7	*G. capensis*	*C. hottentotus*	0.009	11.814
8	*G. capensis*	*F. mechowii*	1.000	0.044
9	*G. capensis*	*B. suillus*	1.000	0.202
10	*F. damarensis*	*C. hottentotus*	0.502	4.003
11	*F. damarensis*	*F. mechowii*	0.927	1.973
12	*F. damarensis*	*B. suillus*	0.910	2.088
13	*C. hottentotus*	*F. mechowii*	0.097	7.328
14	*C. hottentotus*	*B. suillus*	0.005	12.747
15	*F. mechowii*	*B. suillus*	1.000	0.020

Results of multiple comparisons among groups (APDT x BM)				
Test for pair-wise difference in slope :			P-value : 0.00062306	
	Species_1	**Species_2**	**p-value**	**TestStat**
1	*H. argenteocinereus*	*G. capensis*	0.841	2.477
2	*H. argenteocinereus*	*F. damarensis*	1.000	0.007
3	*H. argenteocinereus*	*C. hottentotus*	0.868	2.336
4	*H. argenteocinereus*	*F. mechowii*	0.865	2.354
5	*H. argenteocinereus*	*B. suillus*	1.000	0.313
6	*G. capensis*	*F. damarensis*	0.612	3.505
7	*G. capensis*	*C. hottentotus*	0.002	14.548
8	*G. capensis*	*F. mechowii*	1.000	0.073
9	*G. capensis*	*B. suillus*	0.831	2.527
10	*F. damarensis*	*C. hottentotus*	0.386	4.600
11	*F. damarensis*	*F. mechowii*	0.774	2.799
12	*F. damarensis*	*B. suillus*	1.000	0.423
13	*C. hottentotus*	*F. mechowii*	0.053	8.453
14	*C. hottentotus*	*B. suillus*	0.011	11.381
15	*F. mechowii*	*B. suillus*	0.926	1.977

Results of multiple comparisons among groups (APDT x BL)				
Test for pair-wise difference in slope :			P-value : 4.6605e-05	
	Species_1	**Species_2**	**p-value**	**TestStat**
1	*H. argenteocinereus*	*G. capensis*	0.445	4.285
2	*H. argenteocinereus*	*F. damarensis*	0.940	1.873
3	*H. argenteocinereus*	*C. hottentotus*	0.809	2.638
4	*H. argenteocinereus*	*F. mechowii*	1.000	0.282
5	*H. argenteocinereus*	*B. suillus*	1.000	0.000
6	*G. capensis*	*F. damarensis*	1.000	0.668
7	*G. capensis*	*C. hottentotus*	<0.001	25.174
8	*G. capensis*	*F. mechowii*	0.995	1.104
9	*G. capensis*	*B. suillus*	0.020	10.247
10	*F. damarensis*	*C. hottentotus*	0.718	3.044
11	*F. damarensis*	*F. mechowii*	0.987	1.322
12	*F. damarensis*	*B. suillus*	0.936	1.903
13	*C. hottentotus*	*F. mechowii*	0.648	3.351
14	*C. hottentotus*	*B. suillus*	0.199	5.958
15	*F. mechowii*	*B. suillus*	1.000	0.395

APPENDIX 5.9. Test for equality of slopes and pairwise comparisons of RMA regressions for the periosteal module (diameters) for intralimb comparisons. Top: forelimb comparisons. Bottom: hindlimb comparisons.

Results of multiple comparisons among groups (TDU vs TDH)				
Test for pair-wise difference in slope :			P-value : 0.0042965	
	Species_1	Species_2	p-value	TestStat
1	*H. argenteocinereus*	*G. capensis*	1.000	1.008
2	*H. argenteocinereus*	*F. damarensis*	1.000	0.831
3	*H. argenteocinereus*	*H. glaber*	1.000	0.480
4	*H. argenteocinereus*	*C. hottentotus*	1.000	0.750
5	*H. argenteocinereus*	*F. mechowii*	1.000	0.264
6	*H. argenteocinereus*	*B. suillus*	1.000	0.089
7	*G. capensis*	*F. damarensis*	**0.010**	12.211
8	*G. capensis*	*H. glaber*	1.000	0.066
9	*G. capensis*	*C. hottentotus*	1.000	0.053
10	*G. capensis*	*F. mechowii*	0.878	2.783
11	*G. capensis*	*B. suillus*	0.999	1.130
12	*F. damarensis*	*H. glaber*	0.479	4.677
13	*F. damarensis*	*C. hottentotus*	**0.023**	10.626
14	*F. damarensis*	*F. mechowii*	1.000	0.066
15	*F. damarensis*	*B. suillus*	0.600	4.109
16	*H. glaber*	*C. hottentotus*	1.000	0.008
17	*H. glaber*	*F. mechowii*	0.990	1.652
18	*H. glaber*	*B. suillus*	1.000	0.319
19	*C. hottentotus*	*F. mechowii*	0.939	2.362
20	*C. hottentotus*	*B. suillus*	1.000	0.729
21	*F. mechowii*	*B. suillus*	1.000	0.909

Results of multiple comparisons among groups (APDU vs APDH)				
Test for pair-wise difference in slope :			P-value : 0.016757	
	Species_1	Species_2	p-value	TestStat
1	*H. argenteocinereus*	*G. capensis*	0.994	1.536
2	*H. argenteocinereus*	*F. damarensis*	0.988	1.716
3	*H. argenteocinereus*	*H. glaber*	1.000	0.004
4	*H. argenteocinereus*	*C. hottentotus*	1.000	0.120
5	*H. argenteocinereus*	*F. mechowii*	1.000	0.327
6	*H. argenteocinereus*	*B. suillus*	0.784	3.273
7	*G. capensis*	*F. damarensis*	1.000	0.003
8	*G. capensis*	*H. glaber*	0.991	1.630
9	*G. capensis*	*C. hottentotus*	0.462	4.765
10	*G. capensis*	*F. mechowii*	0.803	3.184
11	*G. capensis*	*B. suillus*	1.000	0.566
12	*F. damarensis*	*H. glaber*	0.980	1.891
13	*F. damarensis*	*C. hottentotus*	0.199	6.547
14	*F. damarensis*	*F. mechowii*	0.747	3.449
15	*F. damarensis*	*B. suillus*	1.000	0.911
16	*H. glaber*	*C. hottentotus*	1.000	0.214
17	*H. glaber*	*F. mechowii*	1.000	0.445
18	*H. glaber*	*B. suillus*	0.702	3.651
19	*C. hottentotus*	*F. mechowii*	1.000	0.134
20	*C. hottentotus*	*B. suillus*	0.055	9.020
21	*F. mechowii*	*B. suillus*	0.401	5.087

Results of multiple comparisons among g			TDT vs TDF	
Test for pair-wise difference in slope :			P-value : 0.035831	
	Species_1	Species_2	p-value	TestStat
1	*H. argenteocinereus*	*G. capensis*	0.734	2.974
2	*H. argenteocinereus*	*F. damarensis*	1.000	0.007
3	*H. argenteocinereus*	*C. hottentotus*	0.936	1.905
4	*H. argenteocinereus*	*F. mechowii*	1.000	0.047
5	*H. argenteocinereus*	*B. suillus*	0.955	1.741
6	*G. capensis*	*F. damarensis*	0.051	8.527
7	*G. capensis*	*C. hottentotus*	1.000	0.235
8	*G. capensis*	*F. mechowii*	0.847	2.446
9	*G. capensis*	*B. suillus*	1.000	0.632
10	*F. damarensis*	*C. hottentotus*	0.287	5.225
11	*F. damarensis*	*F. mechowii*	1.000	0.142
12	*F. damarensis*	*B. suillus*	0.234	5.632
13	*C. hottentotus*	*F. mechowii*	0.978	1.478
14	*C. hottentotus*	*B. suillus*	1.000	0.045
15	*F. mechowii*	*B. suillus*	0.987	1.311

Results of multiple comparisons among g			APDT vs APDF	
Test for pair-wise difference in slope :				
	Species_1	Species_2	p-value	TestStat
1	*H. argenteocinereus*	*G. capensis*	0.751	2.900
2	*H. argenteocinereus*	*F. damarensis*	0.894	2.187
3	*H. argenteocinereus*	*C. hottentotus*	0.003	13.539
4	*H. argenteocinereus*	*F. mechowii*	0.478	4.121
5	*H. argenteocinereus*	*B. suillus*	0.758	2.871
6	*G. capensis*	*F. damarensis*	1.000	0.028
7	*G. capensis*	*C. hottentotus*	0.068	7.989
8	*G. capensis*	*F. mechowii*	0.998	0.892
9	*G. capensis*	*B. suillus*	1.000	0.021
10	*F. damarensis*	*C. hottentotus*	0.103	7.225
11	*F. damarensis*	*F. mechowii*	0.996	1.023
12	*F. damarensis*	*B. suillus*	1.000	0.003
13	*C. hottentotus*	*F. mechowii*	0.999	0.834
14	*C. hottentotus*	*B. suillus*	0.017	10.542
15	*F. mechowii*	*B. suillus*	0.994	1.124

CHAPTER 6

Comparative Bone Microstructure and Bone Modeling of African Mole-Rats

"The bony matrix records the effects of circumstances of growth on bone, the influence of the environment and feeding habits, microscopic changes reflecting the gross shape of individual bones, the longevity of the individual, and the many other factors…"

"Phylogenetic as well as ontogenetic studies have not yet been carried out in adequate detail within restricted groups, and such investigations are strongly urged."

Donald Enlow, 1969
THE BONE OF REPTILES

6.1 INTRODUCTION

In the skeletal system, the process responsible for changes in its shape (development) and size (growth) is bone modeling (Frost, 1969, 1987; Parfitt, 2010; Allen & Burr, 2014, also see Ch. 5 for its allometric quantification). Bone modeling involves formation and resorption of bone tissues, processes which are not necessarily coupled (Frost, 1963, 1969, 1987; Parfitt, 2010; Allen & Burr, 2014). This process is equivalent to Enlow's term "growth remodeling" (Enlow, 1962).

Descriptions of patterns of bone modeling in mammals are quite scarce (e.g. Smith, 1960; Enlow, 1963; Goldman *et al.*, 2009; Montoya-Sanhueza & Chinsamy, 2017), and only few of them include the histomorphometric quantification of its bone dynamics (e.g. Sontag, 1986; Erben, 1996; Montoya-Sanhueza & Chinsamy, 2017). Similarly, most studies have focused on single species, with only primates receiving considerably more attention at family level (e.g. McFarlin, 2006, Warshaw, 2008, McFarlin *et al.* 2016). Yet, several decades ago already Enlow (1969) said, "*Phylogenetic as well as ontogenetic studies have not yet been carried out in adequate detail within restricted groups, and such investigations are strongly urged*." It is essential that in order to advance our understanding of bone growth mechanisms and its structural dimensions, it is a necessary to consider the analysis of specific animal groups (Enlow, 1969), as well as a wider breath of non-model organisms with unique phenotypes (e.g. Franz-Odendaal & Hockman, 2019).

A recent study assessing molecular adaptations in bathyergids have found a series of positively selected genes accounting for the expression of metabolism,

aging, reproduction and morphological features (Davies *et al.*, 2015). These authors suggested that the development of mineralized structures in bathyergids have a genetic component, especially for "*odontogenesis, positive regulation of osteoblast differentiation, regulation of bone resorption, biomineral tissue development and regulation of bone remodeling*" (Davies *et al.* 2015; pp. 3095). Despite the role of certain genes on the development of the skeletal system in mammals (Hall, 1978; 2015), other external epigenetic postnatal factors such as diet, behavior, biomechanical load and/or reproduction can also play a role in the final shape of bones (e.g. Cameron & McClure, 1988; Boag & Boonstra, 1988; Zelditch, 2005; Minelli, 2015; Montoya-Sanhueza & Chinsamy, 2017). Thus, most organs integrate organ-extrinsic cues (e.g. nutritional status, mechanical loading) with organ-intrinsic information (e.g. genetic programs, local signals) into a growth response that adapts to changing environmental conditions and ensures that the size and shape of an organ are coordinated with the rest of the body (Roselló-Díez & Joyner, 2015). However, it is not completely known how these factors interact during prenatal stages of development or during regulation of bone (re)modeling in postnatal stages.

One of the most remarkable features reported for some bathyergid species in the last 10 years are their high bone compactness (thick cortical walls) and scarce bone resorption throughout life, which resulted in a positively imbalanced mineral metabolism with low levels of bone loss during life (osteopenia) (e.g. Pinto *et al.*, 2010; Montoya-Sanhueza & Chinsamy, 2017, 2018; Carmeli-Ligati *et al.*, 2019). The process of cortical thickening, including high mineral bone density (BMD) is genetically regulated in mammals such as rodents and humans (Beamer *et al.*, 1996; Roselló-Díez & Joyner, 2015), so similar regulation factors for the skeletal system of bathyergids is expected.

6.1.1 Factors Regulating Bone Modeling

Bone modeling is a mechanism which has a strong physiological and biomechanical regulation, and more specifically by endocrine and load-bearing factors (Hall, 2015). It is known that increased mechanical load and activity are important stimulators of bone formation, as well as inhibitors of bone resorption (e.g. Burger & Veldhuijzen, 1993; Whedon & Heaney, 1993; Hillam & Skerry, 1995; Carter *et al.* 1996; Carter & Beaupre, 2001). Mechanical factors also have important effects on bone growth during early ontogeny (e.g. Hillam & Skerry, 1995; Turner, 2004; Baron & Horne, 2005). Thus, because of different loads, bone structure and tissue distribution (bone geometry) will result in a specific phenotype. For example, bones having the same cross-sectional area but different moments of inertia (i.e. a measure of bone geometry) will be the product of different mechanical loads such as bending or torsion (Pinto *et al.*, 2010). Nevertheless, mechanical loads are not only exerted by load-bearing processes, but also by muscle activity, which has strong effects on bone growth and geometry, even in prenatal life (e.g. Sharir *et al.*, 2011; Felsenthal & Zelzer, 2017). For instance, in the absence of mechanical loads during embryogenesis, the osteoblast distribution around the bone diaphysis is altered, producing changes in the final shape of the bone (becoming more circular), which leads to the development of mechanically

inferior bones (Sharir *et al.*, 2011). The cellular components responsible of such alterations during postnatal bone modeling are osteoblasts and osteoclasts, which can alter proliferation, self-renewal, differentiation, matrix production and mineralization (Genetos & Jacobs, 2013). Thus, deciphering how bone modeling and its components work and interact, is fundamental to understand the adaptive ability of bones, as well as how they were positively selected.

In this chapter, the main objective is to compare the bone microstructure of African mole-rats during postnatal ontogeny to determine the patterns of bone modeling among species. It is hypothesized that due to differences in external bone morphology among bathyergids, they will show different bone modeling patterns (in each bone), which will be evidenced by different composition of bone tissue matrices (histodiversity). Additionally, species with higher bone growth rates (depicted from Ch. 5) will show increased amounts of rapidly deposited bone tissues (i.e. woven bone, compact coarse cancellous bone and perhaps parallel-fibered bone tissues), while species with slow growth rates will show predominance of slowly deposited bone tissues (lamellar bone, lamellated bone, and perhaps parallel-fibered bone tissues). Due to the relevance of the pectoral girdle and forelimb bones during excavation and burrow construction, the humerus and ulna will show faster growth rates as compared to hindlimb bones.

Two main methodologies are implemented to understand the similarities and differences in the pattern of postnatal bone modeling in four species of bathyergids. The study of bone growth and development can be addressed using static or dynamic histological methodologies. Both are based on the visualization of histological sections from decalcified or undecalcified bone samples throughout the microscope. Static histology record parameters of the bone at one point in time in the life of the individual, while dynamic histology (and dynamic histomorphometry) can record cellular activity and its effects on the bone matrices during a defined period of time (Stout & Crowder, 2012; Allen & Burr, 2014). These methodologies will focus principally on histological descriptions of the intramembranous module (i.e. periosteal osteogenesis in the diaphysis of long bones).

Bone modeling in bathyergids has been previously assessed only in *B. suillus* (Montoya-Sanhueza & Chinsamy, 2017). Additionally, the physiology of African mole-rats with low metabolic rates and specific thermoregulatory capabilities, are also considered to have an impact on the morphogenesis of the periosteal module. Due to the extent of this study, for first time analyzing the bone microstructure and bone modeling of a complete rodent family, a discussion considering the implications of bone modeling and remodeling in rodents is also included in this chapter.

6.2 MATERIAL AND METHODS

A total of 133 individuals of both sexes, including four species were studied: *Heterocephalus glaber* (n = 83), *Heliophobius argenteocinereus* (n = 30), *F. mechowii* (n = 30) and *Cryptomys hottentotus natalensis* (n = 10). The study sample comprises a wide range of ontogenetic stages (newborns, pups, juveniles, subadults and adults). Forelimb (humerus, ulna and radius) and hindlimb bones (femur and

tibia-fibula) from either right or left side were studied. In social species, since reproductive specimens are represented by one or a couple of individuals, the descriptions are based mainly on subordinates, unless the contrary is indicated.

The study of bone growth and development can be addressed using dynamic or static histomorphometric methodologies. Both are based on the visualization of histological sections from decalcified or undecalcified bone samples under light microscopy. Static methodologies record parameters of the bone at one point in time, while dynamic analyses can record cellular activity and its effects on the bone matrices during a defined period (Stout & Crowder, 2012; Allen & Burr, 2014).

6.2.1 Dynamic Bone Histology

In vivo bone labelling is the most common technique used for assessing bone dynamics and growth rates. This is typically carried out by using fluorochrome labels (antibiotics), that are incorporated in to the organism and bound to calcium during active mineralization, i.e. osteogenesis (Frost, 1969; Allen & Burr, 2014). Two social bathyergid species were studied, *Heterocephalus glaber* (n = 10) and *Cryptomys hottentotus natalensis* (n = 10). These species were obtained from colonies maintained by Prof. Nigel Bennett at the University of Pretoria (UP). *H. glaber* was selected due to its extraordinary features among mammals, specifically because is usually considered a poikilothermic organism (Buffenstein & Yahav, 1991), while *C. h. natalensis* because represents a generalized and well-studied bathyergid genera (Bennett, 2009). Reproductive and non-reproductive (subordinate) individuals of both sexes were injected multiple times with fluorochromes. Reproductive specimens were included in the analysis to assess the effects of attainment of sexual maturity on bone microstructure. To identify the specimens within colonies, the specimens of *H. glaber* were marked with Pit tags injected subcutaneously, so that a code is available for each individual. For *C. h. natalensis,* the colonies were kept in individual containers and specimens were marked with ink in different parts of their bodies, so that they could be recaptured for subsequent injections.

To monitor bone deposition over an extended period, different fluorochrome injections were administrated every 3-4 months: Engemycin-Oxytetracycline (10%) (Ot), Alizarin (complexone) red (Ar) and Calcein (Cn). The first fluorochrome produces yellowish fluorescence, the second one red fluorescence and the third one green fluorescence. This sequence permitted tracking of bone formation along almost an annual cycle.

After the last injection (Cn), the animals were euthanized within two weeks following the protocol suggested for wild mammals by the "Guidelines of the American Society of Mammalogists" and the "American Veterinary Medical Association – AVMA" (Sikes *et al.*, 2011; Leary *et al.*, 2013). All procedures were carried out on the premises of the UP and by a certified veterinary practitioner. All experiments performed in this project are under the regulation and approval of the Animal Ethics Committee (AEC – UP), under the project "*Skeletal Biology of African mole-rats (Bathyergidae): morphology and ontogeny*", number EC024-17 (PI: G. Montoya-Sanhueza; Supervisor: Prof. N. Bennett).

However, in the following descriptions, only Ar and Cn will be described, since out of the 18 specimens injected with three fluorochromes (+2 controls), none of them registered the first Ot label. Similarly, in a parallel trial consisting of two specimens of *Heliophobius argenteocinereus* also injected with Ot, this fluorochrome was not registered. It is likely that this flurochrome was not assimilated by the individuals or that this antibiotic had a problematic administration that affected all specimens. Further assessment of this antibiotic on bone labeling is required to verify its specificity in mole-rats. Nonetheless, for these reasons, the histological descriptions of this study only focused on the last two labels, the Ar and Cn and are here onwards called "the first injection" (corresponding to Ar) and "the last injection" (corresponding to Cn). Additionally, most of the labeled specimens showed endogenous fluorescence (orange/red) in internal and external contours, which is not associated to the experimental labeling performed in this study (see Fig. 6.3).

This analysis will significantly contribute to the identification of the patterns of bone modeling in bathyergids, such as areas of active bone formation, types of bone tissues deposited and/or cyclicity during bone apposition. This methodology will also help to confirm the origin (endosteal or periosteal) of certain bone tissues that are difficult to track in unlabeled sections (static histology) due to their ambiguous position within the cortex.

6.2.2 Static Bone Histology

Static histology is usually used for the qualitative description of histological features such as presence of osteons, vascularization, cortical drift, bone remodeling, determination of tissue types and age estimation at one point in time. The qualitative description of the bone histology and general microanatomy was identified following Enlow (1963), Francillon-Vieillot *et al.* (1990), Bromage *et al.* (2003) and Chinsamy-Turan (2005, 2012). This nomenclature is based mainly on osteocyte shape and size, mineralized collagen fiber matrix orientation, tissue types and vascularization (e.g. orientation and relative density of canals within the bone). The general shape of the cross-section and size of the medullary cavity were also described (Fig. 6.1). Osteocyte shape and vascular orientation were easily identified under conventional transmitted light, while the pattern of mineralization of the collagen fibers was determined using polarized light microscopy and a gypsum (¼ lambda) plate.

The descriptions are focused on determining intra-element ontogenetic differences among specimens, as well as inter-element differences in individuals. These differences are based on distinctions of the pattern of bone modeling such as appearance of simple vascular canals on bone surfaces, recent bone deposits, resorptive bone surfaces (irregular margins with obliterated areas on the matrices), as well as the presence of cement lines (resting or resorption lines). Patterns of bone modeling followed the experimental and descriptive work of Enlow (1963), Frost (1987), Parfitt *et al.* (1987), Goldman *et al.* (2009) and Parfitt (2010). Since the long bones of bathyergids are composed of thick cortical walls with a diverse arrangement of bone tissues, it is preferable to describe such features considering a compartmentalization of the cortex, i.e. three regions occupying proportional

sectors of the cortex, from internal to external surfaces: endocortical, intracortical and pericortical (Fig. 6.1) (Allen & Burr, 2014).

6.2.3 Preparation of Undecalcified Cross-Sections

Undecalcified thin sections permit a more precise identification of the tissues under polarized light microscope due to the differential orientation of the mineralized collagen fibers (Bromage *et al.* 2003). Standard undecalcified histological procedures (Chinsamy & Raath, 1992) were used to obtain the thin sections for both the dynamic and static bone histology. The midshaft of the diaphysis was selected for comparative purposes since this region is directly implicated with the mechanical behavior of the bone when exposed to different loads and strains, thus allowing to observe the pure axial effects of a tubular structure (Carter & Beaupré, 2001; Brianza *et al.* 2006). This is especially relevant in animals performing parasagittal movements such as scratch-digging species, which are expected to undergo higher bending stresses in this bone region than animals with normal (cursorial or ambulatory) locomotion (Hildebrand, 1985; Biewener & Taylor, 1986; Carter & Beaupré, 2001; Leppänen *et al.*, 2006). In the humerus, the presence of a deltoid tubercle in the midshaft (50% of the bone length) of most bathyergid species (Fig. 6.1, see details in Fig. 4.1, 4.5 in Ch. 4,), affected the tubular cross-sectional geometry of this bone, so the sectioning was performed below this structure (Fig. 1A, B). Studies in other vertebrates have also showed that the midshaft is usually not extensively remodeled and/or resorbed, thus recording the most complete sequence of the ontogenetic development (e.g. Chinsamy-Turan, 2005; Kriloff *et al.* 2008; García-Martínez *et al.* 2011; Quémeneur *et al.* 2013; Montoya-Sanhueza & Chinsamy, 2017).

Transverse sections from the mid-diaphysis were prepared at i) ~50% of the total length from the proximal articular surface of the ulna and femur (and humerus of naked mole-rats, which lacked the development of a deltoid crest), ii) below deltoid tubercle in the humerus of all species (except naked mole-rats), and iii) at the proximal tibio-fibular junction of the tibio-fibula (Fig. 4.4). Thin sections of ~80 – 100 μm thickness were obtained, and high-quality photomicrographs were taken with a Nikon Eclipse E200 Polarizing Microscope and the polarizing Microscope Axio Lab A1 (Department of Biological Sciences - UCT). Further details of the preparations are reported elsewhere (Montoya-Sanhueza, 2014; Montoya-Sanhueza & Chinsamy, 2017). The flurochrome labels were detected using confocal fluorescence microscopy (Zeiss LSM 880 Confocal - Fast AiryScan Technology) at the Confocal and Light Microscope Imaging Facility (Faculty of Health Sciences - UCT).

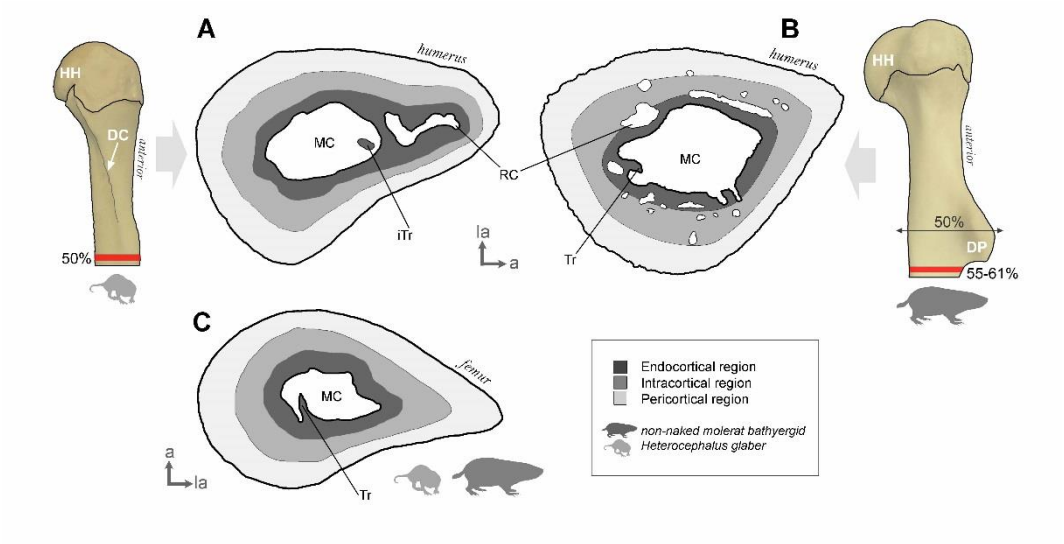

FIGURE 6.1. Long bone cross-sections and main microstructural features described in this study (for humerus and femur). A) Lateral view of the humerus of *Heterocephalus glaber* cut at the 50% from the proximal articular surface (red band), showing the deltoid crest (DC), as well as its generalized bone microanatomy with characteristic elongated shape. B) Lateral view of the humerus of a generalized bathyergid (excluding naked mole-rats), showing the 50% location from the proximal articular surface (double arrowed lined) and the actual 55-61% location where the bones were cut (red band). These percentages vary according to the species (see Table 4.4 in Ch. 4). C) Bone microanatomy of the femur of a generalized bathyergid (including naked mole-rats). Three cortical regions (indicated in shades of gray) were loosely defined in terms of proportional location within the cortex (see Montoya-Sanhueza & Chinsamy, 2017). *Abbreviations*: anterior (a), lateral (la), medullary cavity (MC), resorption cavity (RC), trabeculae (Tr) and isolated trabeculae (iTr) within the MC. Bone cross-sections are not to scale.

6.3 RESULTS

The focus of this chapter is to describe the patterns of bone modeling in limb bones of AMs. Two major sections are included: bone labeling and comparative ontogenetic bone histology. The results of two taxa (*Heterocephalus glaber* and *Cryptomys hottentotus natalensis*) injected with fluorochromes are reported first (bone labeling), and then the detailed bone microstructure of *Heterocephalus glaber*, *Heliophobius argenteocinereus* and *Fukomys mechowii* is described. Each taxon is dealt with separately, and descriptions for each element are described separately.

6.3.1 Bone Labeling

6.3.1.1 *Heterocephalus glaber* (Naked Mole-Rats)

***Body size*.** Figure 6.2 indicates that the body sizes of the specimens studied here (n = 6) are intermediate as compared to the largest and smaller specimens of the total number of individuals that formed part of the complete study (n = 67). Note that the sample included several specimens of known age (triangles in Fig. 6.2). Thus, it can be observed that the specimens treated with fluorochromes had already reached general somatic maturity.

Humeral bone modeling. Most specimens showed thick cortical walls with relatively small MCs. However, the reproductive queen (#506) showed thinner cortical walls and increased cortical porosity, especially in the anterior side of the bone. In general, the bone microanatomy was similar in all specimens, i.e. more or less triangular in shape and elongated towards the anterolateral region (Fig. 6.1 and 6.3), with the medial side being usually concave while the lateral side being convex. Some trabeculae are associated with the endocortical region and sometimes appear isolated within the MC (Fig. 6.3). The bone tissue distribution is quite similar among specimens, showing disorganized tissues in the anterior region (e.g. WB and CCCB). Nonetheless, PFB and PLB were also observed in lateral, medial and posterior sides of the bone. No major histological differences were found among the subordinate specimens. Similarly, the histology of the specimens did not correlate with body size, although one specimen, the #511 showed higher levels of bone formation as compared to the rest (Fig. 6.3D).

All fluorochrome labels were found associated with the endocortical and intracortical regions, with no labels found in the pericortical region (Fig. 6.1 and). This contrasts with the fluorochrome activity found in the periosteal region of the femur (see below), implying that periosteal growth in the humerus ceased before than in the femur. Most bone formation also appeared to be associated with trabeculae in the MC, as well as on the medial side of the endocortical region and in the anterior side of the intracortical region. Most labels correspond to lamellar bone depositions. Endosteal bone resorption was observed on the lateral side. The data suggest that in individuals of intermediate body size, the humerus grows slowly towards the lateral side of the diaphysis.

Ulnar bone modeling. All the specimens showed similar microanatomical (tear-drop) shape. This consisted of thick cortical walls and a small MC. The MC did not show trabeculae. The ulna appeared to be the thickest element among all the limb bones studied. In general, the cortex consisted of mostly PFB and LB, although some patches of WB were also observed. The anterior and posterior sides of the bone were mostly composed of PFB and PLB. Sharpey's fibers were associated with margins of these areas.

Only three individuals showed anabolic activity (#507, #510 and #511) in the ulna. Most bone formation was detected in the posterior side of the endocortical region and associated with LB deposition. In general, this element showed a lower level of bone formation as compared to the humerus (and femur). Considering this, and that only three specimens showed bone formation, it is probably that the ulna may have ceased growth before than stylopodial elements, thus suggesting slower growth rates for this bone during adulthood in comparison to stylopodial elements. This may be related to lower degrees of mineral homeostasis in zeugopodial elements, which may represent either lower bone turnover or unbalanced bone modeling due to higher bone loss. Nevertheless, no significant signs of bone resorption were observed in this bone. Considering the scarce presence of resorption cavities and the scarce osteoblastic activity, this bone seems to have a rather stable mineral homeostasis during these ontogenetic stages, which could be related to functional aspects of the arm. However, the analysis of the ulna of the queen (#506) showed higher levels of intracortical porosity.

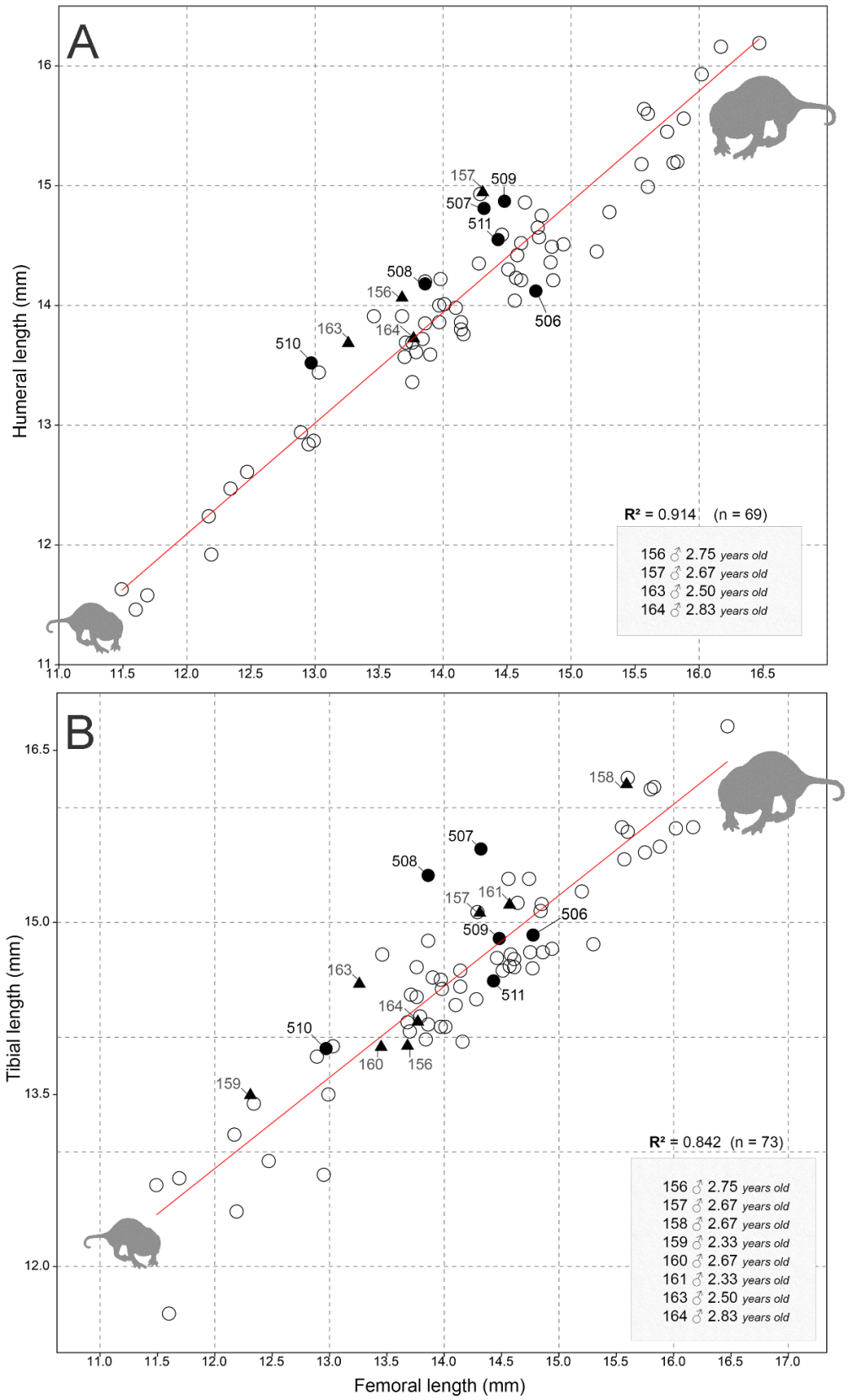

FIGURE 6.2. Scatterplots of limb bone measurements of subordinate naked mole-rats (*Heterocephalus glaber*) for comparison of body sizes. Reduced major axis regressions of humeral (A) and tibial length (B) against femoral length. The sample includes specimens injected with fluorochromes (black circles) and the other specimens not injected (white circles), which includes specimens of known age (triangles).

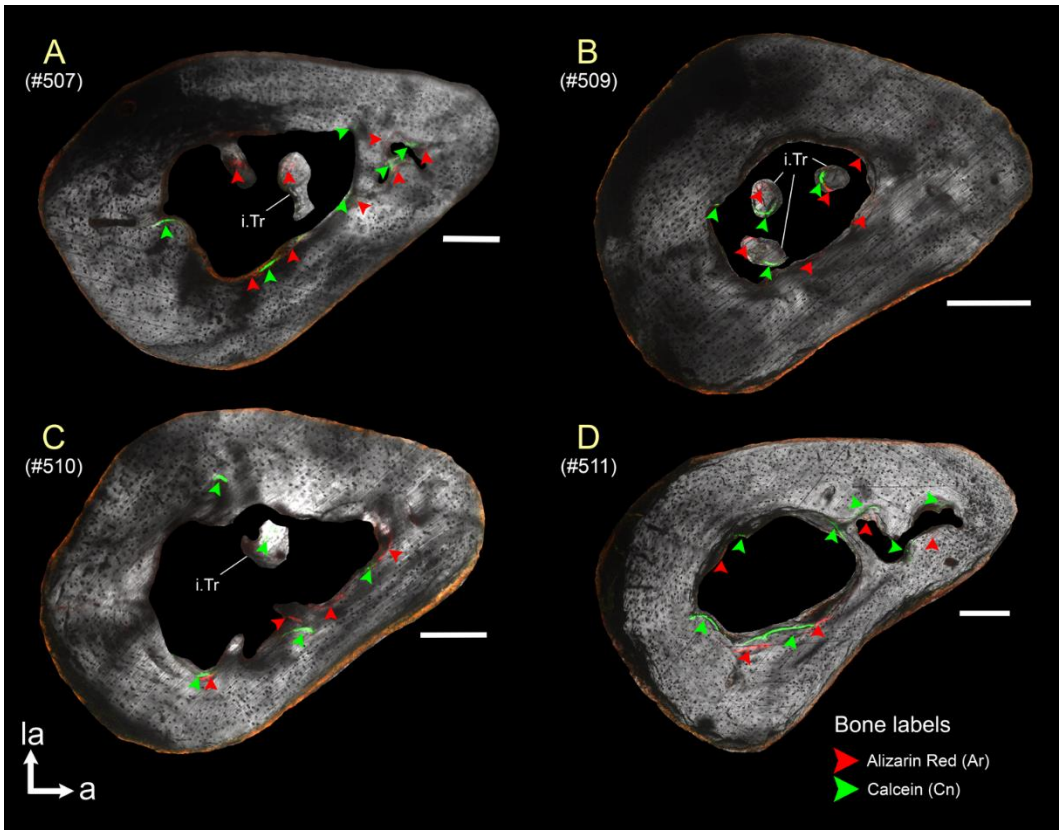

FIGURE 6.3. Fluorochrome double labels in the humerus of *Heterocephalus glaber* (observed by confocal fluorescence microscopy). All specimens are females (A, #507; B, #509; C, #510; D, #511). The internal and external contours of some bones showed endogenous fluorescence in orange/red (see text). Abbreviations: (a) anterior; (la) lateral, (i.Tr) isolated trabeculae. Scale bars = 200 µm.

Femoral bone modeling. All specimens showed similar bone microanatomy, with thick cortical walls and relatively small MC. The lateral side of the bone is clearly defined as a pointy projection. This bone showed more variability in the types of bone tissues observed as compared to the humerus. Most of the cortex is composed of PFB, ELB and PLB. Radial vascularization was more evident.

The most active (anabolic) regions were detected in trabeculae and endocortical regions (medial and lateral sides) (Fig. 6.4). However, most of the fluorochrome bone labels were recorded in the endocortical region, and some of them in the pericortical region, in the region of the tip of the lateral side of bone, close to the distal origin of the third trochanter. Endocortical resorption was more evident in the anteromedial region. These labels indicate a trend of bone deposition towards the lateral side in adults.

Tibial bone modeling. The bone microanatomy of this bone was the most variable among elements analyzed, ranging from circular to ellipsoidal to irregular (triangular). Nevertheless, all specimens showed thick cortical walls and a relatively small MC. The cortex was composed of PFB, PLB and ELB, with some patches of WB.

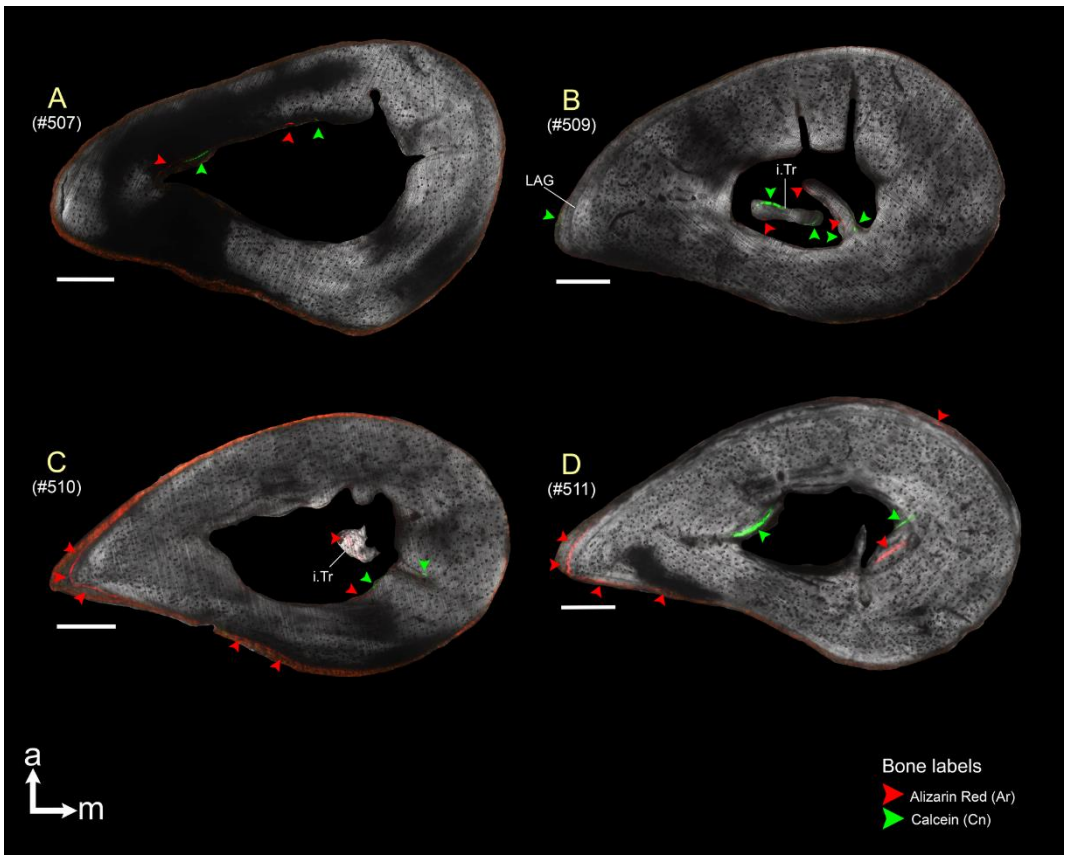

FIGURE 6.4. Fluorochrome double labels in the femur of *Heterocephalus glaber* (observed by confocal fluorescence microscopy). All specimens are females (A, #507; B, #509; C, #510; D, #511). Note the line of arrested growth (LAG) in the lateral tip of the specimen #509. The internal and external contours of some bones showed endogenous fluorescence in orange/red (see text). Abbreviations: (a) anterior; (m) medial, (i.Tr) isolated trabeculae. Scale bars = 200 µm.

In this bone, mostly Cn was observed in endocortical regions, although the specimen #511 appeared to form bone in localized areas of the pericortical region. This bone also seems to show lower bone formation rates as compared to the femur (and humerus). One explanation for this is that imbalance bone modeling occurs in this bone (i.e. higher bone resorption is present in the tibia), although no signs of extensive resorption were observed. This indicates that the tibia has scarce bone loss, like the ulna. This data suggests that zeugopodial bones have a more neutral bone homeostasis, so bone turnover is comparatively lower than seen in stylopodial bones, and this is probably related to the earlier attainment of skeletal maturity hypothesized for these distal elements.

6.3.1.2 *Cryptomys hottentotus natalensis* (Natal Mole-Rats)

Body size. The specimens of *C. h. natalensis* studied here (n = 10) were representative of larger body sizes of the complete sample of *C. hottentotus* included in this study (n = 53, Fig. 6.5). The Figure 6.5 shows the distribution of the fluorochrome labeled specimens based on bone lengths. The sample of *C. h. natalensis* included specimens of known age: #520 and #521 were 18 months old

and were born in captivity (Fig. 6.5), while the other Natal mole-rats were captured in the field.

Humeral bone modeling. The specimens showed different stages of bone modeling. Specimens showed relatively thick cortical walls and large MCs, with the anterior side having thicker cortical walls, and the posterior side being much thinner. Trabeculae were observed, sometimes crossing the MC (Fig. 6.6G). The humeral bone microanatomy was quite variable (Fig. 6.6), which can be explained by the differences in bone modeling. The mediolateral diameter appears to be slightly wider than the anteroposterior diameter (Fig. 6.6).

All injected specimens showed at least one label, five showed only one label and three individuals showed two labels (all females). The largest specimens (two males) showed only the last injection of Calcein (Cn). Two small males showed only the Alizarin red (Ar) label. The females, which were the smaller individuals of the sample showed two bone labels (Ar and Cn).

Fluorochrome labels were mostly found in the endocortical and intracortical regions of the bone, especially on the anterior side (Fig. 6.6B-G). Labels associated with the pericortical region were found in a few individuals and usually associated with the posterior side of the bone (Fig. 6.6 B, E, G). Considering all the specimens, these labels formed a clear pattern of bone growth: the anterior part of the humerus grows mostly by endosteal bone apposition, evidenced by an intracortical label of Ar (first injection) (Fig. 6.6E), usually followed by a label of Cn (last injection) in the endocortical region. This indicates a clear trend for cortical drift towards the anterior side, in the direction of the projection of the deltoid tubercle. Similarly, the labels observed in the anterior region were irregular in shape, following the contour of the endosteal surface. The bone tissues observed in the anterior region were mostly WB, CCCB and ELB. The finding of CCCB in this region is most likely a result of trabecular bone compaction associated with the development of the deltoid tubercle. This indicates that CCCB can also been found in the mid-diaphysis by action of endochondral ossification occurring in the deltoid tubercle.

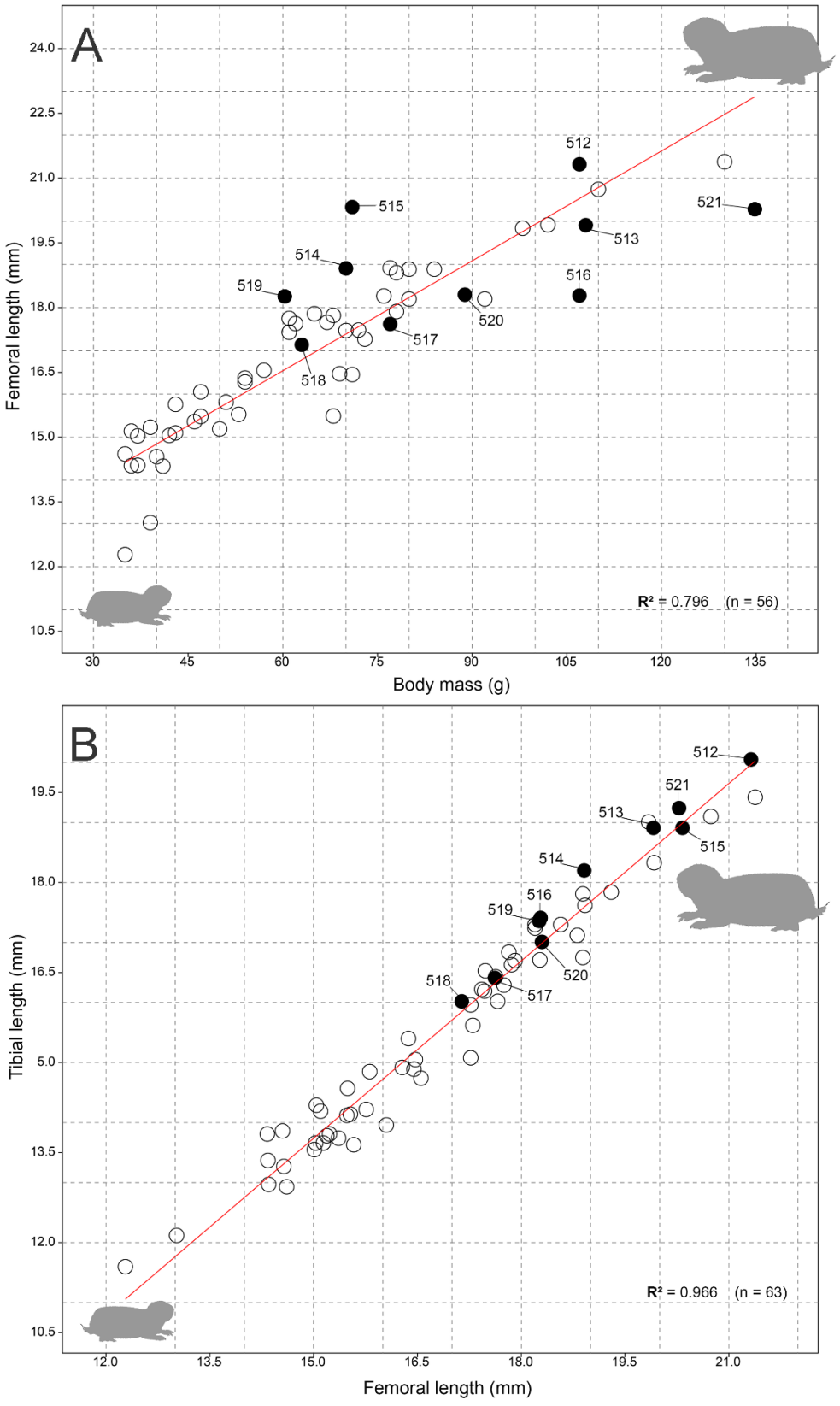

FIGURE 6.5. Scatterplots of limb bone measurements for comparison of body sizes between the Natal mole-rat (black circles - *Cryptomys hottentotus natalensis*) and the common mole-rat (hollow circles - *C. hottentotus*). Reduced major axis regressions of femoral length against body mass (BM) (A) and humeral length against femoral length (B). The sample includes specimens injected with fluorochromes (black circles) and non-injected specimens (white circles). The specimens #520♀ and #521♂ are 18 months old and were born in captivity.

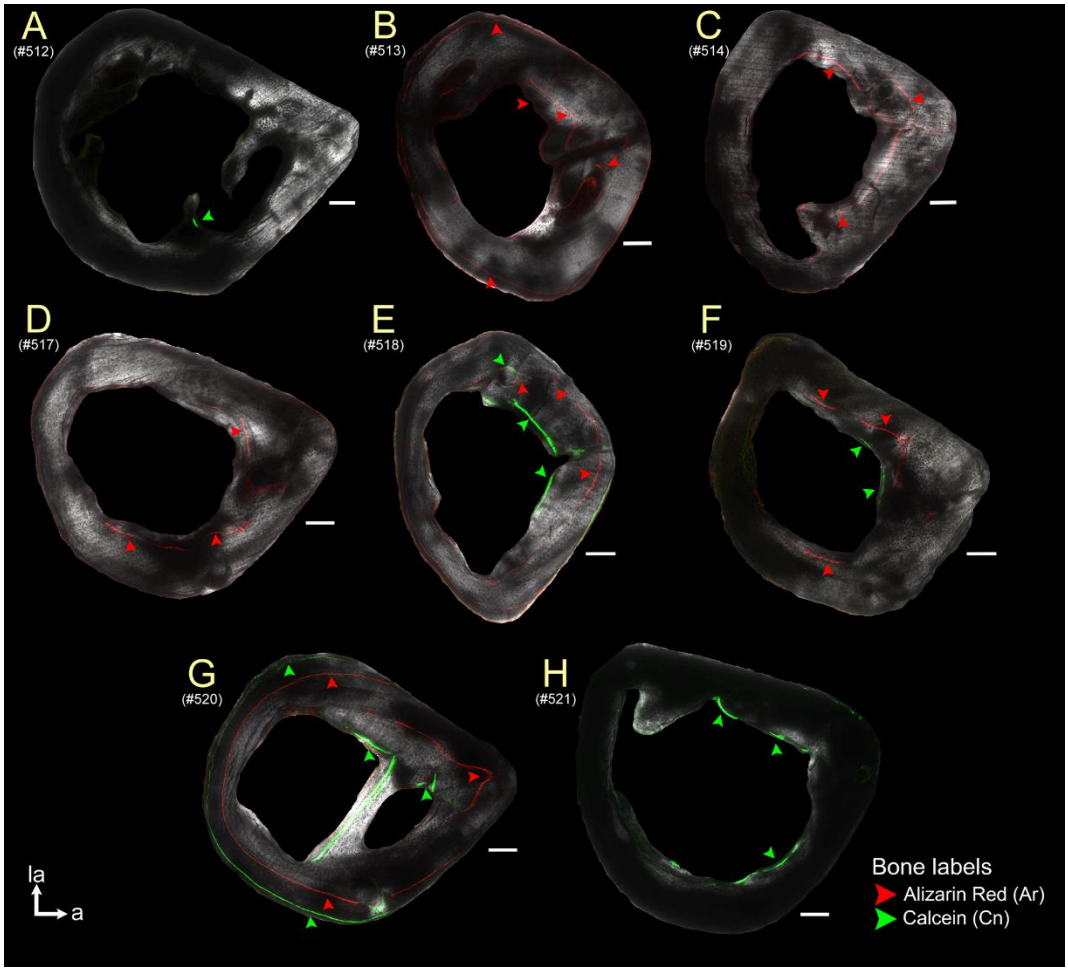

FIGURE 6.6. Fluorochrome double labels in the humerus of *Cryptomys hottentotus natalensis* (observed by confocal fluorescence microscopy). Males (A-C and H) and Females (D-G). The internal and external contours of some bones showed endogenous fluorescence in orange/red (see text). Abbreviations: (a) anterior; (la) lateral. Scale bars = 200 μm.

Ulnar bone modeling. The specimens showed different stages of bone modeling. This bone showed thicker cortical walls as compared to the humerus of the same individual. The MC lacks trabeculae. The posterior side is usually slightly thicker than the anterior side, whereas the medial and lateral sides are thinner. The bone microanatomy and MC are ellipsoidal.

Four specimens showed only one label and three specimens showed both labels, which are all females (Ar and Cn). Considering all the specimens, these labels showed that the bone grows mostly in the anterior and posterior regions. The specimens #518, #519 and #520 showed the clearest bone labels.

Femoral bone modeling. The specimens showed different stages of bone modeling (Fig. 6.7). Generally, this bone showed thick cortical walls and large MCs. No trabeculae were observed. All sides of the bone were relatively similar in thickness. The bone microanatomy and MC are ellipsoidal. Some specimens (3) showed only one flurochrome (either Ar or Cn). Three specimens showed both labels, which are all females (Ar and Cn) (Fig. 6.7). Fluorochrome labels showed endosteal and periosteal bone formation. The specimens #518, #519 and #520 showed the clearest bone labels. Endosteal bone apposition occurred mostly

isometrically around the MC (Fig. 6.7A-F), while periosteal bone growth occurs towards the posterolateral direction (Fig. 6.7F). This growth pattern matches the description of previous studies of *B. suillus* (Montoya-Sanhueza & Chinsamy, 2017). Some specimens showed only the last injection, indicating that bone apposition did not occur at the time of the injection of Ar or because of other factors such as low dosage may have affected the appropriate attachment of the fluorochromes to the bone. In the first case, this would suggest that bone growth was resumed later in ontogeny.

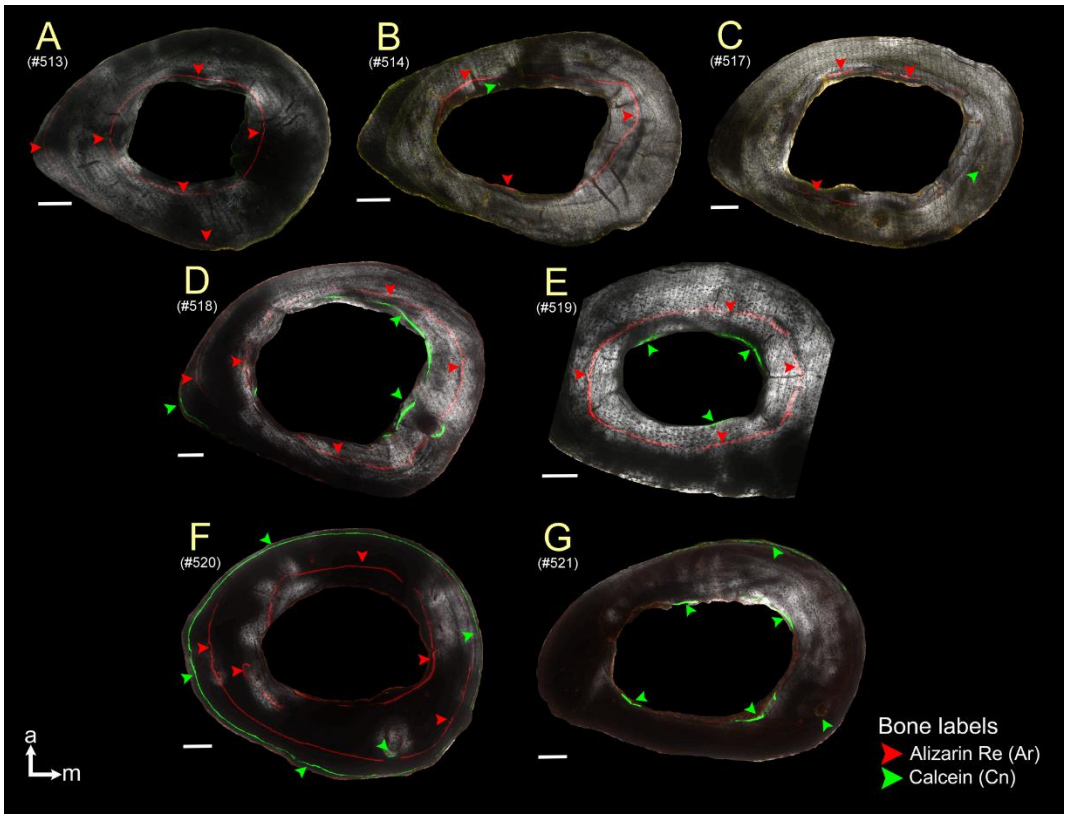

Figure 6.7. Fluorochrome double labels in the femur of *Cryptomys hottentotus natalensis* (observed by confocal fluorescence microscopy). Males (A-B and G) and Females (C-F). The internal and external contours of some bones showed endogenous fluorescence in orange/red (see text). Abbreviations: (a) anterior; (m) medial. Scale bars = 200 µm.

Tibio-fibular bone modeling. The specimens showed different stages of bone modeling. The tibia and fibula were fused in all specimens, although both bones are still clearly differentiated in the cross-sections. The tibia showed thick cortical walls and a well-defined MC, while the fibula is elongated and is significantly smaller in size, usually with an occluded MC. All sides of the bone wall of the tibia were relatively similar in thickness. The fibula fuses to the posterolateral side of the tibia, so that the general microanatomy of this fused bone results in a tear-drop shape. Some specimens showed trabeculae in the tibia, as well as uneven endosteal surfaces. Five specimens showed only one label (either Ar or Cn), and only two specimens showed both labels, which are all females (Ar and Cn). Fluorochrome labels showed endosteal and periosteal bone formation. The

specimens #518 and #520 showed the clearest bone labels. Endosteal and periosteal bone apposition occurred mostly isometrically around bone surfaces.

6.3.2 Comparative Ontogenetic Bone Microstructure

Ontogenetic sequences are described for each taxon separately, first giving a general description of their bone microstructure, and then describing each bone separately during ontogeny.

6.3.2.1 *Heliophobius argenteocinereus*

The sample studied here comprises pups, juveniles and adults of known age from 1 month to 12 years old (n = 30). Thus, the sample encompasses a complete postnatal ontogenetic sequence and a wide range of body sizes.

During the perinatal period, the cortical walls are thick, and the MC is incompletely formed. At this point in bone development, the midshaft microanatomy of the different bones already resembles the general shape of the adults, except for the ulna which differs from the irregular shape of the adults and being subcircular in newborns (Fig. 6.8). The bone matrix is composed of highly vascularized WB (#165-167, Fig. 6.8A). In general, forelimb bones have larger cross-sectional areas as compared to the hindlimb bones. in zeugopodial bones, the MC is formed first, indicating advanced endosteal resorption in these elements. In juveniles, the bone has grown considerably in size from the newborn size, but the cortical walls become thin and the MC shows a considerable expansion in all the bones studied. In juveniles, the ulna and tibia thicken first as compared to the humerus and femur, respectively. The femur seems to be the most delayed in terms of cortical thickening (both in terms of periosteal and endosteal apposition), while the tibia has comparatively smaller MCs sizes than the femur. The ulna also shows growth marks (zonal bone) during juvenile stages. Additionally, from juvenile stages onwards, all the long bones become thicker during ontogeny, and the MC becomes relatively smaller for each bone (Fig. 6.8B). In advanced juvenile stages, thick cortical walls are observed in all bones, although the ulna and tibia showed the thickest cortical walls, and the humerus and femur the least thick. The cortex of juveniles typically showed a homogenous bone tissue composition, comprising mostly of a predominance of PFB and LB, whereas CCCB was not commonly observed in most bones (Fig. 6.8B). The cortex also lacks a dense vascularization, although they showed high cellularity (i.e. high osteocyte density) (Fig. 6.8B). The adults showed variable degrees of cortical thickening, but in general they showed thick cortical walls, and most of the cortex is composed of slowly deposited and highly organized bone tissues (ELB and PLB) (Fig. 6.8C).

In the humerus, cortical walls are thick but not as thick as in the ulna or femur. Endosteal surfaces showed high levels of bone resorption in juveniles, sometimes including a high degree of trabecularization of the endocortical region, so the MC is often not well defined. Endosteal margins become more even and lined by a thin layer of ELB during later stages of ontogeny. The growth of the humerus is marked by the development of the DP, which showed increased intracortical porosity as compared to other regions of the bone and a mixture of bone tissues, including WB, LB and CCCB (Fig. 6.8C). Longitudinal and radial

vascularization are present, but in general they are rather scarce. This lack of vascularization seems to be countered by the high cellularity found in general in all bones. In adults, the lateral side shows more radial canals embedded in a matrix of PFB + PLB, while the medial side has almost no vascularization and is predominantly composed of slowly deposited bone tissues (LB), including LAGs (Fig. 6.8C). In adults, the posterior side shows zonal bone, mostly composed of PFB and LB forming GMs (Fig. 6.8C).

During perinatal stages, the midshaft cross sections of the ulna has a rather circular microanatomy, which becomes ellipsoidal during late stages of perinatal life. The growth pattern of the ulna is quite marked from early life to adulthood: the anterior side is thick and composed of highly vascularized WB, whereas the posterior side is composed of the same matrix, but the bone wall is thinner. Contrarily, the mediolateral aspect grew proportionally less, with one side having reticular vascularization, while the other side is highly compacted with LB. This growth pattern occurs throughout ontogeny and results in the formation of zonal bone in the posterior region (with alternating layers of PFB and LB) with an intracortical layer of WB/CCCB and longitudinal vascularization (i.e. vascularization in the posterior region of the ulna runs parallel to the long axis). This zonal bone can be of two types according to the ontogenetic stage: i) bands of PFB with LB annuli in older stages, and/or ii) bands of WB with thin layers ("annuli") of PFB in younger stages. The anterior side shows a mixture of bone tissues (including CCCB and PLB) and high amount of Sharpey's fibers (SF). The latter probably indicates the interosseous ligament that connects the radius to the ulna. This is observed from early ontogeny. In adulthood, the anterior side is slightly thinner than the posterior cortical wall, indicating that the posterior region continued growing throughout ontogeny, and that the anterior region probably stopped growing due to its proximity to the radius. The mediolateral aspect is clearly identified because the medial side tends to be convex and it is composed predominantly of ELB, whereas the lateral side is rather concave and composed of WB, indicating a slight cortical drift towards the medial side.

The femur grew towards the posterolateral side, and sometimes showed a less marked cortical drift as compared to other species (e.g. *B. suillus*), probably due to the lesser development of the third trochanter. However, other specimens showed a marked cortical drift, although this did not involve localized reduction in cortical thickness in some sides of the section. This means that marked cortical drift can be present without involving a detriment in the thickness of some sides of the bone, and that endosteal bone formation can considerably counteract the resorption occurring on the periosteal surface of that side. No Haversian bone tissue was observed in any bone, and in fact *H. argenteocinereus* showed scarce osteonal development.

The tibia is unfused to the fibula in perinatal specimens, but the fusion occurs in the late juvenile stages, and it is associated with the posterior side of the tibia. In juveniles, the microanatomy of these bones is circular in the tibia and ellipsoidal in the fibula. The region of fusion of these bones is composed of LB. When fusion occurs, both bones maintain independent MCs, although the fibula loses its own MC later in ontogeny, although sometimes some small cavities remain. In general, the MC of the tibia is well-developed and has even margins

throughout ontogeny. The tibio-fibula has relatively thick cortical walls. The cortex is composed of LB with scarce vascularization, while the anterior section (in tibia) is composed of WB with some radial canals. The cortex of the fibula is composed of PFB. In adults, a layer of PLB is observed around the tibio-fibula. Both bones showed high cellularity. Radial and longitudinal vascularization are observed mostly in the tibia, whereas the fibula is rather avascular. Few osteons are observed in the tibia.

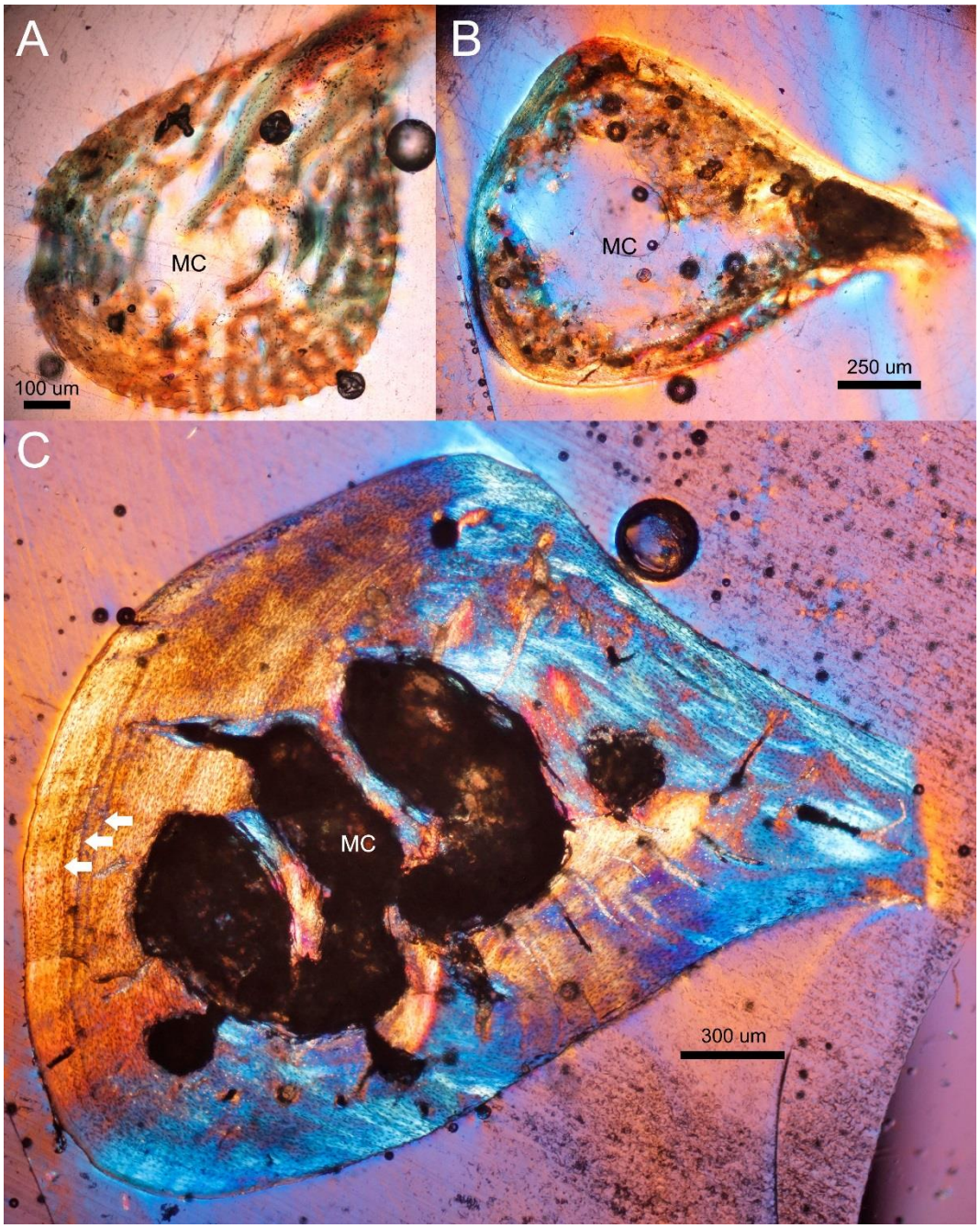

FIGURE 6.8. General humeral bone microstructure of perinatal (A: #165), juvenile (B: #167) and adult (C: #174) *Heliophobius argenteocinereus*. Arrows indicate three lines of arrested growth (LAGs). Abbreviations: MC, medullary cavity.

6.3.2.2 *Fukomys mechowii*

The sample studied here comprises perinatal specimens, juveniles and adults of known age from one day old to 13 years old (n = 30). This sample encompasses a complete postnatal ontogenetic sequence and includes a wide range of body sizes.

Newborns (one day old) specimens showed thick cortical walls with a poorly-developed MC. The bone microanatomy of most bones is generally circular, although the humerus and ulna already showed their main triangular and ellipsoidal shapes, respectively (#196, Fig. 6.9). All bones showed highly vascularized WB matrices, and the endosteal margin is highly trabecularized. Vascularization is mostly laminar in organization. Isometric bone expansion is predominant in most bones, although the ulna already shows a tendency for growing in the anteroposterior regions. Around one month old, specimens had considerably larger bones in terms of cross-sectional area but showed a similar bone matrix composition (highly vascularized WB), although they were less vascularized (#208, Fig. 6.9). At this stage, the MC is more developed and relatively defined by an endocortical region with more organized bone tissues (ELB). This layer of ELB is clearer in the ulna, whereas the rest of the bones have a variable development of this layer. In the femur, the anterior side shows a clear lamellar (LB) organization under polarized light, while the posterior side shows a rapidly growing vascularized WB matrix (#208, Fig. 6.9A). By 4 months, the specimens show differences in the development of the fore- and hindlimbs. The hindlimb bones develop a clear band of ELB around the MC (Fig. 6.9B), whereas the forelimb bones show a less developed (thinner) ELB (#212). This is probably related to the scarce endosteal bone resorption in the hindlimbs, as well as a higher medullary expansion (resorption) of the humerus and ulna. One-year old specimens already show the main gross morphology of the adult phenotype, but are still growing, with no evident endosteal expansion of the MC, indicating that endocortical bone resorption is limited. ELB is deposited and periosteal growth occurs in all bones. The humerus show the highest intracortical porosity among all bones. The bone thickness at this stage is not as high as compared to other species of solitary bathyergids of similar age (e.g. *B. suillus*). Old mature specimens (about 10 years old) showed all bones with thick cortical walls and intact cortices, i.e. without extensive resorption (Fig. 6.9C), except the humerus which it is known to have higher intrinsic intracortical porosity as compared to the other bones (Montoya-Sanhueza & Chinsamy, 2017). In general, the humerus was the larger bone in cross-sectional area in early ontogeny as compared to the ulna, femur and tibia. However, in late ontogeny, the femur is slightly larger in size. Similarly, the midshaft cross-sectional area of the ulna appears larger in early ontogeny as compared to the tibia but is surpassed in size later in life by the tibia. This data suggests higher growth rates in stylopodial elements as compared to zeugopodial elements, although larger bones showed higher intracortical porosity. Forelimbs also seem to show accelerated growth during early ontogeny, which allow them to reach somatic maturity earlier than hindlimbs. Hindlimbs continue growing slowly during life, reaching higher amounts of bone deposition, probably associated to lower bone resorption of these bones.

With respect to the fusion of the tibia and fibula, these bones fuse early in ontogeny, before four days old (#202, Fig. 6.9). The bone surfaces that become

fused are composed of PFB/PLB. It is possible that the fusion occurs because both bones grow towards each other. Ontogenetically earlier staged specimens showed that the growth direction of the tibia was towards the lateral side (Fig. 6.9), so towards the fibula, although the fibula shows a more isometric growth. None of the specimens showed Haversian tissue, but randomly distributed small secondary osteons are present.

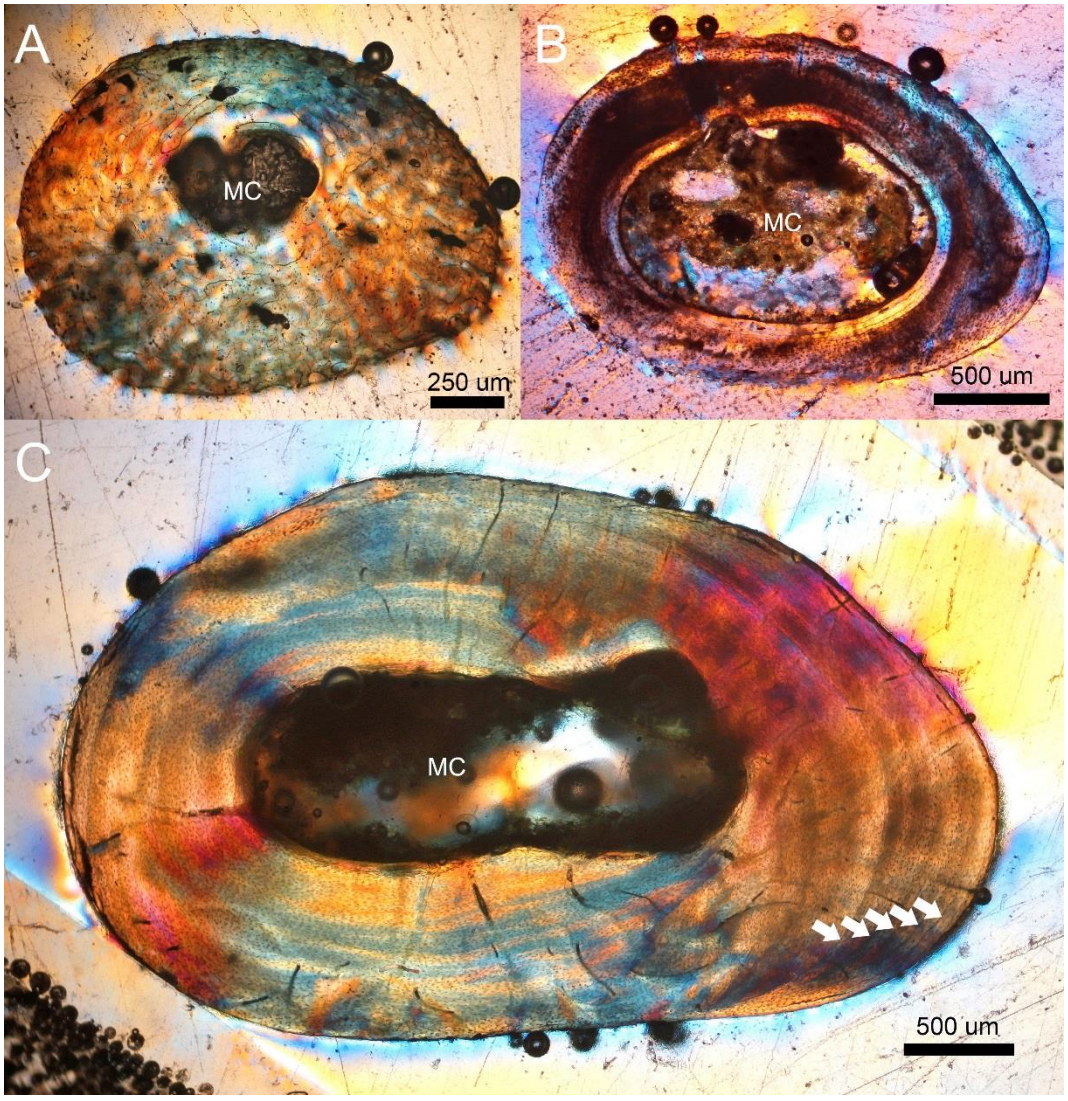

FIGURE 6.9. General femoral bone microstructure of perinatal (A: #202), juvenile (B: #214) and adult (C: #219) *Fukomys mechowii*. Arrows indicate five lines of arrested growth (LAGs). Abbreviations: MC, medullary cavity.

6.3.2.3 *Heterocephalus glaber*

The sample studied here comprises juveniles, as well as subordinate and reproductive adults (n = 60; Fig. 6.2). Some individuals are of known age (Fig. 6.2), and the complete sample comprises a wide range of body sizes (Fig. 6.2).

Individuals of ~4 months old have all bones with thin cortical walls composed of WB and an enlarged MC. No vascularization is observed. The midshaft bone microanatomy of all bones already resembles the general shape of

the adults (Fig. 6.10), although the ulna and tibia have a less differentiated and rather ellipsoidal shape as compared to the adult phenotype. In juveniles, bone thickening occurs especially in zeugopodial elements which show slightly thicker cortical walls than the stylopodial elements. However, at this stage of bone development, the zeugopodial elements have reached their adult microanatomy (#046Fig. 6.10B). In general, the bones grow isometrically from all periosteal bone surfaces and no extensive bone resorption is observed, although the humerus shows more intracortical resorption on the anterolateral side. At this stage, the humerus and femur are similar in shape and the bone matrix indicates similar growth rates during early ontogeny. Some small specimens showed lamellar bone deposits in the endosteal and periosteal regions, indicating that the bone tissue composition changes to a more organized matrix in advanced juveniles. Lamellar bone is variably deposited depending on the bone and region of the cross-section. In the humerus, LB is associated with the endocortical region of the medial side. The anterolateral side of adult bones show a mixture of bone tissues, mostly WB and CCCB (Fig. 6.10C). This region has an irregular periosteal surface, with some longitudinal canals. The concave form of the lateral side of the humerus is still not well-developed. The ulna already shows its adult morphology and is composed of a mixture of bone tissues including LB, PFB and WB. The lateral (concave) side is mostly composed of WB, while the medial side shows zonal bone including bands of WB and PLB (annuli). The anteromedial region is mostly composed of PLB. The femur showed considerable amounts of PLB in the posterior and lateral sides, whereas WB was still observed in the anterior and medial sides. Similarly, ELB also occurs in the anterior and medial regions. This indicates that the growth of the femur occurs towards the posterolateral side, as observed in *B. suillus* (Montoya-Sanhueza & Chinsamy, 2017). The transition between WB and LB depositions is observed clearly in the tibia as well. During ontogeny, the amount of LB in the cortex increases in all bones although remnants of WB, CCCB and PFB can also be observed. In general, secondary osteons (SOs) were limited to 1-3 per bone (Fig. 6.12).

In the humerus, skeletally mature specimens 28 months old (2.33 years) have a more quadrilateral (robust) shape and a reduced MC, with a layer of ELB and endosteal resorption in some areas. Some trabeculae are observed (Fig. 6.3). Thick cortical walls show higher degree of radial vascularization, especially in lateral and posterior sides (Fig. 6.10C). The anterolateral side can show RCs, probably associated with the deltopectoral crest running along the shaft (Fig. 6.10C). Vascularization is in general composed of thin (and unbranched) simple canals. The anterior side show more SFs and a mixture of bone tissues (e.g. WB, CCCB and PFB) with extremely high bone cellularity. LAGs and annuli are observed in the lateral side running around the posterior side. The medial side has more SFs subperiosteally, and some lamellated bone is also observed in subendosteal regions (Fig. 6.10B). The largest individuals show similar bone microstructure to previous ontogenetic stages although some limited endosteal resorption can be observed. The anterolateral side of the bone shows more intracortical resorption, with large RCs (Fig. 6.10C).

In the femur, skeletally mature specimens 34 months old (2.83 years) have thick cortical walls and relatively small MC, although endosteal resorption can be

observed in some specimens. No differentiated layer of ELB can be observed and the endosteal margin is under resorption in some areas. The cortex is composed of mostly subperiosteal PFB, especially on anterior side, although some layers of LB are also observed on the posterior side, as well as in the endocortical and pericortical regions. These regions consist of clear lamellated bone. Bundles of Sharpey's fibers are associated with the periosteal margin of the posterior side. Radial vascularization is observed in the anterior region of the cortex. The tip of the lateral region of the cross-section is composed of LB and show several LAGs. No trabeculae are observed. Apart from the increased bone resorption in some regions and the appearance of intracortical radial and longitudinal vascular canals and small RCs, minimal microstructural changes are observed in older specimens.

The tibia has a subcircular shape in cross-section, with thick cortical walls and a relatively small MC with no trabeculae. The cortex is composed of WB and predominantly PFB, as well as lamellated bone. The bone shows high cellularity in general and no apparent vascularization. A layer of ELB is observed surrounded by a resorption line (RL). This bone also presents several LAGs.

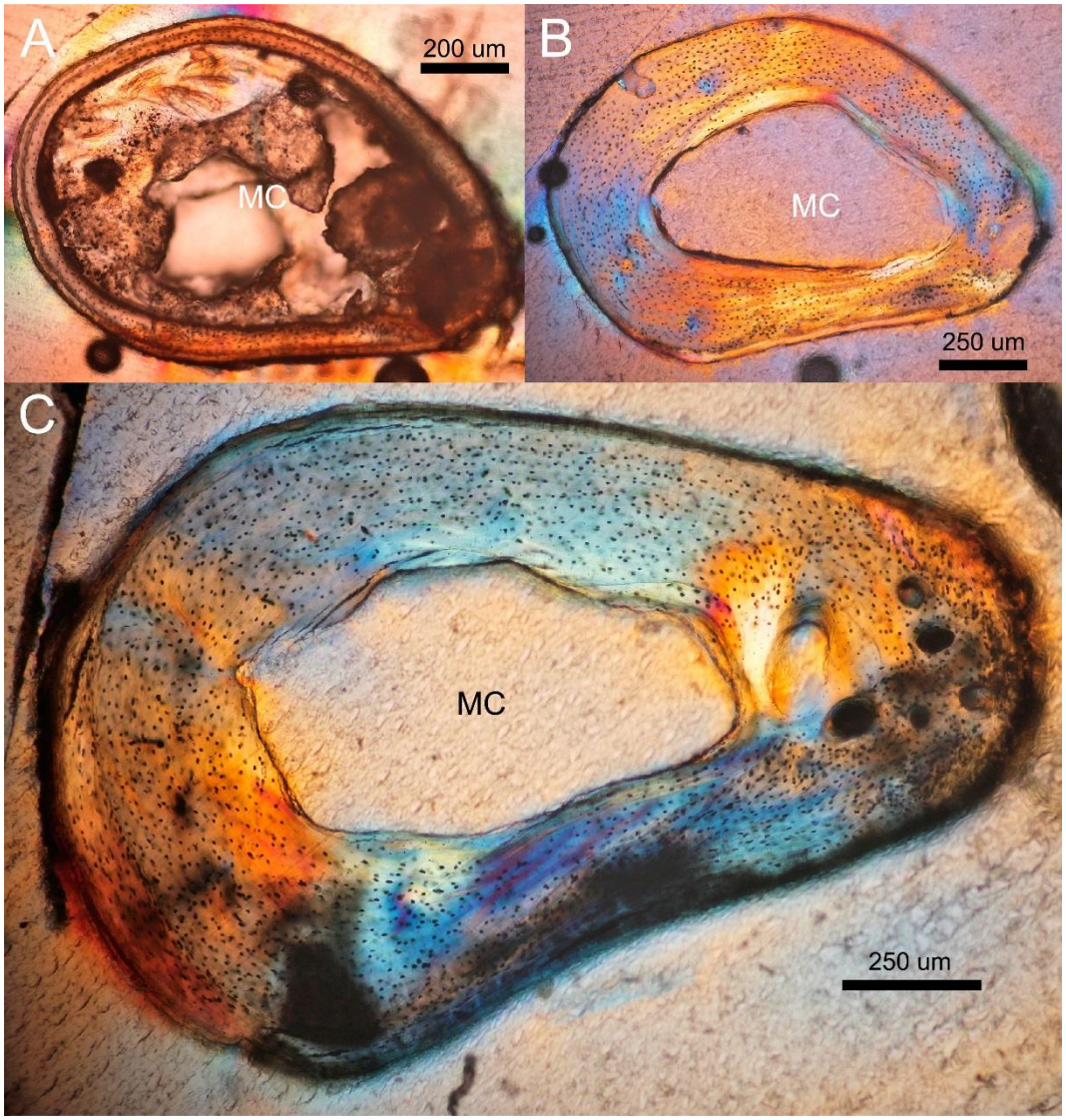

FIGURE 6.10. General humeral bone microstructure of perinatal (A: #046), juvenile (B: #088) and adult (C: #045) *Heterocephalus glaber*. Abbreviations: MC, medullary cavity.

6.4 DISCUSSION

The osteohistological descriptions made in this study represent a unique record of the patterns of bone modeling in African mole-rats (Bathyergidae, Rodentia). In general, osteohistological studies have been essential to understand bone growth and development in vertebrates. In mammals, most of these studies have been carried out to address physiologic and metabolic dynamics associated with osteoporosis and bone healing (e.g. Stout & Crowder, 2012; Allen & Burr, 2014), as well as to assess mechanical and mechanobiological aspects of bone adaptation (e.g. Carter & Beaupré, 2001; Robling *et al.* 2014). A considerable proportion of these studies have been conducted in single species, such as laboratory rodents (*Mus musculus* and *Rattus norvegicus*) and humans, and secondarily in other non-human primates (e.g. Enlow, 1963; Burr, 1992). Ungulates, carnivores and lagomorphs have also been important models to assess metabolic and biomechanical aspects of the skeleton (e.g. Skedros *et al.* 1997, 2004; Jee & Yao, 2001; Martiniakova *et al.* 2003, 2005a). However, until now the only group where a wide ontogenetic and within-family sampling has been done is in primates (McFarlin, 2006; Warshaw, 2008; McFarlin *et al.* 2016). For these reasons, the present study also provides a valuable contribution for the understanding of bone modeling in mammals.

Previous studies assessing appendicular bone microstructure in bathyergids assessed different aspects of its biology and were diverse in the extent of description (e.g. Botha & Chinsamy, 2004; Chinsamy & Hurum, 2006; Pinto *et al.*, 2010; Montoya-Sanhueza, 2014, Montoya-Sanhueza & Chinsamy, 2017, 2018, Montoya-Sanhueza *et al.*, 2019; Carmeli-Ligati *et al.*, 2019). These studies focused on the smallest and largest bathyergds, *H. glaber* and *B. suillus*, respectively. Osteohistological descriptions for all zeugopodial and stylopodial bones were only done for *B. suillus* (Montoya-Sanhueza & Chinsamy, 2017), whilst detailed descriptions of the bone microstructure of naked mole-rats were principally based on 3D scans and histological assessments of the femur only (Pinto *et al.*, 2010; Carmeli-Ligati *et al.*, 2019). Thus, no osteohistological information on bone modeling currently exists for other bones of the skeleton of naked mole-rats. Brief descriptions of femora of few adult specimens were done by Botha & Chinsamy (2004), Chinsamy & Hurum (2006), Edrey *et al.* (2011) and Montoya-Sanhueza & Chinsamy (2016). The latter study also included a brief description of the histology of adult humeri of naked mole-rats. In the current study, a comprehensive analysis of the long bone ontogeny of four species of AMs, including naked mole-rats, is provided and describes the histodiversity, matrix composition, bone modeling, osteonal formation (remodeling), secondary reconstruction, and cortical drift, among other aspects.

The main features observed during the ontogeny of African mole-rats are the increased cortical thickening of all long bones and the scarce endosteal and intracortical bone resorption (Fig. 6.5-6.6, 6.8-6.10). These processes contrast with the observations among most surface-dwelling mammals, where diaphyseal bone shows relatively large medullary cavities and thin cortical walls, mostly due to endosteal bone resorption (Carrier, 1983; Heinrich *et al.*, 1999; Lammers & German,

2002; Castanet, 2006; Young *et al.*, 2010). Similarly, surface-dwelling mammals show more pronounced bone loss with ageing as a result of osteopenia, which occurs at endosteal and intracortical surfaces (Duque & Watanabe, 2011). The scarce resorption evident throughout ontogeny in AMs, suggests that osteopenia is a limited process in AMs, and the lack of bone loss is the main contributor to maintain cortical thickening during ontogeny (Montoya-Sanhueza & Chinsamy, 2018).

The scarce bone resorption of AMs preserves an excellent record of their ontogenetic bone tissue development throughout ontogeny. Several bone tissue types including woven bone (WB), compacted coarse cancellous bone (CCCB), fibrolamellar bone (FLB), parallel-fibered bone (PFB), lamellar bone (LB) and lamellated bone tissues (LLB) were observed during ontogeny. The processes of postnatal osteogenesis are summarized in Table 6.1. In general, newborns and pups of all species (except the newborns of *H. glaber,* which were unavailable) showed highly vascularized WB, and highly compacted cortical walls with a small medullary cavity (Table 6.1; Fig. 6.8A-6.9A). From juvenile stages, most species showed thin cortical walls, which becomes thicker by periosteal and endosteal deposition and subsequently stratified in later ontogenetic stages. Subadults and adults showed thick cortical walls, with zonal bone (Table 6.1; Fig. 6.8C-6.10C). Zonal bone was of two types according to the ontogenetic stage: i) in early juveniles, bands of WB with thin layers ("annuli") of PFB, and/or ii) in adult stages bands of PFB with annuli of LB. This aspect is discussed in detail below. Lamellated bone was also present in some bones and was quite abundant in naked mole-rats (Fig. 6.10C). Growth marks (i.e. annuli and LAGs) were observed in all species and in all bones in a variable number, as well as secondary osteons (see below). For comparative purposes, a detailed description of limb bone modelling in the largest bathyergid, *B. suillus,* can be found in Montoya-Sanhueza & Chinsamy (2017).

TABLE 6.1. Postnatal osteogenesis of African mole-rats. Main features of bone growth are summarized for each species, including thickness of the cortical walls (CT), medullary cavity size (MC), degree of vascularization (VC) and bone tissue types (BT). All species showed a similar growth pattern and bone tissue composition. Bones are thick during perinatal stages (pups) and medullary expansion occurs in juveniles so they exhibit thin CW, especially *Heterocephalus glaber*. Adults show thick CW and a relatively reduced MC. In general all species exhibit high histodiversity, although *H. glaber* showed a more homogeneous bone matrix composition in adults (predominantly PFB and LB, and higher amounts of LLB). *Abbreviations*: Woven bone (WB), parallel-fibered bone (PFB), lamellar bone (LB), compacted coarse cancellous bone (CCCB), lamellated lamellar bone (LLB).

Species	Pups	Juveniles	Adults
H. argenteocinereus	CW= thick; MC= small; VC= high; BT= WB	CW= thin; MC= large; VC= scarce; BT= WB, PFB, LB	CW= thick; MC= variable; VC= scarce; BT= WB, PFB, LB, CCCB, LLB
C.h. natalensis	-	-	CW= thick; MC= variable; VC= scarce; BT= WB, PFB, LB, CCCB
F. mechowii	CW= thick; MC= small; VC= high; BT= WB	CW= thin; MC= large; VC= scarce; BT= WB, PFB, LB	CW= thick; MC= variable; VC= scarce; BT= WB, PFB, LB, CCCB
H. glaber	-	CW= very thin; MC= large; VC= scarce; BT= WB, PFB, LB	CW= thick; MC= variable; VC= scarce; BT= WB, PFB, LB, CCCB
*B. suillus**	-	CW= thin; MC= large; VC= scarce; BT= WB, PFB, LB	CW= thick; MC= small; VC= scarce; BT= WB, PFB, LB, CCCB, LLB

*Based on Montoya-Sanhueza 2017

6.4.1 Bone Labeling

H. glaber and *C. h. natalensis* showed different degrees of bone modeling. Most of the bone formation found in *H. glaber* was associated with endosteal surfaces, including trabeculae of the medullary cavity (Fig. 6.2-6.3). This contrast with the more extensive endosteal and periosteal activity found in bones of *C. h. natalensis* (Fig. 6.5-6.6), which is probably related to ontogenetic differences, although both sample specimens were from somatically mature individuals.

Labeling studies in small mammals are scarce, and have shown that during early ontogeny, periosteal bone growth is predominant, mostly because the extensive endosteal resorption occurring during medullary cavity expansion at these stages (Castanet *et al.*, 2004). In captive grey mouse lemurs *Microcebus murinus,* endosteal bone formation in the tibia appears at one month old (Castanet *et al.*, 2004). In rodents, bone labeling studies are also limited, but Erben (1996) described that trabecular bone from the proximal tibia of aged rats (>6 months old) is mostly composed of bone remodeling at endocortical bone surfaces. The age of the *H. glaber* specimens was unknown, but the fact that most of them showed only endosteal and trabecular bone formation suggests that they were already mature specimens. Indeed, Figure 6.2 shows that the body size of the injected specimens was at an intermediate degree of somatic development. Regarding whether such bone labels represent modeling or remodeling processes in *H. glaber*, as suggested by Erben (1996) for similar processes in rats, is still unknown and deserves additional assessment in naked mole-rats. However, some intracortical sites in the specimen #510 clearly shows bone remodeling, which is demonstrated by lamellar bone being deposited in one side of a resorption cavity (e.g. Fig. 6.3C).

In *C. h. natalensis,* the individual #520 showed the clearest and most complete labels, almost surrounding the complete cross-section (Fig. 6.6G). The individual #521 showed discontinuous endosteal bone formation of only Cn, and no Ar label (Fig. 6.6H). These differences may be related to sexual dimorphism. Sontag (1986a) described that females of old rats (>6 months old) showed mainly resorbing endocortical surfaces. It is likely, that the females undergo more catabolic process in late ontogeny as compared to males, and those differences can explain the different growth dynamics observed. This indicates that sex can have a considerable effect on bone modeling in *C. h. natalensis,* and probably also in other AMs.

6.4.2 Comparative Bone Microstructure and Bone Modeling

The general pattern of bone modeling observed in all bathyergid genera, including ontogenetic series of *Heterocephalus glaber*, *Heliophobius argenteocinereus*, *F. mechowii* and *Cryptomys hottentotus natalensis* appeared to be highly similar among the species, thus suggesting that the mechanism of bone osteogenesis is shared among them. However, *H. glaber* tended to show the most differences. This resembles the quantitative analyses performed in chapters 4-5, where *H. glaber* was the most different species in terms of external morphology and bone growth rates. The following discussion focusses on the forelimb elements, since these have direct implications for digging behavior.

Humerus. The humerus generally had the largest cross-sectional area among all bones in all species. It has a triangular shape which is defined in juvenile stages and it is composed of a disorganized arrangement of different bone tissues, including woven bone (WB), compact coarse cancellous bone (CCCB), parallel-fibered bone (PFB) and lamellar bone (LB). The triangular microanatomy is the result of the projection of the deltoid tubercle, which is already developed in all newborns studied here. The humerus showed the highest level of cortical drift among all bones, as well as increased intracortical and endosteal resorption, and frequent presence of trabeculae throughout ontogeny as compared to other long bones. In *H. glaber,* the cortical drift is less pronounced although they still showed higher intracortical resorption (anterior region) in comparison to other bones (Fig. 6.10C). These features were also reported for the solitary scratch-digger *Bathyergus suillus* (Montoya-Sanhueza & Chinsamy, 2017; Montoya-Sanhueza *et al.*, 2019). These authors suggested that the high cortical drift observed in the humerus is the result of the relocation of the deltoid tubercle during bone growth, and most importantly due to the torsion that the humerus experiences (note that the term deltoid ''crest" was used instead of "tubercle"). These data indicate that the simultaneous processes of humeral torsion and development of tubercles are associated with strong cortical drift and relocation, intracortical resorption, mixture of different bone matrices and high bone turnover.

Strong cortical drift is also evidenced by bone labeling in *C. h. natalensis* (Fig. 6.6). This species showed that the posterior regions of the bone are kept relatively intact during bone relocation (Fig. 6.6E), while the mediolateral and anterior regions are highly resorbed, especially the lateral side. Some individuals showed lamellar bone depositions (PLB) in the medial side, indicating slow growth rates for this area. The direction of such bone dynamics indicates that humeral torsion and cortical drift occurs preferentially towards the medial side of the bone, probably following the mechanical tension exerted by the deltoids muscles which acts in flexing the arm internally against the midline of the body (Hildebrand, 1985).

Montoya-Sanhueza & Chinsamy (2017) proposed a general pattern for the cortical drift observed in *B. suillus,* although they did not mention the orientation of such rotation. The present study confirms that the humerus and deltoid tubercle rotates towards the medial side, which is histologically seen by higher accumulation of slowly deposited tissues on endosteal (ELB) and periosteal (PLB) surfaces, with resorptive pericortical surfaces in the lateral side. Bone labeling also demonstrated that the cortical drift in *H. glaber* is highly reduced (Fig. 6.10C) in comparison to the pattern observed in other bathyergids (Fig. 6.6). This is most likely because of the lack of a deltoid tubercle in this species (see Ch. 4; Fig. 6.1) and therefore a reduced muscular stimulation on the bone diaphysis can be assumed. In humans, a functional imbalance between medial and lateral rotational muscles seems to be important for the degree of humeral torsion (Cowgill, 2007). Likewise, in the absence of muscle activity, bone eminences or superstructures like the deltoid tubercle, are significantly smaller or completely lost (Felsenthal & Zelzer, 2017). This study represents the first comprehensive histological description of the humeral rotation in mammals and highlights the effects of muscle activity

and presence of superstructures on the degree of cortical drift and bone modeling in the humerus.

The ulna. The ulna typically has an ellipsoidal bone shape, which is established early in ontogeny, usually before other bones. This contrast with the allometric findings of Montoya-Sanhueza *et al.* (2019), where the humerus appeared to be the first bone to reach maturity in the scratch-digger *B. suillus*. This observation needs further quantification of bone tissue matrices and inclusion of known age individuals to clarify the timing of bone growth between the humerus and ulna. Bone modeling is mostly appositional in the anterior and posterior regions of the bone during ontogeny, while mediolateral aspects grew considerably less, mostly since the lateral side is under resorption and the medial side show mostly LB depositions, thus showing a slight cortical drift towards the medial side. The anterior side usually showed a mixture of bone tissues (including CCCB and PLB) and high amount of Sharpey's fibers (SF) associated with the interosseous ligament that maintains the radius connected to the ulna. The dynamic histology analysis showed that mature individuals showed less bone formation as compared to the humerus. This indicates that the ulna ceased its growth before the humerus. In this sense, the ulna matures and ceases its growth earlier than the humerus. In *G. capensis*, the ulna was relatively subcircular in shape, which contrast with other social bathyergids and the solitary *Bathyergus*. In *B. suillus*, the ulna is quite narrow (i.e. elongated in anteroposterior cross-sectional view), which is suggested to decrease the surface area of the forearm for a maximized soil breakup (lose sand) during parasagittal scratch-digging. A more circular bone shape in *G. capensis* would be the result of its mostly chisel-tooth digging strategy, which would not require ulnar specializations to maximize scratch-digging ability.

6.4.3 Limb Bone Growth in Subterranean and Fossorial Mammals: a Review

Comparison with other subterranean and fossorial taxa are limited due to the scarcity of such studies. Only a few recent studies have analyzed the ontogenetic bone histology of highly fossorial mammals: the largest subterranean and scratch-digging mammal, *Bathyergus suillus* (n = 42, Montoya-Sanhueza & Chinsamy, 2017), the large aardvark, *Orycteropus afer* (n = 4, Legendre & Botha-Brink, 2018) and the nine-banded armadillo *Daypus novemcinctus* (n = 6, Heck *et al.*, 2019). These studies have shown that such fossorial taxa have thick cortical walls in their long bones, which indicates a strong functional relationship associated with the digging activity. However, some differences exist between bathyergids and other fossorial species.

The diaphysis of long bones in bathyergids, including the largest bathyergid, *B. suillus* (Montoya-Sanhueza & Chinsamy, 2017) is comprised of a mixture of both periosteal and endosteal bone tissues (Fig. 6.8-6.10). However, Legendre & Botha-Brink (2018) mention that most of the cortical limb bones of the aardvark are comprised of compacted coarse cancellous bone (CCCB), which has an endosteal origin. In this species, the periosteal bone is highly resorbed in all long bones and is reduced to a thin outer layer and suggesting a pattern of strong cortical drift and a different pattern of bone modeling from that observed in bathyergids. Heck *et al.* (2019) describe a similar pattern for the armadillo, where

the cortex of the long bones of the smallest (youngest) individual is composed of CCCB and WB, while the cortex of the largest specimens is primarily CCCB with thickened endosteal bone and thin outer cortices of PLB and PFB. Thus, most cortical thickening in these large fossorial species are the result of endosteally formed bone tissues.

This pattern contrasts with that of most large mammals, in which cortical bone at the midshaft is mostly of periosteal origin, while CCCB is usually resorbed during ontogeny due to considerable medullary cavity expansion (Montoya-Sanhueza & Chinsamy, 2017; Legendre & Botha-Brink, 2018). As suggested by Legendre & Botha-Brink (2018), it is likely that the presence of higher amounts of CCCB is related to the influence of body size in fossorial mammals. In terms of development, this tissue is normally formed in all mammals during endochondral ossification and bone compaction, and its presence in the midshaft of long bones is the result of reduced endosteal bone resorption during ontogeny (Montoya-Sanhueza & Chinsamy, 2017). Recently, Garrone *et al.* (2019) described variable amounts of CCCB in long bones of adults of the saltatorial rodent, the plains vizcacha, *Lagostomus maximus* (Chinchillidae), which is a medium size scratch-digging mammal that inhabits communal burrows. The rock hyrax, *Procavia capensis* (Hyracoidea: Paenungulata), a specialized climber also maintains CCCB in the cortex of adults, although to a lower proportion as compared to *B. suillus* (Montoya-Sanhueza *et al.*, 2016). Semiaquatic rodents have also shown the development of these tissues (Enlow 1962; Geiger *et al.* 2013). These findings indicate that limited endosteal resorption in adult mammals is not exclusive to subterranean or fossorial species, and that inhibition of endosteal resorption can be related to different factors mediated by bone modeling. These findings suggest that the proportion of CCCB in the midshaft regions of mammals and other vertebrates is rather dependent on two main factors: (i) the amount of endosteal resorption during early and middle stages of ontogeny, and (ii) the degree of cortical drift, which can erode some sides of the bone wall more than others (Montoya-Sanhueza & Chinsamy, 2017). Further research is needed to assess the variations in amount of CCCB in long bones, as well as its biomechanical implications in bone strength.

6.4.4 Zonal Bone in Mammals: Implications for Bathyergids

The finding of stratified cortical bone (zonal bone) and growth marks in all African mole-rats, and almost all their bones has several implications that will improve our understanding of the relationship between bone growth and metabolism in mammals. Zonal bone and the appearance of growth marks in vertebrates reflects the growth history of the bone (Klevezal & Kleinenberg 1967; Reid, 1981; Castanet *et al.*, Klevezal, 1996; 1993; Chinsamy-Turan 2005, 2012; Castanet, 2006), although its causes were not completely understood until recently (Castanet *et al.*, 1993, 2004). Zonal bone was typically associated with ectothermic animals, as a reflection of their lowered capacity to sustain high metabolic rates, thus reflecting periodic interruptions of bone growth related to seasonal conditions and environmental stresses (Enlow, 1966, 1969). This view accounted for a direct effect of environmental and external factors on the skeletal growth of individuals. On the

contrary, mammals (and birds), considered to be organisms that "generate constant" rates of metabolism and high growth rates were generally assumed to show continuous bone depositions without presence of growth marks (Chinsamy-Turan 2005, 2012). However, several extant and extinct mammals have zonal bone and/or growth marks (e.g. Klevezal & Kleinenberg 1967; Castanet *et al.*, 1993, 2004; Klevezal, 1996; Chinsamy-Turan, 2005, 2012; Castanet, 2006; Chinsamy & Hurum, 2006; Köhler & Moya-Sola, 2009; Montoya-Sanhueza, 2010; García-Martínez *et al.*, 2011; Köhler *et al.*, 2012; Straehl *et al.*, 2013; Kolb *et al.*, 2015; Montoya-Sanhueza & Chinsamy, 2017), thus complicating our understanding of the origin of these histological features and its periodicity. In recent years, alternative explanations have been proposed, specifically linking the physiology of the species with the periodicity of bone deposition, mainly focusing on seasonal fluctuations of their metabolic rates, thermoregulatory strategy, hormonal activity and photoperiod (e.g. Castanet *et al.*, 2004; Castanet, 2006; Köhler *et al.*, 2012). These findings support previous suggestions that growth marks and bone stratification were basically related to endogenous rhythms, and that they are mainly synchronized and/or reinforced by environmental cycles (seasonality) (Castanet *et al.*, 1993). In a pioneering study, Castanet *et al.* (2004) performed one of the first studies to test the reliability of using lines of arrested growth (LAGs) for age determination in a small primate, the mouse lemur (*Microcebus murinus*). Using known aged individuals and bone labeling techniques, they showed that LAGs were highly correlated with the seasonal cycle of photoperiodicity, rather than to ontogenetic age. However, one of the seminal contributions in this area is by Köhler *et al.* (2012), who associated the patterns of seasonal bone growth of a wide range of large ruminant species with their metabolic and energetic characteristics. These authors comprehensively studied wild ruminants from tropical to polar environments, showing that cyclical growth is a universal trait of homoeothermic endotherms, and that bone growth is arrested during the unfavorable season concurrently with decreases in body temperature, metabolic rate and bone-growth-mediating plasma insulin-like growth factor-1 levels (Köhler *et al.*, 2012).

These studies demonstrate the close relationship between postnatal bone morphogenesis and physiological rhythms and environment. This approach also highlights the evolutionary significance of eutherian mammals to associate maximum rates of bone accrual with high, sustained metabolic rates during the favorable season (Köhler *et al.*, 2012), which contrasts with the previous --implicit-- hypothesis that bone growth in mammals was always "relatively constant" and that environmental stresses had a negative effect on those growth rates thus diminishing or ceasing bone formation.

However, it is necessary to understand that despite the traditional classification of vertebrates as being either endothermic or ectothermic (McNab, 2000), there is a growing body of literature reporting temporal variability of such strategies within populations (Moshkin *et al.*, 2007; Angilletta *et al.*, 2010; Boyles *et al.*, 2011; Kohler *et al.*, 2012; and references therein). For example, it is known that individuals undergo seasonal fluctuations during the unfavorable (usually dry) season and use complex energy-conserving strategies including cyclical variation in body core temperature, resting metabolic rate, and associated changes in hormonal levels (Kohler *et al.*, 2012, and references therein). This results in

deviations from a high and constant body temperatures, which has been loosely termed heterothermy (Boyles *et al.*, 2011). This results from the hypothesized high energetic and ecological costs of maintaining strict homeothermy (Angilletta *et al.*, 2010; Boyles *et al.*, 2011), so multiple external factors are known to affect these thermoregulatory patterns in endotherms, including food availability and ambient temperature (Boyles *et al.*, 2011). In this sense, environmental stresses may not affect directly skeletal growth but thermoregulatory conditions in endotherms, which consequently affects bone modeling. Using similar analogy, Chinsamy (1990) much earlier suggested that some theropod dinosaurs may have had the ability to lower their metabolism sufficiently (i.e. heterothermy) to produce annuli in their compacta, which would indicate endothermic strategies like hibernation and aestivation found in modern mammals and birds. However, this hypothesis was still considering the effects of environmental stresses as the main driver responsible for the formation of growth marks (Chinsamy, 1990). Further research on extant vertebrates is needed to understand how different metabolic and energetic strategies are related to osteogenesis during ontogeny.

In the case of bathyergids, it is known that they have low body temperatures and metabolic rates (Buffenstein & Yahav, 1991; Bennett *et al.*, 2009; Šumbera, 2019), as well as slow somatic growth rates (Bennett *et al.*, 1991) in comparison to surface-dwelling mammals of similar body size. Bathyergids do not undergo hibernation, although they can experience torpor. Energy expenditure, body temperature and metabolic rates are known to fluctuate between seasons in some species, thus indicating heterothermic capabilities (Šumbera, 2019). Field studies in *F. damarensis* have shown that variation in body temperature varies between seasons in much the same way as in heterothermic species, although just to a lesser degree (Boyles *et al.*, 2011; Streicher *et al.*, 2011). Additionally, it has been reported that *H. glaber* also undergoes changes in body temperature during reproduction (Urison & Buffenstein, 1995). Thus, zonal bone described for AMs in the current study could be related to intrinsic metabolic fluctuations, and therefore deserves a more thorough investigation.

A remarkable feature among bathyergids is the less stratified cortices of naked mole-rats, although they showed growth marks regardless of sex (Fig. 6.4). Such less marked stratification of the cortex in all limb bones can be related to the unique thermoregulatory capabilities of naked mole-rats. This species is usually considered a poikilothermic mammal (see Šumbera, 2019), although they can also show more complex thermoregulatory mechanisms, including endothermic characteristics during huddling behavior and reproduction (Yahav & Buffenstein, 1991; Hislop & Buffenstein, 1994; Šumbera, 2019). Despite this, the bone matrix composition in adult naked mole-rats appears distinct from that of other mole-rats, having essentially lamellar and lamellated bone tissues, as well as scarce vascularization (Fig. 6.10). These observations clearly indicate very low intramembranous bone growth rates for naked mole-rats. This was also observed in mature specimens injected with fluorochromes, which showed scarce bone formation, and were usually associated with endocortical bone formation (Fig. 6.3-6.4). This, along with slow periosteal (and endochondral) bone growth rates (reported in Ch. 5), suggest that somatic growth and skeletal growth is considerably lower as compared to other bathyergids, but that it is also relatively

stable during adult stages, i.e. slow and sustained growth is present in most individuals.

The recent work by Carmeli-Ligati *et al.* (2019, p. 6, 11) reported that the femoral cortex of naked mole-rats "*is composed entirely of circumferential lamellar bone, with sparse blood supply … and that they do not contain un-remodeled calcified cartilaginous islands*". It seems that these authors refer to the distribution of LB around the entire cortex as the circumferential lamellar bone (Enlow, 1963), while the calcified cartilaginous islands are central zones of the cortical bone that resulted from the endosteal compaction or coalescence (Cadet *et al.*, 2003) of trabecular (cancellous) bone at metaphyseal regions of the bone. These calcified regions were originally termed as cancellous compact coarse bone (CCCB) by Enlow (1963), and represent a common component of mammalian bone, although its extent varies along the diaphysis, during ontogeny and depending on the taxa analyzed (Enlow & Brown, 1958; Montoya-Sanhueza & Chinsamy, 2017). By using quantitative backscattered electron imaging, Bach-Gansmo *et al.* (2013) demonstrated that these islands (i.e. CCCB) have a significantly higher degree of mineralization than the surrounding bone, so these regions likely play an important role in rat cortical bone mechanical properties. Because of the composed nature of CCCB (Enlow, 1962), this tissue can show a mixture of different bone matrices including calcified bone, WB and LB. However, despite the wide ontogenetic sample that Carmeli-Ligati *et al.* (2019) studied, these researchers did not mention the presence of other bone matrices like WB, CCCB and PFB. Nevertheless, these tissues were clearly identified in the present study, including the femora, thus indicating that the histodiversity of naked mole-rat long bones is as high as in other bathyergids and other rodents. The presence of such tissues was also previously mentioned in brief descriptions of the femur and humerus of naked mole-rats (Chinsamy & Hurum, 2006; Montoya-Sanhueza & Chinsamy, 2016).

Regarding previous descriptions of the bone histology in naked mole-rats, Chinsamy & Hurum (2006) described and an inner, richly vascularized region consisting of a more woven type of bone tissue, and suggested that its compacta was formed at a more rapid rate than that of some Mesozoic eutherian genera (*Zalambdalestes* and *Barunlestes*), and indeed more rapidly than those of many other extant small eutherians (e.g. moles, bats, marmots, squirrels), which tend to have rather poorly vascularized compacta (Enlow & Brown 1958). The finding of subperiosteal WB in the thick compacta of *H. glaber* is reminiscent of earlier ontogenetic stages and may not necessarily indicate faster growth rates in young naked mole-rats as compared to other small mammals. In this sense, the adult bone microstructure of moles, bats, marmots and squirrels appears to show slowly deposited bone tissues in adulthood (Enlow & Brown 1958), although their ontogenetic bone microstructure have not been comprehensively described, so it is probably that they also have a mixture of FLB, WB, and/or PFB in early postnatal life. Indeed, the histology of a phylogenetically wide range of adult bats shows the presence of WB, PFB and LB (see images in Lee & Simons, 2015). Edrey *et al.* (2011) assertively described LAGs on the lateral side (tip) of the femur (as this study also found), although they erroneously commented that such growth marks indicate fast growth patterns. LAGs indicate the cessation of appositional growth in bones (Castanet *et al.*, 1993; Klevezal, 1996; Chinsamy, 2005). Growth marks were also

observed in several specimens of *H. glaber* studied here (#511, Fig. 6.4). Chinsamy & Hurum (2006) reported the lack of LAGs in one specimen (femur) of *H. glaber*, suggesting that this could be because the animal was from a captive colony (so would not have had to endure seasonal fluctuations) and that this may also occur naturally in this species in the wild, since it lives in burrows and therefore experiences minimal ambient fluctuations. In the present study, LAGs were found in the limb bones of captive naked mole-rats. Thus, the absence of growth marks in the original study of a single femur (Chinsamy & Hurum, 2006) is most likely due to the reduced number of specimens analyzed by these authors.

Furthermore, although the hypogeous niche represent a considerably highly stable environment in comparison to aboveground niches for subterranean mammals (Šumbera, 2019), these organisms still undergo seasonal thermoregulatory dynamics (Moshkin *et al.*, 2007; Boyles *et al.*, 2011). This provides support to the fact that the variable thermoregulatory and metabolic dynamics of subterranean mammals can generate growth marks in skeletal tissues as a reflection of their endogenous rhythms and physiology, regardless whether the environment is stable or not. Thus, zonal bone and growth marks in *H. glaber* may form part of the plesiomorphic thermometabolic strategy for energy conservation present in mammals suggested to affect bone modeling in mammals (Kohler *et al.*, 2012).

6.4.5 Bone Remodeling in Bathyergidae: the Case of Naked Mole-Rats

In bathyergids, bone remodeling, i.e. development of secondary osteons (Haversian systems), has been histologically demonstrated only for long bones of *B. suillus* (Montoya-Sanhueza & Chinsamy, 2017, 2018). Secondary osteons in this large and solitary species were scarce and randomly distributed in the intracortical regions, usually associated with WB, as well as showed high variation in size and shape (Montoya-Sanhueza & Chinsamy, 2017). Additionally, the number of secondary osteons increases slightly during ontogeny, although they do not develop dense Haversian tissue in any bone (Montoya-Sanhueza & Chinsamy, 2017). Similar observations were made in this study, i.e. all the species showed isolated secondary osteons of variable sizes and shapes, as well as in different stages of osteonal formation (Fig. 6.11B), although individuals never developed dense Haversian tissues. Thus, bone remodeling occurs to a limited extent in bathyergids.

Out of the 83 naked mole-rats analyzed in this study, 38 individuals showed development of secondary osteons (Fig. 6.12). In general, the humerus was the most common bone presenting secondary osteons (SO), followed by the femur, and much less frequent in the ulna and tibia. This indicates that the process of osteonal development in naked mole-rats is limited, but not non-existent as suggested by previous reports (see below), and that osteonal development (Haversian remodeling) was less frequent in zeugopodial bones, which are smaller in cross-sectional area, probably as an adaptation to reduce weakening of smaller bone surfaces. These structures were present in subordinate and reproductive individuals, regardless of their ontogenetic stage, and were evidenced by the development of small resorption cavities infilled with bone matrix or mineralized

osteoid. The SOs were usually rounded, although some showed irregular shapes. An eroded canal was observed when the SO was incompletely formed. This data indicates that SOs were at different stages of maturity. Secondary reconstruction of enlarged RCs was more irregular in shape and extended over larger surfaces of the bone. In general, all somatically mature specimens normally showed resorption cavities in their cortices, which were not infilled with bone to form secondary osteons.

High levels of bone remodeling were observed in reproductive specimens, mostly females (Fig. 6.12), which are known to increase their metabolism during reproduction. Urison & Buffenstein (1995) showed that the metabolic rate of pregnant females of naked mole-rats was 1.4-fold higher as compared to non-reproductive individuals, probably inducing higher bone turnover due to reproductive demands needed for pup development. Additionally, Pinto *et al.* (2010) reported extensive evidence of endocortical bone resorption in late pregnancy and during lactation, as probably indicating the beginning of bone remodeling in naked mole-rats. In this regard, there are hardly any studies of the effects of reproduction on subterranean mammals, although Montoya-Sanhueza & Chinsamy (2018) recently comprehensively described and quantified the effects of reproduction on females of *B. suillus,* which showed marked subendosteal secondary reconstruction. Additionally, experimental studies have reported how Sprague–Dawley rats with low-calcium diet have elevated intracortical remodeling and a greater number of secondary osteons during lactation (Ruth, 1953; Ross *et al.*, 2017). These data on laboratory and wild rodent populations show the increased bone turnover (and bone remodeling) generated during reproductive cycles in a wide range of rodent taxa. It is important to note that studies in rodents (genus *Apodemus*) have shown that neither pregnancy, nor lactation cause a cessation of skeletal growth, so the reproductive cycle in mammals is not expected to stimulate the formation of resting lines due to bone growth cessation (Klevezal, 1996).

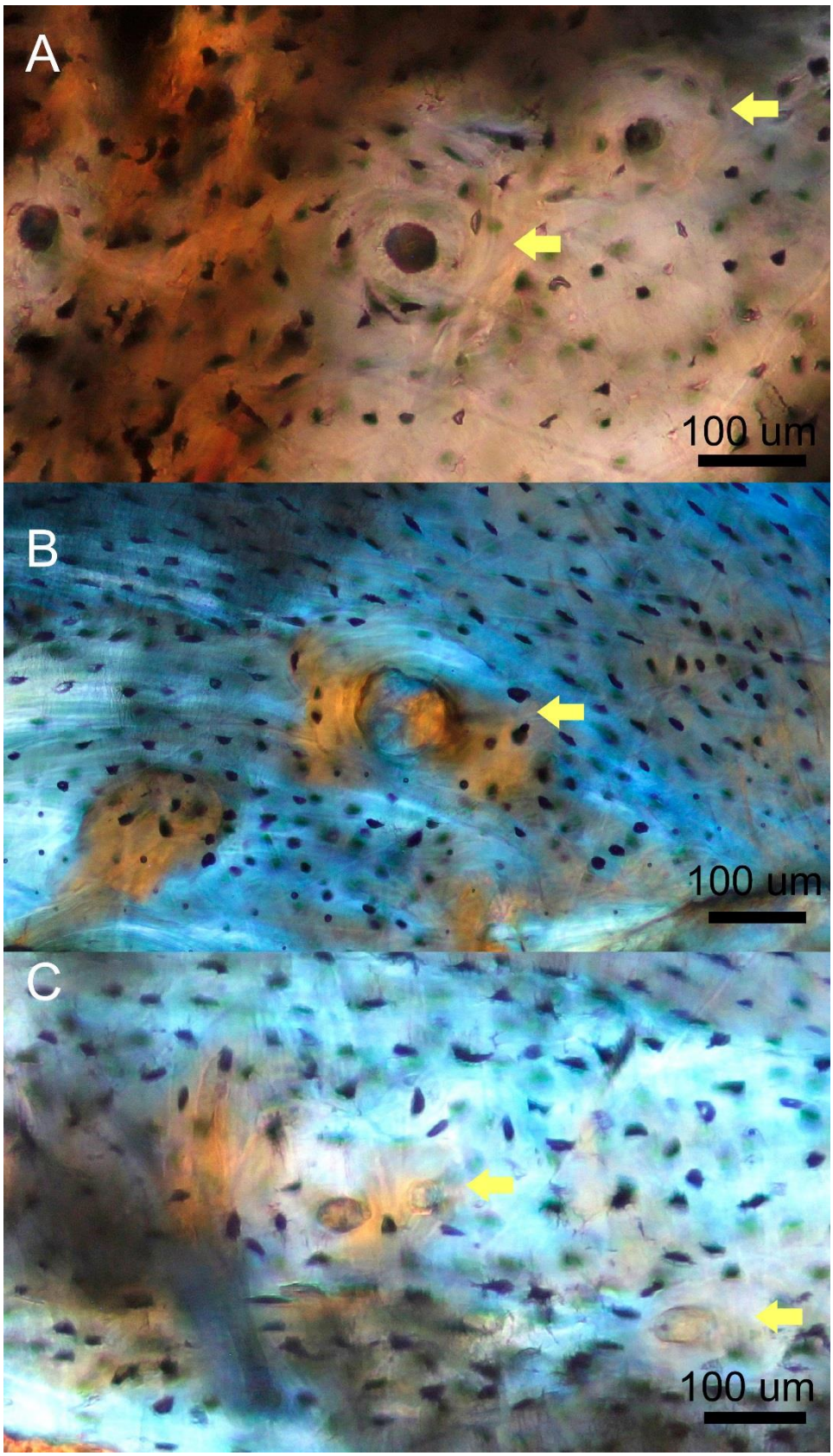

FIGURE 6.11. Remodeling activity and development of secondary osteons in femora of Bathyergidae. A) *Heliophobius argenteocinereus* (#180). B) *Fukomys mechowii* (#222). C) *Cryptomys hottentotus natalensis* (#523). Arrows indicate secondary osteons.

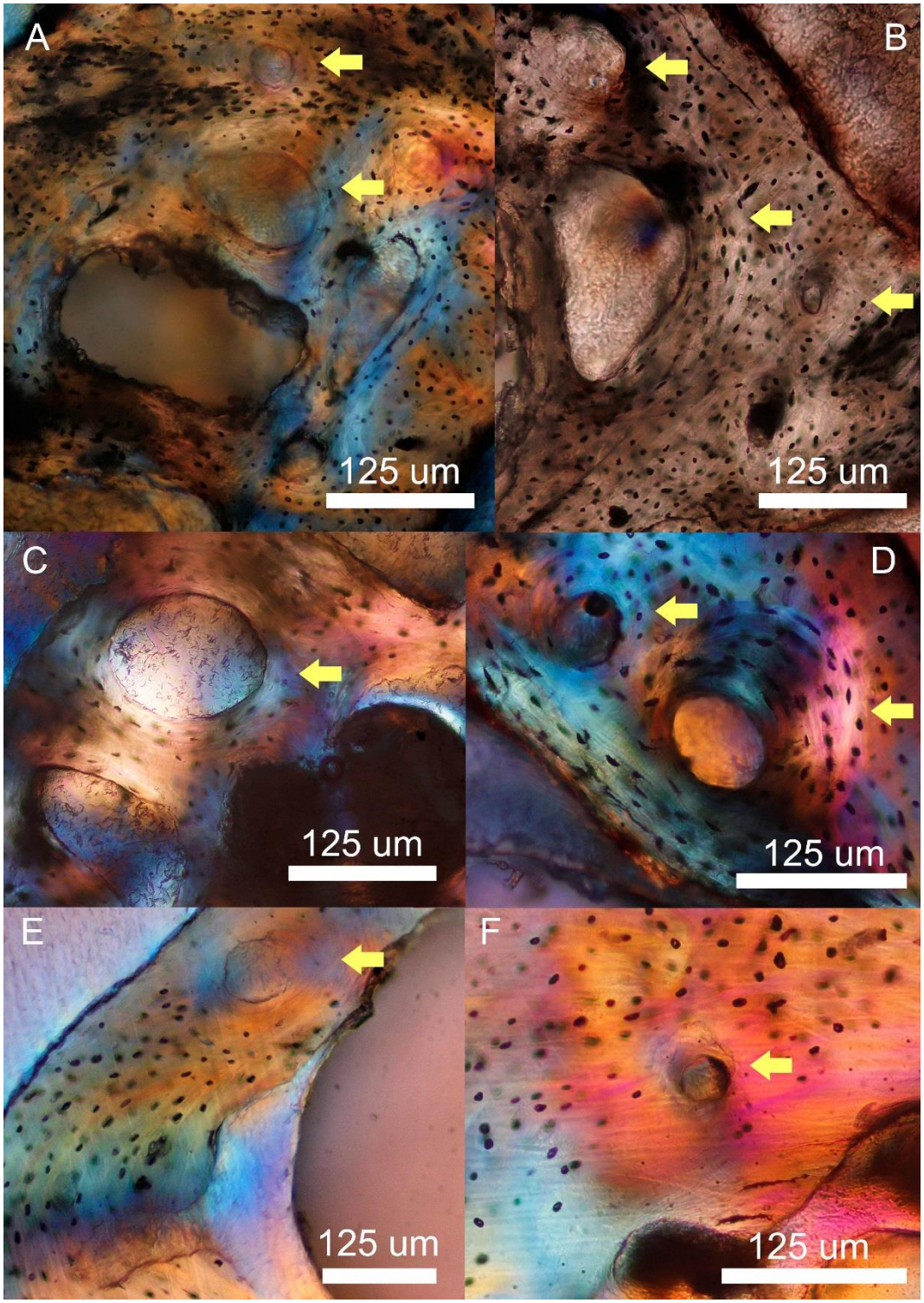

FIGURE 6.12. Remodeling activity and development of secondary osteons in females of *Heterocephalus glaber*. A-B) Humerus (#079). C) Femur (#079). D) Tibia (#079). E) Femur (#506). F) Femur (#510). Arrows indicate secondary osteons. All the specimens are queens, except the individual #510, which is of unknown sex.

Curiously, some authors have mentioned that naked mole-rats have either i) numerous osteons and high bone remodeling (e.g. Bufffenstein, 2008; Edrey *et*

al., 2011) or that ii) they completely lack bone remodeling (Carmeli-Ligati *et al.*, 2019). Based on unpublished data, Buffenstein (2008, p. 443) mentioned the presence of many secondary osteons. In a subsequent study, Edrey *et al.* (2011) mentioned that there is a considerable variability in osteon number and size in *H. glaber*. Regarding the large number of osteons, Carmeli-Ligati *et al.* (2019, p. 2) commented that "*...they base this conclusion on the observation of a few round objects in transverse sections of the femoral diaphysis, but these appear to us to be either primary osteons or blood vessels, and thus do not indicate remodeling.*" Based on the present contribution, those structures resemble resorption cavities (eroded longitudinal vascular canals), and thus they only indicate incomplete remodeling and not secondary osteons (Montoya-Sanhueza & Chinsamy, 2017). Previous histological descriptions of *H. glaber* did not report presence of secondary osteons (Botha & Chinsamy, 2004; Chinsamy & Hurum 2006; Currey *et al.*, 2017), although Chinsamy & Hurum (2006) described that some enlarged erosion cavities are visible in the compacta and that vascular canals lack osteonal development. On the other hand, Carmeli-Ligati *et al.* (2019) reported the complete lack of osteons (primary and secondary) and remodeling in the cortex of a large ontogenetic sample of naked mole-rats (n = 61).

6.4.6 Bone Remodeling, Secondary Osteons, and Haversian Bone Tissue in Mammals and Rodentia

Due to constant confusions in the published literature about the bone histology of rodents and remodeling processes, it is necessary to clarify some misconceptions. Several authors have stated that rodents lack bone remodeling (e.g. Carmeli-Ligati *et al.*, 2019). To address this issue, it is necessary to clarify some terminology. Secondary osteons (Haversian systems) are structural units of the cortical bone, developed by the coupled activity of osteocytes and bone lining cells (osteoblasts and osteoclasts) (Frost, 1963; Parfitt, 2010). This cell complex is also termed as basic multicellular unit (BMU), and its formation follows three main stages: activation, formation of erosion cavities by osteoclasts and the subsequent refilling of such cavities by centripetal bone apposition (Parfitt, 2010). The resulting BMU shows a series of features from which it can be histologically identified, i.e. delimited margins (cement line) and concentric lamellae around the Haversian canal (Martin *et al.*, 1998; Currey, 2002). Bone remodeling represents the molecular, cellular and physiological process by which BMUs are formed (Frost, 1963; Parfitt, 2010; Sims & Martin, 2014). Secondary osteons have been described for a wide range of mammals and vertebrates (Foote 1916, 1911; Enlow 1956; Locke, 2004; Currey *et al.*, 2017) and therefore bone remodeling is present in all these taxa. The development of a BMU results in the formation of one secondary osteon, which can be found isolated, form groups or form dense Haversian patches in the bone (Jaworski, 1992; Hillier et al. 2007). When dense aggregations of secondary osteons form several generations developing and covering a defined bone surface, this is called dense Haversian bone tissue, and represents a specific subtype of bone tissue (Enlow, 1963; Jaworski, 1992). Thus, SOs should not be synonymized with Haversian bone, which is a specific bone formed by multiple and/or successive SOs. Certainly, again, this type of bone tissue is developed by formation of multiple BMUs and

therefore by bone remodeling. However, several researchers have mistakenly synonymized bone remodeling with dense Haversian tissue, thus creating confusion when trying to understand its origin, significance and development.

Furthermore, the bone microstructure of one of the closest relatives of Bathyergidae, the Cape porcupine, *Hystrix africaeaustralis* (Old World porcupines - Hystricidae) (Bennett & Faulkes, 2000; Faulkes *et al.*, 2004), also shows secondary osteons (Fig. 6.13). This species is the largest African rodent, and its presence suggests that the development of secondary osteons (and therefore bone remodeling), in relation to *H. glaber*, is plesiomorphic within Phiomorphia.

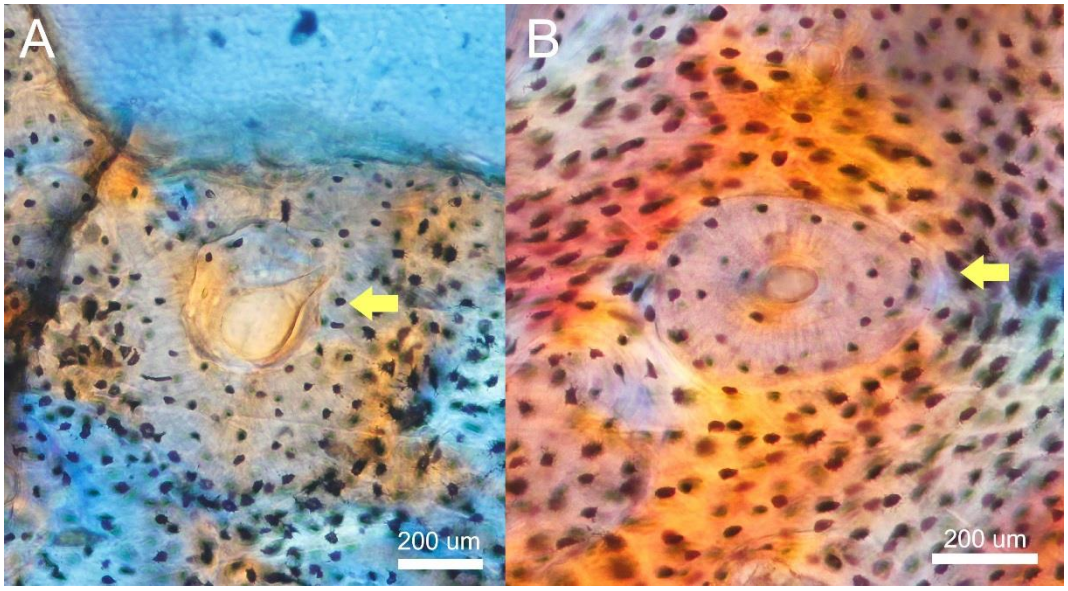

FIGURE 6.13. Secondary osteons in the humerus of the closest relative of Bathyergidae, the Cape porcupine *Hystrix africaeaustralis*. Secondary osteons can vary considerably in morphology and size, even within the same individual and bone region: A) irregular shape. B) ellipsoidal shape. Arrows indicate secondary osteons.

These observations also provide additional support to the hypothesis that bone remodeling in small-sized mammalian lineages such as Rodentia could be related to calcium regulation and mineral homeostasis, as suggested by some authors for mammals (Currey, 2002, and references therein) and not uniquely a result of increased mechanical strains as suggested by other authors working mostly on larger mammals (Martin *et al.*, 1998; Currey, 2002, and references therein).

Apart from rodents, bats (Chiroptera) also have sparse development of secondary osteons and complete lack of dense Haversian bone tissue (Enlow & Brown, 1958). This is interesting when considering that bats, like mole-rats (Dammann & Burda, 2009) also have extraordinarily prolonged lifespans among mammals (Dammann & Burda, 2009). Because Rodentia represents nearly half of the current mammalian diversity, with more than 2261 species (>40%), followed by bat diversity representing the second largest mammalian order, with nearly 1270 described species (>23%), they encompass more than 63% of the mammals of the world. Considering this, it is logical to suggest that i) bone remodeling is a rather

restricted process in mammals, and occurs regardless of lifespan constrains (Currey *et al.*, 2017), and that ii) dense Haversian bone is not developed in most mammalian species. Further research is needed to address the origin and specific functions of extensive bone remodeling (i.e. formation of dense Haversian bone tissue) among different vertebrates.

6.5 CONCLUSIONS

Bathyergids share similar bone modeling patterns, and the size and shape of their long bones are attained by similar growth processes. The newborns studied showed that these perinatal stages also have thick cortical walls, mostly composed by FLB and a reduced medullary cavity. In adulthood, all long bones showed thick cortical walls, although during juvenile stages they showed thin cortical walls. This indicates that the expansion of the medullary cavity is prioritized and synchronized with periosteal bone formation during early postnatal ontogeny, with subsequent deposition of endosteal bone in the medullary cavities in more subadult stages. Wide variation in cortical thicknesses were also observed in some species, indicating that the periosteal module, and probably also the endosteal module, may have a lesser genetic component as compared to the endochondral module. Previous observations in chapters 3 and 4 agree with this and suggest that local bone adaptation in postnatal life may be highly regulated by modifications on the morphogenesis of the intramembranous module. Based on the thickness of their cortical walls, zeugopodial bones also appeared to mature before than stylopodial bones, although this deserves additional assessment and quantification. In the forelimb, anteroposterior diameters showed presence of zonal bone depositions, indicating variable rates of bone formation for those regions, and are usually associated with a mixture of intermediate and rapidly deposited bone tissues, whereas mediolateral regions showed more slowly deposited bone tissues. In the femur, the contrary occurred. It is likely that periosteal ossifications may be prioritized in anteroposterior regions of the cortex to increase resistance to bending during digging behavior, although a direct effect of muscles acting on those areas is also possible. In general, all bathyergids showed low levels of bone remodeling, and do not ever develop Haversian bone. In the case of naked mole-rats, formation of secondary osteons is limited, and bone remodeling is higher in reproductive specimens, most likely due to the high rates of bone turnover during reproduction. Overall, the process of bone remodeling is restricted in rodents, and the fossorial bathyergids are not an exception.

CHAPTER 7

Skeletal Adaptations and Osteogenesis in Bathyergidae: A Summary

7.1 GENERAL DISCUSSION

In comparison to their ecophysiological and behavioral aspects, the skeletal system of African mole-rats has been comparatively less studied. The current PhD thesis has considerably contributed to our knowledge on these aspects, and the following discussion reviews the main findings of the four research chapter (Chapters 3-6), as well as includes the main implications of these findings for understanding the interactions between fossorial adaptations in mammals and the morphogenetic processes generating the phenotype of long bones in bathyergids, as well as its implications for other mammals.

Chapter 3 explored the postnatal development of the highly specialized scratch-digger, the Cape dune mole rat, *Bathyergus suillus* (Bathyergidae). This is the largest subterranean mammal, which lives in sandy soils of the Western Cape of South Africa. By performing a multiscale approach of their long bone microanatomy and relating developmental changes of their external anatomy, limb function and changes in animal behavior as maturation commences, this study revealed how a combination of both genetic and behavioral factors related to scratch-digging impacted on limb maturation. Multivariate analysis showed that the specialized phenotype of this species underwent considerable morphological changes during ontogeny, e.g. juveniles showed externally more robust bones with thin cortical walls, whereas adults presented slender bones with significantly thicker cross-sections. Such changes are probably related to the increased digging demands and agonistic behaviors of the developing young. However, other anatomical features such as greater external epicondylar robustness, well-developed olecranon, teres major and deltoid processes were already expressed perinatally, suggesting that genetic factors played a major role in their development.

Several aspects are integrated for first time in this chapter. The morpho-functional analysis of fossorial mammals has usually considered the calculation of indices based on mediolateral aspects of their diaphysis (e.g. ulnar robustness index - URI). However, the main axis being loaded (bending strains) during parasagittal scratch-digging in tetrapods is the anteroposterior axis (Montoya-Sanhueza *et al.*, 2019, and references therein). These aspects are reviewed and corrected indices were included in the analysis, showing that, for example, the

mediolateral robustness of the ulna (URI) did not vary throughout ontogeny in *B. suillus* (Fig. 3.3), while the anteroposterior robustness of the ulna (URI*) increased considerably its thickness during ontogeny (Fig. 3.2). This indicated that there was a stronger adaptive signal for the corrected index (URI*), most likely indicating local bone adaptation associated with the increased digging demands of the adults. Since this index was highly informative in terms of functional adaptation of the ulna, it represents an appropriate index to estimate bending loads, and it should be implemented in further research of fossorial mammals, as well as ecomorphological specializations of vertebrates in general.

The inclusion of different structural dimensions on the analysis of bone shape (i.e. the multiscale approach), contributed considerably to understand how morphological changes and development are tightly related to the shifts in behavior during life. As the pups become more active and increased their digging demands, an increase in cortical thickening and bone elongation was also observed (Fig. 3.7). Previous studies have hypothesized that mammalian juveniles have more robust bones in external morphology as a trade-off to increase geometric robusticity and hence reduce the risk of fractures of "weaker" young bone matrix, as well as to increase their effective force by altering muscles' line of action and thus compensating for their lower muscular development (Carrier, 1983; Young *et al.*, 2010; Echeverría *et al.*, 2014). This may explain the more robust external anatomy of newborns and juveniles of *Bathyergus*, while thicker cortical walls in adults will provide higher bending resistance to increased muscle loading due to higher digging demands (Casinos *et al.*, 1993; Echeverría *et al.*, 2014). Similarly, adults with slender bones would also contribute to increase locomotor performance.

This research also represents the first time that developmental modules have been applied to long bones. This aspect has been widely applied to cranial features in a wide range of vertebrates and have showed interesting patterns of variation and interaction between different components of the skeletal system (Hall, 2015). One of the most common models to which this has been applied is the mammalian dentary, which is known to be historically the result of the fusion of several bones during mammalian evolution (Hall, 2015), and that has been identified as comprising several modules that behave differently through growth and development (Hall, 2015). This conceptualization was lacking for long bones, most likely because of the assumption that long bones are independent units without historical evidence of fusion of different bones. However, long bones are complex structures that show differential developmental regions, with specifically different ossification processes accounting for different aspects of their phenotype during morphogenesis. Thus, long bones reach their final phenotype (sizes and shape) by a modular process involving intramembranous and endochondral ossifications (Fig. 5.1). These two processes were identified as relatively independent modules in this thesis. Such processes work together to generate the changes in size and shape of bones, and under a histological point of view, they are part of the bone modeling process (Montoya-Sanhueza & Chinsamy, 2017, and references therein). Bone modelling represents the uncoupled cellular activity of bone formation and bone resorption, and which is regulated by different intrinsic and external factors. In this chapter, the main results obtained from the

comparison between bone modules was that endochondral and periosteal modules in *B. suillus* showed distinct growth rates and amount of variance: the periosteal module showed a higher variability and tended to grow faster than the endochondral module. This was further corroborated for all bathyergids in Ch. 4.

Nevertheless, these findings are not exclusive of bathyergids. Based on previous studies of growth patterns in mammals, it was seen that this process of modularity is also present in other species, thus representing a highly relevant phenomenon for understanding the adaptation and evolution of skeletal systems. In this sense, it is known that intramembranous ossification has complex network of mechanosensory receptors that stimulated its local adaptation (Currey, 2002). The understanding of these aspects is fundamental to reveal the causes of bone adaptation, and represents a potential venue of research in bone biomechanics and analysis of bone microstructure.

The aim of Ch. 4 was to investigate the morphological diversity and intraspecific variation of the phenotype of seven species of adult bathyergids: *Bathyergus suillus, Heliophobius argenteocinereus, Georychus capensis, Cryptomys hottentotus, Fukomys damarensis, Fukomys mechowii* and *Heterocephalus glaber*. The main goal of this chapter was to determine which anatomical features of the appendicular system are shared between species, and how these are related to their specific social behaviors, digging strategies and locomotor ability. African mole-rats build extensive and complex burrow systems, mostly with their chisel-like incisors, and only *Bathyergus* uses their long fore-claws for soil excavation. However, all bathyergids use their forelimbs (and hindlimbs) as fundamental tools to both help during excavation and push the soil out of the burrows. Based on this information, it was hypothesized (*Hypothesis A*, Ch. 1) that the type of social strategy observed in bathyergids influenced the morphology of their appendicular skeleton, since a cooperative lifestyle would compensate for individual optimization of anatomical structures for burrow construction. Thus, it was expected that solitary taxa (*Heliophobius, Georychus* and *Bathyergus*) will show a more specialized ("morphologically divergent") appendicular anatomy as compared to social taxa (*Heterocephalus, Fukomys* spp. and *Cryptomys*), which will have a more generalized or simplified limb morphology. Additionally, it was expected that scratch-digging species like *B. suillus* will show a higher degree of morphological specialization in their limbs as compared to chisel tooth digging taxa (*Heterocephalus, Fukomys* spp., *Cryptomys, Heliophobius* and *Georychus*), due to higher anatomical specialization to maximize scratch-digging behavior (i.e. soil breakup).

The results showed that, in general, bathyergids shared a similar gross appendicular anatomy, which is composed of the typical features associated with increased fossorial ability, i.e. higher humeral epicondylar index (EIh), robust diaphysis (HRI), index of fossorial ability (IFA), presence of a distally located deltoid process (RDP) and fusion of tibia and fibula (Fig. 4.5-4.6). Nevertheless, these features were not necessarily more specialized as compared to other fossorial mammals. The fossorial mammals analyzed in previous studies (e.g. Samuels & Van Valkenburgh, 2008) showed higher mean values for traits like the humeral epicondylar index (EIh), index of fossorial ability (IFA) and mediolateral robustness of the ulna (URI) as compared to bathyergids. This indicates that a fully

subterranean lifestyle does not always requires a maximum level of skeletal specialization, at least in bathyergids.

Despite the generalized anatomy within Bathyergidae, multivariate comparisons and multiple ordination of the morpho-functional indices, showed some differences among species, mostly associated with their digging ability and locomotor performance (Fig. 4.9-4.10). These aspects were better visualized when the bathyergid species were classified into novel ecomorphological groups, to understand the interrelationship between phenotype and their social systems and digging behaviors. This classification included solitary scratch-diggers, solitary chisel-tooth diggers and social chisel-tooth diggers, thus comprising their major structural, functional and ecological aspects of their subterranean lifestyle. The results of this investigation showed that in general, social species appeared to have a phenotype more specialized to increase digging ability and locomotor performance, whereas solitary species showed a relatively less specialized fossorial phenotype, and a diminished locomotor ability. This may contribute to foraging strategies in social species which are known to have more complex and relatively longer burrow systems as compared to solitary species (Le Comber *et al.* 2002, 2006). Despite clear differences between groups, the original hypothesis (*Hypothesis A*, Ch. 1) of increased limb specialization in scratch-diggers was not supported, and social species (except *H. glaber*) showed better specializations for scratch-digging. It was concluded that factors such as social strategy may be modulating the appendicular phenotype through morphogenetic modifications (see below).

One set of morpho-functional indices associated with the locomotor performance, i.e. the crural index (CI), the brachial index (BI) and the intermembral index (IMI) provided important information about the appendicular system of bathyergids. Bathyergids showed relatively symmetrical intralimb and interlimb proportions as compared to other surface-dwelling mammals. The intermembral index (IMI) of adult bathyergids is higher (0.87) as compared to the generalized condition for large surface-dwelling (terrestrial) mammals, which have larger hindlegs than forelegs (0.75, Howell, 1965). Similarly, Lehmann (1963) found that the length of the hindlimbs of other subterranean mammals like *Geomys*, *Ctenomys*, and *Tachyoryctes* are more nearly equal to the length of the forelimbs and differs from the non-fossorial forms and *Rattus,* in which there is a tendency for the hindlimbs to be longer. This was also noted in Ch. 3 for *B. suillus* (Montoya-Sanhueza *et al.,* 2019). The fact that subterranean mammals move through narrow spaces, usually in long burrow systems (Sherman *et al.*, 1991; Bennett & Faulkes, 2000), may imply that their limb proportions (endochondal ossification module) undergo special selective pressures. Previous behavioral experiments in the head lift digger, *Spalax leucodon ehrenbergi* have showed important modifications in their locomotor pattern due to postural challenges, specifically switching its hindlimb function to act as forelimbs (Eilam *et al.*, 1995). Anatomically, it has been hypothesized that this process is facilitated by having symmetric limb proportions and elongated bodies, allowing equal bidirectional locomotion of the animal within burrows thus emphasizing equal propulsive action of both limbs (Novacek, 1980). For these reasons, in this study was suggested that symmetrical limb proportions may be related to maximize equal bidirectional locomotion within

burrows by maintaining equal propulsive action of the fore- and hindlimbs. Thus, the high IMI found in bathyergids and other fossorial mammals may not represent a fossorial adaptation for excavation *per se*, but a morphological specialization for bidirectional locomotion in burrows and narrow spaces (Montoya-Sanhueza *et al.*, 2019). The implications of such modification of the limb proportions on the osteogenesis of limb bones are discussed in the next section.

Regarding the appendicular anatomy of bathyergids, the fusion of the tibia and fibula was previously associated with its fossorial condition (De Graaff, 1979; Landry, 1999; Patterson & Upham, 2014). However, only *H. glaber* showed an unfused condition of the tibia and fibula. Overall, the phenotype of *H. glaber* is rather simplified, showing some similarities with the sister groups of Bathyergidae, the petromurids, and Phiomorpha, the histricines. These groups show unfused epiphyses (and lack of a deltoid process in the humerus), so in this thesis it is suggested that the condition of *H. glaber* may most likely reflect its basal condition within the family (Faulkes *et al.*, 2004; Upham & Patterson, 2015). The morphometric analysis of the cranial morphology of bathyergids performed by Gomes Rodrigues *et al.* (2015) showed that chisel-tooth diggers and scratch diggers (i.e., *Bathyergus*) show specialized crania and mandibles, and this sets apart *Heterocephalus* from other mole-rats. This information also supports the idea that naked mole-rats have a distinctive -simplified- phenotype as compared to other fossorial animals, and that having a highly subterranean and colonial lifestyle, may not require the same level of skeletal specializations for scratch-digging as other fossorial mammals. Overall, this indicates that the morphological adaptations observed in subterranean and fossorial mammals are not as homogenous as previously thought, but instead they constitute a wide range of morphological transitions that vary in terms of the ecological and biological aspects of the species, and sometimes they can result in a complex combination of phenotypes. The role of phylogeny in the evolution of fossorial traits is an aspect that must be considered in future research.

In Ch. 5, two hypotheses were assessed. The first is related to the relative bone growth rates between fore- and hindlimbs (*Hypothesis B,* in Ch.1). Previous studies on extant mammals showing various locomotor modes, gaits, postures and sizes that included marsupials, lagomorphs, rodents, scandentians and primates, found that hindlimb elements generally grow much faster than the homologous forelimb elements (Carrier, 1983; Lammers & German, 2002; Schilling & Petrovitch, 2006; Young, Fernandez & Fleagle, 2010). Since the pectoral girdle and forelimb bones are important for burrow construction in bathyergids (e.g. Genelly, 1965; Jarvis & Sale, 1971), the humerus, ulna and humerus+ulna were expected to show faster growth rates as compared to their serial homologues, the femur, tibia-fibula, femur+tibia-fibula, respectively. It was therefore expected that the forelimb elements would show higher slopes, thus indicating comparatively faster/earlier rates of maturity than hindlimb bones. This study showed that all bathyergids have a relatively similar skeletal growth, irrespective of social behavior or digging strategy, although some differences can be seen in some bones (e.g. tibia-fibula). Contrary to the initial hypothesis, here it was demonstrated that the femur and tibia (and the hindlimb as a whole) showed similar growth rates to the humerus

and ulna (and to the forelimb). This explains the relatively symmetrical limb proportions found in chapters 3 and 4.

It is likely that forelimb growth rates represent an increased growth rate in relation to hindlimbs in bathyergids as an adaptation to balance the growth of this limb with that of the hindlimb, although a synchronized reduction in hindlimb growth rates is also possible. This latter can be observed in the tibia-fibula, which showed the lowest growth rates among bathyergids (Table 5.7). Consequently, the relatively symmetrical bone proportions between limbs in bathyergids may be the result of acceleration of the rates of bone formation on the growth plate of the forelimbs, and a reduction in growth plate activity of the hindlimbs. Additionally, it is suggested that the original ideas suggesting faster growth rates for hindlimbs, are most likely a reflection of the scarce assessment of other non-terrestrial mammals, including subterranean species.

The second hypothesis (*Hypothesis C*, Ch. 1), explored the differences in growth rates between endochondral and intramembranous ossifications during ontogeny. It was expected that because of the differences in the timing of epithelial cell production and growth plate conservatism (predetermination), endochondral ossification will show a more stable pattern of bone growth, and therefore faster growth rates as compared to intramembranous ossification which rather will be more variable due to the constant *de novo* cell formation at periosteal surfaces. In this study, clear differences in the growth pattern between the periosteal and endochondral modules were observed, thus partially supporting the initial hypothesis C, since only some periosteal modules showed relatively higher growth rates, while endochondral modules were more similar in each bone. The most significant difference between endochondral and intramembranous modules was the higher degree of variation of the periosteal module, which appeared to be considerably less dependent on body size (and age) and genetic factors. These results highlight the relevance of considering developmental modularity of long bones in further assessments of bone adaptations, especially for understanding the differential effects of intrinsic and extrinsic factors regulating endochondral and periosteal (intramembranous) ossification and maturity.

Additionally, based on the results of Ch. 4, where external bone morphology was found to be similar among all bathyergid species, except for *H. glaber*, it was expected that the latter would show comparatively lower growth rates. The results show that naked mole-rats have the most distinct growth patterns among bathyergids, with clear neotenic features in the development of their appendicular system. This suggest a consequent increment of the bone growth rates of all other bathyergid species during their evolution. The lower growth rates observed in naked mole-rats is probably related to their less specialized appendicular morphology (i.e. humerus and tibia), which contrasts with the more specialized and more morphologically complex condition of the humerus and tibia of the other bathyergids. This agrees with McNamara's (1997) suggestion that acceleration implies fast growing of structures (peramorphosis), which involves more shape change and an increase in structural/morphological complexity, while the contrary occurs under neotenic conditions, which implies slow growth (paedomorphosis), which involves less shape change and decrease in complexity.

The current study has considerably improved our understanding of growth patterns in subterranean mammals, as well as helped to determine the mechanisms behind the short-legged phenotype typically attributed to this ecomorphological group. This study also demystified previous hypothesis suggesting that mammals have developmental constrains in their appendicular system and that most mammals show isometric or positive allometric scaling of their long bones (Kilbourne & Makovicky, 2012). The data obtained here suggest that the interplay of functional aspects such as foraging and locomotion in narrow spaces (burrows) may have had a stronger effect on the independent modulation and selection of forelimb and hindlimb proportions of subterranean mammals, through modifications on their growth patterns. In this regard, a recent study assessing the external and internal morphology of stylopodial bones of a wide range of rodents with different locomotor strategies showed that subterranean and fossorial species were the only ecomorphological group to consistently show increased rates of humeral and femoral morphological evolution (Hedrick *et al.*, 2020). This latter study supports the idea that the subterranean niche imposes strong selective pressures in the phenotype of mammals.

Generalizations about a common body plan in growth rates among mammals must be taken cautiously since growth rates are known to vary considerably in bones (Currey, 2002). It is most likely that such interpretations result from the small sample studied, which is composed mainly of species with a terrestrial (surface-dwelling) lifestyle, and that terrestrial --aboveground-- locomotion and its associated limb bone growth patterns cannot be restricted to the use of simplified allometric approaches and constrained phylogenetic sampling. These approaches are useful for certain questions. Importantly, the current research has showed that although some species have similar slopes (test for equality of slopes), they showed different growth patterns and allometric trends. This indicates that simplified allometric approaches are not a good estimator of the developmental patterns occurring in mammals, so caution must be put for generalizations on limb bone growth. Allometric approaches are highly simplified, approximate formulas that can be applied to a wide range of phenomena, but they are neither a dogma nor a definitive explanation for natural processes (Von Bertalanffy, 1968).

The final chapter of this thesis (Ch. 6) provides a comprehensive description of the patterns of bone modeling in bathyergids and includes an assessment of their bone dynamics using fluorochrome labeling. Until now, the only group where a wide ontogenetic and within-family research has been done is in primates (Castanet *et al.*, 2004; McFarlin, 2006; Warshaw, 2008; McFarlin *et al.* 2016). In fact, several decades ago Enlow (1969) said, "*Phylogenetic as well as ontogenetic studies have not yet been carried out in adequate detail within restricted groups, and such investigations are strongly urged*." The present study on bathyergids provides a valuable contribution for the understanding of bone modeling not only in rodents, but also in mammals.

In this chapter, four bathyergid species were studied in order to test different hypothesis: *Heterocephalus glaber* (*n* = 83), *Heliophobius argenteocinereus* (*n* = 30), *F. mechowii* (*n* = 30) and *Cryptomys hottentotus natalensis* (*n* = 10). The first hypothesis (*Hypothesis D*, Ch 1) suggests that all bathyergid species will show

similar bone modeling patterns, which will be evidenced by similar composition of bone tissue matrices (histodiversity) in the diaphyseal cortical bone. This follows the fact that the general long bone anatomy of most bathyergids is relatively similar (Fig. 4.5-4.6). Indeed, all bathyergids analyzed showed increased cortical bone thickening during ontogeny, as well as low rates of endosteal bone resorption. Cortical thickening was reached mostly by endosteal and periosteal bone depositions, which is similar to the findings made previously for *B. suillus* (Montoya-Sanhueza & Chinsamy, 2017). Also, all species showed high histodiversity including woven bone, parallel-fibered bone, lamellar bone, compacted coarse cancellous bone and lamellar lamellated bone. Similarly, all species showed limited remodeling (i.e. development of secondary osteons) and they do not develop Haversian bone tissues. Naked mole-rats were the exception to some of these features, for example showing very limited remodeling activity.

The second hypothesis assessed in this chapter (Hypothesis E) was that the species with higher bone growth rates will show increased amounts of rapidly deposited bone tissues (i.e. WB, CCCB and perhaps PFB) bone tissues, while species with slow growth rates will show predominance of slowly deposited bone tissues (LB, LLB, and perhaps PFB). However, as observed in Ch. 5, most species showed similar periosteal growth rates (Table 5.10, 5.11), and their cortical walls were composed of similar bone tissues (see Ch. 6), although some differences in the amounts of bone tissues deposited were observed at intraspecific and interspecific level. Further quantitative analysis of such features is needed to identify the causes of such variations.

The last hypothesis assessed here (*Hypothesis F*, Ch. 1) was associated with the maturity of certain bones. Given that the pectoral girdle and forelimb bones are important during excavation and burrow construction, it was hypothesized that the humerus and ulna will show faster growth rates as compared to hindlimb bones. This was expected to be seen by forelimb bones maturing earlier than hindlimb bones, and histologically this will be evident by the humerus and ulna showing more rapidly deposited bone tissues as compared to the femur and tibia of the same individual. A similar pattern is expected for zeugopodial and stylopodial elements, where the former will show tissues with higher bone growth rates.

The results of the study showed that all bathyergids have zonal bone, which consists of the stratified deposition of different bone matrices including the variable presence of growth marks such as annuli and/or lines of arrested growth (LAG) (Reid, 1981). This zonal bone can be of two types according to the ontogenetic stage and bone analyzed: i) bands of PFB with LB annuli in older stages, and/or ii) bands of WB with thin layers of PFB in younger stages. The finding of a stratified cortical bone and growth marks in all African mole-rats, and almost all their bone cross-sections have several implications for understanding the relationship between osteogenesis and metabolism in mammals. The periodicity of bone deposition (zonal bone) in mammals has been linked to the physiology of the species (i.e. primates and ruminants), specifically to the seasonal fluctuations of their metabolic rates, thermoregulatory strategy, hormonal activity, bone/energy homeostatic biorhythms and photoperiod (e.g. Castanet *et al.*, 2004; Castanet, 2006; Bromage *et al.*, 2009; Köhler *et al.*, 2012). In comparison to surface-dwelling mammals of similar body size, bathyergids have low body temperatures

and metabolic rates (Buffenstein & Yahav, 1991; Yahav & Buffenstein, 1991; Zelová *et al.*, 2007; Bennett *et al.*, 2009; Šumbera, 2019), as well as slow somatic growth rates (Bennett *et al.*, 1991; Ch. 5). Additionally, although they do not undergo hibernation, they can experience torpor (Šumbera, 2019), and some physiological traits such as energy expenditure, body temperature and metabolic rates are known to fluctuate between seasons in some species, thus indicating heterothermic capabilities (Sedláček, 2007a, b (in begall); Boyles *et al.*, 2011; McKechnie & Mzilikazi, 2011; Streicher *et al.*, 2011; Zelova *et al.*, 2011; Šumbera, 2019). Thus, the different types of zonal bone that can be seen in bathyergids may be related to such metabolic fluctuations, and therefore deserves further investigation.

A remarkable feature among bathyergids is the apparently less stratified cortices of naked mole-rats, although they showed growth marks regardless of sex (Fig. 6.4). Such less marked stratification of the cortex in all limb bones can be related to the unique thermoregulatory capabilities of naked mole-rats: this species is usually considered a poikilothermic mammal (but see Šumbera, 2019). Despite this, the bone matrix composition in adult naked mole-rats appears to be distinct from that of other mole-rats, in having essentially lamellar and lamellated bone tissues, as well as scarce vascularization (Fig. 6.10). These observations clearly indicate very low intramembranous bone growth rates for naked mole-rats. This was also observed in mature specimens injected with fluorochromes, which additionally showed scarce bone formation, and even when this occurred it was usually restricted to the endocortical surfaces (Fig. 6.3-6.4). This, along with slow periosteal (and endochondral) bone growth rates (reported in Ch. 5), suggest that somatic growth and skeletal growth in *H. glaber* is considerably lower as compared to other bathyergids, but that it is also relatively stable during adult stages.

Furthermore, although the hypogeous niche represent a highly stable environment in comparison to aboveground niches, subterranean organisms still undergo seasonal thermoregulatory dynamics (Moshkin *et al.*, 2007; Boyles *et al.*, 2011) and formation of zonal bone with growth marks, thus indicating that the main morphogenetic processes of osteogenesis are to some extent decoupled from environmental stresses and fluctuations, and that periodicity of bone depositions are rather a reflection of their endogenous physiological rhythms. This is further supported by the fact that the specimens of *H. glaber* recovered from captive colonies, still develop growth marks. The scarce endosteal and intracortical bone resorption observed in all bathyergids, as well as their scarce remodeling activity, contributes considerably to preserve an excellent record of their bone morphogenesis. This aspect may also explain the findings of zonal bone in bathyergids, since most of other surface-dwelling mammals undergo extensive endosteal resorption and consequent medullary expansion during ontogeny. The osteohistological descriptions made in this study represent a unique record of the patterns of bone modeling in African mole-rats (Bathyergidae, Rodentia), and contributes considerably to understand these processes among mammals.

7.2 CONCLUDING REMARKS

7.2.1 Functional Anatomy, Disparity and Ontogeny

- The limb bones of bathyergids share a highly fossorial phenotype, which is relatively similar to other small fossorial mammals. Thus, morphological disparity among most genera (*Bathyergus, Heliophobius, Georychus, Cryptomys* and *Fukomys*) is low, and differences are principally quantitative. The inclusion of naked mole-rats in the analysis results in a clear distinction of this taxon from other genera, especially in terms of features of the humeral anatomy and tibial and fibular configuration.
- Both chisel-tooth diggers and scratch-digger species have highly specialized limb bones indicating increased fossorial ability. However, naked mole-rats (*Heterocephalus glaber*) showed the lack of typical anatomical features of fossorial mammals such as deltoid process in the humerus and distal fusion of tibia and fibula, which contributed considerably to characterize its appendicular skeleton as having a more simplified -ambulatorial- phenotype. It is concluded that although a subterranean lifestyle imposes strong selective pressures on limb phenotypes, other factors, probably associated with social behavior and digging strategy are also involved in the fossorial adaptation of limb bones.
- Ecomorphological groups (i.e. solitary scratch-diggers, solitary chisel-tooth diggers and social chisel-tooth diggers) successfully determined the main morphological features characterizing each groups: social species appeared more specialized for digging ability and locomotor performance, while solitary species showed a relatively less specialized fossorial ability and diminished locomotor capacities.
- The levels of morphological specialization seem to be associated with the variation found in limb bones. The naked mole-rats showed the most simplified phenotypes within the family, but they showed the highest levels of skeletal variation (and larger morphospace) than other bathyergid species.
- Zeugopodial elements showed higher variation in external shape as compared to stylopodial elements. Similar pattern was found for bone growth rates, where distal elements are less correlated than proximal ones. This was linked to the idea of a modular proximo-distal pattern, where zeugopods, by being in direct contact with the more variable autopodial elements, adapt following a bottom-up sequence of bone adaptation synchronized to the changes occurring in the autopodial modules.
- Regarding the development of morphological specializations in the solitary scratch-digger *Bathyergus suillus,* it was shown that several morphological changes occur at different periods during perinatal and early postnatal life. Based on morpho-functional indices and bone microanatomy, the bones involved in direct scratch-digging behavior (e.g. humerus) undergo less morphological changes during ontogeny than bones not involved in such behaviors (e.g. femur). This indicated a certain degree of canalization of highly specialized bones like the humerus, and similar patterns are expected to see in other bathyergids. The fact that different dimensions of the bone such as functional lengths (endochondral modules), diaphyseal diameters (periosteal module), epicondyles (mixed module) and bone superstructures (endochondral module) show distinct developmental (heterochronic) patterns, indicated differential (intrinsic or extrinsic) regulation of such processes.

7.2.2 Adaptations to Locomotion within Burrows

- Fore- and hindlimbs develop at similar growth rates, resulting in relatively symmetrical limb proportions. It is suggested that this represents an adaptation to the subterranean lifestyle, principally to maximize quadrupedal locomotion within burrows.
- As observed in other surface-dwelling mammals with specialized saltatorial locomotor modes, the morphological changes observed during the ontogeny of *B. suillus* are also associated with shifts in postural behavior and locomotion during development.
- It is concluded that the effects of living in a dense medium and narrow spaces have an important effect on locomotor behavior, which is reflected on stronger selective pressures for phenotypical modifications of the limb bones in bathyergids. Social species have a phenotype more specialized to increase digging ability and locomotor performance, whereas solitary species showed a relatively less specialized fossorial phenotype, and a diminished locomotor ability. This seems to be related to their foraging strategies, social organization and burrow architecture.

7.2.3 Bone Modeling, Bone Microstructure and Cortical Bone Thickening

- All bathyergids have long bones with thick cortical walls in adulthood, which represents a microstructural adaptation to maximize the biomechanical properties of the bone to resist bending and torsion during digging activities. Nevertheless, intraspecific and interspecific differences were observed for this feature, which was also observed in the generalized higher degrees of variability found in the periosteal (intramembranous) module.
- All bathyergids showed scarce endosteal and intracortical bone resorption during ontogeny, which permitted the maintenance of bone tissues deposited earlier in life. Additionally, all species showed limited remodeling (i.e. development of secondary osteons) and they do not ever develop Haversian bone tissues. These characteristics indicate that despite the modeling activity during early postnatal development, they have very low rates of bone turnover during adulthood.
- Changes in increased bone robustness in *B. suillus* (thickening of cortical bone walls) are most likely associated with internal factors (hormonal activity) linked associated to the attainment of skeletal maturity and/or sexual maturity. The fact that most of subordinate (non-sexually mature) specimens born in captivity (e.g. *H. glaber* and *Fukomys damarensis*) showed thick cortical walls, suggest that attainment of sexual maturity played a lesser role for cortical thickening in such species. It is suggested that solitary species reach skeletal and sexual maturity synchronically. Thus, external factors such as increased digging demands and agonistic behaviors during early life of the developing young in solitary species may also contribute to reaching peak bone mass, as occurs in other rodents and humans (see Montoya-Sanhueza & Chinsamy, 2017, and references therein). The development of bone phenotypes involves a complex interplay of both endogenous and external factors affecting its morphogenesis.

7.2.4 Osteogenesis and Bone Modules

- Excluding *H. glaber*, most bathyergids have conservative endochondral growth rates indicating similar growth plate activity. This may explain the symmetric limb proportions found in all species.

- The endochondral and periosteal modules have different dynamics irrespective of social behavior or digging strategy in bathyergids. In general, the periosteal module showed relatively higher growth rates and a higher degree of variation as compared to the endochondral module, thus appearing to be considerably less dependent on body size and genetic factors. Similar observations in other mammals demonstrate that this represent a global pattern of bone ossification and may explain how modules adapt through local bone adaptation during ontogeny and how modules change during evolution.
- Given the basal phylogenetic position of naked mole-rats among bathyergids, and the fact that they have the lowest growth rates within the family, a neotenic condition is suggested for this taxon, and consequently accelerated bone growth rates are hypothesized for the evolution of the other bathyergids.

7.3 FUTURE DIRECTIONS

The current research highlighted the interaction between social behavior of Bathyergidae and bone adaptations. However, further research is needed to assess what are the specific differences in the amount and type of digging behavior performed by different fossorial species. In the case of social species, the individual's contribution within a colony and burrow activity are also needed to be assessed. Similarly, the development of fossorial behaviors during ontogeny at species-specific level, would also contribute to understand the synchronicity between morphological specializations and activity.

The effects of captivity on limb development of mole-rats are not yet fully understood. Experimental designs at species-specific level will contribute substantially to understand such processes.

Similarly, the findings of differences in the patterns of bone ossification highlights the relevance of considering developmental modularity of long bones in further assessments of bone adaptation. The inclusion of a wider range of subterranean and fossorial mammals is also necessary

In a phylogenetic sense, it would be important to assess the evolution of certain anatomical traits associated with fossoriality in bathyergids such as development of superstructures in bones. The testing of different evolutionary patterns among subterranean and fossorial mammals can be considered.

In general, there is still a much-needed gap in our understanding of bone growth and development in response to locomotor and physiological adaptations within specific mammalian families. It is likely that the main patterns of bone adaptation are highly dependent on the group analyzed, thus a better understanding of these processes will result from the multivariate assessment of a wider range of mammalian families rather than studying single species.

References

Alberch P, Gould SJ, Oster GF, Wake DB. 1979. Size and shape in ontogeny and phylogeny. Paleobiology 5: 296–317.

Allen M, Burr D. 2014. Bone Modeling and Remodeling (Ch. 4). In: *Basic and Applied Bone Biology* (eds DB Burr, M Allen), pp. 373. Academic Press, Elsevier, London.

Assis, A.P.A., Costa, B.M.A., Rossoni, D.M., Melo, D., and Marroig, G. 2016. Modularity and Integration. In: Kliman, R.M. (ed.), Encyclopedia of Evolutionary Biology. vol. 3, pp. 34–40. Oxford: Academic Press.

Atchley WR, Hall BK. 1991. A model for development and evolution of complex morphological structures. Biological Reviews 66: 101–157.

Barčiová L, R. Šumbera & H. Burda, 2009. Variation in the digging apparatus of the subterranean silvery mole-rat, *Heliophobius argenteocinereus* (Rodentia, Bathyergidae): the role of ecology and geography. *Biol J Linn Soc,* 97:822–831.

Baron R, & Horne W. 2005. Regulation of osteoclast activity. In: *Bone Resorption* (eds F Bronner, M C.Farach-Carson, J Rubin), pp. 189. Springer-Verlag, London.

Bronner F, Farach-Carson M, & Rubin J (Eds). Springer Vol.2, Series Topics in Bone Biology. London. 189 pp.

Bateman N. 1954. Bone growth: a study of the grey-lethal and microphthalmic mutants of the mouse. *Journal of Anatomy* **88**, 212–262.

Beamer W, Donahue L, Rosen C, Baylink D. 1996. Genetic Variability in Adult Bone Density Among Inbred Strains of Mice. Bone 18: 397–403.

Begall S, Burda H, Schleich C. **2007.** *Subterranean Rodents. News from underground.* Springer-Verlag, Berlin, Heidelberg.

Bennett, NC. 2013. *Cryptomys hottentotus* Forest Giant Squirrel; pp 655–658 in Happold, D. C. D. (ed.) 2013. Mammals of Africa: Volume III. Bloomsbury Publishing, London.

Bennett, NC, & H, Burda. 2013. *Cryptomys mechowi*. Pp. 659-660 in Mammals of Africa. 3. Rodents, hares and rabbits (M. Happold and D. C. D. Happold, eds.). Bloomsbury Publishing. London, United Kingdom.

Bennett NC, 2009. African mole-rats (family Bathyergidae): models for studies in animal physiology. *Afr Zool*, 44:263–270.

Bennett NC, Faulkes CG, Hart L, Jarvis J. **2009.** *Bathyergus suillus* (Rodentia: Bathyergidae). *Mammalian Species* **828**, 1–7.

Bennett NC, & Faulkes CG. 2000. African Mole Rats: Ecology and Eusociality. Cambridge, UK: Cambridge University Press.

Bennett, N.C. & G.H. Aguilar. 1995. The reproductive biology of the Zambian mole-rat, *Cryptomys mechowi* (Rodentia : Bathyergidae). Afr. J. ZooL, 30 : 1 -4.

Bennett NC, Jarvis J, Aguilar GH, & Mcdaid EJ. 1991. Growth and development in six species of African mole-rats (Rodentia: Bathyergidae). Journal of Zoology 225: 13–26.

Bennett, N. C., Jarvis, J. U. M. & Wallace, D. B. 1990. The relative age structure and body masses of complete wild-captured colonies of two social mole-rats, the common mole-rat,

Cryptomys hottentotus hottentotus and the Damaraland mole-rat, *Cryptomys damarensis*. J. Zool. 220, 469–485.

Bennett, N.C., Jarvis, J.U.M., Davies, K.C., 1988. Daily and seasonal temperatures in the burrows of African rodent moles. South Afr. J. Zool. 23, 189–195.

Berkovitz B, Faulkes CG. 2001. Eruption rates of the mandibular incisors of naked mole-rats (*Heterocephalus glaber*). Journal of Zoology 255:461–466

Biewener AA, Bertram JEA. 1993. Mechanical loading and bone growth *In Vivo*. In: *Bone Volumen 7 Bone Growth - B* (ed BK Hall), pp. 353. CRC Press, Boca Raton.

Biewener BA, Taylor CR. 1986. Bone strain: a determinant of gait and speed? Journal of Experimental Biology. 123: 383–400.

Boag, PT, Boonstra, R. 1988. Quantitative genetics of life history traits in meadow voles (*Microtus pennsylvanicus*). Evolution of Life Histories of Mammals (ed. M.S. Boyce), pp. 149-168. Yale University Press, London.

Botha J, Chinsamy A. 2004. Growth and life habits of the Triassic cynodont *Trirachodon*, inferred from bone histology. Acta Palaeontologica Polonica, 49: 619–627.

Boyles, J.G., Verburgt, L., McKechnie, A.E., Bennett, N.C., 2012. Heterothermy in two mole-rat species subjected to interacting thermoregulatory challenges. J. Exp. Zool. Part Ecol. Genet. Physiol. 317, 73–82.

Brianza SZM, Delise M, Ferraris M et al. 2006. Cross-sectional geometrical properties of distal radius and ulna in large, medium and toy breed dogs. *Journal of Biomechanics* **39**, 302–11.

Brodt MD, Silva MJ. 2010. Aged mice have enhanced endocortical response and normal periosteal response compared with young-adult mice following 1 week of axial tibial compression. J Bone Miner Res.; 25(9):2006-2015. doi:10.1002/jbmr.96

Bromage TG, Goldman HM, McFarlin SC et al. 2003. Circularly polarized light standards for investigations of collagen fiber orientation in bone. *Anatomical record. Part B, New anatomist* **274**, 157–68.

Buffenstein, R, T. Park, M. Hanes, J.E. Artwohl. Naked mole rat. In: M.A. Suckow, K.A. Stevens, R.P. Wilson (Eds.), The Laboratory Rabbit, Guinea Pig, Hamster, and Other Rodents., Elsevier (2012), pp. 1055-1074.

Buffenstein R, Pinto. 2009. Endocrine function in naturally long-living small mammals. *Mol. Cell. Endocrinol.* 299: 101–111.

Buffenstein R. 2008. Negligible senescence in the longest living rodent, the naked mole-rat: insights from a successfully aging species. J. Comp. Physiol. B, 178, 439–445. http://doi.org/10.1007/s00360-007-0237-5

Buffenstein R, Jarvis J, Opperman LA et al. 1994. Subterranean mole-rats naturally have an impoverished calciol status, yet synthesize calciol metabolites and calbindins. *European journal of Endocrinology* **130**, 402–409.

Buffenstein R, Yahav, 1991. Is the naked mole-rat, *Heterocephalus glaber*, a poikilothermic or poorly thermoregulating endothermic mammal? *J Therm Biol.* 16:227–232.

Burda, H, R. Šumbera & S. Begall. 2007. Microclimate in Burrows of Subterranean Rodents – Revisited. In Begall S, Burda H, Schleich C. (Eds). *Subterranean Rodents. News from underground.* Springer-Verlag, Berlin, Heidelberg.

Burda, H., R. L. Honeycutt, S. Begall, O. Grütjen, & A. Scharff. 2000. Are naked and common mole-rats eusocial and if so, why? Behavioral Ecology and Sociobiology 47:293–303.

Burger EH, Veldhuijzen JP. 1993. Influence of mechanical factor on bone formation, resorption and growth in vitro. In: *Bone Volumen 7 Bone Growth - B* (ed BK Hall), pp. 368. CRC Press, Boca Raton.

Burr DB, Akkus O. 2014. Bone morphology and organization. In: *Basic and Applied Bone Biology* (eds DB Burr, M Allen), pp. 373. Academic Press, Elsevier, London.

Burr, DB. 1992. Estimated intracortical bone turnover in the femur of growing macaques: implications for their use as models in skeletal pathology. The Anatomical Record 232:180–9.

Busch C, Antenucci D, Valle j. C del, Kittlein MJ, Malizia AI, Vassallo A, Zenuto RR. 2000. Population Ecology of Subterranean Rodents. In: Lacey EA,, In: Patton JL, In: Cameron GN, eds. Life Underground: the biology of subterranean rodents. Chicago: University of Chicago Press, 183–226.

Cadet ER, Gafni RI, McCarthy EF, McCray DR, Bacher JD, Barnes KM, Baron J (2003) Mechanisms responsible for longitudinal growth of the cortex: coalescence of trabecular bone into cortical bone. J Bone Joint Surg Am 85:1737–1748

Cameron, GN, Mcclure PA. 1988. Geographic variation in life history traits of the hispid cotton rat (*Sigmodon hispidus*). Pp. 33-64 in Evolution of the life histories of mammals (M. S. Boyce, ed.). Yale University Press, New Haven, Connecticut.

Candela AM, Picasso MBJ. 2008. Functional Anatomy of the Limbs of Erethizontidae (Rodentia, Caviomorpha): Indicators of Locomotor Behavior in Miocene Porcupines. Journal of Morphology 269: 552–593.

Carleton, A. (1941). A comparative study of the inferior tibio-fibular joint. J. Anat., Lond., 76, 45-55.

Carmeli-Ligati S, Anna Shipova, Maïtena Dumont, Susanne Holtz, Thomas Hildebrandt, Ron Shahar. 2019 The structure, composition and mechanical properties of the skeleton of the naked mole-rat (*Heterocephalus glaber*). Bone Volume 128, November 2019, 115035.

Carrier R. 1983. Postnatal ontogeny of the musculo-skeletal system in the Black- tailed jack rabbit (*Lepus californicus*). *Journal of Zoology, London* **201**, 27–55.

Casinos A, Quintana C, Viladiu C. 1993. Allometry and adaptation in the long bones of a digging group of rodents (Ctenomyinae). *Zoological Journal of the Linnean Society* **107**, 107–115.

Castanet J. 2006. Time recording in bone microstructures of endothermic animals; functional relationships. *Comptes Rendus Palevol* **5**, 629–636.

Castanet J, Croci S, Aujard F et al. 2004. Lines of arrested growth in bone and age estimation in a small primate: *Microcebus murinus*. *journal of zoology of london* **263**, 31–39.

Chimimba, C. T., A. M. Sichilima, C. G. Faulkes, & N. C. Bennett. 2010. Ontogenetic variation and craniometric sexual dimorphism in the social giant mole-rat, *Fukomys mechowii* (Rodentia: Bathyergidae), from Zambia. African Zoology 45:160-176.

Chinsamy A, Hurum J. 2006. Bone microstructure and growth patterns of early mammals. *Acta Palaeontologica Polonica* **51**, 325–338.

Cowgill LW. 2007. Humeral torsion revisited: a functional and ontogenetic model for populational variation. *American journal of physical anthropology* **134**, 472–480.

Cox PG, Hautier L. 2015. Evolution of the Rodents: Advances in Phylogeny, Functional Morphology and Development. Cambridge: Cambridge University Press.

Cox, P. G. and Faulkes, C. G. (2014). Digital dissection of the masticatory muscles of the naked mole-rat, *Heterocephalus glaber* (Mammalia, Rodentia). PeerJ 2, e448.

Cubo J, Ventura J, Casinos A. 2006. A heterochronic interpretation of the origin of digging adaptations in the northern water vole, *Arvicola terrestris* (Rodentia: Arvicolidae). Biological Journal of the Linnean Society 87: 381–391.

Cubo J, Azagra D, Casinos A, Castanet J. 2002. Heterochronic detection through a function for the ontogenetic variation of bone shape. Journal of Theoretical Biology 215: 57–66.

Cubo J. 2000. Process heterochronies in endochondral ossification. Journal of Theoretical Biology 205: 343–353.

Currey, M.N. Dean, R. Shahar, Revisiting the links between bone remodeling and osteocytes: insights from across phyla, Biol. Rev. Camb. Philos. Soc. 92 (2017) 1702–1719.

Currey J. 2002. Bone. Structure and Mechanics. Princeton University Press, Oxfordshire, UK.

Churakov, G., Sadasivuni, M. K., Rosenbloom, K. R., Huchon, D., Brosius, J., & Schmitz, J. (2010). Rodent evolution: Back to the root. Molecular Biology and Evolution, 27(6), 1315–1326.

Dammann P, Burda H. 2007. Senescence patterns in African mole-rats (Bathyergidae, Rodentia). In: Begall S, In: Burda H., In: Schleich C, eds. Subterranean Rodents : News from Underground. Heiderberg, Germany : Springer-Verlag, 251-263.

Davies et al., 2015. Family Wide Molecular Adaptations to Underground Life in African Mole-Rats Revealed by Phylogenomic Analysis. *Mol Biol Evol*; 32 (12): 3089-3107.

Davies KC, Jarvis JUM. 1986. The burrow systems and burrowing dynamics of themole-rats *Bathyergus suillus* and *Cryptomys hottentotus* in the fynbos of the south-western Cape, South Africa. Journal of Zoology (A) 209:125–147.

Davis DD (1964) The giant panda: A morphological study of evolutionary mechanisms. Fieldiana: Zoology 3:1-339

De Blocq A. 2016. 'Bon voyage' to UCT's naked mole rats. (visited on January, 2020). https://andrewdeblog.weebly.com/home/bon-voyage-to-ucts-naked-mole-rats

De Graaff, G. 1979. Molerats (Bathyergidae, Rodentia) in South African National Parks: notes on the Taxonomic "isolation" and Hystricomorph Affinities of the family. Koedoe, Vol 22, (1): a653.

De Souza RL, Matsuura M, Eckstein F, Rawlinson SC, Lanyon LE, Pitsillides AA. 2005. Non-invasive axial loading of mouse tibiae increases cortical bone formation and modifies trabecular organization: a new model to study cortical and cancellous compartments in a single loaded element. Bone ;37(6):810-818. doi:10.1016/j.bone.2005.07.022

Dengler-Crish C, Catania KC. 2009. Cessation of Reproduction-Related Spine Elongation After Multiple Breeding Cycles in Female Naked Mole-Rats. Anatomical Record (Hoboken) 292: 131–137.

Dengler-crish CM, Catania KC. 2007. Phenotypic plasticity in female naked mole-rats after removal from reproductive suppression. Journal of Experimental Biology 210: 4351–4358.

Denys, C. 2011. Rodents Ch. 2. In T. Harrison (ed.), Paleontology and Geology of Laetoli: Human Evolution in Context. Volume 2: Fossil Hominins and the Associated Fauna, Vertebrate Paleobiology and Paleoanthropology.

Dodson, P. (1975). Functional and ecological significance of relative growth in Alligator. J. Zool. 175, 315–355.

Doherty, A. H., Ghalambor, C. K. & Donahue, S. W. 2015. Evolutionary physiology of bone: bone metabolism in changing environments. Physiology 30, 17-29.

Duque G, Watanabe K. 2011. *Osteoporosis Research. Animal Models* (G Duque and K Watanabe, Eds.). London: Springer London.

Echeverría AI, Becerra F, Vassallo A. 2014. Postnatal Ontogeny of Limb Proportions and Functional Indices in the Subterranean Rodent *Ctenomys talarum* (Rodentia: Ctenomyidae). Journal of Morphology 275: 902–913.

Edrey et al., 2011. Endocrine function and neurobiology of the longest-living rodent, the naked molerat. *Exp Gerontol*, 46:116–123.

Eilam D. 1997. Postnatal development of body architecture and gait in several rodent species. Journal of Experimental Biology 200: 1339–1350.

Eilam D, Adijes M, Vilensky J. 1995. Uphill Locomotion in Mole Rats: A Possible Advantage of Backward Locomotion. Physiology & Behavior 58: 483–489.

Elissamburu A, Santis L De. 2011. Forelimb proportions and fossorial adaptations in the scratch-digging rodent *Ctenomys* (Caviomorpha). Journal of Mammalogy 92: 683–689.

Elissamburu A. 2010. Estudio biomecánico y morfofuncional del esqueleto apendicular de *Homalodotherium* Flower 1873 (Mammalia, Notoungulata). Ameghiniana 47: 1–17.

Elissamburu A, Vizcaino SF. 2004. Limb proportions and adaptations in caviomorph rodents (Rodentia: Caviomorpha). Journal of Zoology. 262: 145–159.

Ellerman J. R. 1956. The Subterranean Mammals of the World. Transactions of the Royal Society of South Africa, 35:1, 11-20.

Enlow DH. 1963. Principles of Bone Remodeling. An Account of Post-natal Growth and Remodeling Processes in Long Bones and the Mandible. Springfield, IL: Charles C. Thomas.

Enlow DH. 1962. A Study of the Post-Natal Growth and Remodeling of Bone. *American Journal of Anatomy* **110**, 79–101.

Erben RG. **1996.** Trabecular and Endocortical Bone Surfaces in the Rat: Modeling or Remodeling? *The Anatomical record* **246**, 39–46.

Esteve-Altava B. 2017. Challenges in identifying and interpreting organizational modules in morphology. Journal of Morphology 278: 960–974.

FCAT, 1998. Terminologia Anatomica.

Fabre P-H, Hautier L, Dimitrov D, Douzery EJP. 2012. A glimpse on the pattern of rodent diversification: a phylogenetic approach. BMC Evolutionary Biology 12:88

Fang, X., Seim, I., Huang, Z., Gerashchenko, M.V., Xiong, Z., Turanov, A.A., Zhu, Y., Lobanov, A.V., Fan, D., Yim, S.H., Yao, X., Ma, S., Yang, L., Lee, S.-G., Kim, E.B., Bronson, R.T., Šumbera, R., Buffenstein, R., Zhou, X., Krogh, A., Park, T.J., Zhang, G., Wang, J., Gladyshev, V.N., 2014. Adaptations to a subterranean environment and longevity revealed by the analysis of mole rat genomes. Cell Rep. 8, 1354–1364.

Faulkes, CG., N.C. Bennett. 2009. Reproductive skew in African mole-rats: behavioral and physiological mechanisms to maintain high skew. Ch. 13. In Reproductive Skew in Vertebrates: Proximate and Ultimate Causes, ed. Reinmar Hager and Clara B. Jones. Published by Cambridge University Press.

Faulkes CG, Verheyen E, Verheyen W, Jarvis JUM, Bennett NC. 2004. Phylogeographical patterns of genetic divergence and speciation in African mole-rats (Family: Bathyergidae). Molecular Ecology, 13:613-629.

Felsenthal N, Zelzer E. 2017. Mechanical regulation of musculoskeletal system development. Development 144: 4271–4283.

Francillon-Vieillot H, de Buffrénil V, Castanet J. 1990. Microstructures and mineralization of vertebrate skeletal tissues. In: *Skeletal biomineralizations: patterns, processes and evolutionary trends* (ed Carter J), pp. 471–530. Van Nostrand Reinhold, New York.

Frandsen A, Nelson M, Sulon E et al. 1954. The effects of various levels of dietary protein on skeletal growth and endochondral ossification in young rats. *The Anatomical Record* **119**, 247–265.

Franz-Odendaal, Hockman, 2019. Non-model organisms and unique approaches are needed for the future of evo-devo. Editorial. *Developmental Dynamics*. DOI: 10.1002/dvdy.71

Frost HM. 1969. Tetracycline-based histological analysis of bone remodeling. *Calcified tissue research* **3**, 211–237.

Frost HM. 1987. Bone "mass" and the "mechanostat": a proposal. *The Anatomical record* **219**, 1–9.

García-Martínez R, Marín-Moratalla N, Jordana X et al. 2011. The ontogeny of bone growth in two species of dormice: Reconstructing life history traits. *Comptes Rendus Palevol* **10**, 489–498.

Garrone, MC., IA. Cerda & RL. Tomassini (2019) Ontogenetic variability in the limb bones histology of plains vizcacha (*Lagostomus maximus*, Chinchillidae, Rodentia): implications for life history reconstruction of fossil representatives, Historical Biology. DOI: 10.1080/08912963.2019.1648450

Geiger, M., L. a. B. Wilson, L. Costeur, R. Sánchez, and M. R. Sánchez-Villagra. 2013. Diversity and body size in giant caviomorphs (Rodentia) from the northern Neotropics—a study of femoral variation. Journal of Vertebrate Paleontology 33:1449–1456.

Genelly, R. E. 1965. Ecology of the common mole-rat (*Cryptomys hottentotus*) in Rhodesia. Journal of Mammalogy 46:647-665.

Goldman HM, McFarlin SC, Cooper DML et al. 2009. Ontogenetic patterning of cortical bone microstructure and geometry at the human mid-shaft femur. *Anatomical record* **292**, 48–64.

Goldstein B. 1972. Allometric Analysis of Relative Humerus Width and Olecranon Length in Some Unspecialized Burrowing Mammals. Journal of Mammalogy, Vol. 53(1): 148-156.

Gomes Rodrigues H, Sumbera, R (2015), Dental peculiarities in the silvery mole-rat: an original model for studying the evolutionary and biological origins of continuous dental generation in mammals. PeerJ 3:e1233; DOI 10.7717/peerj.1233

Gomes Rodrigues H, Šumbera R, & Hautier L. 2015. Life in burrows channelled the morphological evolution of the skull in rodents: the case of African mole-rats (Bathyergidae, Rodentia). Journal of Mammalian Evolution. doi: 10.1007/s10914-015-9305-x

Gomes Rodrigues H, Marangoni P, Sumbera R, Tafforeau P, Wendelen W, Viriot L. 2011. Continuous dental replacement in a hyper-chisel tooth digging rodent. Proceedings of the National Academy of Sciences of the United States of America 108:17355–17359

Gould, S. J. (1967). Evolutionary patterns in pelycosaurian reptiles: a factor-analytic study. Evolution 21: 385-401.

Gould, S.J. 1966. Allometry and size in ontogeny and phylogeny. Biological Reviews 41:587–640.

Hall BK. **2015.** *Bones and Cartilage. Developmental and evolutionary skeletal biology.* Academic Press, Elsevier, London.

Hall BK. 1978. Developmental and Cellular Skeletal Biology. New York: Academic Press.

Hamilton, W J Jr. 1928. *Heterocephalus*, the Remarkable African Burrowing Rodent. The museum of the brooklyn institute of arts and sciences, Vol 3(5).

Hammer Ø, Harper DAT, Ryan PD. 2001. PAST: Paleontological Statistics Software Package for Education and Data Analysis. Palaeontologia Electronica 4: 1–9.

Happold, D. C. D. 2013. Mammals of Africa. Volume III: Rodents, Hares and Rabbits. Bloomsbury Publishing, London.

Hart L, Chimimba CT, Jarvis JUM, O'Riain J, Bennett NC. 2007. Craniometric Sexual Dimorphism and Age Variation in the South African Cape Dune Mole-Rat (Bathyergus suillus). Journal of Mammalogy 88: 657–666.

Heck CT, Varricchio DJ, Gaudin TJ, Woodward HN, Horner JR (2019) Ontogenetic changes in the long bone microstructure in the nine-banded armadillo (Dasypus novemcinctus). PLoS ONE 14(4): e0215655.

Henry EC, Dengler-Crish CM, Catania KC. 2007. Growing out of a caste--reproduction and the making of the queen mole-rat. Journal of Experimental Biology 210: 261–268.

Herbst, M., J. U. M. Jarvis, and N. C. Bennett. 2004. A field assessment of reproductive seasonality in the threatened wild Namaqua dune mole-rat (*Bathyergus janetta*). Journal of Zoology 263:259–268.

Hildebrand M. 1978. Insertions and functions of certain flexor muscles in the hind leg of rodents. Journal of Morphology 155(1):111-122

Hildebrand M. 1985. Digging of quadrupeds. In: Hildebrand M,, In: Bramble D,, In: Liem K,, In: Wake DB, eds. Functional Vertebrate Morphology. Massachusetts and London: The Belknap Press of Harvard University Press, 89–109.

Hillam R, Skerry TM. **1995.** Inhibition of bone resorption and stimulation of formation by mechanical loading of the modeling rat ulna *In Vivo*. *Journal of bone and mineral research* **10**, 683–689.

Hill, WC., A. Porterr, . T. Bloom J, Seago A., Nd. D. Southwick. Field and laboratorys tudies on the naked mole-rat (*Heterocephalus glaber*). Proceedings of the Zoological Society of London 128:455-513.

Hillier, M.L. and Bell, L.S. (2007), Differentiating Human Bone from Animal Bone: A Review of Histological Methods. Journal of Forensic Sciences, 52: 249-263. doi:10.1111/j.1556-4029.2006.00368.x

Hislop, M.S., Buffenstein, R., 1994. Noradrenaline induces nonshivering thermogenesis in both the naked mole-rat (*Heterocephalus glaber*) and the Damara mole-rat (*Cryptomys damarensis*) despite very different modes of thermoregulation. J. Therm. Biol. 19, 25–32.

Holtze S, Braude S, Lemma A, et al. 2018. The microenvironment of naked mole-rat burrows in East Africa. Afr J Ecol.; 56:279–289.

Hopkins, SS, Davis, EB. 2009. Quantitative morphological proxies for fossoriality in small mammals. Journal of Mammalogy, 90(6): 1449–1460.

Hörner K, Leoffler K, Holtzmann M. **1997.** Vergleich der histologischen Struktur der Kompakta der langen Röhrenknochen bei Maus, Hamster, Ratte, Meerschweinen, Kaninchen, Katze und Hund während der Altersentwicklung. *Anatomia, Histologia, Embryologia* **26**, 289–295.

Howell B. 1965. Speed in mammals, their specialization for running and leaping. New York and London: Hafner Publishing Company.

Huxley, J.S. 1932 (1993). Problems of relative growth. Johns Hopkins University Press, Baltimore.

IUCN, 2020. Bathyergidae Family. Visited December, 2019. https://www.iucnredlist.org/search?taxonomies=100537&searchType=species

Janse Van Rensburg, L., Chimimba, C.T., Van Der Merwe, M., Schoeman, A.S. & Bennett, N.C. 2004. Relative age and reproductive status in *Cryptomys hottentotus pretoriae* (Rodentia: Bathyergidae) from South Africa. Journal of Mammalogy 85: 58–65.

Jarvis J. 2013. Family Bathyergidae, Molerats. In: Happold D, ed. Mammals of Africa Volume III. Rodents, hares, and rabbits. London: Bloomsbury, 641–670.

Jarvis J. 2003. African mole-rats (Bathyergidae). In: Hutchins M,, In: Kleiman D,, In: Geist V,, In: McDade M, eds. *Grzimek's Animal Life Encyclopedia: Mammals V, Volume 16*. Farmington Hills, MI: Gale Group, 339–350.

Jarvis, J. U. M. 1981. Eusociality in a mammal: Cooperative breeding in naked mole-rat colonies. Science 212:571-573.

Jarvis JUM., & PW. Sherman. 2002. *Heterocephalus glaber.* Mammalian Species, No. 706: 1-9.

Jarvis JUM, O'Riain MJ, Bennett NC, & Sherman PW. 1994. Mammalian eusociality: a family affair. Trends Ecol Evol 9:47–51

Jarvis J, O'Riain MJ, McDaid E. 1991. Growth and factors affecting body size in

naked mole-rats. in The Biology of the Naked Mole-rat, eds. Sherman, P. W., Jarvis, J. U. M. & Alexander, R. D. (Princeton Univ. Press, Princeton), pp. 258–383.

Jarvis J, Sale J. 1971. Burrowing and burrow patterns of East African mole-rats Tachyoryctes, Heliophobius and Heterocephalus. Journal of Zoology 163:451–479.

Jasinoski SC, Chinsamy A 2012. Mandibular histology and growth of the nonmammaliaform cynodont *Tritylodon*. *Journal of Anatomy* **220**, 564–579.

Jaworski, Z. F. G. (1992). Haversian systems and Haversian bone. In Bone, Volume 4: Bone Metabolism and Mineralization (B. K. Hall, ed.), pp. 21–45. CRC Press, Boca Raton, FL.

Jee WS, Yao W. 2001. Overview: animal models of osteopenia and osteoporosis. *Journal of musculoskeletal & neuronal interactions* **1**, 193–207.

Jones Kate E., Safi Kamran. 2011. Ecology and evolution of mammalian biodiversity. 366. Phil. Trans. R. Soc. B

Kilbourne BM, & Makovicky PJ. 2012. Postnatal long bone growth in terrestrial placental mammals: Allometry, life history, and organismal traits. J Morphol 273:1111–1126.

Kingdon, J., Happold, D., Hoffmann, M., Butynski, T., Happold, M. & Kalina, J. (eds) 2013. Mammals of Africa. Volume I: Introductory Chapters and Afrotheria. Bloomsbury Publishing, London. 2013.

Kingdon, J. & Hoffmann, M. (eds) 2013. Mammals of Africa. Volume V: Carnivores, Pangolins, Equids and Rhinoceroses. Bloomsbury Publishing, London.

Kinlaw A. 1999. A review of burrowing by semi-fossorial vertebrates in arid environments J. Arid Environ., 41 (2): 127-145.

Klevezal GA. 1996. *Recording Structures of Mammals. Determination of Age and Reconstruction of Life History*. A.A. Balkema, Rotterdam.

Klevezal GA, Kleinberg SE. 1967. *Age Determination of Mammals from Annual Layers in Teeth and Bones*. Jerusalem, Israel: Translated from Russian by the Israel Program for Scientific Translations.

Kley N, Kearney M. 2007. Adaptations for digging and burrowing. In: *Fins into Limbs. Evolution, Development, and Transformation* pp. 433. The University of Chicago Press, London.

Klingenberg CP. 2013. Cranial integration and modularity: insights into evolution and development from morphometric data. Hystrix.;24:43–58.

Köhler M, Marín-Moratalla N, Jordana X et al. 2012. Seasonal bone growth and physiology in endotherms shed light on dinosaur physiology. *Nature* **487**, 358–361.

Köhler, M., and S. Moyà-Solà. 2009. Physiological and life history strategies of a fossil large mammal in a resource-limited environment. Proceedings of the National Academy of Sciences of the United States of America 106:20354–8.

Kolb C, Scheyer TM, Veitschegger K et al. 2015a. Mammalian bone palaeohistology: a survey and new data with emphasis on island forms. *PeerJ* **3**: e1358.

Koyabu D, Endo H, Mitgutsch C, Suwa G, Catania KC, Zollikofer CP, Oda Sichi, Koyasu K, Ando M, Sánchez-Villagra MR. 2011. Heterochrony and developmental modularity of cranial osteogenesis in lipotyphlan mammals. EvoDevo 2: 1–18.

Kriloff A, Germain D, Canoville A et al. 2008. Evolution of bone microanatomy of the tetrapod tibia and its use in palaeobiological inference. *Journal of Evolutionary Biology* **21**, 807–826.

Lacey EA, Patton J, Cameron G. 2000. *Life Underground. The Biology of Subterranean Rodents.* The University of Chicago Press, London.

Lagaria A, Youlatos D. 2006. Anatomical Correlates to Scratch Digging in the Forelimb of European Ground Squirrels (*Spermophilus citellus*). Journal of Mammalogy 87: 563–570.

Lanyon LE, Sugiyama T, Price JS. 2009. Regulation of Bone Mass: Local Control or Systemic Influence or Both? *IBMS BoneKEy* 6: 218–226.

Lavocat R. 1978. Rodentia and Lagomorpha. In: Maglio V,, In: Cooke HBS, eds. Evolution of African Mammals. Cambridge: Harvard University Press, 69–89.

Leary, S., Underwood, W., Lilly, E., Anthony, R., Cartner, S., Corey, D., & Division, A. W. 2013. AVMA Guidelines for the Euthanasia of Animals: 2013 Edition. Schaumburg: Association, American Veterinary Medical.

Lee, Simons (2015) Wing bone laminarity is not an adaptation for torsional resistance in bats. PeerJ 3:e823; DOI 10.7717/peerj.823.

Legendre LJ, Botha-Brink J. Digging the compromise: investigating the link between limb bone histology and fossoriality in the aardvark (*Orycteropus afer*). PeerJ 2018; 6:e5216. https://doi.org/10.7717/peerj. 5216 PMID: 30018860

Lehmann T, Vignaud P, Likius A, Mackaye HT, Brunet M. 2006. A sub-complete fossil aardvark (Mammalia, Tubulidentata) from the Upper Miocene of Chad. Comptes Rendus Palevol 5(5):693–703.

Leppänen O, Sievänen H, Jokihaara J, Pajamäki I, Järvinen TL. 2006. Three-Point Bending of Rat Femur in the Mediolateral Direction: Introduction and Validation of a Novel Biomechanical Testing Protocol. Journal of Bone and Mineral Research 21: 1231–1237.

Lessa EP, Vassallo AI, Verzi DH, Mora MS. 2008. Evolution of morphological adaptations for digging in living and extinct ctenomyid and octodontid rodents. Biological Journal of the Linnean Society 95: 267–283.

Lessa E, Thaeler C. 1989. A Reassessment of Morphological Specializations for Digging in Pocket Gophers. Journal of Mammalogy, 70(4): 689-700. doi:10.2307/1381704

Li XQ, Klein L. 1990. Decreasing rates of bone resorption in growing rats *In Vivo*: Comparison of different types of bones. *Bone* **11**, 95–101.

Lin Y-F, Konow N, Dumont ER. 2019. How moles walk; it's all thumbs. Biol. Lett. 15: 20190503.

Linstedt, S. L., & S. D. Swain. 1988. Body size as a constraint of design and function. pp. 93-106. In M. Boyce (lot. cit.).

López-Aguirre, C., Hand, S.J., Koyabu, D. et al. 2019. Postcranial heterochrony, modularity, integration and disparity in the prenatal ossification in bats (Chiroptera). BMC Evol Biol 19, 75.

Luo Z Xi, Meng Q jin, Ji Q, Liu D, Zhang Y guang, Neander A. 2015. Evolutionary delopment in basal mammaliaforms as revealed by a docodontan. Science 347: 760–765.

Luo Z Xi, Wible JR. 2005. A Late Jurassic Digging Mammal and Early Mammalian Diversification. Science 308: 103–107.

Maier, W. & Schrenk, F. 1987. The hystricomorphy of the Bathyergidae, as determined from ontogenic evidence. Zeitschrift Für Säugetierkunde, 52, 156-164.

Marcy AE, Hadly EA, Sherratt E, Garland K, Weisbecker V. 2016. Getting a head in hard soils : Convergent skull evolution and divergent allometric patterns explain shape variation in a highly diverse genus of pocket gophers (*Thomomys*). BMC Evolutionary Biology: 1–16.

Martin RB, Burr DB, Sharkey N. 1998. *Skeletal Tissue Mechanics*. New York: Springer-Verlag.

Martin A. P., Palumbi S. R. (1993). Body size, metabolic rate, generation time, and the molecular clock. Proc. Natl. Acad. Sci. USA 90, 4087–4091. 10.1073/pnas.90.9.4087

Martiniaková M, Omelka R, Chrenek P et al. 2005a. Changes of femoral bone tissue microstructure in transgenic rabbits. *Folia Biologica (Praha)* **51**, 140–144.

Martiniaková M, Vondráková M, Fabi M. 2003. Investigation of the microscopic structure of rabbit compact bone tissue. *Scripta Medica (BRNO)* **76**, 215–220.

Mason MJ, Cornwall HL, Smith ES. J. (2016) Ear Structures of the Naked Mole-Rat, *Heterocephalus glaber*, and Its Relatives (Rodentia: Bathyergidae). PLoS ONE 11(12): e0167079.

Maunz, M., & German, R. Z. (1997). Ontogeny and limb bone scaling in two new world marsupials, *Monodelphis domestica* and *Didelphis virginiana*. Journal of Morphology, 231, 117–130.

Mcfarlin SC, Terranova CJ, Zihlman AL et al. 2016. Primary bone microanatomy records developmental aspects of life history in catarrhine primates. *Journal of Human Evolution* **92**, 60–79.

McFarlin, S. 2006. Ontogenetic variation in long bone microstructure in catarrhines and its significance for life history research. Anthropology, The City University of New York, New York, pp.

McIntosh, A. F. and Cox, P. G. (2016a). The impact of gape on the performance of the skull in chisel-tooth digging and scratch digging mole-rats (Rodentia: Bathyergidae). R. Soc. Open Sci. 3, 160568.

McIntosh, A. F. & Cox, P.G. 2016b. Functional implications of craniomandibular morphology in African mole -rats (Rodentia: Bathyergidae). Biol. J. Linn. Soc. 117: 447 -462.

McNab BK. 2002. The Physiological Ecology of Vertebrates. Ithaca and London: Associates, Comstock Publishing.

McNab, 1966. The metabolism of fossorial rodents: a study of convergence. *Ecology* 47, 712–733.

Meier PS, Bickelmann C, Scheyer TM, Koyabu D, Sánchez-Villagra MR. 2013. Evolution of bone compactness in extant and extinct moles (Talpidae): exploring humeral microstructure in small fossorial mammals. BMC Evolutionary Biology 13:55.

Minelli A. 2015. Grand challenges in evolutionary developmental biology. Front. Ecol. Evol. 2:85. doi: 10.3389/fevo.2014.00085

Montoya-Sanhueza, G, Wilson LAB & Chinsamy A. 2019. Postnatal development of the largest subterranean mammal (*Bathyergus suillus*): Morphology, osteogenesis, and modularity of the appendicular skeleton. Developmental Dynamics. DOI: 10.1002/dvdy.81.

Montoya-Sanhueza G & Chinsamy A. 2018. Cortical bone adaptation and mineral mobilization in the subterranean mammal *Bathyergus suillus* (Rodentia: Bathyergidae): effects of age and sex. PeerJ 6:e4944; DOI 10.7717/peerj.4944

Montoya-Sanhueza, G & A. Chinsamy. 2017. Long bone histology of the subterranean rodent *Bathyergus suillus* (Bathyergidae): ontogenetic pattern of cortical bone thickening. Journal of Anatomy, 230:203-233.

Montoya-Sanhueza, G & Chinsamy A. 2016. Bone microstructure of two highly specialised subterranean rodents: *Bathyergus suillus* and *Heterocephalus glaber* (Bathyergidae). Biennial Conference Palaeontological Society of Southern Africa (PSSA). Abstract book. Stellenbosch, South Africa, 45.

Montoya-Sanhueza, G. 2014. Bone microstructure of the subterranean rodent *Bathyergus suillus* (Rodentia: Bathyergidae). Master's Thesis. Department of Zoology, University of Cape Town, South Africa.

Morgan CC, Verzi DH, Olivares AI, Vieytes EC. 2017. Craniodental and forelimb specializations for digging in the South American subterranean rodent *Ctenomys* (Hystricomorpha, Ctenomyidae). Mammalian Biology 87: 118–124.

Morgan CC. 2015. The postcranial skeleton of caviomorphs: morphological diversity, adaptations and patterns. Ch 5. SAREM Series A - Mammalogical Research, Vol 1: 167-198.

Morgan E, Barnes G, Einhorn T. 2010. The bone organ system: Form and Function. In: *Fundamentals of Osteoporosis* (eds R Marcus, D Feldman, D Nelson, C Rosen), pp. 1-23. Academic Press, Elsevier, London.

Moshkin M., Novikov E., Petrovski D. 2007. Skimping as an Adaptive Strategy in Social Fossorial Rodents: The Mole Vole (*Ellobius talpinus*) as an Example. In: Begall S., Burda H., Schleich C.E. (eds) Subterranean Rodents. Springer, Berlin, Heidelberg.

Moss ML (1977) A functional analysis of fusion of the tibia and fibula in the rat and mouse. Acta Anat 97, 321–332.

Murray PDF. 1936. Bones: A Study of the Development and Structure of the Vertebrate Skeleton. Cambridge: Cambridge University Press.

Nevo E. 1999. Mosaic Evolution of Subterranean Mammals. Regression, Progression and Global Convergence. Oxford: Oxford University Press.

Nevo E. 1979. Adaptive convergence and divergence of subterranean mammals. Annu Rev *Ecol Evol Syst*, 10:269–308.

Olson EC, & Miller RL. Morphological integration. Chicago and London: Chicago University Press; 1958.

Omerbašić D., Smith E. S. J., Moroni M., Homfeld J., Eigenbrod O., Bennett N. C., Lewin G. R. 2016. Hypofunctional TrkA accounts for the absence of pain sensitization in the African naked mole-rat. Cell Reports, 17(3), 748–758.

O'Connor TP, Lee A, Jarvis J, Buffenstein R. 2002. Prolonged longevity in naked mole-rats: age-related changes in metabolism, body composition and gastrointestinal function. Comparative Biochemistry and Physiology. Part A, Molecular & Integrative Physiology, 133(3), 835–42.

O'Regan HJ, Kitchener AC. The effects of captivity on the morphology of captive, domesticated and feral mammals. Mamm Rev. 2005;35:215–30

O'Riain MJ, Jarvis J, Alexander R, Buffenstein R, Peeters C. 2000. Morphological castes in a vertebrate. Proceedings of the National Academy of Sciences of the United States of America 97:13194–7.

O'Riain MJ, Jarvis J, 1998. The dynamics of growth in naked mole-rats: the effects of litter order and changes in social structure. *J. Zool. (London),* 246, 49–60.

O'Riain, M. J. 1996. Pup Ontogeny and Factors Influencing Behavioural and Morphological Variation in Naked Mole-Rats, *Heterocephalus glaber* (Rodentia, Bathyergidae). University of Cape Town.

Parfitt AM. **2010.** Skeletal Heterogeneity and the Purposes of Bone Remodeling: Implications for the Understanding of Osteoporosis. In: *Fundamentals of Osteoporosis* (eds R Marcus, D Feldman, D Nelson, C Rosen), pp. 537. Academic Press, Elsevier, London.

Park, T.J., Reznick, J., Peterson, B.L., Blass, G., Omerbasic, D., Bennett, N.C., Kuich, P H J L, Zasada, C., Browe, B.M., Hamann, W., et al. (2017). Fructose-driven glycolysis supports anoxia resistance in the naked mole-rat. Science 356, 307–311.

Partha R, Chauhan BK, Ferreira Z, Robinson JD, Lathrop K, Nischal KK, Chikina M, Clark NL. 2017. Subterranean mammals show convergent regression in ocular genes and enhancers, along with adaptation to tunneling. Elife 6:e25884.

Patterson BD, Upham NS. 2014. A newly recognized family from the Horn of Africa, the Heterocephalidae (Rodentia: Ctenohystrica). Zoological Journal of the Linnean Society 172: 942–963.

Pélabon, C. Geir H. Bolstad, Camilla K. Egset, James M. Cheverud, Mihaela Pavlicev and Gunilla Rosenqvist. 2013. On the Relationship between Ontogenetic and Static Allometry. The American Naturalist , Vol. 181, No. 2, pp. 195-212.

Penz, O., Fuzik, J., Kurek, A. et al. 2015. Protracted brain development in a rodent model of extreme longevity. Sci Rep 5, 11592.

Percival & Richtsmeier. 2017. Building Bones: Bone Formation and Development in Anthropology. Cambridge University Press. Cambridge, UK. 319 pp.

Pérez MJ, Barquez RM, Díaz MM. 2017. Morphology of the limbs in the semi-fossorial desert rodent species of *Tympanoctomys* (Octodontidae, Rodentia). ZooKeys 710: 77–96.

Phillips. L. 1885. Note on *Heterocephalus glaber*. Proc. Zool. Soc. London. Pp. 611.

Pinto et al. 2010. Lack of sexual dimorphism in femora of the eusocial and hypogonadic naked mole-rat: A novel animal model for the study of delayed puberty on the skeletal system. *Bone*, 46:112–120.

Pratt CW. 1959. Postnatal changes in the shaft of the rat's femur. *Journal of anatomy* **93**, 309–22.

Pratt CW. 1957. Observations on osteogenesis in the femur of the foetal rat. *Journal of anatomy* **91**, 533–544.

Prochel, J., Begall, S., Burda, H. 2013. Morphology of the carpal region in some rodents with special emphasis on hystricognaths. Acta Zoologica (Stockholm) 95: 220–238.

Purdie DW, Aaron JE, Selby PL. 1988. Bone histology and mineral homeostasis in human pregnancy. *british journal of obstetrics and gynaecology* 95: 849–854.

Quemeneur S, de Buffrénil V, Laurin M. 2013. Microanatomy of the amniote femur and inference of lifestyle in limbed vertebrates. *Biological Journal of the Linnean Society* 109: 644–655.

Quinn G., M. Keough. 2002. Experimental Design and Data Analysis for Biologists. Cambridge University Press, Cambridge.

R Core Team, (2015). R: A language and environment for statistical computing. 2.15.3 ed. Vienna, Austria: R Foundation for Statistical Computing.

Raff RA, Wray GA. 1989. Heterochrony - developmental mechanisms and evolutionary results. J Evol Biol.; 2(6):409–34.

Ray S, Botha J, Chinsamy A. 2004. Bone histology and growth patterns of some nonmammalian therapsids. Journal of Vertebrate Paleontology **24**, 634–648.

Ray S, Chinsamy A. 2004. *Diictodon feliceps* (Therapsida, Dicynodontia): bone histology, growth, and biomechanics. Journal of Vertebrate Paleontology 24: 180–194.

Reed, Ch. 1954. Some Fossorial Mammals from the Tertiary of Western North America. Journal of Paleontology, Vol. 28, No. 1. 102-111

Reichman, O.J., Seabloom. E.W. 2002. The role of pocket gophers as subterranean ecosystem engineers Trends Ecol. Evol., 17: 44-49.

Reichman OJ, Smith SC. 1990. Burrows and burrowing behavior by mammals. In: Genoways HH, ed. Current Mammalogy. New York and London: Plenum Press, 197–244.

Retief, L., Bennett, N.C., Jarvis, J.U.M. et al. Subterranean Mammals: Reservoirs of Infection or Overlooked Sentinels of Anthropogenic Environmental Soiling?. EcoHealth 14, 662–674 (2017).

Rolian C. 2008. Developmental basis of limb length in rodents: evidence for multiple divisions of labor in mechanisms of endochondral bone growth. Evolution and Development 10: 15–28.

Rose J, Moore A, Russell A, Butcher M. 2014. Functional osteology of the forelimb digging apparatus of badgers. Journal of Mammalogy 95: 543–558.

Ruby, JG, M Smith, R Buffenstein (2018). Naked mole-rat mortality rates defy Gompertzian laws by not increasing with age. eLife 7:e31157.

Russell AF, Carlson AA, McIlrath GM, Jordan NR, Clutton-Brock T. 2004. Adaptive size modification by dominant female meerkats. Evolution 58, 1600–1607. (doi:10.1111/j.0014-3820.2004.tb01739.x)

Salton JA, Sargis EJ. 2008. Evolutionary Morphology of the Tenrecoidea (Mammalia) Forelimb Skeleton. In: Sargis E,, In: Dagosto M, eds. Mammalian Evolutionary Morphology, A Tribute to Frederick S. Szalay. Dordrecht: Springer Netherlands, 51–72.

Samuels JX, Valkenburgh B Van. 2008. Skeletal Indicators of Locomotor Adaptations in Living and Extinct Rodents. Journal of Morphology 269: 1387–1411.

Sánchez-Villagra MR. 2002. Comparative patterns of postcranial ontogeny in therian mammals: An analysis of relative timing of ossification events. Journal of Experimental Zoology 294: 264–273.

Sanger TJ, Norgard EA, Pletscher LS, Bevilacqua M, Brooks VR, Sandell LJ, Cheverud JM. 2011. Developmental and Genetic Origins of Murine Long Bone Length Variation. Journal of Experimental Zoology. Part B, Molecular and Developmental Evolution 316: 146–161.

Sansalone, G., Colangelo, P., Loy, A. et al. 2019 Impact of transition to a subterranean lifestyle on morphological disparity and integration in talpid moles (Mammalia, Talpidae). BMC Evol Biol 19, 179.

Sansalone G, Colangelo P, Kotsakis T, Loy A, Castiglia R, Bannikova AA, Zemlemerova ED, Piras P. 2018. Influence of Evolutionary Allometry on Rates of Morphological Evolution and Disparity in strictly Subterranean Moles (Talpinae, Talpidae, Lipotyphla, Mammalia). Journal of Mammalian Evolution 25: 1–14.

Sahd, L., Bennett, N. C., & Kotzé, S. H. (2019). Hind foot drumming: Mor-phological adaptations of the muscles and bones of the hind limb inthree African mole-rat species. Journal of Anatomy,235, 811–824.

Scharff, A., S. Begall, O. Grütjen, & H. Burda. 1999. Reproductive characteristics and growth of Zambian giant mole-rats, *Cryptomys mechowi* (Rodentia: Bathyergidae). Mammalia, 63: 217-230.

Schilling, N., & A. Petrovitch. 2006. Postnatal allometry of the skeleton in *Tupaia glis* (Scandentia: Tupaiidae) and *Galea musteloides* (Rodentia: Caviidae)–a test of the three-segment limb hypothesis. Zoology109:148–163.

Seney ML, Kelly DA, Goldman BD, Šumbera R, Forger NG. 2009. Social Structure Predicts Genital Morphology in African Mole-Rats. PLoS ONE 4(10): e7477. doi:10.1371/journal.pone.0007477

Sharir A, Stern T, Rot C, Shahar R, Zelzer E. 2011. Muscle force regulates bone shaping for optimal load- bearing capacity during embryogenesis. Development 138: 3247–3259.

Shea, B. T. 1993. Bone growth and primate evolution. 133-157. In Hall, B. K. (ed.). Bone Volume 7: Bone growth - B. CRC Press, Boca Raton, FL, 353 pp.

Sherman, P. W., J. U. M. Jarvis, and R. D. Alexander. 1991. The biology of the naked mole-rat. Princeton University Press, New Jersey.

Sikes, R., Gannon, W. L., & Animal Care and Use Committee. 2011. Guidelines of the American Society of Mammalogists for the use of wild mammals in research. Journal of Mammalogy, 92(1), 235–253. http://doi.org/10.1644/10-MAMM-F-355.1

Silva MJ, Brodt MD, Hucker WJ (2005) Finite element analysis of the mouse tibia: estimating endocortical strain during three-point bending in SAMP6 osteoporotic mice. Anat Rec 283, 380– 390.

Simpson, G. G., Roe, A. & Lewontin, R. C. (1960). Quantitative zoology. 2nd ed. New York: Harcourt, Brace & World.

Skedros JG, Hunt KJ, Bloebaum RD. **2004.** Relationships of loading history and structural and material characteristics of bone: development of the mule deer calcaneus. *Journal of morphology* **259**, 281–307.

Skedros JG, Su SC, Bloebaum RD. 1997. Biomechanical implications of mineral content and microstructural variations in cortical bone of horse, elk, and sheep calcanei. *Anatomical Record* **249**, 297–316.

Skinner J, & Chimimba CT (eds). 2005. The mammals of the Southern African Region. Cape Town, South Africa: Cambridge University Press.

Skulachev VP, Holtze S, Vyssokikh MY, Bakeeva LE, Skulachev MV, Markov AV, Hildebrandt TB, Sadovnichii VA. Neoteny, Prolongation of Youth: From Naked Mole Rats to "Naked Apes" (Humans). Physiol Rev 97: 699–720, 2017.

Smith JW. 1960. Collagen fibre patterns in mammalian bone. *Journal of anatomy* **94**, 329–344.

Sontag W. 1986. Quantitative measurements of periosteal and cortical-endosteal bone formation and resorption in the midshaft of male rat femur. *Bone* **7**, 55–62.

Spicer, JI. 2006. A Physiological Approach to Heterochrony. In Comparative Developmental Physiology. Contributions, Tools, and Trends. By Warburton, SJ, WW Burggren, B Pelster, CL. Reiber, & J Spicer (Eds). Oxford University Press. NY, USA.

Spradling, T. A., M. S. Hafner, and J. W. Demastes. 2001. Differences in rate of cytochrome-b evolution among species of rodents. Journal of Mammalogy 82:65–80.

Stein B. 2000. Morphology of Subterranean Rodents. In: Lacey EA,, In: Patton J,, In: Cameron GN, eds. Life Underground: the biology of subterranean rodents. Chicago: The University of Chicago Press, 19–61.

Stern T, Aviram R, Rot C et al. 2015. Isometric scaling in developing long bones is achieved by an optimal epiphyseal growth balance. *PLOS Biology* **13**, e1002212.

Stout S, Crowder C. 2012. Bone remodeling, histomorphology, and histomorphometry. In: *Bone Histology. An Anthropological Perspective* (eds C Crowder, S Stout), pp. 375. CRC Press, Boca Raton.

Straehl FR, Scheyer TM, Forasiepi AM et al. 2013. Evolutionary patterns of bone histology and bone compactness in xenarthran mammal long bones. *PloS one* **8**, e69275.

Stathopoulos S, Bishop JM, O'Ryan C (2014) Genetic Signatures for Enhanced Olfaction in the African Mole-Rats. PLoS ONE 9(4): e93336.

Šumbera, 2019. Thermal biology of a strictly subterranean mammalian family, the African mole-rats (Bathyergidae, Rodentia) - a review. *Journal of Thermal Biology*, 79:166-189.

Šumbera, R., V. Mazoch, H. Patzenhauerová, M. Lövy, J. Šklíba, J. Bryja & H. Burda. 2012. Burrow architecture, family composition and habitat characteristics of the largest social African mole-rat: the giant mole-rat constructs really giant burrow systems. Acta Theriologica 57:121-130.

Šumbera, R., Chitaukali, W.N., Elichová, M., Kubová, J., Burda, H., 2004. Microclimatic stability in burrows of an Afrotropical solitary bathyergid rodent, the silvery mole-rat (*Heliophobius argenteocinereus*). J. Zool. 263, 409–416.

Šumbera, R., Burda, H., Chitaukali, W.N., 2003. Reproductive biology of a solitary subterranean bathyergid rodent, the silvery mole-rat (*Heliophobius argenteocinereus*). J. Mammal. 84, 278–287.

Szalay F. S. & Sargis E. J. 2001. Model-based analysis of postcranial osteology of marsupials from the Palaeocene of Itaboraí (Brazil) and the phylogenetics and biogeography of Metatheria. Geodiversitas 23 (2): 139-302

Taylor P, Jarvis J, Crowe T, Davies KC. 1985. Age determination in the Cape molerat Georhychus capensis. S.-Afr. Tydskr. Dierk. 20: 261–267.

Thomas, H. G., P. W. Bateman, S. C. Le Comber, N. C. Bennett, R. W. Elwood, and M. Scantlebury. 2009. Burrow architecture and digging activity in the Cape dune mole rat. Journal of Zoology 279:277–284.

Thompson D'AW 1917. On growth and form (Cambridge University Press, Cambridge).

Thorley J, Katlein N, Goddard K, Zottl M, Clutton-Brock T. 2018. Reproduction triggers adaptive increases in body size in female mole-rats. Proc. R. Soc. B 285: 20180897.

Tian J, Azpurua C, Hine A, Vaidya M, Myakishev-Rempel J, Ablaeva Z, Mao E, Nevo V, Gorbunova A, Seluanov (2013) High-molecular-mass hyaluronan mediates the Cancer resistance of the naked mole rat. Nature 499:346–349.

Tomlin DH, Henry KM, Kon SK. **1953.** Autoradiographic study of growth and calcium metabolism in the long bones of the rat. *British journal of nutrition* **7**, 235–252.

Turner CH. 2004. Biomechanical Aspects of Bone Formation. In: *Bone Formation, Volume 1, Series Topics in Bone Biology* (eds F Bronner, M Farach-Carson)), pp. 160. Springer-Verlag, London.

Upham, N., Patterson, B.D., 2015. Evolution of caviomorph rodents: a complete phylogeny and timetree for living genera, in: Vassallo, A.I., Antenucci, D. (Eds.), Biology of Caviomorph Rodents: Diversity and Evolution. SAREM Series A, Buenos Aires, pp. 63–120.

Urison, N., Buffenstein, R., 1995. Metabolic and body temperature changes during pregnancy and lactation in the naked mole-rat (*Heterocephalus glaber*). Physiol. Zool. 68, 402–420. https://doi.org/10.1086/physzool.68.3.30163776.

Van Daele PA1, Herrel A, Adriaens D. 2009. Biting performance in teeth-digging African mole-rats (*Fukomys*, Bathyergidae, Rodentia). Physiol Biochem Zool. 2009 Jan-Feb;82(1):40-50. doi: 10.1086/594379.

Van Daele PAAG, Faulkes CG, Verheyen E, Adriaens D. 2007. African mole-rats (Bathyergidae): a complex radiation in tropical soils. In: Begall S, Šumbera R, Schleich CE (eds) Subterranean Rodents: News from Underground. Springer-Verlag, Berlin, Heidelberg, New York, pp 358–373

Van Wassenbergh, S., Heindryckx, S., & Adriaens, D. (2017). Kinematics of chisel-tooth digging by African mole-rats. Journal of Experimental Biology, 220(23), 4479– 4485.

Von Bertalanffy, L. 1968. General System Theory. Foundations, Development, Applications. New York, George Braziller, 1968.

Vassallo AI. 1998. Functional morphology, comparative behaviour, and adaptation in two sympatric subterranean rodents genus *Ctenomys* (Caviomorpha: Octodontidae). J Zool, 244:415–427.

Vianey-Liaud M, Hautier L, Marivaux L. 2015. Morphological disparity of the postcranial skeleton in rodents and its implications for paleobiological inferences: the case of the extinct Theridomyidae (Rodentia, Mammalia) In: Cox FG, Hautier L, eds. Evolution of the rodents: advances in phylogenetics, functional morphology and development. Cambridge: Cambridge University Press. 538-588

Vizcaíno SF, Bargo S, Cassini GH, Toledo N. 2016. Forma y función en paleobiología de vertebrados. La Plata, Buenos Aires: Editorial de la Universidad de La Plata (EDULP).

Vizcaíno SF, Bargo MS, Kay RF, Milne N. 2006. The armadillos (Mammalia, Xenarthra, Dasypodidae) of the Santa Cruz Formation (early – middle Miocene): An approach to their paleobiology. Palaeogeography, Palaeoclimatology, Palaeoecology 237: 255–269.

Vizcaíno SF, Milne N. 2002. Structure and function in armadillo limbs (Mammalia: Xenarthra: Dasypodidae). Journal of Zoology of London 257: 117–127.

Vizcaíno SF, Fariña RA, Mazzetta G V. 1999. Ulnar dimensions and fossoriality in armadillos. Acta Theriologica 44: 309–320.

Wallace IJ, Demes B, Judex S. 2017. Ontogenetic and Genetic Influences on Bone' s Responsiveness to Mechanical Signals. In: Percival C,, In: Richtsmeier J, eds. Building bones. Bone formation and development in anthropology. Cambridge, UK: Cambridge University Press, 233–253.

Warton DI, Wright IJ, Falster DS, & Westoby M. 2006. Bivariate line-fitting methods for allometry. Biol Rev Camb Philos Soc, 81:259–291.

Wayne, R. K. 1986. Cranial morphology of domestic and wild canids: the influence of development on morphological change. Evolution 40:243–261.

Whedon D, Heaney R. 1993. Effects of physical inactivity, paralysis, and weightlessness on bone growth. In: *Bone Volumen 7 Bone Growth - B* (eds BK Hall), pp. 368. CRC Press, Boca Raton.

White, C. R., Matthews, P. G. D. and Seymour, R. S. (2006). Balancing the competing requirements of saltatorial and fossorial specialisation: burrowing costs in the spinifex hopping mouse, Notomys alexis. J. Exp. Biol. 209, 2103-2113.

Wilson LAB, Schradin C, Mitgutsch C, Galliari FC, Mess A, and Sanchez-Villagra MR. 2010. Skeletogenesis and sequence heterochrony in rodent evolution, with particular emphasis on the African striped mouse, Rhabdomys pumilio (Mammalia). Organisms Diversity & Evolution 10(3):243-258.

Winkler, A., Christiane Denys, D. Margaret Avery. 2010. Fossil Rodents of Africa (Ch. 7). In: Cenozoic Mammals of Africa. Werdelin, L., and W. J., Sanders (Eds.). University of California Press. 1040 pp.

Yahav, S., & Buffenstein, R., 1991. Huddling behavior facilitates homeothermy in the naked mole rat *Heterocephalus glaber*. Physiol. Zool. 64, 871–884.

Young AJ, Bennett NC. 2010 Morphological divergence of breeders and helpers in wild Damaraland mole-rat societies. Evolution 64, 3190–3197. (doi:10.1111/j.1558-5646.2010.01066.x)

Young JW, Fernandez D, Fleagle JG. 2010. Ontogeny of long bone geometry in capuchin monkeys (*Cebus albifrons* and *Cebus apella*): implications for locomotor development and life history. Biology Letters 6: 197–200.

Zelditch ML. 2005. Developmental regulation of variability. Pp. 249-276 in: Hallgrímsson B, Hall BK, eds, Variation: A central concept in biology. Burlington, MA: Elsevier.

Zelová et al., **2010.** Cost of digging is determined by intrinsic factors rather than by substrate quality in two subterranean rodent species. *Physiology & Behavior* 99:54–58.

The more you look at the summit,
the longer it will take you to reach it.

G. Montoya, 2020